Vniversitat ɖɖ València

Faculty of Medicine and Dentistry

Department of physiology

Doctoral Program in Physiology

"Identification of new biomarkers for phenotypical characterization in peripheral neuropathies"

Marta Seco Cervera

May, 2017

Supervised by:

Dr. Federico V. Pallardó Calatayud (co-director and Tutor)

Dr. José Luis García Giménez (co-director)

Dr **Federico V. Pallardó Calatayud**, Catedrático del Dpto. de Fisiología de la Universitat de València

Dr **José Luis García Giménez**, profesor asociado del Dpto. de Fisiología de la Universitat de València

CERTIFICA/N:

Que la presente memoria, titulada "**Identification of new biomarkers for phenotypical characterization in peripheral neuropathies**", corresponde al trabajo realizado bajo su dirección por Dña. **Marta Seco Cervera**, para su presentación como Tesis Doctoral en el Programa de Doctorado en Fisiología de la Universitat de València.

Y para que conste firma/n el presente certificado en Valencia, a 30 de Mayo de 2017.

Fdo. Federico V. Pallardó Calatayud   Fdo. José Luis García Giménez

Agradecimientos

"Si se cree y se trabaja, se puede" – Diego Pablo Simeone

Con estas palabras me gustaría empezar este apartado tan simple pero tan lleno de sentimiento. Sentimiento de gratitud. Porque como si este proyecto de tesis ha llegado hasta aquí ha sido por eso porque se ha creído y se ha trabajado. Y por ello quiero dar las gracias al Dr. Federico V. Pallardó. Aún con sus múltiples tareas que conlleva el cargo de Decano de la Facultad de Medicina siempre intenta tener un hueco para cualquier cosa que necesites. También me gustaría dar las gracias a mi otro director y gran amigo el Dr. José Luis García Giménez, o como yo lo denomino mi padre científico. Este hombre sobre natural siempre está ahí cuando lo necesitas para cualquier cosa sea para una duda técnica, para ayudarte a solucionar cualquier "marrón" de los que aparecen a menudo en el laboratorio, aunque él este inmerso en diez mil "marones" más o para enseñarte cada día una cosa nueva. Eres un ejemplo a seguir como científico. A los dos, gracias por aconsejarme siempre que te tenido una consulta, por ser comprensivos cuando ha sido necesario, por solucionar "marrones" y por en definitiva ayudarme a conseguir que este proyecto de tesis llegara a término.

Me gustaría dedicar unas palabras de agradecimiento a toda la gente que me rodea y ha sido participe en este proyecto de tesis directa o indirectamente:

A todos los integrantes de mi laboratorio qué, aunque somos los "raritos" como nos denominan algunos, hemos sido bastantes: Isa muchas gracias por ayudar y saber dónde estaba todo o donde se podía conseguir, para mí la categoría de técnico de laboratorio siempre te ha quedado pequeña. A Sergio por su por su aprecio a los "rojos" y sus cuidados de cultivos. A los fugaces estudiantes: Marta Belda, Alba, Jenny, Aitor y alguno más que seguramente se me olvide, gracias por hacer los días de laboratorio más entretenidos. Mención especial al señor Galluuu porque aún me estoy riendo del día de la tarta de gominolas, ¡eres muy grande! A los bioinformáticos Pablo, el ruso y Dayme, la perraaa suciaaa que se dedica a arrastraaaarmeee ya tu sabe' gracias por todo, sobre todo a Dayme porque sin su brillantez con los análisis informáticos todavía estaríamos perdidos con los datos de secuenciación. Te quiero mil sorraaa. A José (o José Francisco o Francisco José) por proporcionarnos dulces del

paraíso de la Beata Inés que sapigués que te voliem sols per això :P). A les perles de la Ribera baixa Ester i Carla sou un solet les dos. Al Dr. Litos, también conocido como Carlos Romà, por sus sabias palabras y sus correcciones. A la pareja cubana Gisselle y Guillermin por traer salsa y alegría al laboratorio además proporcionar muchos sabios consejos. A Eva por hacer resolver todas las diferencias estadísticamente significativas. A los nuevos estudiantes que están por el labo: Inma, Rosa, Carmen (happy flower), Jesús y Martina por hacer de estos días de escritura más amenos. A Pili, por sus sugerencias que siempre nos permiten mejorar.

A los laboratorios compis, tanto a los chic@s que han ido pasando por el labo de Viña, como los vecinos de enfrente "linces": Xavi, Dani y Ana. Porque robarnos mutuamente material, nunca ha sido tan agradable, eh linces :P

I want to thanks also, my host laboratory in Boston. Thank you Dr. Richard Gregory, Julie, and all the people in the 9th floor of Karp Building. Specially, I want to thank Dr. Mehdi Pirouz for teach me, be patient with me and make me feel as in my own laboratory.

A Santi, per que des de que vam començar este camí sempre has estat ahí tant en els bons moments com en els roïns. El teu sentit del humor plena el laboratori d'alegría i bon rotllo i això es una cosa molt important en aquesta professió tan sacrificada. Tot lo que te puga agrair es queda curt i tot lo que puga dir de tu també. Eres el meu company de la vida. Te vull moltisim.

Como no agradecer a mis padres y hermano, por su apoyo, su cariño y su comprensión. Sin vosotros no hubiera sido posible nada de esto. Os quiero.

A mi pequeña Lula, porque sabe cómo alegrarme solo con un lametón suyo y nunca, nunca me ha fallado.

A mis tíos y primos, por creer siempre en mí y porque "Joróbate Flanders" era una frase que debía aparecer en esta tesis.

A mis abuelos, tanto el que está con nosotros como los que ya no. Porque estaríais orgullosos de este trabajo y con vuestro amor y cariño conseguisteis que yo sea la persona que soy a día de hoy.

Al resto de personas que no son familia de sangre, pero como si lo fueran: Patricia, Mari Tere, JM, Patri, Javi, Adrian, Junior, Carmen, Carmen Ibáñez, José, Irene y María.

A Bojana desde que llegaste al labo fuimos inseparables y ahora no sé qué haría yo sin mi happy flower farmacéutica. A pesar de que estés "lejos" sabes que te echo de menos y que tu apoyo está presente siempre.

A mi Pauliiii, porque eres mi bombonsito, mi corasón, mi guapiii. Mil gracias por estar ahí siempre y animarme como solo tú sabes. Eres una gran amiga y una gran persona que siempre tendrás un sitio mi corazón.

A mis florecillas de Boston, Elena y Julia. Los días que pasamos allí no los podré olvidar ya que sois de lo mejor que una se puede encontrar. Queda pendiente un reencuentro.

To my dear roommate and friend Margo, thank you for give me all your love and make my staying in Boston as comfortable and happy than one can image. I miss our hang out together and cheers with "Quién no apoya, no….". And remember "Hay un amigo en mi"

A mis amigos de la Uni Irene, Parra, Juan Ángel, Sergio y Ceci aunque nos vemos poco siempre estamos ahí entre las sombras.

A mis biopetorris, Carmen, Jesús, Cris, Pablo e Inma por compartir momentos insólitos; sois mis desechos favoritos y os quiero mogollón.

A Raul, Jorge, las Silvias, Manu, Cristina, Saray, Víctor y Laila por estar siempre ahí. ¡Gracias chicos!

A las prostis pero, sobre todo los petits porque sabéis motivar a la gente y contagiar vuestra alegría y ganas de vivir. Somos Gallos!!

Abbreviations

2D-DIGE	2D-Differential In Gel Electrophoresis
CEIB	Biomedical Research Ethics Committee
CMT	Charcot-Marie-Tooth disease
CMTNS	Charcot-Marie-Tooth Neuropathy Score
CNS	Central Nervous System
Ct	Threshold cycle
DRG	Dorsal Root Ganglia
FRDA	Friedreich's ataxia
FXN	frataxin gene
GAA	Guanine-adenine-adenine
GSH	Reduced Glutathione
GSSG	Oxidised Glutathione
KEGG	Kyoto Encyclopaedia of Genes and Genomes
MDA	Malondialdehyde
miRNA	microRNA
NGS	Next-Generation Sequencing
PMP22	Peripheral myelin protein 22 gene
PNS	Peripheral Nervous System
OMIM	Online Mendelian Inheritance in Man
RNS	Reactive Nitrogen Species
ROC	Receiver operating characteristic
ROS	Reactive Oxygen Species
RT-qPCR	Reverse Transcriptase- quantitative Polymerase Chain Reaction
SARA	Scale for the Assessment and Rating of Ataxia
SH-SY5Y	Neuroblastoma cell line

Index

0. Resumen

Resumen

0.1. Introducción

Las neuropatías periféricas hereditarias son aquellas enfermedades que afectan al sistema nervioso periférico y cuya etiología reside en un desorden genético hereditario. La neurodegeneración que presentan este tipo de enfermedades se caracteriza por una pérdida progresiva de la función y/o estructura en las neuronas. En el caso de axonopatias el proceso empieza en los extremos distales de los axones largos seguido de una progresión hacia las partes más proximales. Este tipo de desórdenes plantea dificultades en el diagnóstico clínico debido a la variabilidad de síntomas clínicos y a las diferentes variaciones fenotípicas que se presentan en los pacientes.

Especies reactivas del oxígeno (ERO) y especies reactivas del nitrógeno (ERN) son generadas en el metabolismo normal de la célula. Mecanismos enzimáticos y no enzimáticos están presentes también en la célula para mantener estas especies reactivas en equilibrio. Alteraciones en los mecanismos de defensa o en los mecanismos que generan ERO y ERN producen lo que se denomina como estrés oxidativo. Este desbalance, conlleva a un aumento de las especies reactivas dando lugar a daño en el ADN, lípidos y proteínas. La generación de este daño produce ciertas marcas en cada uno de estos tipos de moléculas que pueden ser detectados y utilizados como marcadores de estrés oxidativo.

La enfermedad de Charcot-Marie-Tooth (CMT; ORPHA166) es la neuropatía hereditaria más común y recoge a un grupo heterogéneo de desórdenes con características clínicas, neurofisiológicas, genéticas y patológicas comunes. Las características clínicas que definen este tipo de pacientes son: debilidad y deterioro muscular de las extremidades distales, reflejo osteotendinoso disminuido o ausente, pérdida de la sensibilidad distal y frecuentemente deformidades esqueléticas. Este fenotipo y las características clínicas observadas en pacientes con CMT son consecuencia de una progresiva pérdida axonal en los nervios sensitivos y motores. Este desorden tiene un origen genético diverso con más de 75 genes asociados a la enfermedad de Charcot-Marie-Tooth. El desorden genético que con más frecuencia se encuentra en pacientes con la enfermedad de CMT es una duplicación intracromósomica que incluye a la parte del gen codificante para la proteína periférica

Resumen

de mielina de 22 kDa (PMP22). Este tipo de alteración define un subtipo de la enfermedad denominado CMT subtipo 1A (CMT1A). PMP22 es una proteína integral de la membrana altamente expresada por las células de Schwann mielinizantes del sistema nervioso periférico. Esta proteína forma parte de la región compacta de la vaina de mielina donde tiene una función estructural además de participar en los primeros pasos de la formación de ésta. PMP22 además actúa como mediador entre la célula de Schwann y la matriz extracelular, regulando la proliferación celular y la apoptosis, y ha sido relacionada con las uniones intracelulares. La enfermedad de Charcot-Marie-Tooth, como ya se ha descrito, presenta un fenotipo heterogéneo con un amplio rango de alteraciones genéticas y genes implicados. Además, el debut en la infancia, la diferente progresión y severidad de los pacientes de CMT y la falta de tratamiento para esta enfermedad hereditaria potencia la necesidad de encontrar nuevos biomarcadores de diagnóstico, pronóstico y monitorización de los efectos terapéuticos de los ensayos clínicos.

La ataxia de Friedreich (FRDA; OMIM 229300) es una enfermedad mitocondrial neurodegenerativa con una herencia autosómica recesiva, aunque dentro de las ataxias hereditarias es la más prevalente. A pesar de este último hecho, se considera una enfermedad rara o poco frecuente con un debut en la infancia y que presenta una progresiva pérdida de las neuronas sensitivas en el ganglio dorsal de la raíz y la columna posteriores de la médula. Además de presentar alteraciones en el sistema nervioso periférico, el sistema nervioso central también está afectado detectando alteraciones en el núcleo dentado del cerebelo de estos pacientes. Al mismo tiempo de estas características neurológicas, otras enfermedades concomitantes se han descrito en pacientes de FRDA. Así, los pacientes de FRDA pueden presentar, además de mostrar las características neurológicas, escoliosis, diabetes tipo II y cardiomiopatía hipertrófica. Esta última es la principal causa de muerte en pacientes de FRDA. El fenotipo observado en pacientes de FRDA está causado por una alteración en el número de repeticiones del tripéptido guanina-adenina-adenina (GAA) en el primer intrón del gen que codifica *FXN* que codifica para la proteína frataxina. Alelos con hasta 36 repeticiones son considerados como normales, mientras que más de estas repeticiones puede conllevar la generación de expansiones patogénicas. En el caso de ataxia de Friedreich las repeticiones fluctúan entre 44 y 1700 y generan la disminución

de expresión de la proteína frataxina. La función principal de frataxina no está claramente corroborada, sin embargo, esta proteína se ha visto implicada en diversas funciones. Una de las primeras descritas fue en relación a su capacidad para unir hierro ejerciendo un papel de almacenaje de hierro. Por otro lado, también se la ha relacionado con la formación de los clústers hierro-azufre, imprescindibles para el correcto funcionamiento en la mitocondria de los complejos I, II y III de la cadena de transporte electrónico y la enzima aconitasa, y en la biosíntesis de grupo hemo. Este tipo de ataxia, presenta diferencias en las características clínicas, así como en la progresión de la enfermedad. Además, la presencia de enfermedades concomitantes incrementa la complejidad de esta neuropatía por lo que se está incrementando el estudio de posibles biomarcadores pronóstico de esta enfermedad. No obstante, no existen biomarcadores fiables que puedan estratificar los pacientes según su enfermedad/es concomitante/s (diabetes, escoliosis y cardiomiopatía hipertrófica).

Los microARNs (miARN) son pequeñas secuencias de 22 nucleótidos localizadas en regiones intragénicas y/o intrínsecas de transcritos que codifican para proteínas. Tras su procesamiento por el complejo Drosha-DGCR8 y Dicer, dos hebras complementarias se generan y una es incorporada al complejo de silenciamiento inducido de ARN. Este complejo se une por complementariedad a la secuencia de ARN mensajero de la proteína diana controlando su degradación, y por tanto los niveles de proteína. Estas pequeñas moléculas genómicas han sido descritas como biomarcadores de diferentes enfermedades. Están además implicadas en el desarrollo y correcto funcionamiento del sistema nervioso. Por ello estudios de los perfiles de expresión de estos miARN puede proveer de más conocimiento acerca de los mecanismos patológicos de las enfermedades neurodegenerativas además de servir como biomarcadores de progresión de la enfermedad y monitorización de los tratamientos que se utilicen durante los ensayos clínicos.

0.2. Hipótesis y objetivos

Dada la heterogeneidad fenotípica observada tanto en los pacientes de Charcot-Marie-Tooth como en los de ataxia y la ausencia de marcadores de pronóstico y seguimiento de ensayos clínicos fiables, la necesidad de encontrar nuevos

biomarcadores es más que patente. Análisis de marcadores de estrés oxidativo y de expresión de proteínas pueden proporcionar un perfil de expresión diferencial entre pacientes leves, pacientes severos y controles que puede utilizarse como biomarcadores en este tipo de pacientes. Por otra parte, estudios de expresión diferencial de miARN pueden dilucidar diferencias en el perfil de expresión entre pacientes de FRDA o los diferentes modelos celulares de ataxia de Friedreich y sus respectivos controles que pueden ser nuevos biomarcadores para esta neuropatía.

El principal objetivo de este estudio es encontrar biomarcadores de estratificación clínica, pronóstico y/o monitorización de ensayos clínicos en la enfermedad de Charcot-Marie-Tooth y en la ataxia de Friedreich.

Para ello se pretende llevar a cabo los siguientes objetivos y sub-objetivos:

I. Búsqueda de biomarcadores en plasma de pacientes leves y severos de la enfermedad de Charcot-Marie-Tooth con duplicación en PMP22.

    a. Analizar marcadores de estrés oxidativo en plasma de pacientes leves y severos de la enfermedad de Charcot-Marie-Tooth con duplicación en PMP22.

    b. Explorar la expresión diferencial de marcadores proteómicos en plasma de pacientes leves y severos de la enfermedad de Charcot-Marie-Tooth con duplicación en PMP22 y validar los posibles biomarcadores.

II. Búsqueda de biomarcadores genómicos en plasma de pacientes de ataxia de Friedreich y modelos celulares de la enfermedad (células madre de la mucosa olfativa, fibroblastos y SH-SY5Y).

    a. Evaluación de la representación diferencial de los miARN en muestras de plasma de pacientes de FRDA y controles sanos, análisis bioinfomático de las rutas reguladas por estos miARN y validación de miARN candidatos a biomarcadores y sus rutas diana.

    b. Analizar la expresión diferencial de modelos celulares de la enfermedad (células madre de la mucosa olfativa, fibroblastos y SH-SY5Y), análisis bioinfomático de las rutas reguladas por estos miARN y validación de miARN candidatos a biomarcadores y sus rutas diana

c. Validar el perfil de miARN de muestras de plasma de pacientes de FRDA y controles sanos en modelos celulares de la enfermedad (células madre de la mucosa olfativa, fibroblastos y SH-SY5Y) y sus rutas diana.

0.3. Metodología

Tras obtener la aprobación de los comités éticos y científicos de los hospitales y biobancos implicados en este estudio, se realizó la colecta de las muestras de plasma en tubos EDTA de pacientes de la enfermedad de Charcot-Marie-Tooth (Subtipo 1A) y de ataxia de Friedreich y sus respectivos controles agrupados por edad y sexo. Para el caso de CMT, 42 pacientes caucásicos y 22 sujetos caucásicos sanos se unieron a estudio. Los pacientes se clasificaron según la escala CMTNS en leves si el valor era menor o igual a 15 o en severos si el valor era superior a 15. En el caso de FRDA 25 pacientes caucásicos y 25 controles caucásicos fueron incluidos en el estudio.

Además de las muestras de plasma tres modelos celulares diferentes de ataxia de Friedreich fueron utilizados en este trabajo: líneas celulares de fibroblastos de pacientes de FRDA y fibroblastos de sujetos sanos; líneas celulares de células madre de la mucosa olfativa de pacientes de FRDA e individuos sanos; línea celular de deficiencia en frataxina por interferencia en células de neuroblastoma SH-SY5Y y sus controles.

Para la búsqueda de biomarcadores de estrés oxidativo en muestras de plasma de CMT, se determinaron los niveles de Malondialdehido (MDA) mediante cromatografía liquida de alta presión acoplada a detección con ultravioleta (HPLC-UV). Los niveles de proteínas carboniladas se obtuvieron mediante derivatización de las muestras con el kit *Oxi-Blot*^{TM} *protein oxidation detection kit"* (Millipore, EE. UU.) y posterior inmunodetección con técnica "dot-blot", en la que las muestras son adsorbidas en una membrana de nitrocelulosa y para posteriormente realizar la inmunodetección con anticuerpos específicos. También mediante esta técnica "dot-blot" se obtuvieron los niveles de proteínas nitrosiladas. Las imágenes obtenidas se densitometraron mediante el uso del software imageJ. Para obtener los niveles de glutatión, así como determinar el ratio de glutatión oxidado (GSSG) y reducido (GSH),

se utilizó el kit comercial *"DetectX Glutathione kit"* (Arbor Assays, EE. UU). Por último, mediante el uso del kit *"Cayman's Antioxidant Assay Kit"* (Cayman, EE. UU.) se determinó la capacidad antioxidante total que presentaba cada uno de los grupos analizados.

Para realizar el análisis proteómico de las muestras de plasma de pacientes de la enfermedad de Charcot-Marie-Tooth se realizó mediante el uso de una técnica mejorada de la electroforesis en dos dimensiones: la electroforesis diferencial en gel de dos dimensiones (2D-DIGE). Esta técnica permite identificar las proteínas con expresión diferencial entre un grupo diana (en nuestro caso el grupo leve o severo de pacientes de CMT) y un grupo control. Para ello cada una de las muestras seleccionadas de cada uno de los grupos se tiñe con un fluoróforo de los denominados cyDyes diferente. Este tipo de fluoróforos se unen covalentemente en una proporción uno: uno a la proteína. Además, una mezcla equimolecular de ambas muestras se tiñó con otro fluoróforo Cy diferente a los anteriores para normalizar los niveles de proteínas. Las tres muestras teñidas se incorporaron a una tira de gradiente de pH inmovilizado *"IPG strips"* (24cm, non-lineal pH 3-10, Immobiline DryStrip, GE Healthcare, EE. UU.) y se separaron según su punto isoeléctrico. Posteriormente estas tiras se incorporaron a geles de poliacrilamida donde se realizó la segunda dimensión de la técnica y las proteínas que previamente se habían separado por punto isoeléctrico, se separaron además por tamaño molecular. Los geles fueron escaneados con *"Typhoon™ TRIO"* (GE Healthcare, EE. UU) y analizados con el software Decyder software (GE Healthcare, EE. UU.) que nos determinó los picos con expresión diferencial observados en cada uno de los contrastes realizados. Estos picos identificados en el gen posteriormente fueron extraídos utilizando un equipo *"Ettan spot picker"* (GE Healthcare, EE. UU). Cada una de las muestras obtenidas del análisis 2D-DIGE fueron analizadas por espectrometría de masas o por cromatografía liquida acoplada a espectrometría de masas, identificando así cada una de las muestras que se observaron con expresión diferencial. Para determinar la relevancia de estas proteínas en el contexto de la enfermedad de Charcot-Marie-Tooth, se realizó un estudio bioinformático con la herramienta web PhenUMA, en la que se realizó un primer análisis de similitudes fenotípicas que presenta el gen mutado en estos pacientes (PMP22) y posteriormente otro análisis de relaciones fenotípicas entre los

genes relacionados con PMP22 por presentar rasgos fenotípicos similares al ser alterados y los genes de las proteínas identificadas en el análisis 2D-DIGE. Por último, se realizó una validación de la proteína gelsolina mediante el uso de ensayos de inmunodetección ligados a enzimas (ELISA), en concreto el kit comercial *"Human plasma (soluble) gelsolin ELISA kit"* (Aviscera Biocience, EE. UU.).

En el caso de los análisis genómicos de miARN, a partir de las muestras de plasma de pacientes de FRDA y controles o precipitado de las diferentes líneas celulares presentes en los tres modelos de FRDA mencionados anteriormente se aisló la fracción pequeña de ARN. En el caso de las muestras de plasma se realizó mediante el uso del kit *"miRNeasy Serum/Plasma kit"* (Qiagen, Termofisher, EE. UU.), mientras que en el caso de los modelos celulares se utilizó el kit *"miRvana miRNA Isolation Kit"* (Applied Biosystems/Ambion, EE. UU.). Una vez aislados los miARN se procedió al análisis de secuenciación de la fracción pequeña de ARN (small-RNA sequencing). Los miARN procedentes de plasma fueron analizados mediante la plataforma Ilumina. Para ello, previamente a la secuenciación se generó una biblioteca de ADN complementario (cADN) utilizando para ello los kits *"RNA Library Prep Set for Illumina" (Set 1&2)* (New England Biolabs, EE. UU.). Estas bibliotecas fueron empleadas para la generación de los "clústers" y la secuenciación en la plataforma de *"Illumina HiScanSQ platform"* (50 bp single read; Illumina, EE. UU.). Los resultados obtenidos fueron analizados para determinar su calidad mediante el software FastQC y alineadas con el genoma humano de referencia Hg18 y la base de datos de miARN miRBase v21 utilizando para ellos los paquetes "Subread" y "Rsubread". Por otro lado, los miARN procedentes de los modelos celulares fueron secuenciados mediante la tecnología "Ion Torrent". La generación previa de la biblioteca de cADN por tanto se realizó mediante el kit, correspondiente para esta plataforma de secuenciación, *"Ion Total RNA-Seq Kit v2"* (Life Technologies/Thermo fisher, EE. UU.). Estas bibliotecas de cADN se utilizaron para generar las "beads" que se incorporaron al chip que posteriormente se introduciría en el secuenciador *"Ion Proton sequencer"* (Life Technologies/Thermo FIsher, EE. UU.). Las secuencias obtenidas fueron alineadas con el genoma de referencia Hg19 y la base de datos de miARN miRBase v21. La expresión de los miARN procedentes de plasma fueron normalizadas y se seleccionaron aquellos que tenían una expresión diferencial con una tasa de falso descubrimiento (FDR) de 1e-4. En el

caso de los miARN de modelos celulares la expresión diferencial de estos fue calculada utilizando los paquetes del software R denominados "EdgeR" y "DESeq" 2. Por último, se determinaron las proteínas diana de regulación de los miARN detectados con expresión diferencial mediante el uso de la sección *DIANA-microT-CDS* del servidor web *DIANA v5.0* y *"DIANA-miRPath" v3.0* para determinar las rutas moleculares en las cuales están las dianas de los miARN. Estos miARN fueron validados mediante técnicas de cuantificación basadas en la reacción en cadena de la polimerasa (RT-qPCR), así como la evaluación de los niveles de ARN mensajero de las dianas del miR-330-3p. Por último, se realizaron análisis estadísticos Chi-cuadrado para determinar si los miARN encontrados con expresión diferencial en plasmas de pacientes de ataxia de Friedreich respecto a sus controles permitían estratificar a los pacientes según su enfermedad concomitante (diabetes o cardiomiopatía). Además, se realizaron análisis de curvas de Característica Operativa del Receptor (ROC) para determinar la especificidad y la sensibilidad de los miARN. Todos estos análisis se realizaron mediante el uso del software *SPSS* versión 20 (IBM Corporation, EE. UU.). El resto de análisis estadísticos no especificados se realizaron mediante el uso del software *"Graphpad Prism"* versión 6 (GraphPad Software, EE. UU.).

0.4. Resultados y discusión

Las enfermedades neurodegenerativas presentan una alta variabilidad fenotípica y genotípica, por ello es de especial relevancia la obtención de nuevos biomarcadores que permitan mejorar el conocimiento sobre la estratificación de pacientes, la progresión de la enfermedad y la monitorización de tratamientos analizados en ensayos clínicos. En esta tesis se ha pretendido obtener biomarcadores de estrés oxidativo y proteómicos en plasmas pacientes de la enfermedad de Charcot-Marie-Tooth con duplicación en gen de la proteína PMP22 y biomarcadores genómicos, en concreto miARN, en plasmas de pacientes de ataxia de Friedreich y modelos celulares de esta enfermedad.

En la búsqueda de biomarcadores de estrés oxidativo en los plasmas de CMT, se analizaron los niveles de daño proteico por estrés oxidativo mediante los niveles de proteínas carboniladas y nitrosiladas. También se determinaron los niveles de daño oxidativo en lípidos mediante los niveles de malondialdehido (MDA). Sin embargo, no se entraron diferencias en ninguno de ellos. Tampoco se observaron diferencias en los niveles de capacidad antioxidante total, ni en los niveles de glutatión total y cociente GSSG/GSH, por lo que parece que no hay marcadores de estrés oxidativo en plasmas de pacientes de la enfermedad de Charcot-Marie-Tooth con duplicación en el gen PMP22 (CMT1A).

Por otra parte, en el análisis proteómico mediante la técnica 2D-DIGE, se identificaron veinte proteínas con expresión diferencial entre pacientes de CMT (pacientes leves y pacientes severos) comparados con los sujetos sanos. Estas proteínas fueron: Afamina, Región C de la cadena kappa de las inmunoglobulinas, Plasminógeno, Factor B del complemento, gelsolina, Antitrombina-III, Apolipoproteína A-IV, Haptoglobina, Clusterina, Componente C6 del complemento, Cadena del fibrinógeno, Vitronectina, Serotransferrina, Kininogeno-1, Alfa-1-antitrypsina, Alfa-2-HS-glicoproteina, Alfa-1B-glicoproteina, Proteína de unión a vitamina D, Apolipoproteína E y Apolipoproteína A-I. De estas proteínas solo diecisiete mostraron tener relación con PMP22 a través de otras proteínas que al ser mutadas tenía un fenotipo similar al observado en la duplicación de PMP22 al analizarlas con el software PhenUMA. Gelsolina es una de las proteínas identificadas con expresión diferencial

Resumen

entre pacientes leves de CMT y pacientes severos al compararlos con los sujetos sanos. Esta proteína está relacionada con PMP22 a través de otras proteínas relacionadas fenotípicamente con esta última y además ha sido descrita con niveles alterados en otra neuropatía, la amiloidosis familiar tipo finlandesa. Por ello se validaron los niveles de esta proteína en los tres grupos estudiados (pacientes leves, pacientes severos y controles). Sin embargo, no se observaron diferencias en los niveles de gelsolina entre estos grupos. Además, también se analizó la correlación entre la edad de los pacientes de CMT o controles y los niveles de esta proteína, ya que en el caso de la amiloidosis familiar si se observó una relación entre los niveles de esta proteína y la edad. En el caso de los pacientes de CMT, una ligera correlación se observó entre la edad y los niveles de gelsolina, pero no suficiente para que las diferencias en los niveles de gelsolina puedan ser explicados por las diferencias de edad. En el caso de los pacientes no se observó correlación. Todos estos resultados muestran que gelsolina no es un buen biomarcador para la enfermedad de Charcot-Marie-Tooth. Del resto de proteínas identificadas, la proteína de unión a vitamina D ha sido descrita como biomarcador en otras enfermedades neurodegenerativas. Otras proteínas implicadas en la coagulación como son plasminógeno y la antitrombina III se han descrito como alteradas en diferentes enfermedades del sistema nervioso. Otras proteínas como son la cadena gamma del fibrinógeno y la vitronectina también se encuentran alteradas en otras neuropatías. Por su parte los factores B y componente C6 del complemento están relacionados con enfermedades neurodegenerativas y distrofias neuroaxonales respectivamente. Las lipoproteínas clusterina (también conocida como Apolipoproteína J), Apolipoproteína A-IV, Apolipoproteína E y Apolipoproteína A-I han sido encontradas con niveles alterados en diferentes neuropatías además de en nuestro estudio. Esto indicaría una alteración del metabolismo de las lipoproteínas en la enfermedad de Charcot-Marie-Tooth y se explicaría por su papel en la organización de las zonas ricas en lípidos derivados de colesterol, por ello este estudio muestra diferentes proteínas con expresión diferencial, y con asociación con otras enfermedades neurodegenerativas, que pueden ser posibles biomarcadores proteómicos para la enfermedad de Charcot-Marie-Tooth.

Resumen

El estudio de biomarcadores en la ataxia de Friedreich se realizó mediante el análisis del miRNoma en plasmas de pacientes y en tres modelos diferentes de esta enfermedad ya que estas moléculas puedes ser potenciales biomarcadores de diagnóstico, pronóstico y monitoreo de ensayos clínicos.

En el caso del miRNoma de las tres líneas celulares hemos detectado diferente perfil de expresión entre los casos y los controles de cada una de ellas (fibroblastos, células madre de la mucosa olfativa y líneas celulares de SH-SY5Y). Al comparar los diferentes perfiles de expresión de los 3 modelos no se encontraron miRNAs que aparecieran en todos ellos, pero si se detectaron al realizar comparaciones entre un grupo y otro de los dos grupos restantes. Así, hsa-miR-10b-5p se encuentra en los perfiles de expresión de fibroblastos y líneas celulares SH-SY5Y. hsa-miR-409-3p, hsa-miR-3117-3p, hsa-miR-106b-3p, hsa-let-7a-2-3p, hsa-miR-15a-3p, and hsa-miR-106b-5p están expresados diferencialmente en líneas celulares SH-SY5Y y células madre de mucosa olfativa. hsa-miR-10b-5p, hsa-miR-106b-3p, hsa-miR-15a-3p, and hsa-miR-106b-5p fueron validados en las tres líneas celulares. Además, también se analizaron las rutas en las que están implicadas las dianas de los miARN detectados con expresión diferencial. El metabolismo de lípidos es una ruta que tiene algunas dianas de los miARN detectados (la sintetasa de ácidos grasos y la acil-CoA ácido graso sintasa 4) y ha sido descrita como alterada en modelos de mosca de FRDA. Otra ruta destacada en el contexto de ataxia de Friedreich es la ruta de señalización de AMPK donde *FOXO3* es una de las dianas además de Akt, mTORC y la propia AMPK. FOXO3 es un factor de transcripción que fomenta la expresión del gen *FBXO32* gen cuya expresión puede potenciar la atrofia o hipertrofia muscular. La expresión de este gen fue analizada en las tres líneas celulares observando que su nivel estaba elevado en todas ellas.

En el análisis del miRNoma de las muestras de plasma, encontramos siete miARN circulantes que tienen expresión diferencial entre pacientes de ataxia de Friedreich y sujetos control (hsa-miR-128-3p, hsa-miR-625-3p, hsa-miR-130b-5p, hsa-miR-151a-5p, hsa-miR-330-3p, hsa-miR-323a-3p, hsa-miR-142-3p). Además, al realizar análisis para estratificar los pacientes encontramos que el mir-323a-3p presenta niveles más elevados en aquellos pacientes con cardiomiopatía hipertrófica con una alta sensibilidad (88.9%) y una aceptable especificidad (62.5%). Este miARN puede ayudar a los clínicos en la generación de algoritmos que predigan la cardiomiopatía en este

tipo de enfermos, contribuyendo a un diagnóstico y pronóstico temprano previo a la detección por procedimientos estándar. En el análisis de las rutas en las que participan las dianas de los siete miARN encontramos la oxidación de los ácidos grasos y el metabolismo central del carbono, ambas alteradas en FRDA y que pueden contribuir al daño cardiaco en los pacientes de ataxia de Friedreich. Otra ruta, también observada en el caso del estudio del miRNoma en las tres líneas celulares, fue la ruta de señalización AMPK. En este caso además de AMPK, AKT y mTORc, otras proteínas de la ruta como FOXO1, PTEN, ATM o PI3K están también reguladas por estos miARN. Para determinar la importancia de estos miARN en el contexto celular se validaron en los modelos celulares descritos anteriormente (fibroblastos, SH-SY5Y y células madre de la mucosa olfativa), observando que los niveles del miR-330-3p estaban alterados en todos ellos. Por ello se pretendió determinar los niveles de expresión génica de algunas de sus dianas (*FOXO1*, *LDHA*, *PDHA*, and *SOD2*), observando que la expresión de estas dianas no está regulada por el miR-330-3p en exclusividad, pero este puede estar ejerciendo un papel importante en la fisiopatología de la ataxia de Friedreich.

Otras rutas con dianas de los miRNA son la ruta de señalización por insulina cuya desregulación también ha sido descrita en modelos animales y celulares de ataxia de Friedreich y que tiene como consecuencia la aparición concomitante de diabetes tipo II en pacientes de esta enfermedad.

Por último, es destacable la ruta de señalización Wnt/β-catenin en la que algunos miRNA tienen como diana la catenina CTNNB1, mientras que otros entre ellos miR-323a-3p tienen como diana la ATPasa transportadora de calcio del retículo sarcoplásmico, ATP2A2. Nosotros proponemos que la disminución de estas proteínas por parte de estos miARN puede generar un aumento de Ca^{+2} que conduzca a la activación de genes de crecimiento y remodelación cardiaca favoreciendo la aparición de la hipertrofia cardíaca en pacientes de FRDA. Además, como se ha explicado anteriormente el miR-323-3p tiene unos niveles más elevados en pacientes con este tipo de patología y se encuentra sobreexpresado en los modelos celulares de células madre de mucosa olfativa y SH-SY5Y, lo que concuerda con nuestra hipótesis.

Todos estos hechos ponen de relevancia la importancia de los miARN en la fisiopatología de la ataxia de Friedreich proporcionando diversos candidatos para la

terapia personalizada de estos pacientes y generando nuevo conocimiento acerca de las bases moleculares y fisiológicas que subyacen a esta neuropatía.

0.5. <u>Conclusiones</u>

Este estudio mejora el conocimiento acerca de la fisiopatología de estas enfermedades neurodegenerativas raras. Se muestra una serie de posibles biomarcadores implicados en rutas fisiológicas y moleculares subyacentes a estas enfermedades, que están afectados también en otras enfermedades neurodegenerativas. Por último, proponemos el miR-323a-3p como biomarcador de cardiomiopatía hipertrófica en pacientes con ataxia de Friedreich así como un posible mecanismo por el cual una desregulación de éste generaría el defecto cardíaco.

Resumen

1. Introduction

1.1. Peripheral nervous system

The complex assemblage of nerves and specialized cells and structures that forms the nervous system have as function the coordination and signalling integration to and from different parts of body. This system could be separated in two main parts. Brain and spinal cord are two components of one of main part called central nervous system (CNS). The cranium and the vertebral canal of spine protect these components respectively. Second part, called peripheral nervous system (PNS), is formed by nerves (cranial and spinal nerves) and ganglia outside of brain and spinal cord (peripheral ganglia, such as Dorsal Root Ganglia) that connects CNS with the rest of the body (Figure 1).

PNS can be divided into somatic nervous system (transmits voluntary signals from CNS to rest of the body) and autonomic nervous system (controls involuntary responses to adjust physiological functions). The last one is always working either in its parasympathetic or sympathetic state. In PNS those nerves that transmit information from the body to CNS are called afferent or sensory, meanwhile the nerves that transmit signals from CNS to the rest of the body are called efferent or motor.

The fast and correct conduction of information is achieved thanks to myelin sheath. Myelin is formed by the wrapping of the plasma membrane of myelinating glial cells (called Schwann cells in PNS)[1] along the axons, with exceptions in some regions with high concentration of sodium and potassium channels, known as Nodes of Ranvier, that facilitate the saltatory conductions of impulses[2]. Also, unmyelinated axons are present in the CNS in closely packed bundles without any glial cells separating them. Whereas in the PNS are always ensheathed in Schwann cells. Unmyelinated axons show reduced conductivity of impulses compared with myelinated ones, due to absence of myelin sheath and the small diameter[3].
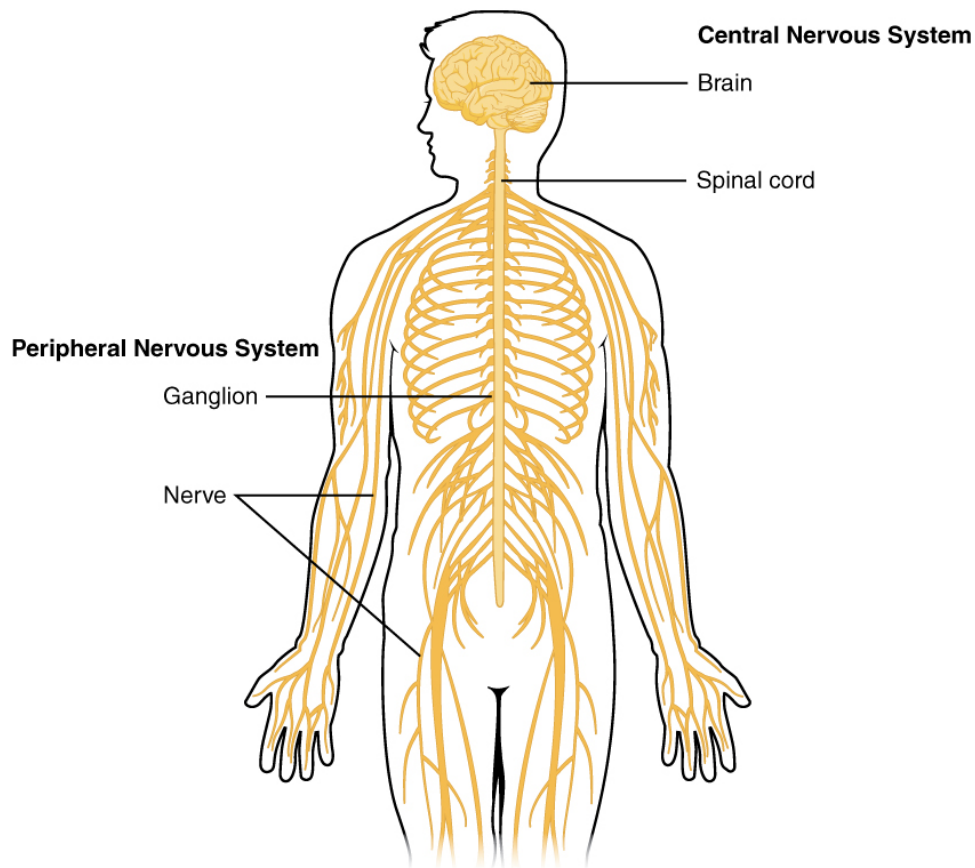
Figure 1. Schematic representation of central nervous system and peripheral nervous system. (Image obtained from 8.81 version of Textbook OpenStax [4])

1.1.1. Afferent or sensitive nerves

Primary afferent nerves transmit impulses from sensory receptors in the skin or viscera to the secondary sensory neurons of the spinal cord dorsal horns for central processing. The somas of the primary afferent neurons are contained in dorsal root ganglia (DRG) with a pseudo-unipolar structure. This pseudounipolarity is denominated when the cell body of the neuron is situated in DRG and the axon has two branches, bifurcating one to a peripheral and the other one to spinal cord. Each DRG is identified with C, T, L or S letter according to section of spinal cord (cervical, thoracic, lumbar or sacral, respectively) and, in a rostro-caudal order, the number of corresponding vertebra.

Primary afferent neurons are characterized according to degree of myelination and axon size of. Aα- and Aβ-fibers are the largest and heavily myelinated neurons that transfer information of proprioception and innocuous mechanoreception, respectively. Aδ-fibers are small and myelinated neurons that

mainly convey fast sharp pain and temperature sensation, but a few of them are responsible of low threshold mechanosensation information transport. Small unmyelinated fibers, called C-fibers, transmit sensation of temperature, slow dull pain and itch[5]. Diverse modality of neurons project axons specifically to some laminae of the spinal cord; in dorsal horn laminae I and II is where terminate nociceptive afferents neurons, whereas mechanosensitive neurons mainly end in laminae III and IV. Proprioceptive neurons terminate in the ventral spinal cord where they synapse with motor neurons [6] (Figure 2).
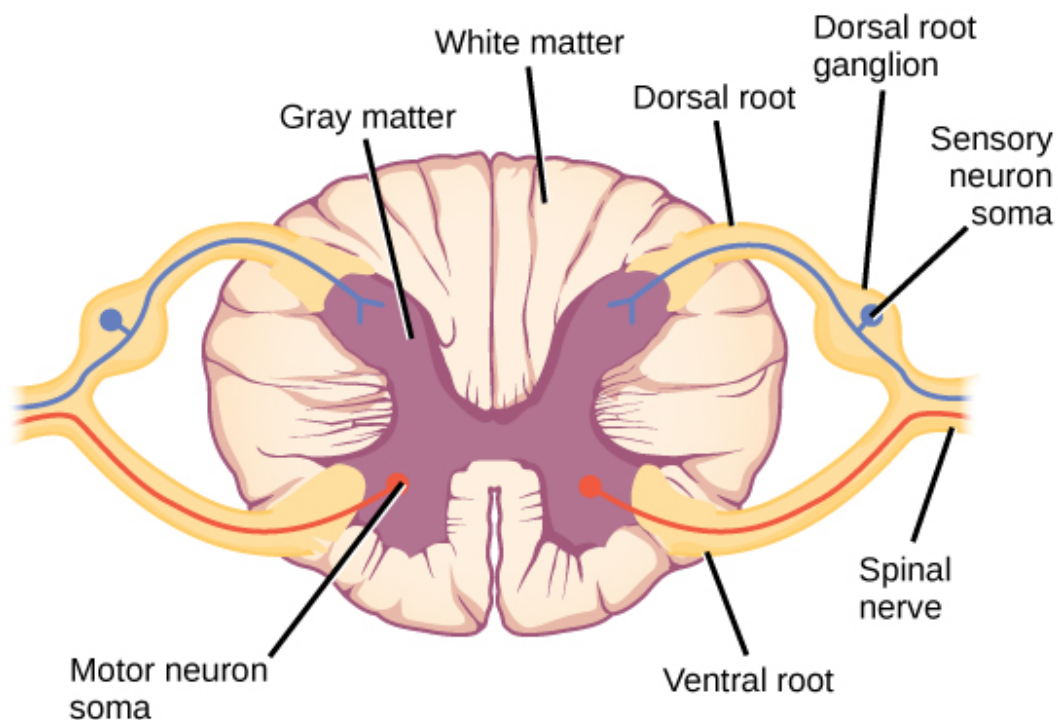
Figure 2. Schematic representation of cross section of spinal cord. (Figure obtained from http://www.newhealthadvisor.com/Spinal-Cord-Cross-Section.html)

1.1.2. Efferent or motor neurons

Efferent nerves, also called motoneurons, transfer information from central nervous system to effector organs (muscles or glands). Upper motoneurons are one main type of efferent nerves that originates from cerebral cortex, whereas lower motoneurons, second main type, are situated in the brainstem and spinal cord. The body cell of those from spinal cord, is localized in the ventral horn of the grey matter and the axon projects to peripheral effectors

through the ventral root. Lower motoneurons receive information from upper efferent neurons, sensory neurons and interneurons.

1.1.3. Neurological disorders

Neurological disorders are electrical, biochemical or structural anomalies that can affect the nervous system (central and peripheral). The protection of CNS prevents most types of injuries, however when some of the anomalies appear then they produce more important consequences than injuries in PNS. PNS diseases, also called peripheral neuropathies, are part of common and many rare diseases with a heterogeneous aetiology, pathology and severity that could affect one peripheral nerve (mononeurpathy) or multiple nerves (polyneuropathy). Among the possible aetiology of peripheral neuropathies those with a genetic hereditary origin are called peripheral hereditary neuropathies.

Peripheral hereditary neuropathies can be categorized into 1) h*ereditary motor-sensory neuropathies* when primary sensitive and motoneurons are affected; 2) *hereditary sensory neuropathies* or 3) distal *hereditary motor neuropathy*, when exclusively sensory neurons or distal lower motoneurons are affected, respectively; 4) *hereditary brachial plexus neuropathy* when brachial plexus and upper motoneurons are affected; 5) *hereditary sensitive autonomic neuropathies* when primary sensory and autonomic neurons are affected; and hereditary neuropathy with liability to pressure palsies when an individual nerve suffer a pressure[7].

Neurodegeneration is characterized by progressive loss of function, structure or both, in neurons. This process often begins at distal ends of long axons, followed by distal-to-proximal progression in a phenomenon called "dying-back neuropathy", typical of neuropathies denominated axonopathies, such as amyotrophic lateral sclerosis, spinal muscular atrophy or spinocerebellar disorders[8]. Neurodegeneration can also occur when Schwann cells are affected, since the myelin sheath is crucial for function and maintenance of peripheral nerves. Loss of myelin, demyelination, in one or several internodes is often followed by remyelination generating concentric proliferation of Schwann cells that generates a structure called "onion-bulb". This structure is observed in some types of Charcot-Marie-Tooth (CMT) disease[9].

Peripheral neuropathies have some difficulties in clinical diagnosis, since high variability of clinical symptoms and frequently different forms of the disease are associated with peripheral neuropathies[10-12].

1.2. Oxidative stress

An important element of cellular physiology is to maintain redox homeostasis, meaning to keep balanced antioxidant and pro-oxidant levels. Oxidative stress is generated by an imbalance between antioxidant and pro-oxidant species levels, which results in an oxidative damage. Reactive oxygen species (ROS) and reactive nitrogen species (RNS) are a wide spectrum of molecules (Table 1) that are generated as a consequence of enzymatic and non-enzymatic mechanisms. Vital roles in different biological processes (such as biological molecules synthesis, cell growth, blood pressure modulation, cell signalling, immune response, and smooth muscle relaxation) are played by ROS and RNS [13-15].

Table 1. Main Reactive oxygen species (ROS) and reactive nitrogen species (RNS) [16].

Name	Symbol
Superoxide ion	$O_2^{\bullet-}$
Hydrogen peroxide	H_2O_2
Hydroxyl	$HO^\bullet$
Peroxyl radical	$ROO^\bullet$
Singlet oxygen	$O_2^{\frac{1}{2}}\Delta g$
Nitric oxide	$NO^\bullet$
Peroxynitrite	$ONOO^-$
Nitrosyl	HNO
Nitrite	NO_2^-
Nitrate	NO_3^-
S-nitrosothiol	$RSNO$
Carbon monoxide	CO

The Electron transport chain in mitochondria is the major source of ROS into the cell, produced mainly as a result of partial reduction of molecular oxygen during the process of oxidative phosphorylation, and generating superoxide anion ($O_2^{\bullet-}$). In addition to this major source of ROS there exist other systems that can produce ROS

such as peroxisomes, NADPH, xanthine oxidase, RNS and plasma membrane redox system, lysosomes, and protein folding processes [17]. The principal source of RNS is NO$^\bullet$ generated by amino acid metabolism of L-arginine which is converted to L-citrulline by nitric oxide synthases (NOS)[18]. When NO reacts with O_2^- oxidant peroxynitrite (ONOO$^-$) is generated, which reacts relatively slowly with most biological molecules such as nitrotyrosine, nitrotryptophan and nitrated lipids. These subproducts are used as relevant biological markers of persistent oxidative stress[19].

Increased levels of free radicals induce damage in lipids, proteins, and DNA. The end products of this damage are trustworthy and relatively direct makers of oxidative stress. Different products of DNA damage, including 8-hydorxydeoxyguanosine (8-OH-dG), 8-hydroxyadenide, and 7-methyl-8-hydroxyguanine, have been detected in humans[20,21]. Protein carbonyls and protein nitrosylation are used mainly as protein oxidation markers[22]. Damage in polyunsaturated fatty acids leads to the formation of highly reactive electrophilic aldehydes such as malondialdehyde (MDA), 4-hydroxy-2-nonenal (HNE) or acroleine[23].

1.2.1. Antioxidant systems

Mechanisms of defence against exposure to different free radicals, such as physical barriers, preventive, and repair processes have been developed. Antioxidants systems can be classified in two categories: enzymatic antioxidants and non-enzymatic antioxidants and some of them are discussed below.

1.2.1.1. *Enzymatic antioxidants*
1.2.1.1.1. *Superoxide dismutase (SOD)*

Superoxide dismutase catalyses, in the first line of defence against free radicals, the reduction of highly reactive radical anion $O_2^{\bullet-}$ into oxygen and the less reactive H_2O_2 molecule, with the coordinated action of catalase or peroxidase enzymes that remove generated H_2O_2. Three different forms of SOD are found in different cellular localizations: cytosolic copper/zinc-SOD (CuZnSOD, SOD1), mitochondrial manganese-SOD (MnSOD, SOD2), and extracellular superoxide dismutase (SOD3).

Catalase (CAT)

As described above, catalase remove hydrogen peroxide generating molecular oxygen and water using either iron or manganese as a cofactor. Catalase localization is mainly in peroxisomes.

1.2.1.1.3. *Glutathione peroxidase (GPx)*

Other enzyme, as it is mentioned before, that catalyses the reduction of H_2O_2 generated by SOD is glutathione peroxidase. In addition, Gpx is able to catalyse the reduction of lipid peroxides using, as in the case of hydrogen peroxide, reduced glutathione (GSH) and generating also oxidized glutathione (GSSG). GPx is a selenium-peroxidase with six different isoforms that are present in both cytosol and mitochondria. To reconvert the GSSG into GSH a flavoprotein enzyme called glutathione reductase (GRx) is needed, using NADPH as reducing power source[24].

1.2.1.1.4. *Thioredoxin (TRX)*

TRX system is the most important disulphide reductase system, which can donate electrons (using NADPH as source of reduction power) to a big amount of proteins and seems to be essential for DNA synthesis and oxidative stress defence. Thioredoxin system is formed by thioredoxin (Trx) isoforms (mitochondrial isoform TRX2, cytosolic isoform TRX1, and testis isoform TGR) and thioredoxin reductase (TrxR), that regenerates oxidized thioredoxin[25].

1.2.1.1.5. *Peroxiredoxins (Prdx)*

These enzymes are peroxidases that reduce also hydrogen peroxide, and other compounds as organic hydroperoxides and peroxynitrite [26].

1.2.1.2. *Non-enzymatic antioxidants*

Non-enzymatic antioxidants act as scavengers or chelating agents without enzymatic reactions. These molecules are categorized as metabolic antioxidants (such as lipoid acid, glutathione, L-arginine, coenzyme Q10, melatonin, uric acid, bilirubin, transferrin, etc.) or nutrient (dietary sources)-based (such as vitamin E, vitamin C, carotenoids, flavonoids, omega-3 and omega-6 fatty

acids, etc.) antioxidants[27]. Some of these non-enzymatic antioxidants are described below:

1.2.1.2.1. *Glutathione (GSH)*

Glutathione is a tripeptide (gamma-glutamylcysteinyl glycine) that can react with both oxidizing and electrophilic species (such as ROS). In addition, GSH can detoxify many drugs and xenobiotics and, as described above, is a cofactor for a GSH peroxidase family of enzymes. Reduced/oxidized glutathione (GSH/GSSG) ratio is used as a marker of cellular redox state level[24].

1.2.1.2.2. *Vitamin E*

Vitamin E is an antioxidant soluble in fats that prevents cell membranes from ROS damage such as peroxyradicals in fatty acids oxidation [28].

1.2.1.2.3. *Vitamin C*

Ascorbic acid or vitamin C is a water-soluble antioxidant that plays a role in free radical scavenging by electron transfer. Moreover, it is a cofactor for some enzymes that have a role in the antioxidant defence [29].

1.2.1.2.4. *Ubiquinone*

Coenzyme Q10 or ubiquinone acts as an electron carrier in its central function in the electron transport chain. Furthermore, coenzyme Q10 act as a free radical-scavenging antioxidant.

1.2.2. Oxidative stress and neuropathy

Reactive species of oxygen and nitrogen are also implicated in many pathophysiological disorders and diseases as diabetes[30], obesity, cancer, cardiovascular diseases and neurodegenerative diseases [31-33]. Oxidative damage can result as a consequence of increased ROS and RNS production or decreased protection systems[34]. Contribution of oxidative stress in neurodegenerative initiation and progression is under discussion, due to vulnerability of nervous system to ROS and RNS because of the elevated metabolic rate, its low efficient mechanisms of oxidative defence, and its decreased levels of cellular turnover. As main source of ROS, mitochondria defects or alterations in the correct function of electron transport chain

cause increased ROS. Mitochondrial DNA (mtDNA) is an easy target for ROS due to the lack of protective histones in mtDNA together with reduced repair capacity. Moreover, to maintain polarity of highly polarized neurons normal mitochondrial dynamics are required[35] , and disturbances on this pathway seems generate oxidative stress, aging and neurodegeneration[36]. Mitochondrial disorders with neurological deficits or degeneration (such as Friedreich's ataxia, and Leigh Syndrome [37]) and most common neurodegenerative diseases as Alzheimer disease and Parkinson disease [34] show mitochondrial dysfunction and oxidative stress, representing one of the most common features in neurodegenerative diseases.

On the other hand, antioxidant defence systems are altered in neurodegenerative diseases. Overexpression of CuZnSOD in neuroblastoma cells has shown less susceptibility to beta-amiloid neurotoxicity [38], and also mutations in this protein are involved in amyotrophic lateral sclerosis (ALS) and Friedreich's ataxia [39,40]. Alzheimer models of neurodegeneration have demonstrated a neuroprotective role of catalase [41]. Thioredoxin overexpression has showed a neurotoxicity protection in *Drosophila* model of Machado–Joseph disease and a suppressor activity of a substrate of the E3 ubiquitin ligase implicated in Parkinson disease [42]. Moreover, thioredoxin has decreased levels in fibroblasts from patients of Lafora disease [43] and has a close relationship with the proteasome that has decreased levels of activity in this neurodegenerative disease[44], in Alzheimer's disease [45], and in Parkinson's disease [46]. In addition, glutathione levels are important to avoid oxidative stress and neurodegeneration in brain[47] . In Friedreich's ataxia fibroblasts, it has been found decreased levels of GSH[48]. Furthermore, in another neurodegenerative disorder such as ataxia with vitamin E deficiency decreased levels of GSH were also found. Reinforcing this idea of oxidative stress in neurodegenerative disorders, studies performed in animal models of neurodegenerative diseases have demonstrated that supplementation with vitamin E delays neurodegeneration, although it was not demonstrated in human studies[49,50]. As occurs for vitamin E, the neuroprotective antioxidant role of vitamin C is described in neurodegenerative animal models but not in human studies [51]. Finally, coenzyme Q10 is demonstrated to be neuroprotective in several studies including clinical studies of a diverse neurodegenerative disorders, such as Huntington disease [52] and Parkinson disease[53].

1.3. <u>Charcot-Marie-Tooth disease</u>

In 1886, the same neurological syndrome was described for the first time by Charcot and Marie in Paris, and Tooth in England. They described this disorder as a hereditary syndrome which most common features include: skeletal deformities, progressive distal muscle wasting and weakness, and attribution to a peripheral nerve disorder. Nowadays, this neurological syndrome is known as Charcot-Marie-Tooth (CMT; ORPHA166) the most common hereditary neuropathy and with diverse prevalence in different populations and regions: 82.3 cases per 100,000 population in Norway[54], 10.8 per 100,000 in Japan[55] or 18.1 per 100,000 in UK[56].

CMT disease contains a heterogeneous group of disorders with similar clinical, neurophysiological, genetic and pathological features. More than 75 genes have been described to be associated with CMT and other related neuropathies [57]. Classically CMT has been categorized by motor nerve conduction velocities (NCVs) in CMT1, a demyelinating form with symmetrically more decreased NCV (<38m/sec) than normal (>45m/sec); CMT2 an axonal form with normal, or slight decreased, NCV that shows loss of myelinated axons [58]. A third (Intermediate CMT) form that shows axonal and demyelinating features and intermediate NCVs is currently recognized [59]. Based on the inheritance pattern and molecular genetic defects, additional subdivisions of CMT disease could be done. CMT can present autosomal dominant (AD) inheritance, autosomal recessive (AR) inheritance or X-linked inheritance. AR forms of CMT1 are sometimes called CMT4 and those forms of CMT2 are frequently referred to as AR-CMT2. AD and AR of intermediate CMT have been respectively named CMTDI and CMTRI. Finally, those CMT forms with X-linked inheritance are known as CMTX. Mathis *et. al*. have recently proposed a modification of nomenclature of CMT and related disorders. This new version takes into account inheritance patterns, primary pathological phenotype (axonal, demyelinating, or intermediate) and causative gene defects [60] (Table 2).

Table 2. New classification of Charcot-Marie-Tooth disease. (adapted from Mathis *et. al.* [60]; AD: autosomal dominant, AR: autosomal recessive, de: desmyelinating, ax: axonal, in: Intermediate, XL: x-linked inheritance).

	Proposed denomination	Gene	Chromosome	MIM	Denomination
CMTde					
AD-CMTde	AD-CMTde-*PMP22dup*	*PMP22 (duplication)*	17p12	118220	CMT1A
	AD-CMTde-*PMP22*	*PMP22*	17p12	118300	CMT1E
	AD-CMTde-*MPZ*	*MPZ*	1q23.3	118200	CMT1B
	AD-CMTde-*LITAF*	*LITAF*	16p13.3	601098	CMT1C
	AD-CMTde-*EGR2*	*EGR2*	10q21.3	607678	CMT1D
	AD-CMTde-*NEFL*	*NEFL*	8p21.2	607734	CMT1F
	AD-CMTde-*FBLNS*	*FBLNS*	14q32.12	-	-
	AD-CMTde-*GJB3*	*GJB3/Connexin 31*	1p34.3	-	-
	AD-CMTde-*ARHGEF10*	*ARHGEF10*	8p23.3	608236	SNCV/CMT1
AR-CMTde	AR-CMTde-*GDAP1*	*GDAP1*	8p21.11	214400	CMT4A
	AR-CMTde-*MTMR2*	*MTMR2*	11q21	601382	CMT4B1
	AR-CMTde-*SBF1*	*SBF1/MTMR5*	22q13.33	615284	CMT4B3
	AR-CMTde-*SBF2*	*SBF2/MTMR13*	11p15.4	604563	CMT4B2
	AR-CMTde-*SH3TC2*	*SHTC2/KIAA1895*	5q32	601591	CMT4C
	AR-CMTde-*NDRG1*	*NDRG1*	8q24.22	601455	CMT4D
	AR-CMTde-*EGR2*	*EGR2*	10q21.3	605253	CMT4E
	AR-CMTde-*PRX*	*PRX*	19q13.2	614895	CMT4F
	AR-CMTde-*HK1*	*HK1*	10q22,1	605285	CMT4G
	AR-CMTde-*FGD4*	*FGD4*	12p11.21	609311	CMT4H
	AR-CMTde-*FIG4*	*FIG4/KIAA0274/SAC3*	6q21	609390	CMT4J
	AR-CMTde-*CTDP1*	*CTDP1*	18q23	604168	CCFDN
	AR-CMTde-*SURF1*	*SURF1*	9q34.2	-	-
CMTax					
AD-CMTax	AD-CMTax-*MFN2*	*MFN2*	1p36.22	609260	CMT2A2
	AD-CMTax-*RAB7*	*RAB7*	3q21.3	605588	CMT2B
	AD-CMTax-*TRPV4*	*TRPV4*	12q24.11	606071	CMT2C
	AD-CMTax-*GARS*	*GARS*	7p14.3	601472	CMT2D
	AD-CMTax-*AARS*	*AARS*	16q22.1	613287	CMT2N
	AD-CMTax-*MARS*	*MARS*	12q13.3	616280	CMT2U
	AD-CMTax-*HARS*	*HARS*	5q31.3	-	-
	AD-CMTax-*NEFL*	*NEFL*	8p21.2	607684	CMT2E
	AD-CMTax-*HSPB1*	*HSPB1/HSP27*	7q11.23	606595	CMT2F
	AD-CMTax-*HSPB8*	*HSPB8/HSP22*	12q13.3	608673	CMT2L
	AD-CMTax-*GDAP1*	*GDAP1*	8q21.11	607831	CMT2K
	AD-CMTax-*MPZ*	*MPZ/P0*	1q23.3	607677/ 607736	CMT2I/CMT2J

	AD-CMTax-*DNM2*	*DNM2*	19p13.2	606482	CMT2M
	AD-CMTax-*DYNC1H1*	*DYNC1H1*	14q32.31	60012	CMT2O
	AD-CMTax-*LRSAM1*	*LRSAM1*	9q33.3	614436	CMT2P
	AD-CMTax-*DHTKD1*	*DHTKD1*	10p14	615025	CMT2Q
	AD-CMTax-*TRIM2*	*TRIM2*	4q31.3	615490	CMT2R
	AD-CMTax-*VCP*	*VCP*	9p13.3	-	-
	AD-CMTax-*TFG*	*TFG*	3q12.2	604436	HMSNP
	AD-CMTax-*KIFSA*	*KIFSA*	12q13.3	604187	SPG10
	AD-CMTax-*mtATP6*	*mtATP6*	-	-	-
	AD-CMTax-Unknown	*Unknown*	12q12q13.2	608591	CMT2G
AR-CMTax	AR-CMTax-*LMNA*	*LMNA*	1q22	605588	CMT2B1
	AR-CMTax-*MED25*	*MED25*	19q13.33	605589	CMT2B2
	AR-CMTax-*GDAP1*	*GDAP1*	8q21.11	607731	CMT2H
	AR-CMTax- *IGHMBP2*	*IGHMBP2*	11q13.3	616131	CMT2S
	AR-CMTax- *C12ORF65*	*C12ORF65*	12q24.31	616155	SPG55
	AR-CMTax- *HSJ1*	*HSJ1*	2q35	604139	CMT2T
CMTin					
AD-CMTin	AD-CMTin-*DNM2*	*DNM2*	19p13.2	606482	CMTDIB
	AD-CMTin-*YARS*	*YARS*	1p35.1	698323	CMTDIC
	AD-CMTin-*MPZ*	*MPZ/P0*	1q23.3	607791	CMTDID
	AD-CMTin-*INF2*	*INF2*	14q32.33	614455	CMTDIE
	AD-CMTin-*GNB4*	*GNB4*	3q26.33	615195	CMTDIF
	AD-CMTin-*NEFL*	*NEFL*	8p21.2	-	-
	AD-CMTin-Unknown	*Unknown*	10q24.1-q25.1	606483	CMTDIA
AR-CMTin	AR-CMTin-*GDAP1*	*GDAP1*	8p21.2	608340	CMTRIA
	AR-CMTin-*KARS*	*KARS*	16q23.2	613641	CMTRIB
	AR-CMTin-*PLEKHG5*	*PLEKHG5*	16q23.1	615376	CMTRIC
	AR-CMTin-*COX6A1*	*COX6A1*	1p36.31	616039	CMTRID
XL-CMT	XL-CMTin-*GJB1*	*GJB1/Connexin 32*	Xq13.1	302800	CMTX1
	XL-CMTde-*GJB1*	*GJB1/Connexin 32*	Xq13.1	302800	CMTX1
	XL-CMTax-*GJB1*	*GJB1/Connexin 32*	Xq13.1	302800	CMTX1
	XL-CMT-*AIFM1*	AIFM1	Xq26.1	310490	CMTX4
	XL-CMT-*PRPS1*	PRPS1	Xq22.3	311070	CMTX5
	XL-CMT-*PDK3*	PDK3	Xq22.1	300905	CMTX6
	XL-CMT-Unknown	*Unknown*	Xq22.2	302801	CMTX2

1.3.1. Clinical features of Charcot-Marie-Tooth disease

The clinical phenotype of Charcot-Marie-Tooth disease is quite homogenous, despite of mutations in many different genes involved in several functions: axonal transport, cytoskeleton elements, gap-junctions forming proteins, transcription factors, heat shock proteins, mitochondrial dynamics, energy production, proteins of myelin, nuclear envelope, amino acid processing, etc. (Summarized in Figure 3). An incorrect function of these proteins generates an axonal degeneration that is dependent of the axon length [61].
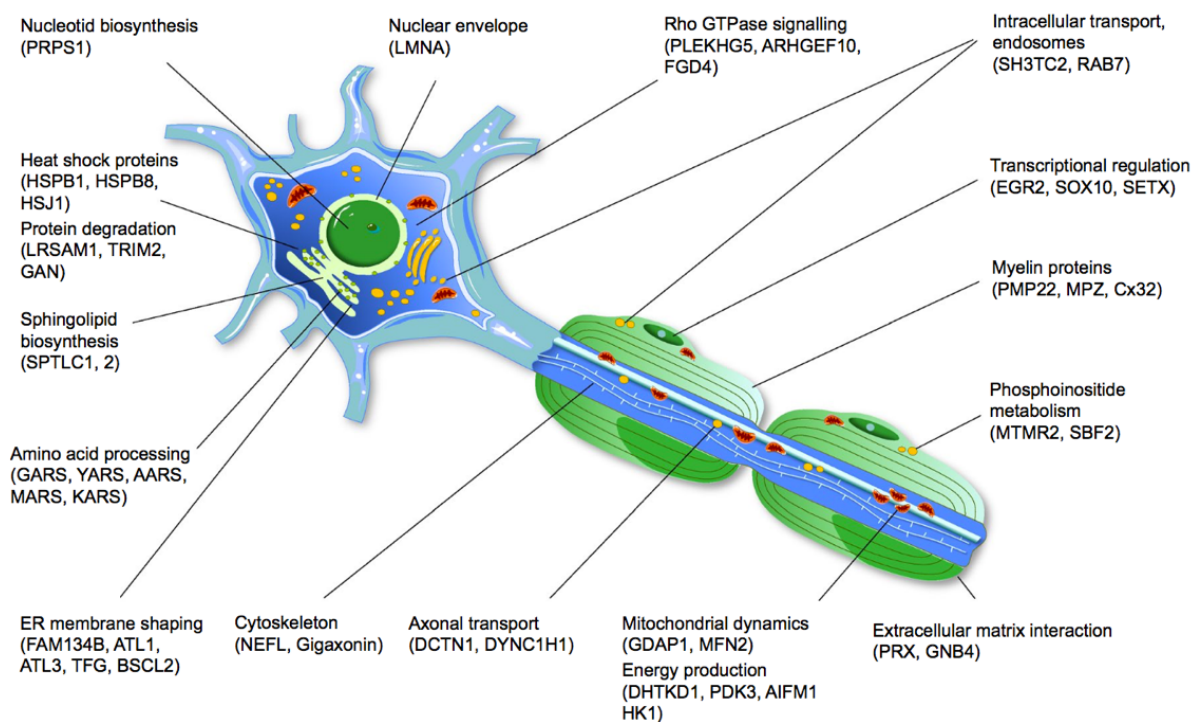
Figure 3. Phatomechanisms proposed of genes involved in Charcot-Marie-Tooth disease. Figure shows genes involved in physiopathology of CMT [9].

Patients affected with this disorder show wasting and weakness of distal limb muscles, produced by length-dependent degeneration of nerves. This motor impairment with atrophy and weakness starts in intrinsic foot muscles and progressively ascends to legs muscles. Legs show the typical inverted champagne bottle appearance but foot drop and steppage gait (in which the patient must lift the leg in an exaggerated way to move the foot) are the first signs observed, followed by weakness of foot plantar flexors. Next step of impairment is lower third of the thigh and hand muscles, and later to the forearms. Claw hand, or as said in French "main en

griffe" is the most common deformity which appears in the progression of Charcot-Marie-Tooth phenotype. It is rare in CMT proximal muscle weakness, and only appears in the most severe patients [58,62].

Sensory loss, as in motor impairment, involves at the beginning feet and legs and later hand and deep tendon reflexes, also with a pattern of length-dependence. However, signs are less obvious than motor ones, and are often subtle. It is common to find loss of touch sensation, vibration and pain. Affection of upper limbs is less frequent and less severely affected[58,62,63]. Skeletal deformities are present in CMT in more than 66% of all patients, and are characterized by *"pes cavus"* with hammer toes, whereas scoliosis is less common. Finally, muscles clamps, cold feet, acro-cyanosis are also recurrent complains[64,65].

Severity of the disease is extremely variable, some patients may show significant disabilities, and meanwhile other may be minimal or even oblivious. Although the disease onset usually arises during the first decades of life, the course of the disease is very slow and extends over decades [61].

CMT1A is the most common hereditary neuropathy, thus it is the best characterized of all subtypes of CMT [62-64,66-68]. CMT1A patients show a relatively benign classical phenotype compared with other subtypes remaining ambulatory the rest of their life. Nevertheless, a broad diversity of severity is shown in this subtype of CMT. Some patients show delayed motor nerve conduction velocities and severe skeletal deformities (*pes cavus*, scoliosis, etc.), which progress to important proximal weakness, that need walking aids, or can become chairbound in rare cases [63,64,67]. On the other hand, normal or near to normal life with slightly or absent symptoms have been reported in other patients. In addition, Garcia *et. al*. reported that identical twins with CMT1A showed important differences in severity. It is unknown why this clinical variability for CMT with the same mutation occurs[69], probably genetic modifiers or epigenetic events could explain the differences between endophenotypes. In CMT1A disease onset appears during childhood or adolescence, showing *pes cavus* or planus, lower-limb areflexia, and wasting and weakness of intrinsic foot muscles followed by peroneal and anterior tibialis muscles. Slight impairment of hand is presented in the first phases of disease and progresses gradually. It is not clear if the progression is constant or associated with age, but it seems that might be slower in adolescence[67],

meanwhile in older patients the progression is faster[62]. Since infancy, abnormalities in electrophysiology can be detected, observing slower NCVs than normal at 2 years.

However, there is not subtle distinction in NCV's after childhood and these do not correlate with severity of disease[67,70]. Reduced motor amplitudes of compound muscle action potential occur in first stages. This fact and the loss of motor units are correlated with clinical impairment, indicating that axonal loss causes weakness, and not reduced conduction velocity (Figure 4)[66].
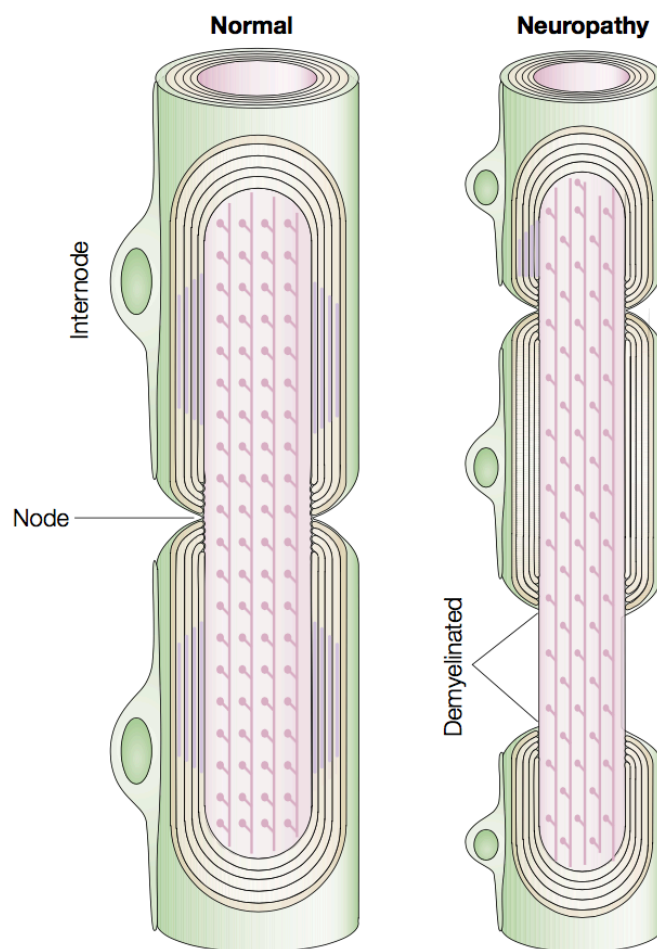
Figure 4. Changes in Charcot-Marie-Tooth disease 1 physiopathology in an overview schema. Internodes of myelin are disappeared and replaced by one or more new internodes with a decreased length, whereas some regions of the axon let demyelinated[71].

1.3.2. *PMP22* gene

The most common neuropathy, CMT1A, is usually caused by heterozygous inheritance of 1.4 mega base duplication on chromosome 17p11.2-p12 that includes *PMP22* gene. *PMP22* is located in chromosome 17q12 of human genome and consists in six conserved exons with an extension of 40-kb (Figure 5) that encode for peripheral myelin protein 22 Kda (PMP22). Exons 1a and 1b are alternatively transcribed to form the first exon of the gene and generates two different transcripts[72] that only differ in 5'untraslated regions and their distribution of tissues: exon 1a has been detected predominantly in the sciatic nerve, in contrast exon 1b has been found in brainstem, spinal cord, skeletal muscle, heart, and sciatic nerve in mouse [73,74]. Altogether exon 2 to 5, without considering the alternatively exon transcriptions mentioned above, comprise the coding region: transmembrane domain is encoded by exon 2, followed by the first extracellular loop encoded by exon 3, next exon 4 encodes the second and half of the third transmembrane domains, and finally exon 5 encodes the rest of third transmembrane domain, second extracellular domain, the fourth transmembrane domain, and the 3' untranslated region[72,75].
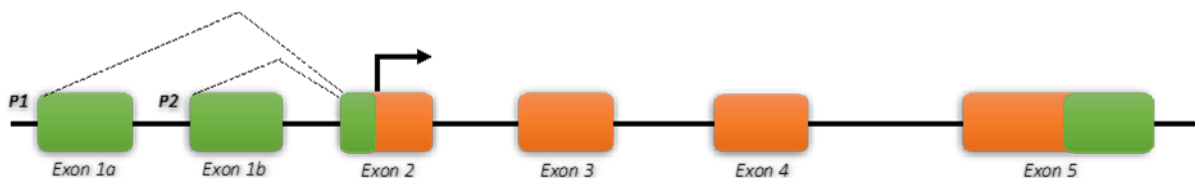
Figure 5. Schematic representation of *PMP22* gene structure. Representation of six exons that contains human PMP22 gene. Untranslated regions are showed in green and coding region are showed in orange. (based on an original figure provided by Li *et. al*[76]).

It has been found a TATA-box-like DNA element in the P1 and P2 promoters of *PMP22* with an island of high content of GCs. In addition, two sites between -1,600 and 2,100 bp of *PMP22* are found to interact with cAMP response element binding (CREB) protein, generating *PMP22* promoter silencing. Moreover, in this region there is a site for sterol regulatory element binding (SREB) protein, which enhances *PMP22* transcription with steroid hormones[77-79]. Flanking *PMP22* there are two homologous DNA sequences, that are the source of CMT1A mutation. Their elevated degree of homology encourages imbalanced crossing over during meiosis, consequently a

duplicated and a deleted allele is generated[80]. The inheritance of a deletion that includes *PMP22* is usually the cause of hereditary neuropathy with liability to pressure palsies (HNPP)[81]. In addition to gene duplications and deletions, more than 40 different *PMP22* mutations cause amino-acid substitutions (missense mutations), premature stops (non-sense mutations) or frameshifts (Figure 6). For example, a missense mutation generates another hereditary neuropathy similar to CMT1A, but more severe, denominated Dejerine-Sottas syndrome (DSS)[82].

1.3.3. PMP22 structure

First structure of PMP22 based in sequence of amino acid showed three putative transmembrane domains with one N-glycosylation site. In addition, N terminus is embedded in the membrane, and both C terminus and the N-glycosylation site are intracellular[83]. Latter, a novel structural prediction models includes a new transmembrane region at the end of protein structure[72]. One of them also suggests that first and fourth transmembrane domains of the previous model are inside of de membrane, but second and third domains are outside of the lipid bilayer[84]. There are many models for PMP22 structure, however N-glycosylation site at Asn 41 has been established in several studies[83,85-87]. D'Urso *et. al.* [88] confirmed intracellular localization of N and C termini and also, they discovered that PMP22 has two extracellular loops. Extracellular loop 1 may mediates a homophilic interaction of two PMP22 proteins, whereas extracellular loop 2 may mediate heterophilic interaction of PMP22 and MPZ[89]. Figure 6 shows a recent model of PMP22 structure, which shows four transmembrane domains with two extracellular domains and one intracellular domain[76]. In addition, extracellular loops in PMP22 protein have seven putative metal ion-coordinating sites that may explain the PMP22 ability to bind Zn(II)[90].
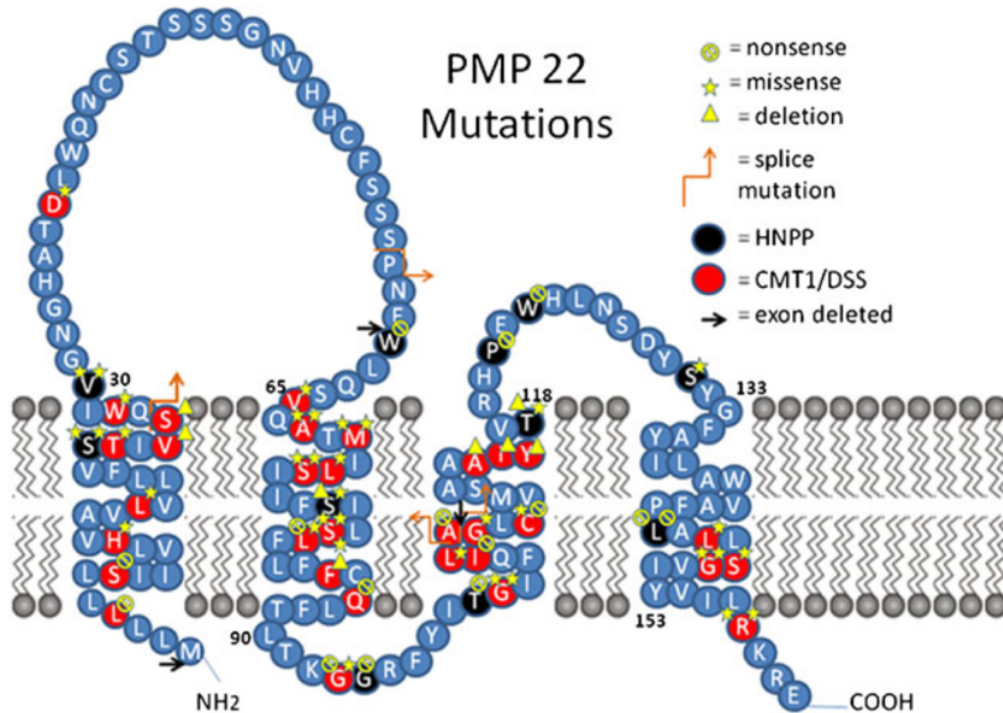
Figure 6. Predicted structure of human PMP22 protein. Schematic representation of PMP22 intracellular, extracellular, and transmembrane domains. Bubbles shows substituted amino acids in Charcot-Marie-Tooth disease 1 (CMT1) and Dejerine-Sottas syndrome (DSS) in red, and hereditary neuropathy with liability to pressure palsies (HNPP) in black [76].

Upregulated levels of PMP22 were observed during axonal contact in myelinating Schwann cells [85,91]. Nevertheless, as it is above-mentioned, PMP22 should have regulated levels in order to maintain them in a narrow range and avoid developing inherited neuropathies caused by reduced or increased PMP22 levels. New PMP22 proteins, as a membrane protein, are kept in endoplasmic reticulum (ER) and Golgi compartments in order to perform translational modifications. N-linked glycosylation in PMP22 precursor of 18kDa before getting the plasma membrane has been showed in Schwann cells[87,92]. This glycosylation of PMP22 protein may prevent the degradation of proteins and subsequent transport to the cell surface.

1.3.4. PMP22 function

Myelin is a specialized cell membrane, with multi-layer spiral structure, that ensheathes axons that are larger than 1 μm in diameter. Schwann cells create the myelin sheath in the PNS and oligodendrocytes in CNS. This structure reduces the electrical current conduction across the membrane in internodes, enhancing the

process of saltatory conduction in which nerve impulses jump between nodes of Ranvier. Myelin sheath has two areas, compact and non-compact, which contain unique proteins. The compact region contains myelin structural proteins PMP22, P0 (Encoded by *MPZ*), and myelin basic protein. Also, cholesterol, sphingolipids, some lipids more specialized like galactocerebroside and sulfatide (sulfated galactocerebroside) are found in this region. The non-compact region is subdivided in two regions: paranode region which contains loops of Schwann cells membrane and proteins such as Cx32, the major gap-junction protein in myelin, myelin associated glycoprotein (MAG), neurofascin 155, and axonal proteins Caspr and Conactin can be found; and in juxtaparanodal region two proteins expressed by axons, potassium channels and Caspr2 protein, can be located[71].

PMP22, as a part of compact region of myelin, has a structural role in the sheath of myelin and it is involved in early myelination steps. PMP22 is necessary for the correct development of peripheral nerves, axon maintenance and stability and width of myelin sheath[93]. Interaction of PMP22 with P0/MPZ protein and the gene-dosage sensitivity of both proteins agree with the hypothesis that precise stoichiometric amount of two proteins are required to correct myelination[94].

In addition to the structural role of PMP22, Schwann cell-extracellular matrix interactions are important to explain the proposed functions of PMP22 in the regulation of cell spreading, cell migration, and apoptosis[95-97]. PMP22 is expressed on the surface of Schwann cells in the first phases of myelination with b4 integrin, and can be co-immunoprecipitated with laminin and a6 integrin[98]. Furthermore, epithelial membrane protein-2, a close homologue of PMP22[99], interacts with ß1 integrins and regulates adhesion[100]. Elevated or inexistent PMP22 levels are observed in a wide number of Schwann cell-axon profiles showing loss of lamina[98]. Proteolipid protein 1 (PLP1) may regulate myelination by interaction with integrins, which form a complex[101] and integrin signalling seems to be crucial for the correct myelination of axons[102]. These facts indicate that PMP22 may be a partner in integrin/laminin complex and act as a mediator in Schwann cells and extracellular matrix interactions.

Other possible function for PMP22 may be as mediator of ubiquitin-proteasomal activity. When PMP22 are synthetized, almost all are poly-ubiquitinated and quickly degraded by the proteasome, whereas only a little portion are assembled in plasma

membrane of Schwann cells[103-105]. Overexpression of PMP22 leads to formation of aggregates or "aggresomes"[104] of dimers or multimers of ubiquitinated PMP22 proteins. Aggresomes are associated with autophagosomes and lysosomes, indicating an activation of autophagy as a compensatory response to decreased proteasomal activity[106]. In the same way, impaired proteasomal function can lead to the formation of aggresomes of PMP22. These aggresomes might alter cell differentiation and cell death, however they might also confer protection by sequestration of toxic proteins[107].

PMP22 interacts also with the chaperon protein calnexin in the endoplasmic reticulum. Punctual mutations in PMP22 increase the association with calnexin that might collaborate in the pathophysiology of CMT disturbing control of the protein folding pathway[108]. In addition, transgenic mice with decreased calnexin function generate characteristics of motor disorder[109].

Finally, PMP22 has some similarities in the primary amino acid sequence with the claudin family of tight junction proteins, and has been involved in the development of blood-nerve and blood-brain barrier [97,110] at intercellular junctions.

1.3.5. Biomarkers in Charcot-Marie-Tooth

As described in previous sections, CMT present a heterogeneous phenotype and a wide range of genetic alterations and genes implicated. In addition to this facts, childhood-onset, different progression and severity of CMT patients, and the lack of a treatment for this hereditary neuropathy enhance the need to find new biomarkers of diagnostic, prognostic, and monitoring of therapeutic effects in clinical trials. These new biomarkers of disease are considered genomic polymorphisms and variants, RNA expression profiles (including miRNAs), proteomic signatures in tissues, metabolomics patterns and molecular structural images. Furthermore, they should improve the clinical scales, such as the "Charcot-Marie-Tooth Neuropathy Score" (CMTNS)[111] used currently in order to evaluate the disease severity.

Nowadays, a new assay of the proximal sciatic nerve called magnetization transfer ratio assay, and based in magnetic resonance imaging was described as a biomarker of myelin content in CMT patients[112]. New studies try to find new

biomarkers for clinical trials monitoring mRNA expression levels from skin biopsies of CMT1A patients [113].

1.4. Friedreich`s ataxia

In 1863, a German pathologist from Heidelberg called Nikolaus Friedreich described for the first time a new disease of spinal cord. Nevertheless, the inheritance nature of the disease was assigned in 1876, and it was 120 years after when the genetic defect that triggers Friedreich Ataxia (FRDA; OMIM 229300) was discovered: an expansion mutation of guanine-adenine-adenine (GAA) repeats in the first intron of frataxin gen (*FXN*), which produces a decreased expression of the FXN protein[114]. This mutation observed in gene encoding FXN protein permitted the confirmation with a genetic diagnosis, and opened a new scientific field with FRDA as a model disorder. GAA repetitions are localized within an AluSx sequence, and this insertion, probably caused by a retroviral insertion, is present in *FXN* gene of higher primates such as Orangutans, Gorillas, and Chimpanzees[115].

FRDA commonly occurs in Caucasians, is rare in Sub-Saharan populations and very rare in the Eastern countries[116,117]. Prevalence in Caucasians is 2-5 per 100,000 people, but recent demography studies of published literature show that FRDA prevalence in Europe shows big regional differences. The existence of a gradient of prevalence from a 5 per 100,000 people in south-west (North of Spain, south and middle of France), and west (Ireland) of Europe to low levels of 1 per 250,000 or lower in north (Scandinavia) and east of Europe (East Germany, east of Austria, Czech Republic, Russia), can explain the regional differences in Europe[118].

There is no cure for FRDA just therapies that may cause a symptomatic effect resulting in improvement of symptoms and/or may interfere with the disease pathogenesis leading to a decreased progression of disease.

Different clinical ataxia rating scales have been described such as the Friedreich Ataxia Rating Scale (FARS), the International Cooperative Ataxia Rating Scale (ICARS), and the Scale for the Assessment and Rating of Ataxia (SARA)[119-121]. All of them measure motor aspects of cerebellar dysfunction including ataxia of stance, gait and limbs.

1.4.1. Clinical features of Friedreich's ataxia

Friedreich's ataxia is the most common hereditary ataxia, with elevated differences in symptomatology between individuals and within families. Instability of the GAA expansion size is approximately responsible of 50% of variability of disease onset[122]. The typical age of onset for FRDA is late in the first decade or early in the second decade of life. However, late-onset cases, with symptoms detectable after 25 years of age, have been described, and symptoms are hardly shown as late as the sixth or seven decades [123].

Neurological features of gait and limb ataxia, lower limb areflexia and dysarthria are observed in almost all cases. A mixed origin of ataxia results from spinocerebellar degeneration, peripheral sensory neuropathy, cerebellar and vestibular pathology, and the posterior adding of the pyramidal disabilities [124]. As a consequence of this mixed origin, mild cerebellar atrophy with loss of the dentate nucleus and its efferent fibres causing superior cerebellar peduncle atrophy can be observed. In addition, dorsal root ganglia show less size, the dorsal spinal roots are thin and grey, and the dorsal columns show an important atrophy generating a spinal cord calibre lower than normal. Spinocerebellar and corticospinal tracts are also decreased[125]. Normal or minimally disturbed brainstem and cerebellum are shown in the early phases of the disease; nevertheless, superior vermis and medulla oblongata are affected in latter stages of the disease[126]. There is a progressive dependence on aids to walking, and also limb ataxia generates daily activities impairments that need fine dexterity[127]. Lower limbs show more obvious pyramidal weakness, a relatively late feature, than upper limbs, preserving normal power of the latter in almost all patients even when they need a wheelchair [127]. An early sign presented by practically all patients is arreflexia predominantly in lower limps and slightly reduced muscle tone[128]. Severe axonal neuropathy with an important affection of sensory action potentials, are showed in neurophysiological studies. In addition, large myelinated fibres proportion are increased in peripheral nerves biopsy, and last, both findings correlate with GAA expansion size [129].

Eye movements abnormalities such as square wave jerks (SWJs) which are characterized by fixation instability interrupted by involuntary saccades, are an early

feature in FRDA patients, and other less common ophthalmic sing is decreased visual acuity. However, visual system impairments are relatively rare [130]. Dysarthria and dysphagia, and also hearing difficulties are common symptoms that produce severe disabilities[131,132].

Other non-neurological features are related with Friedreich's ataxia. Cardiac complications are found very often in FRDA patients, and rarely observed before neurological features. Hypertrophic cardiomyopathy or evidence of left ventricular hypertrophy was found in large number of cases and confirmed by cardiac magnetic resonance imaging. However, there is no correlation between cardiac complications and neurological severity[133]. Also, diabetes mellitus by insulin resistance of peripheral tissues and/or decreased insulin secretion resulting from dysfunction of pancreatic beta cell are associated with FRDA[134]. Finally, skeletal malformations such as scoliosis, and foot abnormalities (*pes cavus* and *talipes equinovarus*) are observed in FRDA patients[128,135].

1.4.2. Frataxin gene (*FXN*)

The majority of FRDA patients are homozygous for an unstable guanine-adenine-adenine (GAA) expansion in the first intron of *FXN* gene that localizes in chromosome 9q21.11 producing decreased protein levels of frataxin. Less common are patients with the GAA expansion in one allele and a punctual mutation in the other allele. Normal alleles have less than 36 GAA repetitions, whereas more than 36 repetitions conduce to pathogenic expansions. In FRDA repetitions fluctuate from 44 to 1,700 repetitions (Figure 7a) [123].

Seven exons make up frataxin gene (exons 1-4, 5a, 5b and 6). Five of them (transcript of 1.3kb from exon 1 to exon 5a) encode for frataxin protein isoform A. There are two more isoforms, (isoform B and B1) encoded by alternative transcripts that contain exon 5b instead of 5a with or without non-coding exon 6. Unmethylated CpG islands containing rate restrictions sites are found in 5'end plus of the first exon of the gene [114]. The promoter of this gene is located in the 1255-bp region extending 5' of Human FXN open reading frame. There is not TATA sequence, but many repetitive retroelements (AluJb, AluY and L2) and mammalian-wide interspersed repeats (MIR)

that act as enhancers of the promoter [136,137] are found. Another promoter modulator is an E-box element that can bind to helix-loop-helix family transcription factors such as muscle-specific factor (MyoD)[137]. Other regulator of frataxin expression may be iron, since deferoxamine (an iron chelator) reduces frataxin expression and also hemin or ferric ammonium citrate produce elevated expression of frataxin [138,139]. Four binding sites for serum responsive factor (SRF; important for neuronal development), transcription factor AP2 (TFAP2; implicated in neural-crest development), CCCTC binding factor (CTCF), and early growth response protein (EGR3) are found in *FXN* gene promoter (Figure 7b)[140,141].

Unusual structures such as intra-molecular triplex, sticky DNA or RNA·DNA hybrids formed by GAA expanded repeats are detected in vitro. In addition, marks of condensed heterochromatin (such as methylation of specific CpG sites, reduction of acetylation levels of histone H3 and H4, and increased levels of tri-methylation of histone H3 in Lys 9) are found in the FXN promoter and intron regions flanking the GAA repeat expansions. These data suggest that both processes may be implicated in frataxin gene silencing[142].
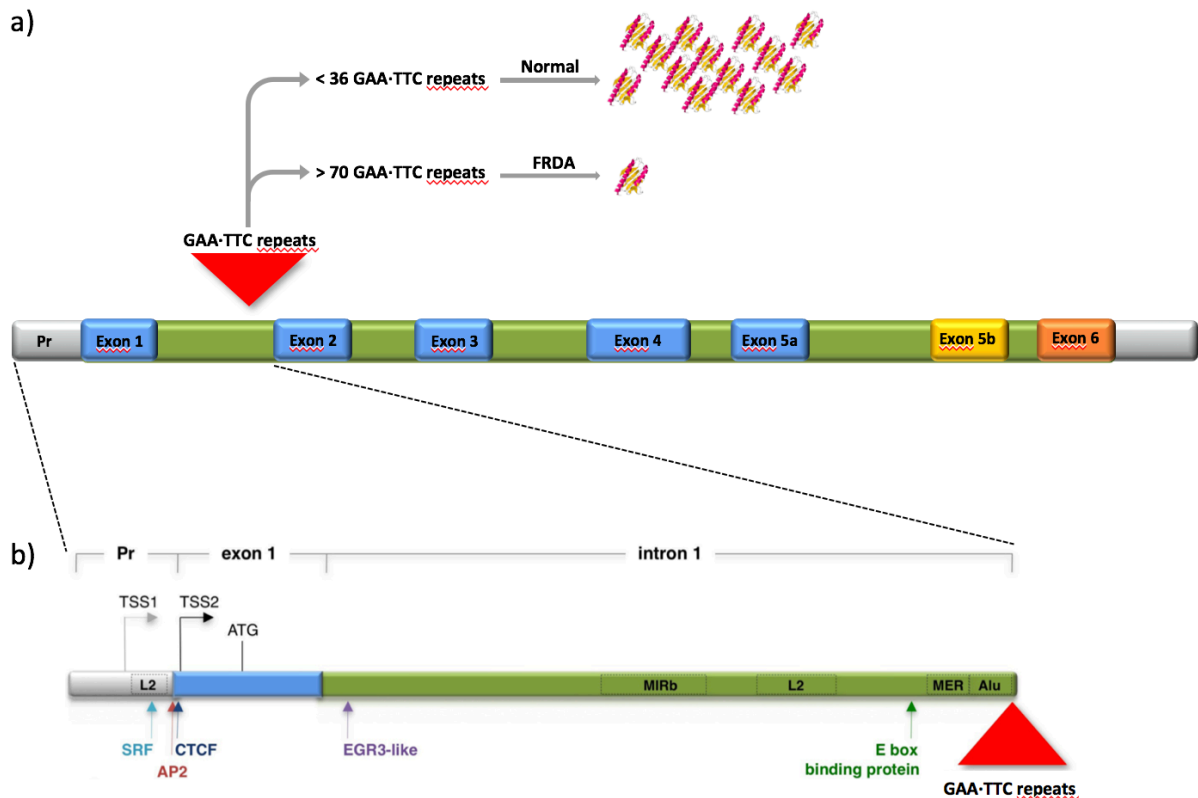
Figure 7. Frataxin gene. a) Schematic representation of FXN gene. Exon 1, 2, 3, 4, and 5a exons (shown in green) encode frataxin protein. Alternative transcripts that includes exon 5b instead of exon 5a, with or without exon 6 (shown in yellow and orange, respectively) encodes less common isoforms of frataxin. b) Schematic representation of 5`end of frataxin gene. Interspersed repeated sequences are indicated by black outlined rectagles. Arrows indicates binding sites localization of activator protein 2 (AP2), serum response factor (SRF), an early growth response protein 3 (EGR3)-like factor, CCCTC-binding factor (CTCF), and an E-box binding protein. (TSS1 and TSS2, transcription start site 1 and 2; pr, promoter; modified from Kumari *et. al.*) [143]

1.4.3. Frataxin structure

Frataxins are small acidic proteins (between 100 and 220 amino acids) highly conserved in most organisms from bacteria to mammalians[144,145]. In humans, due to alternative splicing there are 3 different isoforms (Figure 8a). In addition, a precursor of 210 amino acids and 23kDa of human frataxin is synthesized in cytoplasmic ribosomes and imported to mitochondria thanks to mitochondrial import sequence. The mitochondrial processing peptidase (MMP) performs a process of maturation in two steps in order to eliminate the import sequence. The maturation process consists in a successive generation of intermediate form of 19kDa (42-210 amino acids) and a mature form of 14kDa (81-210; figure 8a)[146,147]. Once the maturation of frataxins proteins are done, they are localized in mitochondrial matrix[148].

Folding of frataxin consists in a large, twisted, five-strand ß–antiparallel sheet, flanked by N- and C-terminal α helices (α1 and α2) and a sixth (and a seventh in human frataxin) ß-strand that intersects the planes to generate an α- ß sandwich structure motive (Figure 8b). An area of negatively charged residues on the helical plane of frataxin are presented, which may be iron-binding sites[149]. Protein-protein interactions can be achieved through mostly uncharged surface of ß-sheets. *In vitro* structural studies of frataxin show that this protein assembles into trimers, hexamers and multimers, nevertheless it is not clear if these structures are present *in vivo*, neither their functional relevance. The most abundant products seem to be the monomeric form of frataxin (81-210 amino acids) [150].
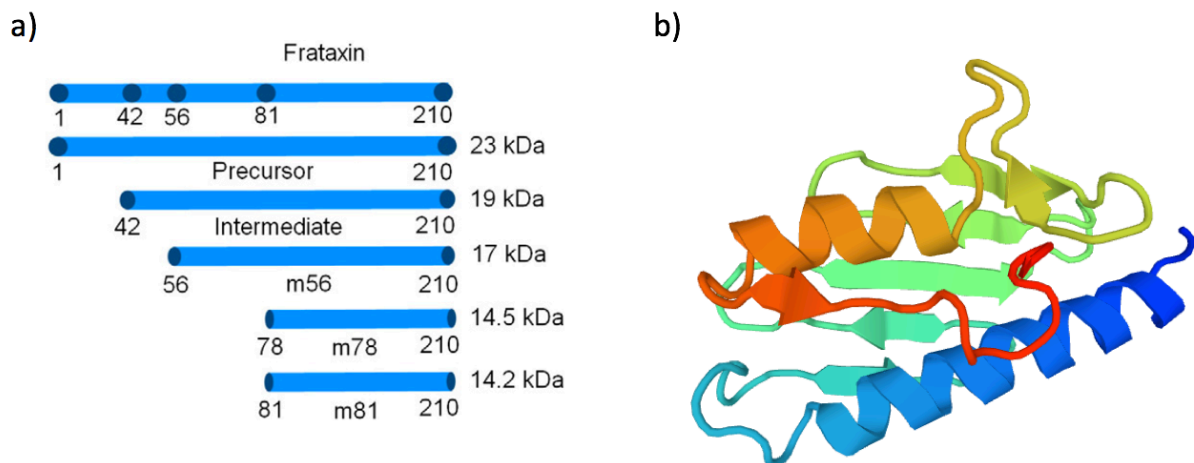
Figure 8. Human frataxin structure. a) Different frataxin forms. Three described mature isoforms: m56 (56-210 amino acids), m78 (78- 210 amino acids), and m81 (81-210 amino acids). The precursor (1-210 amino acids) and the intermediate (42-210 amino acids; image obtained from Marmolino)[151]. b) Frataxin structure showing α helices and a seventh stranded β-antiparallel sheets.

The conserved residues in frataxin among different species, suggest the importance for structural and/or functional role regions. Parts of hydrophobic core contains conserved buried residues that seem to be important for folding, and those conserved residues that localize on the surface of the protein are associated with protein function. FRDA patients with a point mutation on frataxin on one allele and a GAA expansion on the other, result in mutations like I151F, W155R, G130V, and D122Y[152].

Frataxin is expressed in all cells, but there are different FXN mRNAs and frataxin levels depending on the tissue, in almost all cases correlating with those affected in FRDA patients. In humans, heart and spinal cord shows highest levels of expression, whereas in cerebellum, liver, skeletal muscle and pancreas lowest levels of expression are found [114]. Dorsal root ganglia express high levels of frataxin, and are the most vulnerable neurons, therefore showing decreased levels of frataxin.

1.4.4. Frataxin function

The principal function of frataxin is not clear yet, however the early lethality in embryos of FXN knock-out mice remarks the notable importance of frataxin function in cell survival [153]. Several roles have been assigned to frataxin: first, hypothetical function for frataxin was suggested by Isaya's laboratory when they described the iron binding and aggregate formation of yeast homolog of frataxin (Yfh)[154][155]. This facts were supported by the detection of iron deposits in hearts from FRDA patients[156]. However, this does not seem the main function of frataxin, because these aggregates cannot be observed in human frataxin and it only precipitates under a large excess of iron[149]. In addition, it was observed that the aggregates formation did not seem to be essential when frataxin acts as an iron chaperon during the iron-sulfur cluster or heme assembly[157]. More evidences were observed for Fe-S cluster assembly function of frataxin. Both hscA and hscB proteins involved in Fe-S clusters in proteobacteria have identical phylogenetic distribution with the *FXN* gene[158]. Moreover, a mouse model for heart cardiomyopathy of FRDA suggest an involvement of frataxin in Fe-S cluster [159] and with deficiencies in mitochondrial complexes I, II, III and aconitases, enzymes that have an iron-sulfur (Fe-S) cluster, have been described in FRDA patients[160]. Fe-S cluster are found in mitochondria (i.e. several subunits of respiratory complexes, Aconitase, Ferrodexin, Ferrochelatase, the molybdenum cofactor synthesis enzyme MOCS1a, and the membrane associate protein of unknown function MitoNEET), cytosol, and nucleus [151]. Both yeast and human frataxin are found as Fe-S cluster assembly complex binding proteins [161][162]. This complex is composed by the cysteine desulfurase NFS1 and its accessory protein (ISD11), and the Fe-S scaffold protein (ISCU2) when the complex is mostly inactive, whereas activated complex includes

additionally frataxin [163]. NFS1 provides sulfur for Fe-S cluster biosynthesis, meanwhile ISD11 stabilizes and may activate NFS1[164]. ISCU2 acts as a template for cluster assembly and finally FXN stimulates the cysteine desulfurase and Fe-S cluster assembly reactions[165].

Bridwell-Rabb et. al propose a model of Fe-S cluster biosynthesis in which frataxin has a role as allosteric regulator[162]. In this model, Fe-S cluster assembly complex is in an equilibrium between non-functional (helix motive) and functional (coil structure) conformational states. Frataxin binding to the complex stabilizes the coil conformation acting as an allosteric activator (Figure 9).
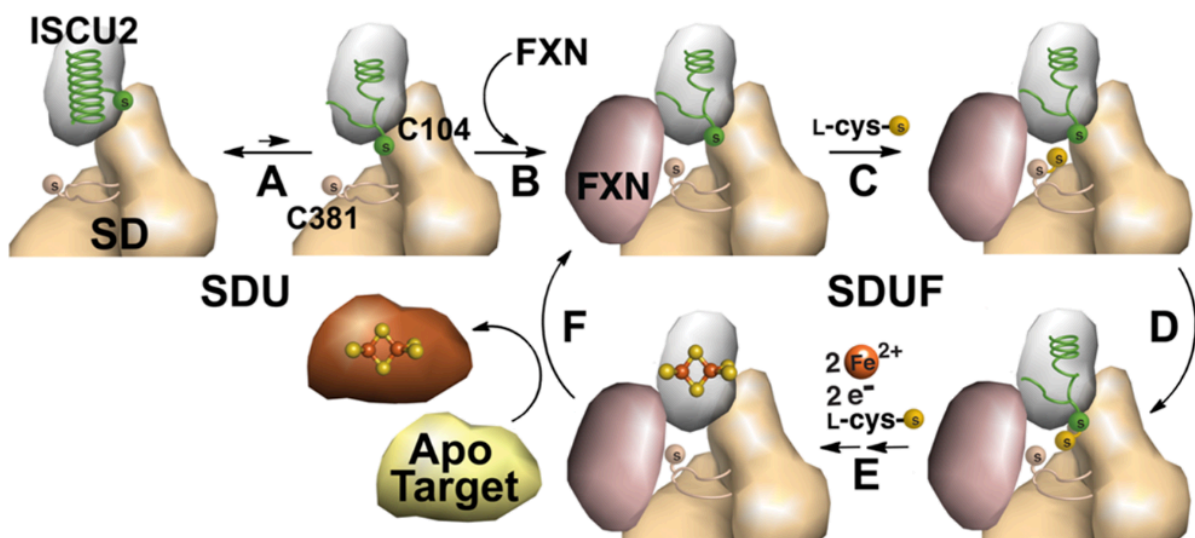
Figure 9. Schematic representation model of the Fe-S assembly complex activated by frataxin. a) Equilibrium of Fe-S cluster assembly complexes between the less stable active (coil; SDUF) and the stable inactive (helix; SDU) conformation. b) Binding of frataxin to coil structural motive for the C-terminal helix switches the equilibrium from inactive form to active form. c) L-cysteine reacts with NFS1 and form on C381 a persulfide species. d) C104 residue of ISCU2 receive sulfur molecule from NFS1. e) Formation of [2Fe-2S] cluster occurs on ISCU2 with the addition of the rest of reaction components. f) The Fe-S cluster is transferred to an apo target, and the active SDUF is re-formed (image from Bridwell-Rabb *et. al*)[162].

An interaction between frataxin and ferrochelatase, the enzyme that catalyses the final step of heme group biosynthesis by inserting the ferrous ion into porphyrin ring, suggests another role of frataxin in heme biosynthesis pathway[166]. In addition, kinetic inhibition of this pathway occurs when frataxin levels are decreased[167].

Frataxin links with mitochondrial aconitase, mitochondrial respiratory chain (complex II) and differential types of chaperons are reported, however the importance of these interactions is not completely clear[168].

1.4.5. Biomarkers in Friedreich's ataxia

Friedreich's ataxia patients have not a currently approved therapy and the number of methods to test the possible efficacy of therapeutic treatments is reduced. All the biomarkers used in FRDA are neurologic, including hole peg test, timed 25 food walk, etc. Thus, targeting and restoring of frataxin expression are main goals for the treatment of FRDA. Currently, frataxin expression in conjunction with other biomarkers (such as deacetylase inhibitor (HDACi) RGFP109/RG2833 [169] or the Nrf2 inducer dimethyl fumarate (DMF)) is used to assess drug therapies. However, little is known about biomarkers that could stratify the patients with the concomitant diseases of FRDA (cardiomyopathy, diabetes, scoliosis, etc.). Nowadays, there are some efforts trying to find new biomarkers for progression of cardiomyopathy in FRDA using imaging technologies [170].

Recent studies have shown that miRNAs are involved in altered gene expression profiles that trigger the development of mitochondrial diseases and cellular redox homeostasis. In fact, miRNAs participate in the regulation of frataxin levels[171,172]. Although a small number of studies have analysed miRNAs in FRDA[173,174], their regulatory role in this disease has not been clearly reported. Of the two previous studies, only one was performed in blood, reporting differential levels of miR-886 in FRDA blood samples[173]. However, miR-886 is not actually a miRNA, and it has been reclassified as a vault RNA in the most recent version of miRbase, v21 (miRNA accession number: MI0005527; available at www.mirbase.org).

The potential of identifying miRNA signatures in FRDA goes beyond the discovery of physiological and molecular pathways underlying this disease. Understanding the phenotypic variability of patients is also necessary for designing the most appropriate therapy for each of them, according to their specific pattern of disease progression.

1.4.6. miRNAs as biomarkers

In recent years, noncoding RNAs (ncRNAs) have added a new level of complexity in DNA-RNA-protein relationship. ncRNAs can be transcribed and participate in regulatory and functional processes[175].

ncRNAs can be categorized by their size in two classes: small ncRNAs (sncRNAs; between 20 and 30 nucleotides) which act as a posttranscriptional regulators of target RNAs via RNA interference (RNAi), and/or modifying other RNAs; and long ncRNAs (lncRNAs, more than 200 nucleotides) [176]. MicroRNAs (miRNAs) are the best characterized sncRNAs. With about 22 nucleotides, there is a huge number of human transcripts, which have been published with sequences and annotations[177], listened in the database miRBase v21 (http://www.mirbase.org/).

miRNAs can be localized in the genome in both intragenic and/or intrinsic regions of transcripts that encode for proteins. Mostly RNA polymerase II and in some cases RNA polymerase III, are the enzymes that transcribe miRNAs[178,179]. Once transcribed as a primary miRNA transcripts (pri-miRNA) in the nucleus, a new stem loop precursor of 70 nucleotides (pre-miRNA) is generated from pri-miRNA in the Drosha-DGCR8 enzyme complex[180]. The new precursor transcript is transported to the cytoplasm through exportin 5, where it is cleaved, generating a mature double-stranded miRNA (between 19 to 24 nucleotides), by the type III Dicer[181]. One of these two strands is loaded into RNA-induced silencing complex (RISC) [182]. This binding permits the identification of target mRNA based in the complementarity of 3'UTR of target gene and miRNA sequence, and controls the degradation of the mRNA target when there is enough complementarity or translational repression of protein expression[183,184]. Some miRNAs are released from cells in membrane-bound vesicles which protect them from RNase activity[185], and for this reason miRNAs could be detected in circulating fluids such as plasma, serum, urine and saliva[186-188]. Besides their role in specific tissues and, recently as a stable molecule in circulating fluids[189], miRNAs have been proposed as biomarkers in some diseases such as cancer[190,191], diabetes[192], neurodegenerative diseases[193], etc.

The small fraction of total RNA in cell (which is lower than in circulating miRNAs), the lack of poly(A) and the short length of mature miRNAs makes difficult the detection of this molecules. However, new commercial column-based kits are useful tools to isolate the small RNA fraction, which consist mostly by miRNAs. In addition, new platforms of next-generation sequencing (NGS), and specifically small RNA-sequencing, have improved the miRNA analysis. In fact, hybridization-based detection allows the determination of miRNAs but with the sequencing-based detection the

possibility of simultaneous detection of known miRNAs and new undiscovered ones has been achieved. Concomitant bioinformatics tools to process information from NGS analysis and to understand the miRNA-mRNA interaction network has been developed[194].

A crucial role of miRNAs in the development and function of nervous system has been reported. Neurons express high number of miRNAs that regulate key pathways for neuronal differentiation, neural patterning, the establishment and maintenance of cell identity, synaptogenesis and neural plasticity[195]. Altered expression of miRNAs has been detected in different neurological disorders, and it has been observed that they could play an important role in the pathogenesis of these disorders[193]. Studies of the role of miRNAs in diabetes describe altered profile of miRNAs associated with cardiovascular complications, nephropathy, retinopathy, and neuropathy [196]. In addition, pancreatic ß-cell fate and pancreas formation, and insulin synthesis and secretion are regulated by miRNAs [197]. Essential roles of miRNAs in cardiovascular pathologies have been described. Furthermore, the heart overexpresses some miRNAs, which control cardiac development and function[198].

Clarification of miRNA signatures could therefore provide a new landscape of pathological mechanisms occurring during the natural history of the disease, since miRNA levels can change with disease progression and pharmacological interventions.

2. Hypothesis and objectives

2.1. Hypothesis

Charcot-Marie-Tooth (CMT) and Friedreich's ataxia (FRDA) are the most common hereditary neuropathy, and the most common hereditary ataxia, respectively. The physiopathology of these two rare diseases is not completely understood and their clinical evaluation is impaired by the lack of specific diagnostic and prognostic parameters. We propose that the evaluation of oxidative stress and the proteomic profile would provide differences between mild CMT patients, severe CMT patients, and controls that could be used as new biomarkers of disease progression. On the other hand, miRNAs analysis would provide different expression profile signatures between patients and controls that may help in the identification and stratification of different phenotypes in FRDA's patients. Furthermore, the miRNome characterization in cellular models may help in the comprehension of the special function of differential expressed miRNAs in the physiopathology of Friedreich ataxia.

2.2. Objectives

The main objective of this study is to find biomarkers for clinical stratification, prognosis and monitoring of clinical trial experiments in Charcot-Marie-Tooth disease and Friedreich's ataxia.

The main objective has two different goals with different sub-objectives:

I. To search for new biomarkers in plasma samples from mild CMT patients, severe CMT patients, and healthy patients

    a. To analyse oxidative stress markers in plasma samples from mild CMT patients, severe CMT patients, and healthy patients.

    b. To explore differential expression of proteomic markers in plasma samples from mild CMT patients, severe CMT patients, and healthy patients and validation of candidate biomarkers

II. To search for new biomarkers in plasma samples of FRDA patients and healthy controls, and in cellular models of FRDA disease (i.e. olfactory mucosa stem cell model, SH-SY5Y, and fibroblasts)

a. To evaluate differential representation of miRNA in plasma samples of FRDA patients and healthy control: bioinformatics analysis of pathways regulated by this miRNAs and validation of possible miRNAs biomarkers

b. To analyse the differential expression of miRNA in cellular models of FRDA disease (i.e. olfactory mucosa stem cell model, SH-SY5Y, and fibroblasts) bioinformatics analysis of pathways regulated by this miRNAs and validation of candidate miRNAs biomarkers and their target pathways.

c. To validate the miRNA profile from plasma samples of FRDA patients and healthy control in cellular models of FRDA disease (i.e. olfactory mucosa stem cell model, SH-SY5Y, and fibroblasts) and their target pathway.

3. Material and methods

3.1. Protocol approval and samples description

3.1.1. Protocol approval by CEIBs

The selection process was carried out in accordance with the relevant clinical guidelines, following standard operation procedures, and with the approval of the ethics and scientific committees. Informed consent was obtained from all participants.

All experimental protocols to perform the experiments in CMT biological samples described in this Thesis were approved by the Biomedical Research Ethics Committee (CEIB) of Hospital La Fe (Valencia), Hospital de Bellvitge (Barcelona), Hospital La Paz (Madrid), and Hospital Virgen del Rocio (Sevilla) and the ethics and scientific committees of CIBERER Biobank (Appendix document 1).

In the same way, all experimental protocols to perform the experiments in FRDA biological samples described in this Thesis were approved by the ethics and scientific committees of the Basque Biobank for Research-OEHUN (www.biobancovasco.org) and the Biobank for Biomedical Research and Public Health of the Valencian Community (IBSP-CV) through the Spanish National Biobank Network (RNBB 2013/12). Ethics and scientific committees of Hospital Clínic Universitari de Valencia was approved in order to obtain samples from CIBERER Biobank (www.ciberer-biobank.es; Spanish Biobank) (Appendix document 2).

The samples were used to create a public sample repository of CMT patients, and healthy controls in the CIBERER Biobank (www.ciberer-biobank.es; Spanish Biobank).

3.1.2. Human plasma

Blood samples were collected from CMT patients, FRDA patients and healthy participants in EDTA tubes. Each sample was centrifuged at 2500 rpm for 10 minutes to separate the plasma and stored at $-80^{o}C$.

3.1.2.1. Participants in Charcot-Marie-Tooth study

A cohort of patients with diagnosis of CMT from four referral hospitals of Spain (Hospital La Fe (Valencia), Hospital de Bellvitge (Barcelona), Hospital La Paz (Madrid),

and Hospital Vírgen del Rocío (Sevilla) participated in the study. A total of forty-six Caucasian CMT1A patients and twenty-two Caucasian healthy subjects were randomly recruited from these hospitals. Patients were tested for corroboration of PMP22 duplication and have not got any other secondary disease that could affect to the neurodegeneration caused by PMP22 duplication. Informed consent was obtained from each subject, either directly or from his or her guardian, and the Ethical Committee of the four hospitals mentioned above approved the protocol of this study. Patients were grouped according to their CMTNS[199]: twenty-five mild CMT patients (CMTNS <15) and twenty-one severe CMT patients (CMTNS> 15).

Samples from healthy volunteers were obtained from the CIBERER's Biobank. As exclusion criteria, we consider subjects with neoplastic diseases, active infection, cardiomyopathy, heart problems, hypertension or diabetes. Healthy volunteers were enrolled by CIBERER Biobank (www.ciberer-biobank.es; Spanish Biobank Registry number).

All samples from CMT patients and healthy volunteers were matched by sex and age (Table 3).

Table 3. List of CMT patients and controls matched by gender and age. *Samples used only for gelsolin levels analysis.

Control			*Mild*			*Control*			*Severe*		
ID	Sex	Age	ID	Sex	Age	ID	Sex	Age	ID	Sex	Age
60*	MALE	12	4	FEMALE	3	22	FEMALE	23	12	FEMALE	20
62*	MALE	12				24	FEMALE	29	68*	FEMALE	22
57*	MALE	13				21	MALE	32	9	MALE	32
59*	FEMALE	12	6	FEMALE	14	20	MALE	34	19	MALE	36
61*	FEMALE	13	7	FEMALE	15	25	MALE	40	14	MALE	39
63*	FEMALE	16	15	FEMALE	18				34	MALE	42
64*	MALE	14	3	MALE	20	52	FEMALE	44	38	FEMALE	44
58*	MALE	15	13	MALE	22				18	FEMALE	47
22	FEMALE	23	2	FEMALE	26	55	MALE	41	17	MALE	50
24	FEMALE	29	5	FEMALE	29	49	FEMALE	49	67*	FEMALE	51
21	MALE	32	11	MALE	32				35	FEMALE	53
20	MALE	34	1	MALE	35				66*	FEMALE	54
23	FEMALE	31	10	FEMALE	32	56	MALE	42	65*	MALE	54
			16	FEMALE	37	51	FEMALE	52	44	FEMALE	56
			31	FEMALE	40	50	FEMALE	54	37	FEMALE	57
			33	FEMALE	41				46	FEMALE	57
52	FEMALE	44	41	FEMALE	42	53	MALE	65	43	MALE	60
			42	FEMALE	42				47	MALE	67
			27	FEMALE	43	54	MALE	65	45	MALE	68
			30	FEMALE	43				39	FEMALE	70
56	MALE	42	29	MALE	45				48	MALE	75
49	FEMALE	49	28	FEMALE	45						
			26	FEMALE	47						
51	FEMALE	52	40	FEMALE	58						
50	FEMALE	54	8	FEMALE	60						
53	MALE	65	32	MALE	63						
54	MALE	65	36	MALE	67						

3.1.2.2. Participants in Friedreich's ataxia study

The study population included patients from different families who had been diagnosed with FRDA. This diagnosis was confirmed by genetic study. Patients with neoplastic diseases and active infection were excluded. Data about age, sex, tobacco use, history of diabetes, cardiomyopathy, medication and therapies and number of repetitions in the mutation and disease duration were recorded. The scale for assessment and rating of ataxia (SARA) was used to measure the clinical severity of the disease[200].

Table 4. List of FRDA patients and controls matched by gender and age.

	PATIENTS			CONTROLS	
ID	SEX	AGE	ID	SEX	AGE
27	FEMALE	26	33	FEMALE	24
38	FEMALE	32	34	FEMALE	33
42	FEMALE	68	49	FEMALE	56
41	FEMALE	48	46	FEMALE	53
2	FEMALE	39	47	FEMALE	38
6	FEMALE	56	47	FEMALE	56
18	FEMALE	38	47	FEMALE	38
5	FEMALE	46	31	FEMALE	44
25	FEMALE	46	31	FEMALE	44
29	MALE	28	35	MALE	30
1	MALE	34	10	MALE	32
4	MALE	35	10	MALE	32
13	MALE	35	10	MALE	32
30	MALE	32	10	MALE	32
14	MALE	41	22	MALE	40
39	FEMALE	49	7	FEMALE	54
17	MALE	47	20	MALE	47
15	MALE	37	21	MALE	39
16	MALE	39	21	MALE	39
3	MALE	52	9	MALE	51
26	FEMALE	37	11	FEMALE	37
40	FEMALE	37	11	FEMALE	37
43	MALE	21	50	MALE	20
37	MALE	19	44	MALE	16
28	FEMALE	29	45	FEMALE	31

Healthy volunteers with no neoplastic diseases, active infection, cardiomyopathy, heart problems, hypertension, or diabetes were enrolled by the Basque Biobank for Research-OEHUN (www.biobancovasco.org) and the Biobank for Biomedical Research and Public Health of the Valencian Community (IBSP-CV) through the Spanish National Biobank Network (RNBB 2013/12).

The participants of both groups (healthy volunteers and FRDA patients) were matched by race, sex and age (Table 4).

3.1.3. Cell lines

Three different cell lines were used in this work: human fibroblasts, stem cells from olfactory bulb and SH-SY5Y cells.

3.1.3.1. Human fibroblasts

Primary fibroblasts from FRDA patients' biopsies and from healthy donors were used in this work. The table 5 shows the characteristics of each individual and also the source of each one.

Fibroblasts were grown using 1:1 mixture of Dulbecco's modified Eagle's medium (DMEM) supplemented with 15% of inactive foetal bovine serum (FBS), 2mM of L-glutamine, and 100mg/mL of penicillin-streptomycin (Gibco, Spain). Cells were maintained at 37°C in a saturated humidity atmosphere containing 20% O_2 and 5% CO_2.

Table 5. Characteristics and identification of FRDA fibroblasts and control fibroblasts. Table shows information of the age, gender and clinical features of individuals from whom fibroblasts have been obtained. Data of GAA repetitions were obtained from García-Gimenez *et. al.* [201] * Kindly obtained from Dra. Marcela Del Río (CIEMAT; Madrid)

Name	ID	GAA REPETITIONS	SOURCE	CLINICAL REPORT	AGE	SEX
FRDA 1	GM04078	370/470	Coriell cell Repository	Ataxia; cardiomyopathy; mild peripheral neuropathy	30	Male
FRDA 2	GM03816	350/470	Coriell cell Repository	Spinal-cerebral degeneration with cardiomyopathy	36	Female
FRDA 3	GM03665	780/780	Coriell cell Repository	limb and gait ataxia; scoliosis; proprioceptive sensory loss;	13	Female
CONTROL 1	GM08402	10/10	Coriell cell Repository	Apparently Healthy	32	Male
CONTROL 2	-	10/10	*	Apparently Healthy	50	Female
CONTROL 3	-	-	*	Apparently Healthy	11	Female

3.1.3.2. Olfactory mucosa stem cells

Olfactory mucosa stem cells from healthy volunteers and FRDA patients were obtained following the procedure detailed by Lanza *et. al.* [202] Cells were kindly gifted by Dr. Javier Diaz-Nido's laboratory and they were grown using 1:1 mixture DMEM and Ham's F12 Nutrient (Gibco, Thermo-fisher; US) with GlutaMAX, Albumax 0,5%, HEPES 5mM, glucose 0.6%, 100mg/mL of penicillin-streptomycin, no-essential amino acids (L-ala 44mM, L-Asn 45mM, L-Asp 40mM, L-Glu 40mM, L-Pro 30 mM) 2µg/ml heparin, N2 (Gibco, Thermo-fisher; US), 10ng/ml hrfGF-2 (Pepro thech Inc, US), 50ng/ml NGF (Sigma, US). 20% of fresh medium was added twice a week. Cells were maintained at 37°C in a saturated humidity atmosphere containing 20% O_2 and 5% CO_2.

3.1.3.3. SH-SY5Y cells

SH-SY5Y cell line was subcloned from original cell line called SK-N-SH, and it was described by first time by Biedler *et. al* [203]. The original SK-N-SH was obtained from bone marrow biopsy of four-years-old woman as described by Biedler *et. al*. [204]. SH-SY5Y cell line is an excellent model for Friedreich's ataxia because of the same developmental origin in neural crest of neuroblastoma cells and dorsal root ganglia affected in FRDA patients.

SH-SY5Y were transfected with vector pLKO.1 in order to obtain a silenced frataxin model. pLKO.1-NT was a control cell line with a sequence of interference RNA not directed. FXN-138.1 and FXN-138.2 were frataxin silenced cell lines with a reduction of 82% and 78% of protein levels, respectively.

SH-SY5Y were grown using 1:1 mixture DMEM and Ham's F12 Nutrient mixture medium supplemented with 10% of inactive foetal bovine serum (FBS), 2mM of L-glutamine, and 100mg/mL of penicillin-streptomycin (Gibco, Thermo-fisher; US). Transfected cells also were grown with 2 µg/ µL of puromycin as a selective marker. Cells were maintained at 37°C in a saturated humidity atmosphere containing 20% O_2 and 5% CO_2. All cell lines were kindly obtained from Dr. Francesc Palau laboratory.

3.2. Measurement of Protein levels

Protein levels of samples were measured using Pierce™ BCA Protein Assay Kit (Thermo Fisher, USA) in plates of 96 wells, following manufacturer's instructions. This assay is based on the reduction of Cu^{+2} to Cu^{+1} by protein in an alkaline medium, the Cu^{+1} generated binds to two molecules of bicinchoninic acid (BCA) generating a purple colour solution. This coloured complex generated is measured at 562nm of absorbance.

Standard dilutions of bovine serum albumin (BSA) were used in order to generate a standard curve, and protein concentration of samples were determined using the following formula:

$$Protein\ concentration\ (mg/ml) = \frac{Sample\ average\ absorbance - (intercept)}{Slope} X\ Dilution$$

3.3. MDA analysis

Malondialdehyde (MDA) is produced as product of membrane lipid peroxidation. As consequence of this oxidation the composition and structure of cellular membranes change, thereby altering the fluidity of the cellular membrane is reduced. Wong *et. al*. [205] described a method where MDA reacts with thiobarbituric acid (TBA) generating a chromogen with absorbance between λ=532-535 nm that could be measured.

25 µL Samples and MDA standards (Merck, Germany) were derivatized with 500 µL Sodium acetate anhydrous buffer 2M, pH 3,5, with TBA 0.2% during 60 min at 95ºC. This incubation generates lipid peroxide hydrolysis releasing MDA molecules that bounds with TBA molecules (MDA-TBA$_2$). 500 µL of KH_2PO_4 buffer 50 mM, pH 6,8, were added to samples and were shacked gently. Finally, after samples were centrifuged 5 min 13000 rpm at 4ºC, 200 µL of KH_2PO_4 Buffer 50 mM, pH 3,5 were added to the same volume of supernatant, and mixed slightly.

Derivatized samples and standards were analysed using a C18 Hypersil GOLD HPLC Column 15cm and 5 µm particle size (Thermo FIsher, USA) with the mobile phase of a mixture of KH_2PO_4 buffer 50 mM, pH 6,8 and acetonitrile (83 of KH_2PO_4 buffer / acetonitrile), flow phase rate of 1.0 mL/min, and under isocratic conditions.

3.4. Immunoblotting Blotting analysis

3.4.1. Dot-Blot

Dot-blotting was used to measure carbonylated proteins and nitrosylated proteins. Samples (20ng) were derivatized using Oxi-Blot™ protein oxidation detection kit (Millipore, USA) following the manufacturer's instructions to detect levels of carbonylated proteins. In case of nitrosylated proteins samples (20ng) were mixed with sample buffer 5x (Tris-HCl 40 mM pH 6.8, EDTA 4mM, SDS 4%, bromophenol blue 0.01%, sacarose 40%, ß-mercaptoethanol 10%) and denaturalized by boiling 5 min at 95ºC. We prepared also negative and positive controls to each experimental process.

Nitrocellulose Transfer Membrane (Whatman, Germany) and one filter paper (Whatman 3MM) were hydrated with 0.05 g/ml of skimmed milk (for nitrosylated proteins) or 0.01 g/ml BSA (for carbonylated proteins) in PBS-Tween solution (Phosphate buffer saline 4mM and Tween 0.1%) and then, were put together with one dried filter paper and 3 towel papers. Samples were dropped in membranes using 1 µL of each sample, including positive and negative controls of carbonylated proteins, and were left to dry for a few minutes. Once membranes were dried, blocking incubation was performed using 0.05 g/ml of skimmed milk (nitrosylated proteins) or 0.01 g/ml BSA (for carbonylated proteins) in PBS-Tween solution during 1h.

After blocking incubation, first antibody incubation was performed using target protein antibody diluted in 0.01 g/ml of skimmed milk or BSA in TBS-Tween solution: anti-carbonylated proteins (1:1000; provided in Kit Oxi-Blot™ protein oxidation detection kit; Millipore, USA) and anti-Nitrotyrosine, clone 1A6 (1:1000; Millipore, USA). Membrane was incubated with appropriate antibody over night at 4ºC and with a softly shaking.

The following day, membranes were washed 3 times with 0.01 g/ml of skimmed milk or BSA in PBS-Tween solution, in order to eliminate no-binding antibody. Then, the membrane was incubated with appropriate second antibody 1 h with gently shaking: goat anti-mouse (1:7500, Calbiochem, Germany), goat anti-rabbit (1:2500, Cell Signaling, USA) all of them with horseradish peroxidase enzyme conjugated.

Three washings with PBS-Tween solution were done in order to eliminate the non-binding antibody. After that, membranes were incubated with reactive of ECL Plus Western Blotting Detection System (GE Healthcare, USA). The images of chemoluminescence were obtained with LAS-4000 (GE Healthcare, USA).

3.4.2. Densitometry analysis

Images obtained from chemoluminescence were analysed with Image J software. Relative density of dots was obtained by analysis of dots in rectangular sections and following measure of relative density of the contents of the rectangle. The rectangular sections enclose the region of interest and were defined as the minimal area that encloses the dots in a band. The regions of interests were analysed with the option "Gels" in the "Analyze" menu of imageJ software and a histogram plot for each rectangle was obtained. The peaks observed for each rectangle correspond to each dot that encloses the rectangle. A straight line in bottom of each peak was drawn in order to eliminate the background noise and separate each peak. The area observed for each peak corresponds to the number of pixels and the intensity and was measure with the tool of imageJ called "Wand". These data about areas was used for detect differences between intensities, and consequently in amount of protein.

3.5. GSSG /GSH ratio

Glutathione (L-gamma-glutamyl-L-cysteinylglycine; GSH), the most important non-enzymatic antioxidant in eukaryotes, is able to reduce H_2O_2 levels when the glutathione peroxidase (GPX) uses it as reductant to generate H_2O. Reduced GSH reacts with another molecule of GSH generating the oxidised form GSSG. Reduction of GSSG to GSH is done by glutathione reductase, which obtains the electrons from the NADPH generating 1 equivalent of $NADP^+$. In addition, glutathione S-transferase catalyse the nucleophilic addition of GSH to electrophiles. Hence, GSSG/GSH ratio is considered a good parameter to measure oxidative stress imbalance.

Based in these facts, GSSG/GSH ratio and total GSH were measured using The DetectX Glutathione kit (Arbor Assays, USA) following the manufacturer's instructions. This kit uses ThioStar® reagent, a fluorescent molecule that produce a highly

fluorescent product when it binds to the free thiol group of GSH. In the first step, ThioStar® binds to free GSH molecules present in samples and the fluorescence is measured with excitation of λ= 390 and emission of λ= 510 nm in Gemini XPS Microplate Reader (Molecular Devices, USA). Total GSH was measured in the same well and with the same parameters of excitation and emission spectra, after addition of a reaction mixture with NADPH and glutathione reductase that converts all GSSG molecules into free GSH, which is measured again using ThioStar® reagent. Afterwards, GSSG concentration was obtained using the next formula:

$$GSSG = \frac{(Total\ GSH - Free\ GSH)}{2}$$

3.6. Total antioxidant activity

Physiologic aerobic metabolism produces reactive oxygen species (ROS). In order to reduce ROS levels and the damage they produce, antioxidant systems were developed by the organisms. These antioxidant systems include enzymes (e.g. superoxide dismutase, catalase, and glutathione peroxidase), macromolecules (e.g. albumin, ceruloplasmin, and ferritin) and small molecules (e.g. GSH, β-carotene, uric acid, bilirubin, and ascorbic acid). The activity of all of them represents the total antioxidant activity.

Total antioxidant activity in our samples was measured using Cayman's Antioxidant Assay Kit (Cayman, USA). This assay is based on the ability of antioxidants presents in the sample to inhibit the oxidation by metmyoglobin of ABTS® (2,2'-Azino-di-[3-ethiylbenzthiazoline sulphonate]) to ABTS®·+. This oxidation product was measured by its absorbance at 750nm in a SpectraMax® Plus 384 Microplate Reader (Molecular Devices, USA) and compared with the antioxidant capacity of Trolox, a tocopherol analogue. The antioxidant capacity was quantified as millimolar Trolox equivalents using the formula:

$$Antioxidant\ (mM) = \frac{Sample\ average\ absorbance - (y - intercept)}{Slope} X\ Dilution$$

3.7. Proteomic analysis

Individual identification and relative quantification of thousands of proteins composing the proteome in a specific time can be performed using an improvement of 2-dimensional electrophoresis called 2D-Differential In Gel Electrophoresis (2D-DIGE). This analysis let separation of proteins first, by isoelectric point in a non-lineal pH gradient strip, and then by size, in a sodium Dodecyl Sulphate Polyacrylamide gel electrophoresis (SDS-PAGE), as occurs in a 2D-Differential electrophoresis. The improvement of 2D-DIGE is that samples are labelled with fluorescent dyes called CyDyes: Cy2, Cy3 and Cy5. CyDyes are covalently attached to proteins (a single protein by fluor dye). Samples are labelled with different dyes, and then proteins are run on the same 2D gel. The advantage of 2D-DIGE is that a mix of 2 analysed samples in the same gel are mixed and labelled with a third CyDye in order to normalize protein levels, therefore analysing simultaneously the different amount of specific proteins in both samples. Fluorescence images of labelled proteins are taken and analysed with Decyder software to detect differential protein expression between two samples [206].

The 2D-DIGE analyses were carried out in the UCIM-University of Valencia Proteomics Unit, a member of ISCIII ProteoRed Proteomics Platform.

3.7.1. Sample preparation

A selection of CMT plasma samples (Table 6) were used in order to perform 2D-DIGE proteomic analysis in Proteomic Unit of Central Research in Medicine Unit (UCIM) from University of Valencia.

Table 6. Selection of CMT plasma samples and dyes used in 2D-DIGE proteomic analysis. The numbers appearing in each box corresponds to one-selected samples. For sample assignation and description please see Table 3.

ID gel	Cy3 Dye	Cy5 Dye	Cy2 Dye
60455	20	26	20+26
60456	27	21	27+21
60457	51	1	51+1
60458	3	52	3+52
60464	53	8	53+8
60465	32	54	32+54
54177	20	17	20+17
54178	43	21	43+21
54179	51	44	51+44
54180	46	52	46+52
52931	53	47	53+47
52932	18	54	18+54

3.7.2. Depletion of main plasma proteins

Main proteins (albumin, IgG, antitrypsin, IgA, Transferrin, Haptoglobin) from plasma samples were depleted using an affinity cartridge "Multiple Affinity Removal Spin Cartridge - Hu-6HC (Human)" (ref. 5188-5341 Agilent Technologies, USA). In order to avoid cartridge saturation a 1:5 dilution of each plasma sample in buffer A (Multiple Affinity Rem Spin Cartridge Reagent Kit 1L Buffer A, Agilent Technologies, ref. 5188-5254, USA) was used. The diluted samples were loaded in the cartridge and centrifuged twice for a better concentration of proteins. In order to avoid substances no desirable like detergent, salts, lipids, phenols, and nucleic acids 2D clean-up (ref: 80-6484-51, GE Healthcare, USA) kit was used as manufacturer's instructions. Later, the pellet was resuspended in SCLB (Standard Cellular Lysis Buffer; Tris-HCl 30mM pH 8.5; Urea 7M; Thiourea 2M; 4% CHAPS) and pH was optimized between 8 and 9.

3.7.3. 2D-DIGE labelling of protein with Cy Dyes

50 µg of protein in SCLB from selected samples of each group (Table 6), were labelled with 1 µl NHs-Cyanine (Cy) dyes (Cy2, Cy3 and Cy5, Amersham CyDye DIGE Fluor, GE Healthcare, USA). Equal amounts of protein from each condition were mixed to prepare a standard pool. The samples were incubated 30 minutes in ice and protected from the light and then dyes were quenched by adding 1 µl of lysine 10 mM

and leaving 10 minutes in ice and darkness. Equal protein amounts from pairs of differentially labelled samples and Cy2 labelled standard were mixed in the same tube with the volume of 2x RBS (Rehydration buffer stock. Urea 7M; thiourea 2M; CHAPS 4%), and reduced in ice during 10 minutes by 5 mg of DTT in 10 μL of Immobilized pH gradient (IPG) buffer (General Electrics, Healthcare, USA).

3.7.4. Protein separation by 2D-DIGE

The IPG strips (24cm, non-lineal pH 3-10, Immobiline DryStrip, GE Healthcare, USA) were rehydrated during at least 12h with 460 μl of RBS buffer, 1 mg of DTT and 5 μl of IPG Buffer. Labelled samples were loaded into loading cup from Ettan IPGphor3 IFU system (GE Healthcare, USA) and the isoelectric focusing was performed following next program: 300W during 4h, gradient from 300W to 1000W during 6h, gradient from 1000W to 10000W during 3h, and finally 10000W during 3h. Strips were equilibrated during 15 min at room temperature, and agitation in equilibration buffer (Tris 50mM pH 7.5; urea 6M; glycerol 30%; SDS 2%; Bromophenol blue 1%) containing 1% of DTT in order to keep the reduced proteins. Then for 15 min in the same buffer and conditions but containing 2.5% of iodoacetamide in order to avoid the oxidation of proteins. When the strips were equilibrated, they were transferred to 12.5% polyacrylamide gels (Acrylamide 40%; Tris 1.5M pH 8.8; SDS 10%; APS 10%; temed) in order to perform a SDS-PAGE electrophoresis. Gels were run in an Ettan DALTSix Device (GE Healthcare, USA) at 25 ºC as follows: 2W/gel during 45 min and then 15W/gel for 3h.

3.7.5. Gels scanning and image analysis

Typhoon™ TRIO (GE Healthcare, USA) was used to scan the gels with 100 μn of resolution and using excitation/emission wavelengths for each dye: Cy2 (488nm/520nm), Cy3 (532nm/580nm), and Cy5 (633nm/670nm). Images were loaded by Image loader module of Decyder software (GE Healthcare, USA) in order to be analysed first by the differential in gel analysis (DIA) module and then by the biological variance analysis (BVA) module of this software. DIA module is able to detect real spots, calculate spot volume/abundances for the Cy2, Cy3, and Cy5 images from a

same gel and normalize the values (Cy3/Cy2 and Cy5/Cy2). BVA module performs the matching of the spots from the images and obtains statistical data of expression levels for each group. When at least a 1.5-fold change was observed, quantitative differences were accepted. Student's t-test was used and the statistical significance of the differences were accepted when p<0.05.

3.7.6. Flamingo Fluorescent staining and spot picking

Gels were fixed for 2h, shaking with fixing solution (40% Ethanol and 10% of acetic acid in bidistilled water). Then Flamingo Fluorescent Gel (Bio Rad, USA) staining was performed in shaking during 2h. The stained gels were scanned on the Typhoon™ TRIO and then the images were exported to Ettan spot picker (GE Healthcare, USA) in order to pick up the samples from the gels.

3.7.7. Protein identification

The proteomic identification was carried out in the SCSIE-University of Valencia Proteomics Unit, a member of ISCIII ProteoRed Proteomics Platform.

3.7.7.1. Mass spectrometry

Samples from 2D-DIGE analysis were digested with sequencing grade modified trypsin (Promega,) as describe *Shevchenko et. al.* [207]. Digestion was stopped with Trifluoroacetic acid 1% (TFA) and digested peptides were concentrated until 7μL. A BSA plug was analysed in the same way to control the digestion process. Previously, the Plate and the acquisition methods were calibrated with 0.5 μL the CM5 calibration mixture (ABSciex, Applied Biosystems, USA), in 13 positions. The resulting mixtures were analysed in a 5800 MALDI TOFTOF (ABSciex, Applied Biosystems, USA) in positive reflectron mode (3000 shots every position). Five of the most intense precursors (according to the threshold criteria: minimum signal-to-noise: 10, minimum cluster area: 500, maximum precursor gap: 200 ppm, maximum fraction gap: 4) were selected for every position for the MSMS analysis. And, MS/MS data was acquired using the default 1kV MS/MS method.

The MS-MSMS information was sent to MASCOT via the Protein Pilot (ABSciex, Applied Biosystems, USA). Database search was performed on Expasy databases. Searches were done with trypsin specificity allowing one missed cleavage and a tolerance on the mass measurement of 100 ppm in MS mode and 0.8 Da in MSMS mode. Carbamidomethylation of Cys was used as a fixed modification and oxidation of Met and deamidation of Asn and Gln as variable modifications.

According to all the parameters a list of proteins ordered by probability of being the analysed protein was obtained.

3.7.7.2.   *Liquid chromatography tandem-mass spectrometry (LC-MS/MS)*

When the MALDI TOF/TOF analysis indicated mixture of proteins, (LC-MS/MS) was performed. 5 µl of every sample (except the main bands) were loaded onto a trap column (NanoLC Column, 3µ C18-CL, 350umx0.5mm; Eksigen, Ireland) and desalted with 0.1% TFA at 3µl/min during 5 min. The peptides were then loaded onto an analytical column (LC Column, 3 µ C18-CL, 75umx12cm, Nikkyo, Japan) equilibrated in 5% acetonitrile 0.1% FA (formic acid). Elution was carried out with a linear gradient of 5-45% B in A for 15min. (A: 0.1% FA; B: ACN, 0.1% FA) at a flow rate of 300nl/min. Peptides were analysed in a mass spectrometer nanoESI qQTOF (5600 TripleTOF; ABSciex, Applied Biosystems, USA). The tripleTOF was operated in information-dependent acquisition mode, in which a 0.25-s TOF MS scan from 350–1250 m/z, was performed, followed by 0.05-s product ion scans from 100– 1500 m/z on the 50 most intense 2-5 charged ions.

The data obtained for the sample were analysed combined for database search. ProteinPilot default parameters were used to generate peak list directly from 5600 TripleTof wiff files. The Paragon algorithm of ProteinPilot was used to search ExPASy protein database with the following parameters: trypsin specificity, iodoacetamide cys-alkylation, taxonomy restricted to *Homo sapiens*, and the search effort set to mode rapid. To avoid using the same spectral evidence in more than one protein, the identified proteins are grouped based on MS/MS spectra by the Protein-Pilot Progroup algorithm. Thus, proteins sharing MS/MS spectra are grouped, regardless of the peptide sequence assigned. The protein

within each group that can explain more spectral data with confidence is shown as the primary protein of the group. Only the proteins of the group for which there is individual evidence (unique peptides with enough confidence) are also listed, usually toward the end of the protein list.

3.8. PhenUMA analysis

PhenUMA analyses were performed in the Laboratory of Francisca Sánchez-Jiménez from University of Malaga, using the same methodology described by Rodriguez-Lopez *et.al*[208].

The web available application PhenUMa displays biological networks using data repositories of biomedical and biomolecular information. This software combines semantic similarity methods with information taken from databases of genetic diseases and biological interactions (Gene Ontology (GO) and Human Phenotype Ontology (HPO)).

HPO and GO were used to calculate the phenotypic similarities between genes and the functional similarities between genes. The inferred relationships between genes and orphan diseases are due to binary relationships. For instance, an inference between two genes will be considered if at least one or more (Online Mendelian Inheritance in Man) OMIM/Orphan diseases are associated with both genes.

Phenotypic similarity network was requested for PMP22 gene, the resulting network was populated with the functional, protein-protein interaction, metabolic and inferred relationships. Low level of confidence for both phenotypic similarities (the 98th percentile) and functional similarities (the 99.5th percentile) were selected.

3.9. Enzyme Linked ImmunoSorbent Assay (ELISA)

Gelsolin validation was performed for plasma samples of human and mice with Human plasma (soluble) gelsolin ELISA kit (Aviscera Bioicence, USA).

All Elisa's assays were performed following manufacturer's protocol and were based in a coated 96 wells plaque where samples and standard curve were detected using a biotinylated tracer antibody and a conjugate of streptavidin-peroxidase. Using

TMB as subtract of peroxidase, concentration of each well was measured at 450 nm using a SpectraMax® Plus 384 Microplate Reader (Molecular Devices, USA). The mean absorbance for each standard concentration was plotted on the vertical (Y) axis (logarithmic scale for gelsolin kit) versus the corresponding concentration on the horizontal (X) axis (logarithmic scale). Final concentration of the proteins was calculated using the following equations:

$$Gelsolin\ (pg/ml) = \frac{Sample\ average\ absorbance - (intercept)}{Slope} X\ Dilution$$

All concentrations were represented versus total protein concentration (mg/ml).

3.10.   miRNA analysis

3.10.1. RNA extraction and quantification

We isolated cell-free total RNA (including miRNAs) from 400 μl of plasma using the miRNeasy Serum/Plasma kit (Qiagen, Termofisher, USA), following the manufacturer's protocol. The RNA was eluted with 25 μL of RNAse-free water twice.

About 10^6 cells from cell lines were used to perform miRNA purification with miRvana miRNA Isolation Kit (Applied Biosystems/Ambion, USA) following manufacturer's instructions. The RNA was eluted with 75 μL of RNAse-free water.

The amount of total miRNAs was evaluated by Nanodrop 2000 and the quality of them was obtained by Small RNA assay Agilent 2100 Bioanalyzer (Agilent Technologies, USA).

3.10.2. Small-RNA sequencing of circulating miRNAs using Illumina technology

Small-RNA sequencing by Illumina method was performed in the Genotyping and Genetic Diagnostic Unit of INCLIVA.

3.10.2.1.   Library Preparation and Next-generation sequencing

Small-RNA libraries were prepared using the NEBNext Multiplex Small RNA Library Prep Set for Illumina (Set 1&2) (New England Biolabs, USA), following the manufacturer's protocol. Briefly, 5' and 3' adapters were ligated with small

RNA samples, followed by a cDNA library construction and incorporation of index tags by reverse transcription-PCR (RT-PCR). The products of this RT-PCR were purified using 6% non-denaturing polyacrylamide gel electrophoresis, and a 145-160 bp size fraction was isolated. The cDNA library samples were used for cluster generation and Illumina sequencing on the HiScanSQ platform (50 bp single read;Illumina, USA).

The first step was to assess the quality of the Illumina raw sequences with the FastQC software. Based on the results obtained, the sequence reads were trimmed to remove sequencing adapters and low quality bases. Once the data were deemed of sufficient quality, they were mapped against the human Hg38 build reference sequence, taken from the UCSC Genome Browser. After that, the intersection between the aligned position of reads and the miRNA coordinates taken from miRBase v21 was performed. The alignment and quantification steps were performed using the Subread[209] and RSubread[210] packages, respectively.

3.10.3. Small-RNA sequencing of FRDA cell lines using Ion Torrent Technology

Small-RNA sequencing by Ion Torrent method was performed by Primbio Research Institute (Exton, USA).

3.10.3.1. *Library Preparation and Next-generation sequencing*

cDNA libraries were constructed using Ion Total RNA-Seq Kit v2 from Life Technologies and manufacturers recommended protocol. miRNA samples were run on the microfluidics-based platform Agilent 2100 Bioanalyzer (Agilent Technologies, USA). to assess yield and size distribution of the RNAs, using the Agilent Small RNA Assay (Agilent Technologies, USA). 15 ng of miRNA was hybridized with Ion Adapters. The hybridized samples were then mixed with a reverse transcriptase master mix to generate cDNA libraries. The purified cDNA libraries were then amplified by PCR using Platinum PCR Super-Mix High Fidelity (Thermo Fisher, USA) and Ion Xpress Barcode reverse and forward primers (Thermo fisher, USA). The amplified cDNA libraries were purified using Nucleic

Acid binding beads, binding buffers and run on Agilent 2100 Bioanalyzer (Agilent Technologies, USA) to determine the yield and size distribution of each library.

Approximately 10 pM of pooled barcoded libraries were used for templating using Life Technologies Ion PI Template OT2 Solutions 200 Kit v3 (Life Technologies/Thermo fisher, USA) and manufacturers recommended protocol. The beads prepared for sequencing were loaded onto a pre-prepared and calibrated Ion P1 chip as directed by Life Technologies Ion P1 Sequencing 200 Kit v3(Life Technologies/Thermo FIsher, USA) protocol. The chip was placed into an Ion Proton sequencer (Life Technologies/Thermo FIsher, USA) and the run was started using Ion torrent miRNAseq run plan that was configured based on type of library, species, number of run flows required, type of plug-in required, adapter-trimming as well as other parameters specific to the miRNA-seq run.

The raw sequences were aligned to the human Hg19 building reference sequence by the Life Technologies Ion Torrent Suite. Aligned BAM files were used for further analysis. BAM files, separated by the specific barcodes, were uploaded to the Strand NGS software (Strand NGS, USA). Quality control was assessed by the Strand NGS program, which determined the pre- and post-alignment quality of the reads for each sample. The aligned reads were filtered based on alignment score, match count, mapping quality and average base quality

3.11. Bioinformatic analysis

Bioinformatic analysis and optimization of methodologies and procedures for differential expression and miRNA candidate identification were carried out by miss Dayme González Rodríguez as part of her master thesis entitled "*Estudio de mircroRNAs obtenidos en plasma mediante NGS como bimarcadores en Ataxia de Friedreich*".

The expression data from circulating miRNAs, were normalized using the trimmed mean of M-values (TMM) method[211]. Differential expression analysis was performed between patients and controls. The test used was based on exact statistical methods developed by Robinson and Smyth [212]. It was necessary to estimate miRNA-specific dispersion with a quantile-adjusted conditional maximum likelihood (qCML)

method[212,213]. Dysregulated miRNAs with an FDR of less than 1e-4 were used to calculate a correlation matrix. A logistic regression model with a LASSO penalty[214] was fitted with miRNAs that had a correlation level below 0.7. In order to select the most important miRNAs in the model, a leave-one-out cross validation was performed. All miRNAs that had non-zero coefficients at the value of λ that gave the minimum mean cross-validated error were selected.

On the other hand, differential expression analysis of proton run of cell lines miRNAs was performed using the packages EdgeR and DESeq 2 by means software R. The tests used were exactTest and binomial Wald Test, which are included in the packages of EdgeR and DESeq2, respectively. The results showed correspond to those, which were confident in both tests. For EdgeR, we first filtered those miRNAs that do not show any data of expression. Afterwards, the data were normalized using Calculate normalization factors to calculate the effective size of the library. We represented graphically using the package R by means non-supervised clustering.

Finally, all miRNAs have a large number of potential target sites. The computational approach to predicting miRNA targets helps to narrow down the potential candidates. In our approach, we first used DIANA-microT-CDS accessed from DIANA web server v5.0[215]. This tool shows whether the target was also predicted by miRanda or TargetScan or was experimentally validated in TarBase v7.0. We used the DIANA-miRPath v3.0 functional analysis online suite to identify miRNAs controlling significant molecular pathways annotated on Kyoto Encyclopaedia of Genes and Genomes (KEGG), using as default parameters: experimentally supported interactions from DIANA TarBase v.7.0; a p-value threshold of 0.001; and a microT threshold of 0.8. TargetScan was used to predict targets for hsa-miR-128-3p. To reduce the number of false positive miRNA targets, we applied a false discovery rate (FDR) correction to selected KEGG pathways. The algorithm used in this analysis was a one-tailed Fisher's exact test[216].

3.12.   Real-time qPCR validation of a novel miRNA signature from plasma of FRDA patients and healthy controls

Reverse transcription reactions were performed using TaqMan miRNA Reverse Transcription kit, miRNA-specific stem-loop primers (Part No. 4366597, Applied Biosystems. Inc, CA; US) and 100 ng of input cell-free RNA in 20 μL RT reaction. Real-time PCR reactions were performed in triplicate, in scaled-down 10 μL reaction volumes using 5 μL TaqMan 2x Universal PCR Master Mix (Applied Biosystems /Thermo FIsher, USA) with No UNG, 0.5 μL TaqMan Small RNA assay (20x) (Applied Biosystems /Thermo FIsher, USA) [hsa-miR-128-3p (002216), hsa-miR-625-3p (002432), hsa-miR-130b-5p (002114), hsa-miR-151a-5p (002642), hsa-miR-330-3p (000544), hsa-miR-323a-3p (002227), hsa-miR-142-3p (000464), hsa-miR-16-5p (000391), hsa-miR- 10b-5p (002218); hsa-mir-106b-3p (002380), hsa-mir-106b-5p (000442) and hsa-mir-15a-3p (002419)], 3.5 μL of nuclease free water and 1 μL of RT product. Real-time PCR was carried out on an Applied BioSystems 7900HT thermocycler Applied Biosystems /Thermo FIsher, US)) programmed as follows: 50°C for 2 minutes, 95°C for 10 minutes followed by 45 cycles of 95°C for 15 seconds and 60°C for 1 minute. One of the miRNAs with the most stable counting reads and previously used like endogenous control [217], miRNA hsa-miR-16-5p (000391) and RNU48 (001006), were used to normalize the expression data of plasma and cell lines, respectively, using the delta-delta CT method ($2^{-\Delta\Delta CT}$) [218].

3.13.   Validation of miRNAs as Biomarkers

To assess differences between patients and healthy controls and between different patient subgroups, we performed several statistical tests, using patient phenotype, age, sex, and disease onset as variables. Student's T tests and Mann-Witney tests were applied to compare miRNA fold-change values as a continuous variable in the different groups of study participants (healthy controls, FRDA patients with metabolic disorders and FRDA patients without metabolic disorders). Chi-square tests were employed to compare frequencies between the study groups when the fold-change was converted into a categorical variable (less than 2.5, greater than 2.5).

The coefficient of variation of miR-323a-3p was calculated by dividing the standard deviation by the mean. Variance stabilization was performed on our sequencing data before the coefficient of variation was calculated, as RNA-Seq data tend to follow the Negative Beta Binomial model, and so their SD tends to increase with mean. The data from the microarray datasets, meanwhile, were normalized using the RMA method[219].

The miRNA diagnostic test from each miRNA was validated by Receiver operating characteristic (ROC) curves analysis: area under the curve, diagnostic sensitivity and specificity, positive and negative predictive values. Optimal cut-off points were determined by highest sensitivity plus specificity and efficiency values.

P-values less than 0.05 were considered statistically significant. The data analysis was performed using SPSS version 20 (IBM Corporation).

3.14.   RT-qPCR for gene expression

Reverse transcription reactions were performed using High-Capacity cDNA Reverse Transcription Kit and 200 ng of input cell-free RNA in 20 µL RT reaction.

Real-time PCR reactions were performed in duplicate, in scaled-down 10 µL reaction volumes using 5 µL 2x TaqMan® Universal PCR Master Mix Applied Biosystems /Thermo FIsher, USA) and 0.5 µL TaqMan® Gene Expression Assays (20x) [*LDHA* gene (Hs01378790_g1); *PDHA1* gene (Hs01049345_g1); *FOXO1* gene (Hs00231106_m1); *SOD2* gene (Hs00167309_m1)] to gene expression. Real-time PCR was carried out on an Applied BioSystems 7900HT thermocycler Applied Biosystems /Thermo FIsher, USA) programmed as follows: 50°C for 2 minutes, 95°C for 10 minutes followed by 40 cycles of 95°C for 15 seconds and 60°C for 1 minute. *GAPDH* gene (Hs02786624_g1) was used to normalize the expression data, using the delta-delta CT method ($2^{-\Delta\Delta CT}$) [218].

3.15.   Statistics analysis

For the statistical analysis of the results, the mean was taken as the measurement of the main tendency, and standard deviation (SD) was taken as the

dispersion measurement. Normality test were used for each evaluated parameter in order to use the proper comparison test (Student's t test or Mann–Whitney U test). Statistical differences were assumed when p-value of appropriate comparison test was under 0.05 (*).

4. Results

4.1. Biomarkers in Charcot-Marie-Tooth disease

4.1.1. Patients description

PMP22 duplication was confirmed by genetic study in the 46 CMT1A patients recruited for this work; patients showed no comorbidity that could contribute to the neuropathy. Patients with CMTNS <15 were grouped into mild CMT patients (25) and those with CMTNS > 15 were assigned to severe CMT patients group (21). Table 7 shows age, gender, and CMTNS distribution for each group. As we expected in a neurodegenerative disease, when we grouped the patients by CMTNS, the group with a higher CMTNS (severe group) had also increased age mean (51 years) than mild group (37 years; table 7). In mild group there were less men (29%) than in severe group, in which the presence of men was similar to women (48 %) (Table 7).

22 healthy subjects without neurodegenerative diseases or associated diseases were also participants of this study. 12 healthy volunteers were men (55%), and the mean age of the participants was 43 years (range: 16-56 years).

Table 7. Demographic and clinical features of CMT1A patient's groups and control group.

	Mild *(n=25)*	*Severe* *(n=21)*	*Control* *(n=22)*
Age (mean/range)	37 years (3-67)	51 years (20-75)	43 years (12-65)
Sex (M/F)	7 (28%)/18 (72%)	10 (48%)/11 (52%)	12 (55%)/10 (45%)
CMTNS (mean/range)	9.28 (2-15)	20.52 (16-28)	-

4.1.2. Oxidative stress markers

Plasma samples from CMT patients and control subjects were analysed to evaluate different oxidative stress markers. Oxidative stress protein markers, such as carbonylation and nitrosylation, were determined in both groups of CMT patients and in control samples, but no differences were observed among the three groups (Figure 10 a and b, respectively). Moreover, we analysed fatty acids peroxidation as a marker of oxidative stress by measuring malondialdehyde (MDA) levels. The results showed similar levels in all groups analysed (Figure 10c). In addition, we performed analysis

to determine total antioxidant capacity in patients and control subjects and no differences were observed among groups (Figure 10d). Finally, we determined levels of total glutathione (GSH) and the ratio between reduced GSH and its oxidized form (GSSG) (Figure 10e and 10f, respectively). These data showed that there were no significant differences in oxidative stress markers in plasma neither in mild and severe CMT patients nor in CMT1A patients and control subjects.
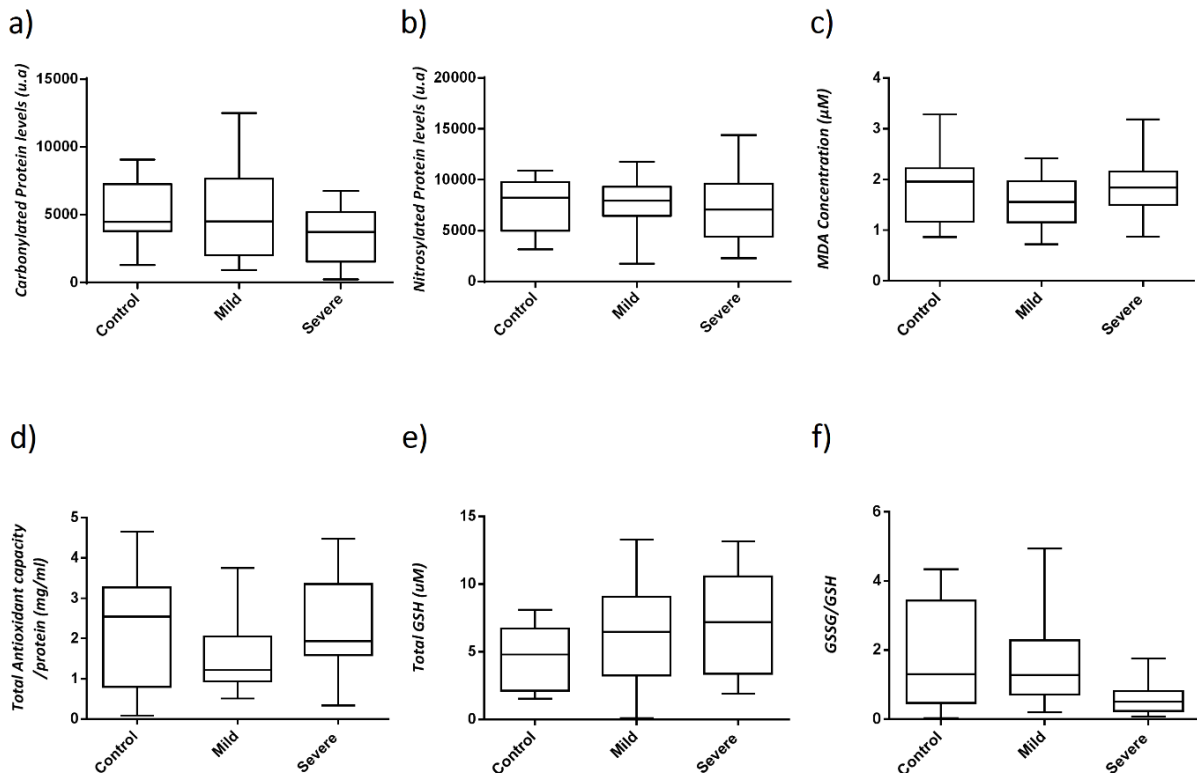
Figure 10. Oxidative stress markers in plasma of mild CMT1A patients group, severe CMT1A patients group, and control group. a) Densitometry of carbonylated protein levels analysed by dot-blotting b) Densitometry of nitrosylated protein levels analysed by dot-blotting c) Malondialdehyde (MDA) levels analysed by HPLC-UV chromatography d) Total antioxidant activity per protein concentration (mg/ml) measured by Total antioxidant activity kit and BCA kit e) Total GSH (µM) levels obtained with "The DetectX Glutathione kit" f) GSSG/GSH ratio analysed with "The DetectX Glutathione kit". All results are represented as mean ± SD.

4.1.3. Proteomic biomarkers

Plasma samples contain a large number and diversity of proteins. In order to detect proteomic biomarkers that may be used as prognostic markers of Charcot-Marie-Tooth disease, we performed a 2D-DIGE analysis. 6 selected samples of each group (Table 6) were run in 6 different gels in the same electrophoresis experiment for mild CMT group and control (mild/control) and severe CMT group and control

(severe/control). We obtained fluorescence levels in all groups analysed for each experiment. All the different fluorescence intensity peaks for each experiment (mild versus control or severe versus control) are shown in appendix figure 1 and appendix figure 2. Differential expression protein spots and their localization in the gel were obtained (Figure 11a). In the mild CMT group eight proteins were detected with differential expression. Among those proteins, four were up-regulated and four were down-regulated (Figure 11b left). In severe CMT group thirty-six proteins were detected with differential expression when we compared it with control group, and fourteen proteins were up-regulated and twenty-two proteins were down-regulated (Figure 11b right).
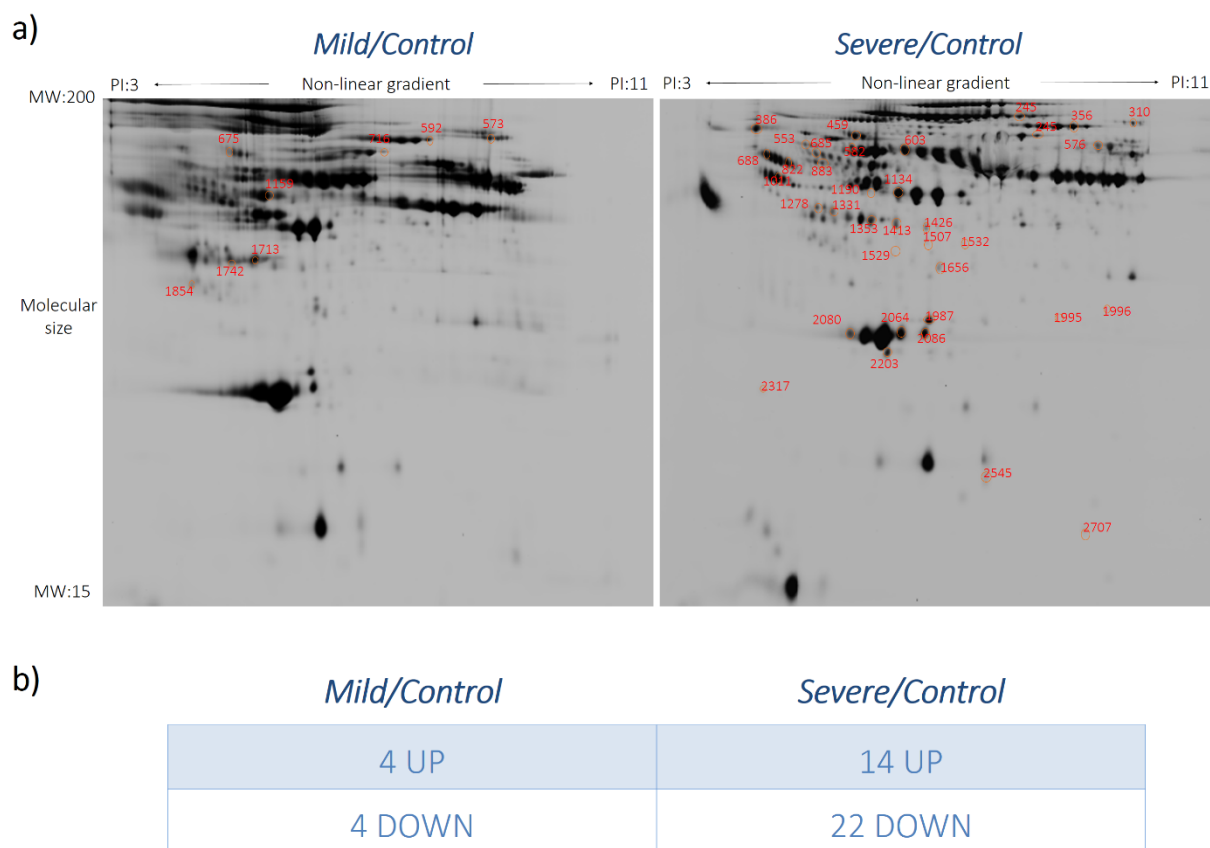
Figure 11. Differential protein expression analysis performed by 2D-DIGE analysis. a) Representation of localization of differential expression proteins in mild CMT group against control group (left panel) and representation of localization of differential expression proteins in severe CMT group against control group (right panel). Circles represent the localization the protein in the gel and number are ID of the unknown proteins. b) Number of proteins upregulated (UP) and downregulated (DOWN) in mild (left) and severe (right) CMT group against control group.

In order to determine which protein corresponds to each spot detected in the 2D-DIGE analysis, we performed mass spectrometry or liquid chromatography tandem-mass spectrometry. All data retrieved from the protein spot are shown in

appendix table 1 and table 2. We summarized the results of each protein obtained from the study of differential expression and its average ratio in Table 8.

The proteomic analysis identified some proteins with differential expression in both experimental groups (Mild vs. Control and Severe vs. Control): plasminogen, complement factor B, afamin, gelsolin, apolipoprotein A-AV, and haptogloblin. Levels of plasminogen were downregulated in mild CMT group and also in severe CMT group. Same pattern was observed in complement factor B protein levels and afamin protein levels. However, we detected high levels of apolipoprotein A-IV and haptoglobin in both mild and severe CMT group compared with control group. Some spots were identified as the same protein; this may be explained with the different post-translational modifications of proteins, such as phosphorylation, that could alter the isoelectric point of the proteins and also generate an electrophoretic mobility shift. Finally, gelsolin levels were upregulated in mild CMT group but it was downregulated in severe CMT group. The rest of identified proteins only appeared in one of the experimental groups: only 2 proteins were detected in Mild CMT patient's vs Control group, whereas 12 proteins were observed only in Severe CMT patient's vs Control group.

Table 8. List of Identified proteins by mass spectrometry and liquid chromatography in both experiments mild CMT group with control group (Mild/Control), and severe CMT group with control group (Severe/Control). Table shows protein name, protein identification code in Uniprot database, gene identification code and average ratio of differential expression measured in a 2D-DIGE analysis.

Protein	ID Uniprot	ID Gene	Mild/Control Average Ratio	Severe/Control Average Ratio
Plasminogen	PLMN_HUMAN	PLG	-1,48	-1,89
Complement factor B	CFAB_HUMAN	CFB	-1,86	-2,60
				-2,48
Afamin	AFAM_HUMAN	AFM	-1,51	-1,95
Gelsolin	GELS_HUMAN	GSN	1,99	-1,72
Antithrombin-III	ANT3_HUMAN	SERPINC1	1,47	
Apolipoprotein A-IV	APOA4_HUMAN	APOA4	1,59	2,99
Haptoglobin	HPT_HUMAN	HP	2,28	2,25
				3,36
				2,91
				3,15
				4,93
				4,38
				6,89
Clusterin	CLUS_HUMAN	CLU	-1,33	
Complement component C6	CO6_HUMAN	C6		-2,17
Fibrinogen gamma chain	FIBG_HUMAN	FGG		-2,47
Vitronectin	VTNC_HUMAN	VTN		-2,95
Serotransferrin	TRFE_HUMAN	TF		-2,65
				-1,68
Kininogen-1	KNG1_HUMAN	KNG1		-1,69
				-2,54
Alpha-1B-glycoprotein	A1BG_HUMAN	A1BG		-1,70
Alpha-1-antitrypsin	A1AT_HUMAN	SERPINA1		5,34
Alpha-2-HS-glycoprotein	FETUA_HUMAN	AHSG		-2,17
Vitamin D-binding protein	VTDB_HUMAN	GC		7,05
Apolipoprotein E	APOE_HUMAN	APOE		-1,98
Ig kappa chain C region	IGKC_HUMAN	IGKC		9,75
				10,13
Apolipoprotein A-I	APOA1_HUMAN	APOA1		-1,82
				-1,64
				-1,93

With the aim of determining which proteins were more relevant in PMP22 duplication context, we analysed interactions previously described between differential expressed proteins genes and PMP22 gene. First, we analysed, using PhenUMA software, the interactions between PMP22 and other genes that could have any phenotypic and functional relationship. We observed that PMP22 has phenotypic association with other genes, most of them mutated in other types of CMT, as shows figure 12. These genes generate similar phenotype when the protein, which they encode is mutated. Moreover, we showed other kind of interactions between genes phenotypically related to PMP22: protein-protein interactions, biological process co-association, and cellular co-localization. However, direct relationship between the mutated gene and genes of differential expression proteins previously detected were not observed.
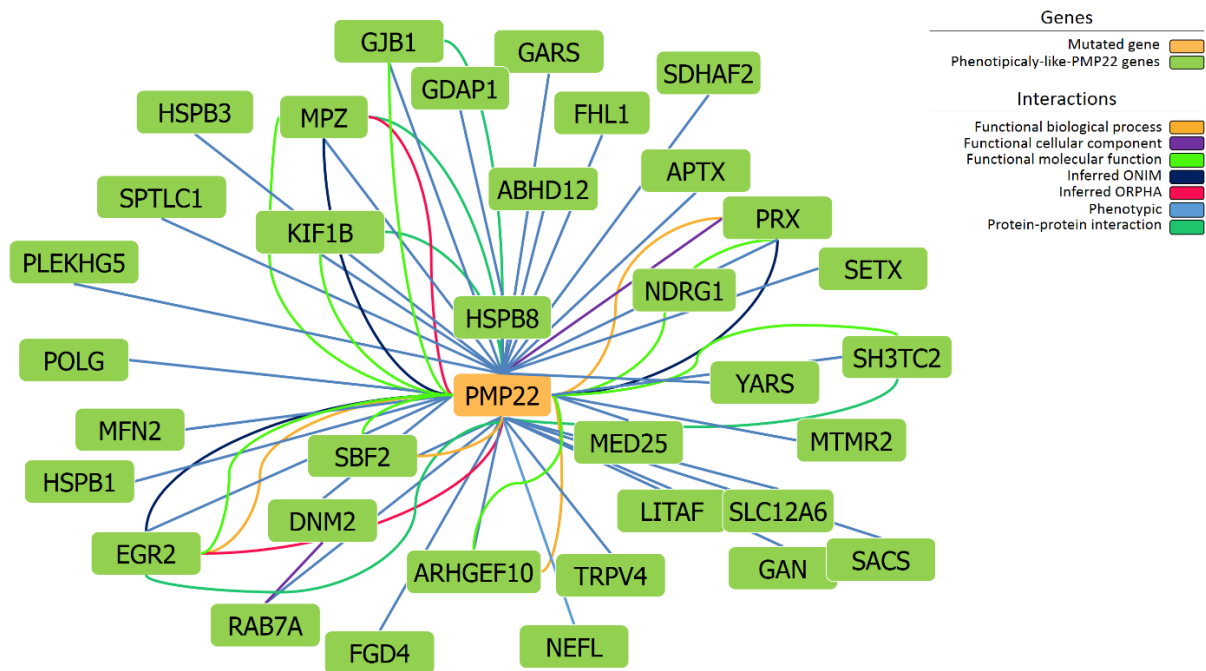
Figure 12. Interactions of PMP22 with other genes. Boxes represent mutated gene PMP22 and genes with phenotypic relationship with PMP22. Lines represent interactions between genes (see legend for details). glycyl-tRNA synthetase (GARS); ganglioside induced differentiation associated protein 1 (GDAP1); gap junction protein Beta 1 (GJB1); myelin protein zero (MPZ); heat shock protein family B (Small) member 3 (HSPB3); serine palmitoyltransferase long chain base subunit 1 (SPTLC1); four and a half LIM domains 1 (FHL1); succinate dehydrogenase complex assembly factor 2 (SHDAF2); ataxin (APTX); abhydrolase Domain Containing 12 (ABHD12); kinesin family member 1B (KIF1B), periaxin (PRX); pleckstrin homology and RhoGEF domain containing G5 (PLEKHG5); senataxin (SETX); N-myc downstream regulated 1 (NDRG1); heat shock protein family B member 8 (HSPB8); DNA polymerase Gamma, catalytic subunit (POLG); SH3 domain and tetratricopeptide repeats (SH3TC2); tyrosyl-tRNA synthetase (YARS); mitofusin 2 (MFN2); mediator complex subunit 25 (MED25); myotubularin related protein 2 (MTMR2); SET binding factor 2 (SBF2); heat shock protein family B member 1 (HSPB1); dynamin 2 (DNM2); lipopolysaccharide induced TNF factor (LITAF); solute carrier family 12 member 6 (SLC12A6); early frowth response 2 (EGR2); Rho guanine nucleotide exchange factor 10 (ARHGEF10); transient receptor potential cation channel subfamily V member 4 (TRPV4); gigaxonin (GAN); sacsin molecular chaperone (SACS); member RAS oncogene family (RAB7A); RhoGEF and PH domain containing 4 (FGD4); neurofilament Light (NEFL).

For these reason, in order to detect indirect relationships between PMP22 and proteins with differential expression detected in 2D-DIGE experiments, we performed a new PhenUMA analysis using those genes phenotypically related to PMP22 (Figure 12) and those genes from proteins differentially expressed in CMT1A groups. We considered indirect relationship when we detected an association between two genes through other gene. We obtained indirect interactions of PMP22 gene with genes of differentially expressed proteins, through genes with similar phenotype to PMP22 (Figure 13). From the interactome showed in figure 13 we observed that some proteins were directly related to genes with similar phenotype to PMP22: serotrasferrin receptor (TF); alpha-1-antitrypsin (SERPINA1); antithrombin-III (SERPINC1); alpha-2-HS-glycoprotein (AHSG); clusterin (CLU); apolipoprotein E (APOE);

gelsolin (GSN); apolipoprotein A1 (APOA1); vitamin D-binding protein (GC); plasminogen (PLG); complement factor B (CFB); apolipoprotein A-IV (APOA4); haptoglobin (HP); complement component C6 (C6), fibrinogen gamma chain (FGG); vitronectin (VTN) and kininogen-1 (KNG1).
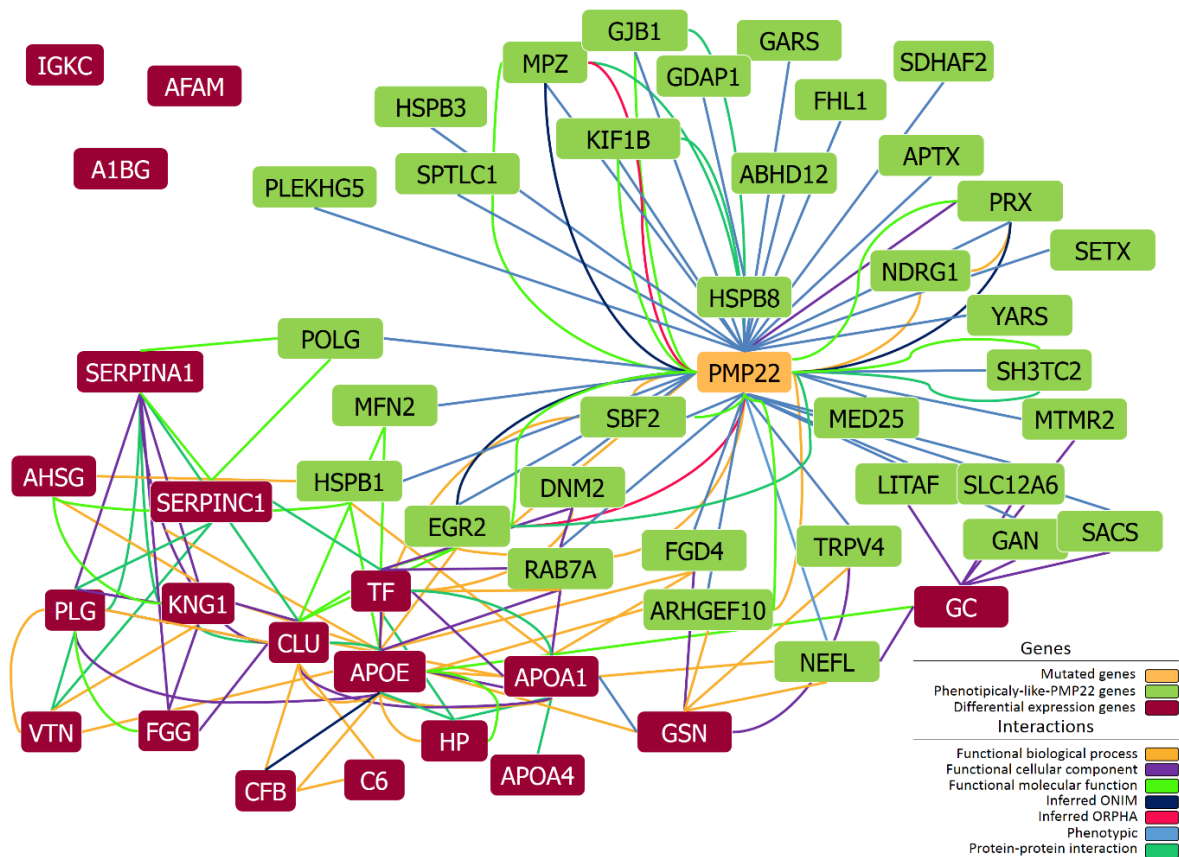

Figure 13. Interactions of PMP22 with genes of differential expressed proteins through genes with similar phenotype to PMP22. Boxes represent mutated gene (PMP22), genes with phenotypic relationship with PMP22, and genes from differential expressed proteins. Lines represent different interactions between genes (See legend for details). glycyl-tRNA synthetase (GARS); ganglioside induced differentiation associated protein 1 (GDAP1); gap junction protein Beta 1 (GJB1); myelin protein zero (MPZ); heat shock protein family B (Small) member 3 (HSPB3); serine palmitoyltransferase long chain base subunit 1 (SPTLC1); four and a half LIM domains 1 (FHL1); succinate dehydrogenase complex assembly factor 2 (SHDAF2); aprataxin (APTX); abhydrolase Domain Containing 12 (ABHD12); kinesin family member 1B (KIF1B), periaxin (PRX); pleckstrin homology and RhoGEF domain containing G5 (PLEKHG5); senataxin (SETX); N-myc downstream regulated 1 (NDRG1); heat shock protein family B member 8 (HSPB8); DNA polymerase Gamma, catalytic subunit (POLG); SH3 domain and tetratricopeptide repeats (SH3TC2); tyrosyl-tRNA synthetase (YARS); mitofusin 2 (MFN2); mediator complex subunit 25 (MED25); myotubularin related protein 2 (MTMR2); SET binding factor 2 (SBF2); heat shock protein family B member 1 (HSPB1); dynamin 2 (DNM2); lipopolysaccharide induced TNF factor (LITAF); solute carrier family 12 member 6 (SLC12A6); early frowth response 2 (EGR2); Rho guanine nucleotide exchange factor 10 (ARHGEF10); transient receptor potential cation channel subfamily V member 4 (TRPV4); gigaxonin (GAN); sacsin molecular chaperone (SACS); member RAS oncogene family (RAB7A); RhoGEF and PH domain containing 4 (FGD4); neurofilament Light (NEFL); serotrasferrin receptor (TF); alpha-1-antitrypsin (SERPINA1); antithrombin-III (SERPINC1); alpha-2-HS-glycoprotein (AHSG); clusterin (CLU); apolipoprotein E (APOE); gelsolin (GSN); apolipoprotein A1 (APOA1); vitamin D-binding protein (GC); plasminogen (PLG); complement factor B (CFB); apolipoprotein A-IV (APOA4); haptoglobin (HP); complement component C6 (C6), fibrinogen gamma chain (FGG); vitronectin (VTN); kininogen-1 (KNG1); afamin (AFAM); alpha-1-B glycoprotein (A1BG); immunoglobulin Kappa constant (IGKC).

Taking together the results from table 8 and Figure 13, gelsolin was the only protein that has a direct interaction with some genes with similar phenotype to PMP22 and also differential expression in mild CMT/Control and severe CMT/Control 2D-DIGE experimental groups. Moreover, Paunio *et. al*. detected altered gelsolin levels in serum from patients with familial amyloidosis, Finnish type, when compared with serum of healthy subject [220].

Therefore, we decided to perform experimental analysis with the aim of confirm differential expression of gelsolin observed in 2D-DIGE experiments. Enzyme-Linked Immunoassays (ELISA) were performed to detect levels of this protein in plasma samples of mild CMT1A patients, severe CMT1A patients and healthy subjects. Concentration of gelsolin was normalized with the total concentration of proteins in each sample. On the contrary to 2D-DIGE experiments we did not detect any significant difference between the three groups analysed (Figure 14a). In addition, we performed correlational analysis in order to determine if gelsolin levels showed a dependence with age of subjects (Figure 14b) as occurs in familial amyloidosis, Finnish type[220].
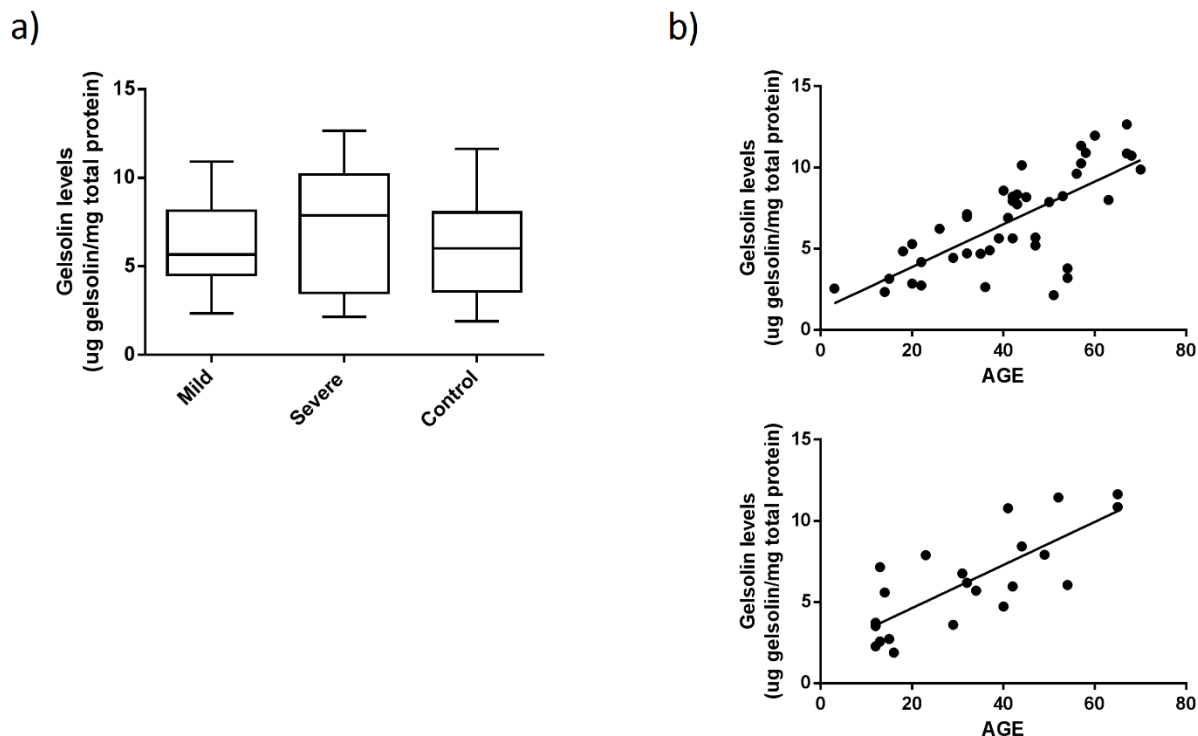

Figure 14. Gelsolin levels in plasma samples of CMT1A patients and healthy subjects analysed by ELISA assays. a) Gelsolin levels in mild CMT group (Mild), severe CMT group (Severe), and healthy subjects (Control). Results represent mean ± SD. b) Correlation between gelsolin levels and age in CMT1A patients (upper panel) and healthy subjects (bottom panel).

We detected a slight correlation between age and gelsolin levels in CMT1A patients ($r^2 = 0.5262$) but not significant enough to confirm that there exists an interdependence of gelsolin levels with age in patients (Figure 14b upper panel), because only 52.62% of changes in gelsolin levels could be explained by age. Furthermore, we analysed this correlation in samples from healthy controls. We detected a correlation between gelsolin levels and age in control samples ($r^2 = 0.6029$; figure 14b bottom panel) but as it was observed for patients, coefficients were not significant enough to clearly confirm a correlation between gelsolin levels and age. As in the work by Paunio *et. al.* [220], there was not strong data to confirm a correlation between gelsolin levels and age in control samples.

4.2. Biomarkers in Friedreich's ataxia

4.2.1. Epigenetic Biomarkers in different models of FRDA

4.2.1.1. *Identification of differentially expressed miRNAs using NGS*

miRNA samples of three different human cell lines (fibroblasts, olfactory mucosa stem cells, and frataxin deficient model in SH-SY5Y cell) were analysed by NGS.

First, we performed an exploration of the expression levels of all miRNAs in the three different human cell lines, and the analysis showed how these three lines were separated from each other (Figure 15) according to miRNA expression levels. Moreover, as presented in figure 15, olfactory mucosa stem cells from patients (OFRDA1 and OFRDA2) showed similar expression levels of miRNAs between them, and this expression pattern was different from control cell line (OControl1). SH-SY5Y cell lines (pLKO) and frataxin deficient cell lines (FXN-138.1 and FXN-138.2) showed a similar behaviour than in stem cells.
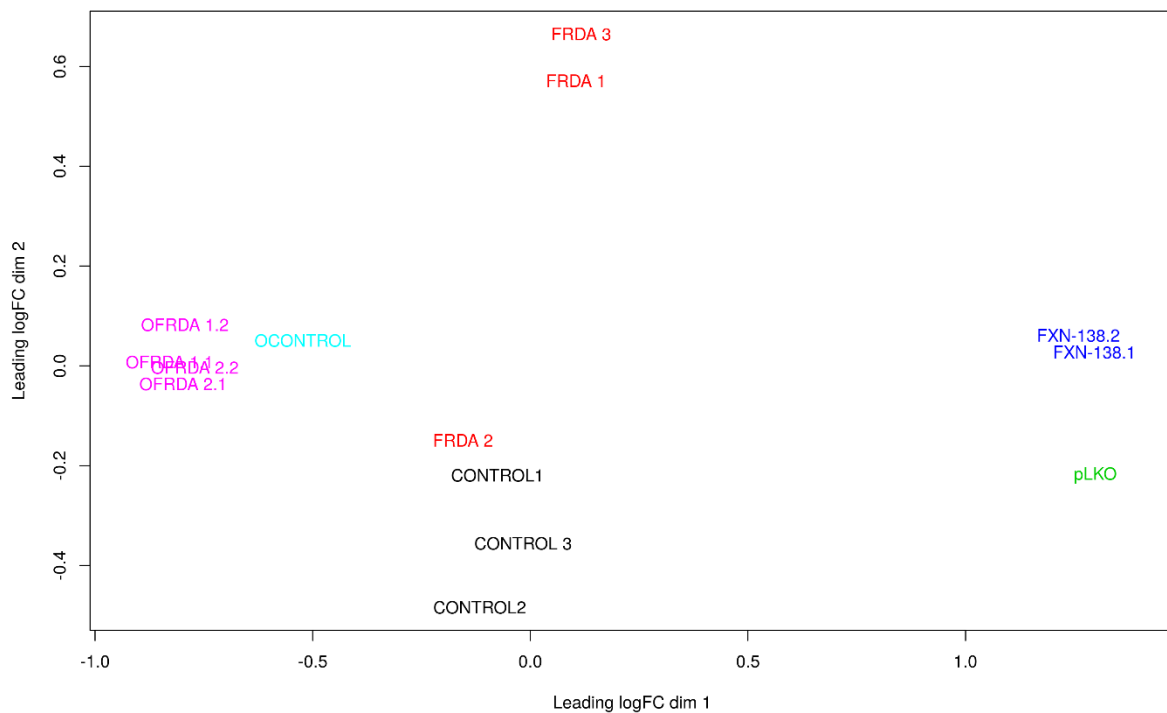
Figure 15. Multidimensional scale plot with all miRNAs and samples of fibroblasts (middle), olfactory mucosa stem cells (left), and frataxin deficient model in SH-SY5Y cells (right). Expression levels of all miRNAs permit to differentiate cell lines analysed, and also inside of each cell line those from patients or frataxin deficient model from their respective control. Just one sample from human fibroblasts (FRDA2) was misclassified. Red colour indicates samples from patients or frataxin deficient model; blue colour indicates samples from controls.

Finally, human fibroblasts samples of patients (FRDA1 and FRDA3) presented different miRNAs expression levels when compared to control samples (Control 1, Control 2, and Control 3). However, miRNA profiles of sample FRDA2 resembles more controls than the miRNA expression profiles showed by patients FRDA1 and FRDA3. We analysed only fibroblasts samples and we observed that FRDA2 showed similar miRNAs expression levels to control samples (Control 1 and Control 2), instead of patient's samples (FRDA1 and FRDA3). Also Control 3 showed different expression level of miRNAs to other controls (Figure 16).
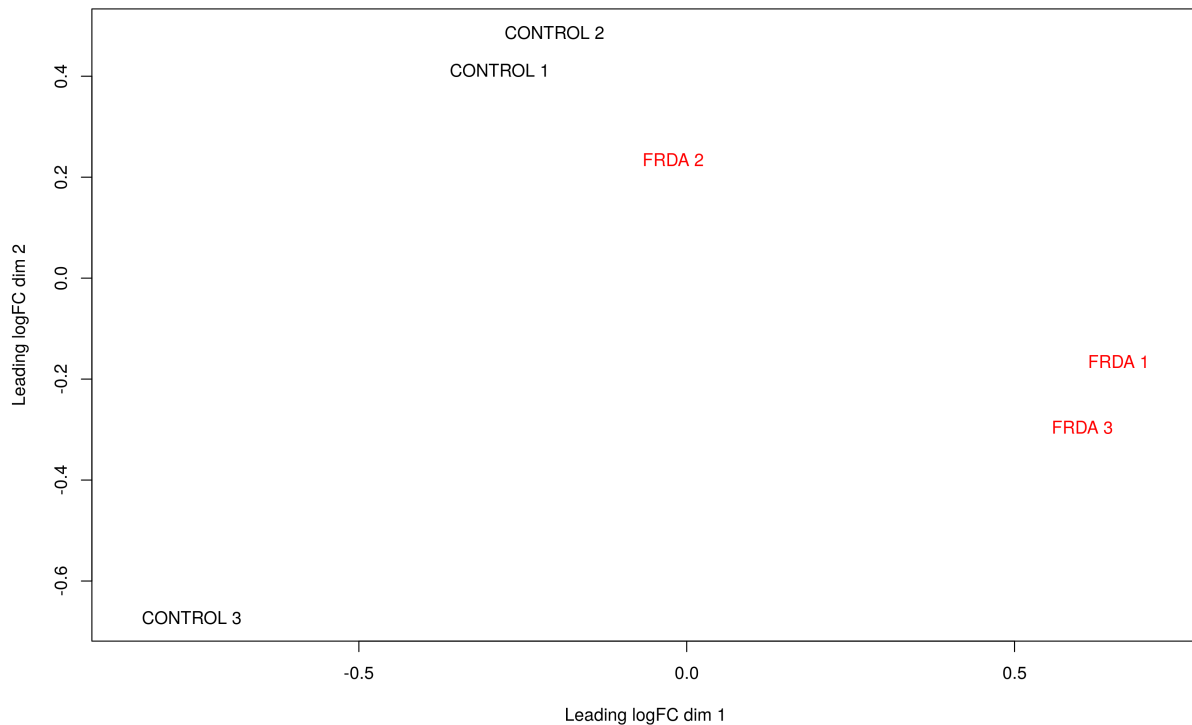
Figure 16. Multidimensional scale plot with all miRNAs and samples of fibroblasts. Expression levels of all miRNAs permit to differentiate control samples (FRDA1 and FRDA2) from patient's fibroblasts (FRDA1 and FRDA3). FRDA2 and Control 3 were misclassified. Red colour indicates samples from patients or frataxin deficient model; blue colour indicates samples from control.

Differential expression analysis between FRDA samples and controls for each cell line was performed. In olfactory mucosa stem cells, differential expression analysis between samples from FRDA cells and controls showed twenty-three miRNAs with differential expression: thirteen were downregulated (hsa-let-7a-2-3p, hsa-miR-15a-3p, hsa-miR-140-5p, hsa-miR-301a-5p, hsa-miR-24-2-5p, hsa-miR-27a-5p, hsa-miR-93-5p, hsa-miR-93-3p, hsa-miR-106b-5p, hsa-miR-106b-3p, hsa-miR-7-1-3p, hsa-let-7d-3p, and hsa-miR-452-3p) and ten were upregulated (hsa-miR-625-3p, hsa-miR-665, hsa-miR-127-3p, hsa-miR-370, hsa-miR- 494, hsa-miR-134, hsa-miR-409-3p, hsa-miR-146a-5p, hsa-miR-31-5p, and has-miR-31-3p; figure 17).

Figure 17. Heat map of differential expressed miRNAs in samples of olfactory mucosa stem cells. Differential expression oft-three miRNAs separate samples of olfactory mucosa stem cells from patients (red line) and olfactory mucosa stem cells from control (blue line).

SH-SY5Y cell model showed thirty-six miRNAs with differential expression between control (pLKO) and frataxin-deficient cell model (FXN-138.1 and FXN-138.2), when differential expression analysis was performed (Figure 18). Fourteen miRNAs showed reduced expression levels (hsa-miR-483-5p, hsa-miR-483-3p, hsa-miR-19b-1-5p, hsa-miR-337-5p, hsa-miR-337-3p, hsa-miR-376a-3p, hsa-miR-409-3p, hsa-miR-1247-5p, hsa-miR-1247-3p, hsa-miR-375, hsa-miR-296-3p, hsa-miR-301b, hsa-miR-3200-3p, and hsa-miR-3619-5p) and twenty-two showed increased expression levels (hsa-miR-34a-5p, hsa-miR-34a-3p, hsa-miR-199a-3p, hsa-miR-181b-3p, hsa-miR-125b-5p, hsa-miR-125b-1-3p, hsa-miR-21-5p, hsa-miR-21-3p, hsa-miR-26b-5p, hsa-miR-26b-3p, hsa-miR-26a-1-3p, hsa-let-7g-3p, hsa-miR-218-5p, hsa-miR-218-1-3p, hsa-miR-182-5p, hsa-miR-183-5p, hsa-miR-183-3p, hsa-miR-490-3p, hsa-miR-27b-3p, hsa-miR-500a-5p, hsa-miR-500a-3p, and hsa-miR-500b).
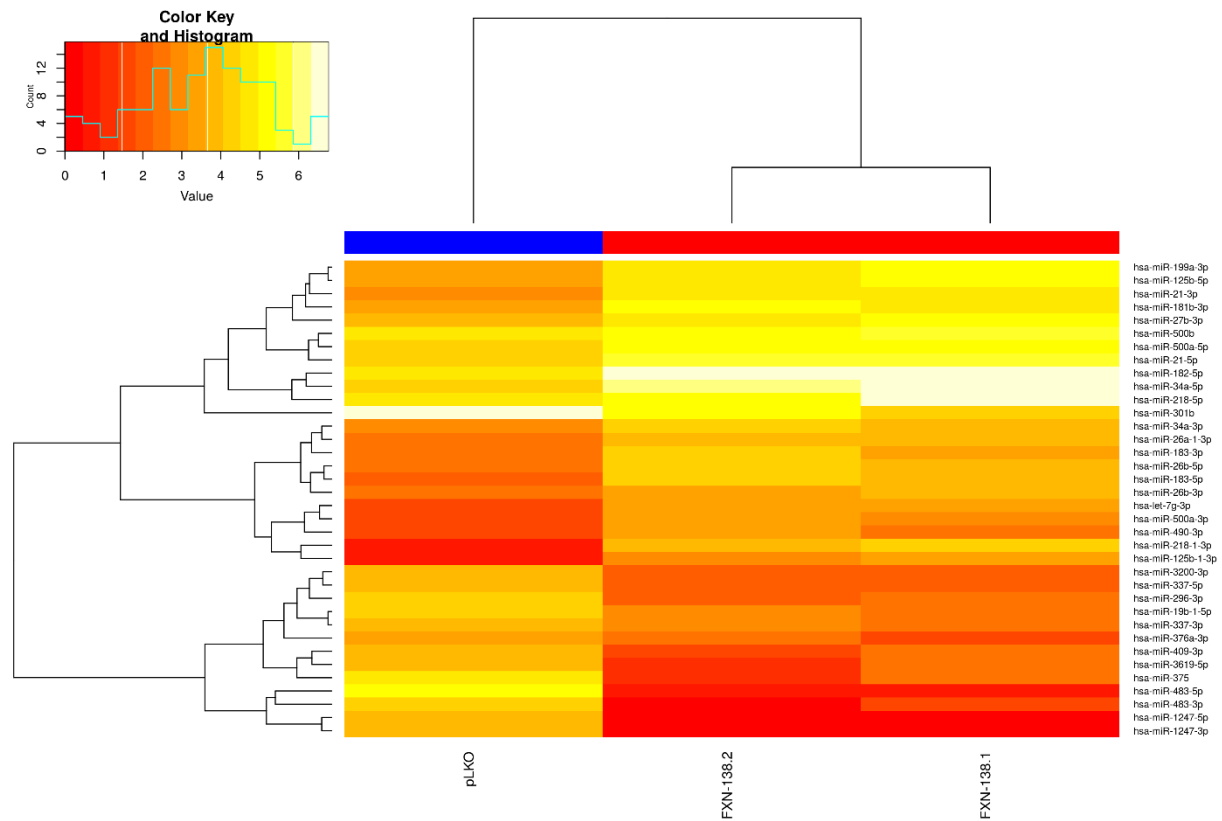
Figure 18. Heat map of differential expressed miRNAs in samples of SH-SY5Y cell models. Differential expressions of thirty-six miRNAs separate samples of frataxin-deficient cell lines (red line) and pLKO control (blue line).

Finally, differential expression analysis in fibroblasts cell line showed that seven miRNAs separate patient's fibroblasts from control's fibroblasts; two miRNAs (hsa-miR-3184-5p and hsa-miR-3529-3p) showed downregulated expression levels and five miRNAs (hsa-miR-143-3p, hsa-miR-22-3p, hsa-miR-423-3p, hsa-miR-532-5p, and hsa-miR-10b-5p) showed upregulated expression levels (Figure 19).

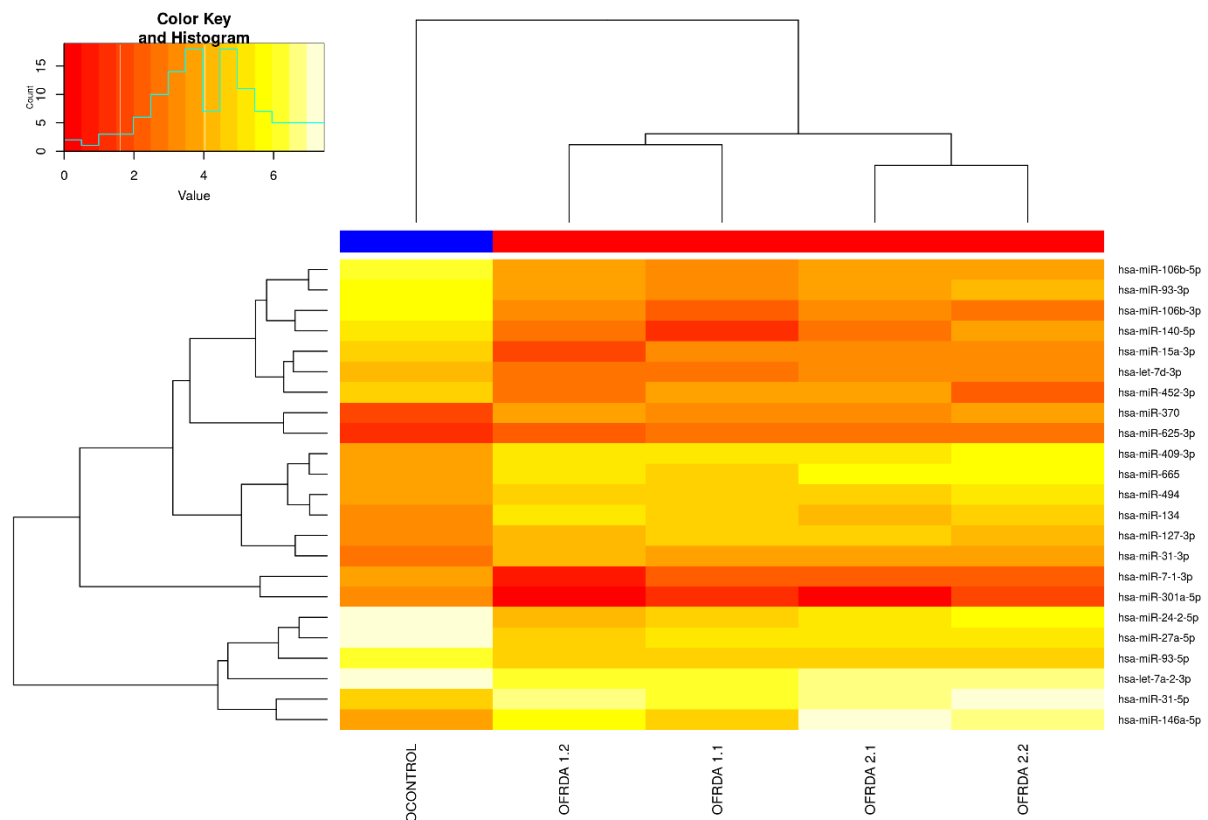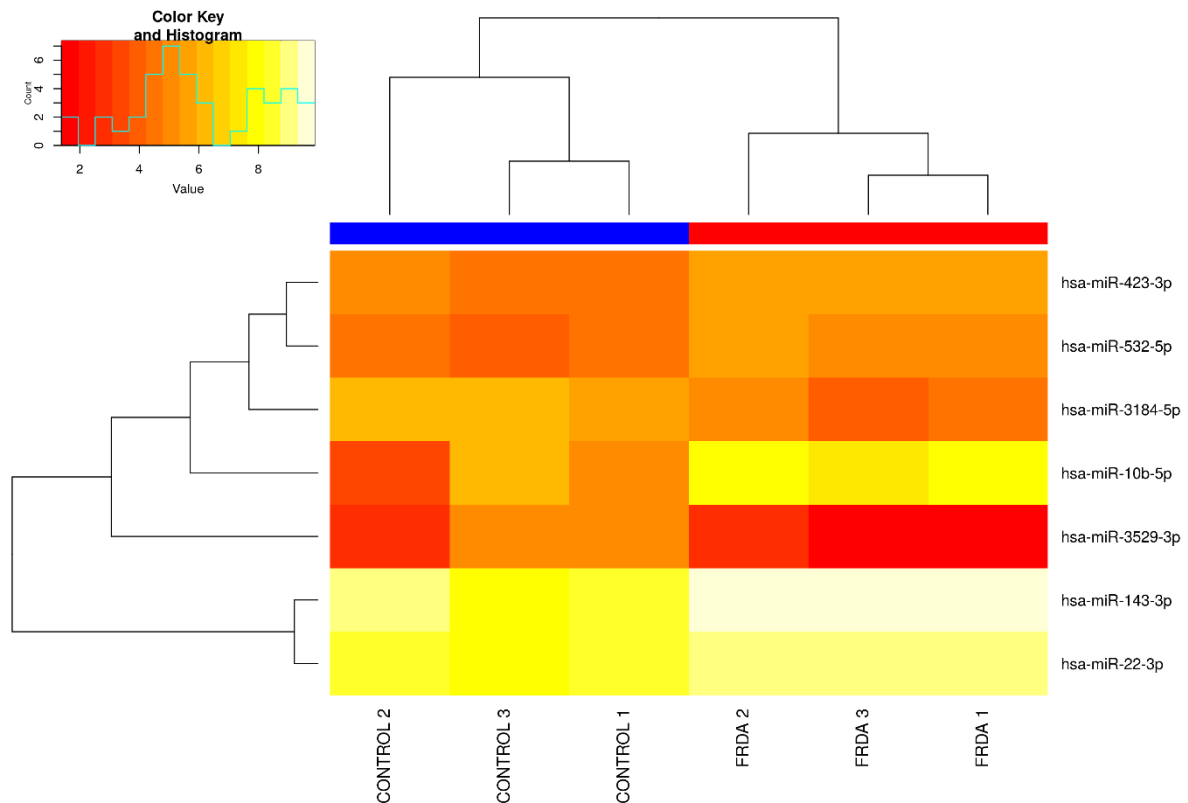**Figure 19. Heat map of differential expressed miRNAs in samples of fibroblasts.** Differential expressions of seven miRNAs separate samples of fibroblasts from patients (red line) and fibroblasts from control (blue line).

Afterwards, we looked for coincidences among miRNA profiles in three cell lines studied (i.e. fibroblasts, olfactory mucosa stem cells and SH-SY5Y).

Comparing the expression profiles of fibroblasts and SH-SY5Y cell models with their respective controls, we observed differential expression only for hsa-miR-10b-5p in both cell types.

When miRNA profiles were compared between olfactory mucosa stem cells an SH-SY5Y, hsa-miR-409-3p, hsa-miR-3117-3p, hsa-miR-106b-3p, hsa-let-7a-2-3p, hsa-miR-15a-3p, and hsa-miR-106b-5p showed differential expression in both cell lines. However, we did not observe any common miRNA between fibroblasts and olfactory mucosa stem cells. In addition, we did not find any miRNA, which was differentially expressed at the same time in each cell line versus its control.

4.2.1.2.   Validation of the differentially expressed miRNAs by RT-qPCR

In order to validate results from NGS by RT-qPCR, four miRNAs were selected by its expression profile (Table 9). These miRNAs were analysed in olfactory mucosa stem cell line: control cell line (n=3) and patients (OFRDA1 and OFRDA2; n=3 each); also in frataxin-deficient models: SH-SY5Y control (n=3), pLKO control (n=3), FXN-138.1 (n=3), and FXN-138.1 (n=3); and finally, in fibroblasts cell lines from FRDA patients (FRDA1, FRDA2, and FRDA3; n=2 each) and controls (CONTROL 1, CONTROL 2, and CONTROL 3; n=2 each). Expression levels were calculated for each miRNA using RNU-48 (small-nucleolar RNA 48) as an endogenous control due to its previously reported use [221-223] and its stable threshold cycle (Ct) values in all the samples analysed by RT-qPCR.

Table 9. miRNAs selected as biomarkers for FRDA cell lines.

miRNA name	Mature sequence	Accession
hsa-miR-10b-5p	uacccuguagaaccgaauuugug	MIMAT0000254
hsa-miR-106b-3p	ccgcacuguggguacuugcugc	MIMAT0004672
hsa-miR-106b-5p	uaaagugcugacagugcagau	MIMAT0000680
hsa-miR-15a-3p	caggccauauugugcugccuca	MIMAT0004488

Expression levels of selected miRNAs in olfactory mucosa stem cell showed similar profile to those observed in NGS analysis. We found that miR-106b-3p, miR-106-5p, and miR-15a-3p showed decreased expression levels in samples of patients (OFRDA1 and OFRDA2) compared to control samples (OCONTROL) in both NGS and RT-qPCR analysis (Figure 20b, 20, and 20d, respectively). However, increased levels for miR-10b-5p were detected in RT-qPCR analysis, which were not observed by NGS analysis. Instead of that decrement, we did not detect differences between patients and control samples (Figure 20a).

Figure 20. Relative expression levels of the miRNAs with different expression levels found in olfactory mucosa stem cells. Levels of a) miR-10b-5p; b) miR-106b-3p; c) miR-106b-5p; d) miR-15a-3p in control cell line (OCONTROL; n=3) and patients (OFRDA1 and OFRDA2; n=3 each). All results are represented as mean ± SD. * indicates p-values <0.05; ** indicates p-values <0.01; *** indicates p-values<0.0001.

In contrast, when we performed RT-qPCR analysis of frataxin-deficient cell models we found a different expression profile than in NGS analysis. Only miR-10b-5p results coincided with that obtained by NGS analysis in which miR-10b-5p showed upregulated levels in both frataxin-deficient cell lines (FXN-138.1 and FXN-138.2) compared to control cell lines (Figure 21a). We found that miR-106b-5p and miR-15a-3p did not show differential expression between control cell line and patient cell lines (Figure 21c and 21d, respectively). On the contrary to NGS analysis, miR-106-3p showed decreased levels in frataxin-deficient cell lines compared to control cell lines (Figure 21b).

a)

b)

c)

d)
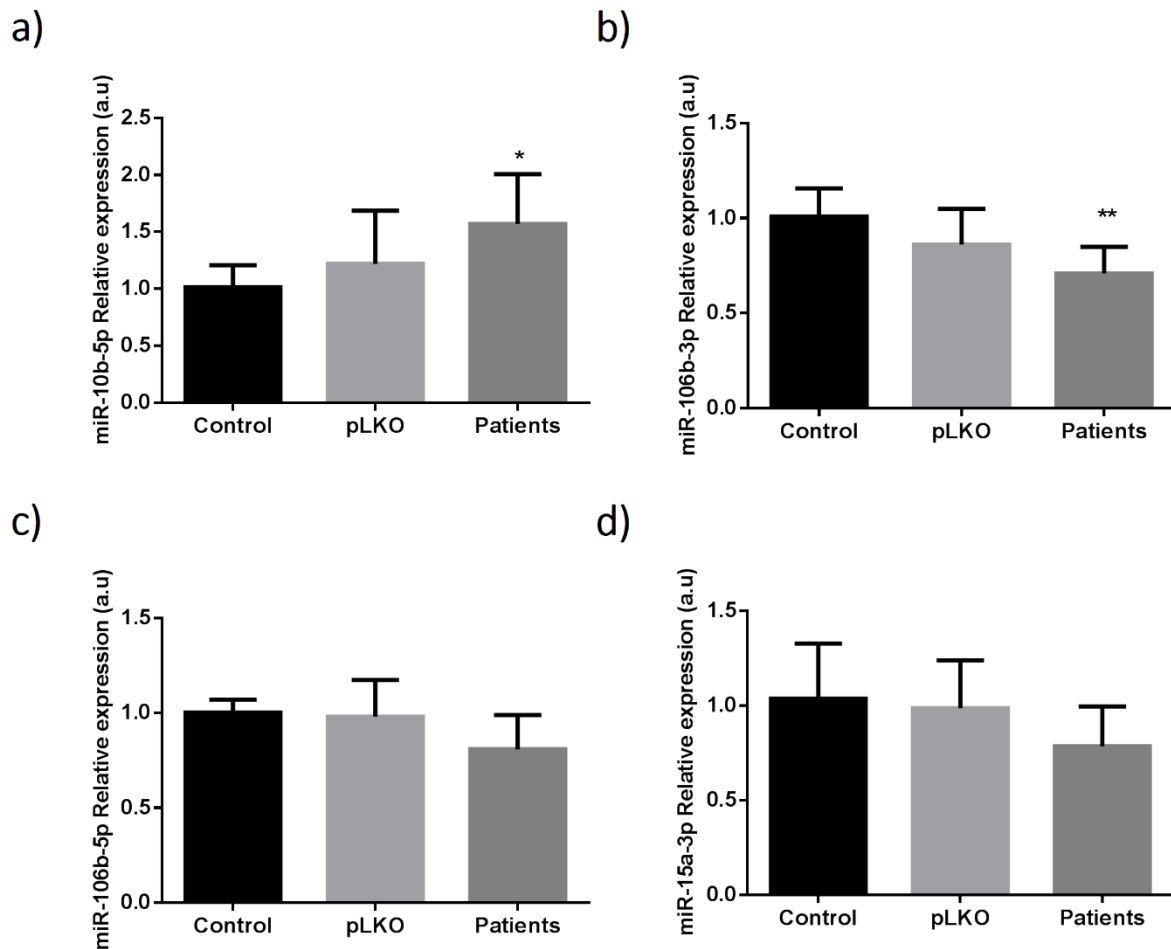
Figure 21. Relative expression levels of the miRNAs with different expression levels found in samples of SH-SY5Y cell models. Levels of a) miR-10b-5p; b) miR-106b-3p; c) miR-106b-5p; d) miR-15a-3p in SH-SY5Y control (n=3), pLKO control (n=3), and deficient frataxin cell lines FXN-138.1 and FXN-138.1 (Patients n=3). All results are represented as mean ± SD.* indicates p-values <0.05; ** indicates p-values <0.01.

Finally, validation analysis of miRNAs by RT-qPCR in fibroblasts cell lines showed the same profile as in NGS analysis. We detected that miR-10b-5p showed increased levels in fibroblasts from patients (FRDA1, FRDA2, and FRDA2) when we compared that result with control cell lines (Control 1, Control 2, and Control 3), as it is observed in NGS analysis (Figure 22a). Furthermore, we did not detect differences between patients and controls in miR-106b-3p, miR-106-5p and miR15a-3p, as occurs in NGS analysis (Figure 22b, 22c, and 22d).
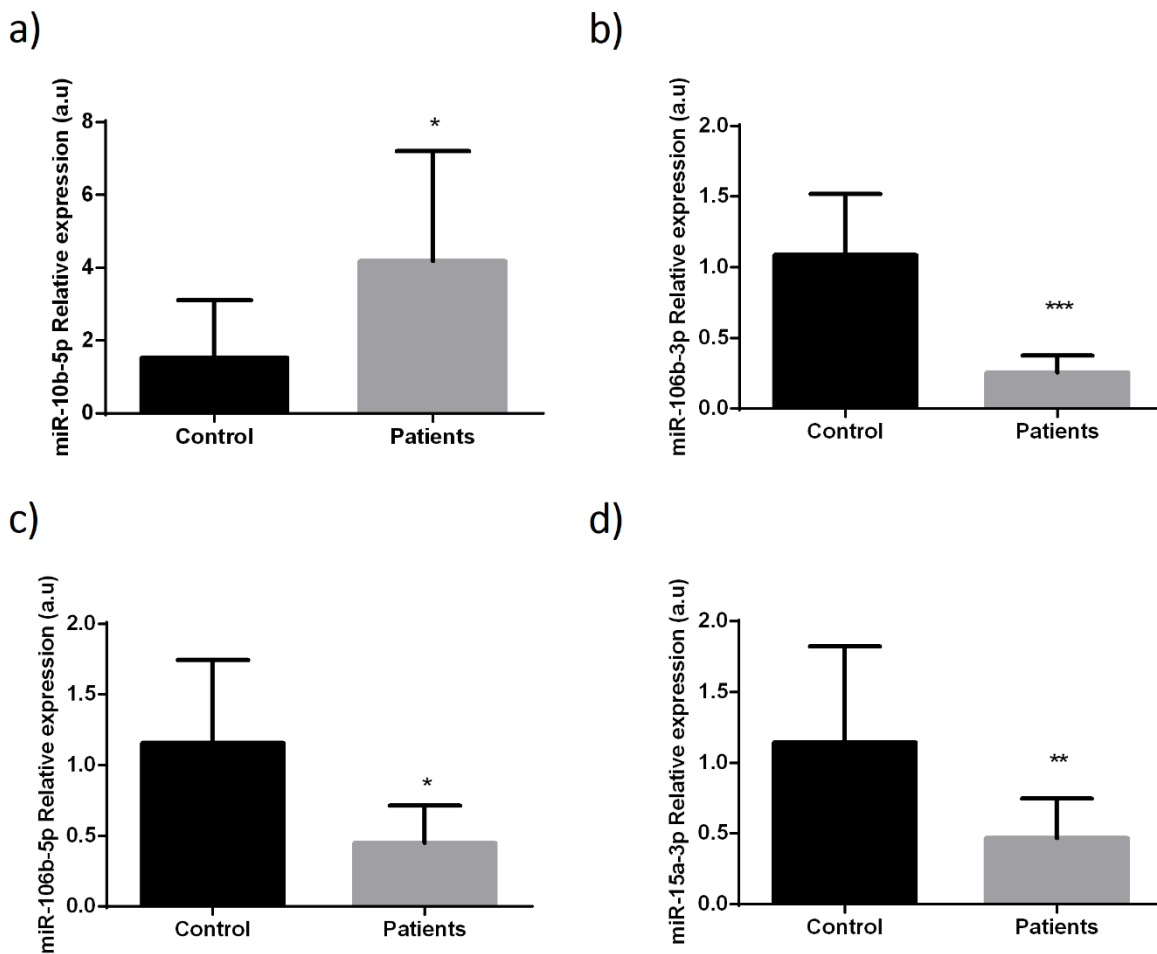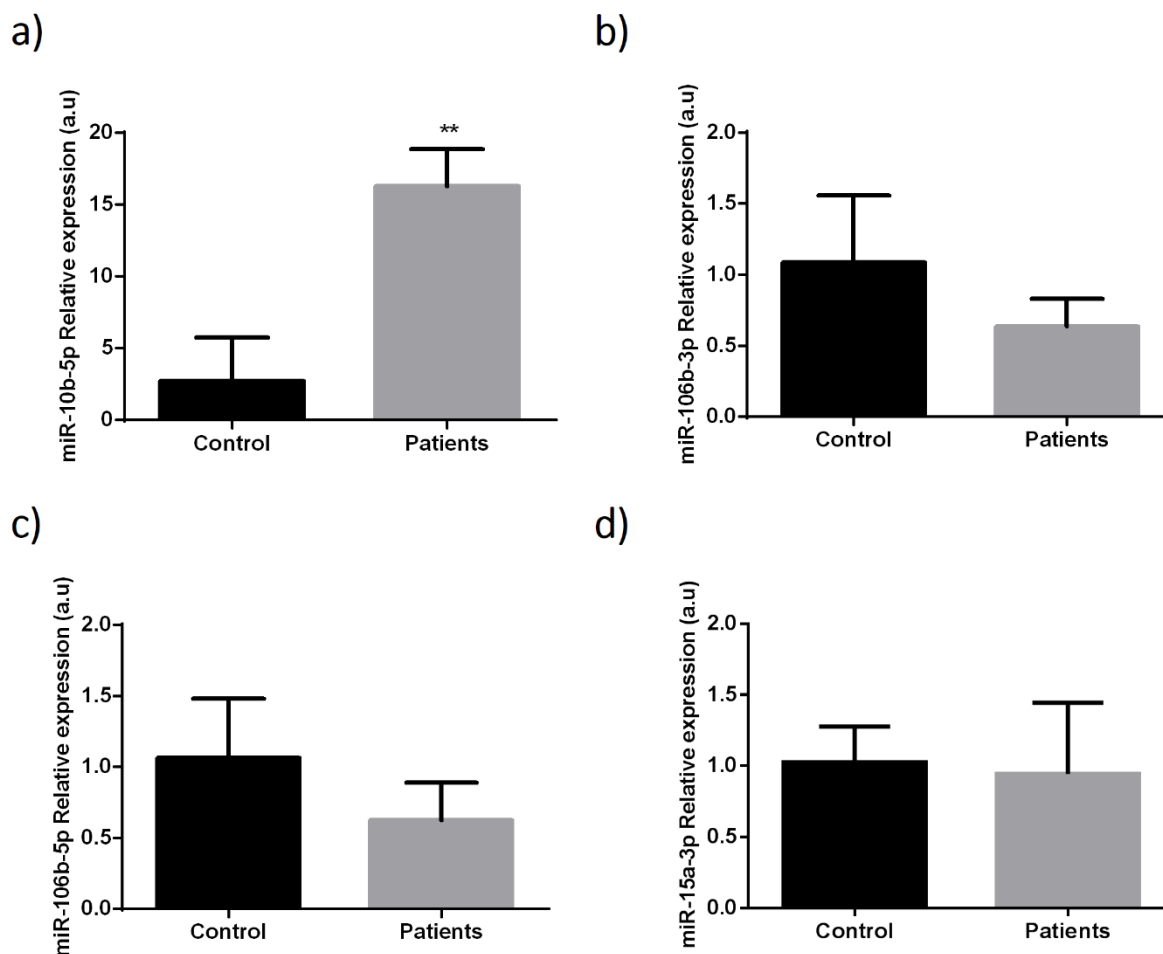
Figure 22. Relative expression levels of the miRNAs with different expression levels found in samples of fibroblasts cell lines. Levels of a) miR-10b-5p; b) miR-106b-3p; c) miR-106b-5p; d) miR-15a-3p in control fibroblasts (Control1, Control2, and Control3; n=3) and fibroblasts from FRDA patients (FRDA1, FRDA2, and FRDA3; n=3). All results are represented as mean ± SD. ** indicates p-values <0.01.

4.2.1.3. Analysis of miRNA targets and pathways in the context of FRDA

With the aim of elucidating the role of those identified miRNAs in FRDA physiopathology, we analysed biochemical networks that were regulated by these post-transcriptional regulators. We performed a DIANA-miRPath v3.0 analysis and a Kyoto Encyclopaedia of Genes and Genomes (KEGG) pathway analysis in the three cell lines, to look for significantly enriched pathways.

In olfactory mucosa stem cells, a total of sixty-six pathways with a false discovery rate (FDR) of less than 0.05 were retrieved in the first study. Nevertheless, we focused our analysis on pathways altered in FRDA pathophysiology and identified nine relevant pathways, which are shown in table 10.

Table 10. KEGG pathways targeted by differential expressed miRNAs in olfactory mucosa stem cell lines.

KEGG pathway	KEGG CODE
Neurotrophin signalling pathway	hsa04722
PI3K/Akt signalling pathway	hsa04151
MAPK signalling pathway	hsa04010
mTOR signalling pathway	hsa04150
FoxO signalling pathway	hsa04068
HIF-1 signalling pathway	hsa04066
Insulin signalling pathway	hsa04910
p53 signalling pathway	hsa04550
TGF-beta signalling pathway	Hsa04350

We performed the same analysis in SH-SY5Y models of frataxin deficiency and control cell lines, and we identified a total of seventy-three pathways, targeted by differential expressed miRNAs, with FDR less than 0.05. We selected sixteen relevant pathways from this list of pathways because they were involved in FRDA physiopathology (Table 11).

Fibroblasts cell lines showed a total of fifty-three pathways in which exist genes targeted by miRNAs with differential expression detected in our study. From this list of pathways, twelve relevant pathways were involved in the context of FRDA pathophysiology, which are shown in Table 12.

Table 11. KEGG pathways targeted by differential expressed miRNAs in frataxin-deficient cell lines and controls

KEGG pathway	KEGG CODE
Neurotrophin signalling pathway	hsa04722
PI3K/Akt signalling pathway	hsa04151
MAPK signalling pathway	hsa04010
mTOR signalling pathway	hsa04150
FoxO signalling pathway	hsa04068
HIF-1 signalling pathway	hsa04066
Insulin signalling pathway	hsa04910
p53 signalling pathway	hsa04115
TGF-beta signalling pathway	hsa04350
Fatty acid biosynthesis	hsa00061
Fatty acid metabolism	hsa01212
Fatty acid elongation	hsa00062
Ubiquitin mediated proteolysis	hsa04120
Protein processing in endoplasmic reticulum	hsa04141
Axon guidance	hsa04360
Huntington's disease	hsa05016

Table 12. KEGG pathways targeted by differential expressed miRNAs in fibroblasts cell lines.

KEGG pathway	KEGG CODE
Neurotrophin signalling pathway	hsa04722
PI3K/Akt signalling pathway	hsa04151
AMPK signalling pathway	hsa04152
mTOR signalling pathway	hsa04150
FoxO signalling pathway	hsa04068
Lysine degradation	hsa00310
Insulin signalling pathway	hsa04910
Huntington's disease	hsa05016
TGF-beta signalling pathway	hsa04350
Fatty acid biosynthesis	hsa00061
Ubiquitin mediated proteolysis	hsa04120
Protein processing in endoplasmic reticulum	hsa04141

As shown in tables 10, 11, and 12, there were many pathways in which participate a high number of miRNAs with differential expression, common to the three cell lines. Moreover, as we said previously, we performed NGS and RT-qPCR of common miRNAs between all cell lines. For these reasons, we analysed pathways targeted by these differentially expressed miRNAs shared between three cell lines, and we identify forty-seven pathways. We listed in table 13, those pathways containing targets of differentially expressed miRNAs, which are relevant in Friedreich's ataxia physiopathology.

Table 13. KEGG pathways targeted by differential expressed miRNAs in all cell lines.

KEGG pathway	KEGG CODE
Neurotrophin signalling pathway	hsa04722
P53 signalling pathway	hsa04115
AMPK signalling pathway	hsa04152
mTOR signalling pathway	hsa04150
FoxO signalling pathway	hsa04068
Lysine degradation	hsa00310
Insulin signalling pathway	hsa04910
MAPK signalling pathway	hsa04010
TGF-beta signalling pathway	hsa04350
Fatty acid biosynthesis	hsa00061
Ubiquitin mediated proteolysis	hsa04120
Protein processing in endoplasmic reticulum	hsa04141

In our analysis, we found that miR-10b-5p and miR15a-3p regulates fatty acid synthase (FASN). Adipose acyl-CoA synthetase-4 (ACSL4) is targeted by miR-106b-3p, hence molecular pathways such as β-oxidation and fatty acid metabolism may be regulated by these miRNAs with altered expression (Figure 23). Other pathway detected in our analysis showed that miR-106b-5p regulates ERO1-like protein alpha (ERO1LA) and ERO1-like protein beta (ERO1LB). Both proteins are targets of miR-106b-5p, thus controlling protein folding and oxidative stress levels in endoplasmic reticulum. Moreover, Glucose-6-phosphatase

catalytic subunit (G6PC) gene, involved in insulin-signalling pathway, is targeted by miR-10b-5p.
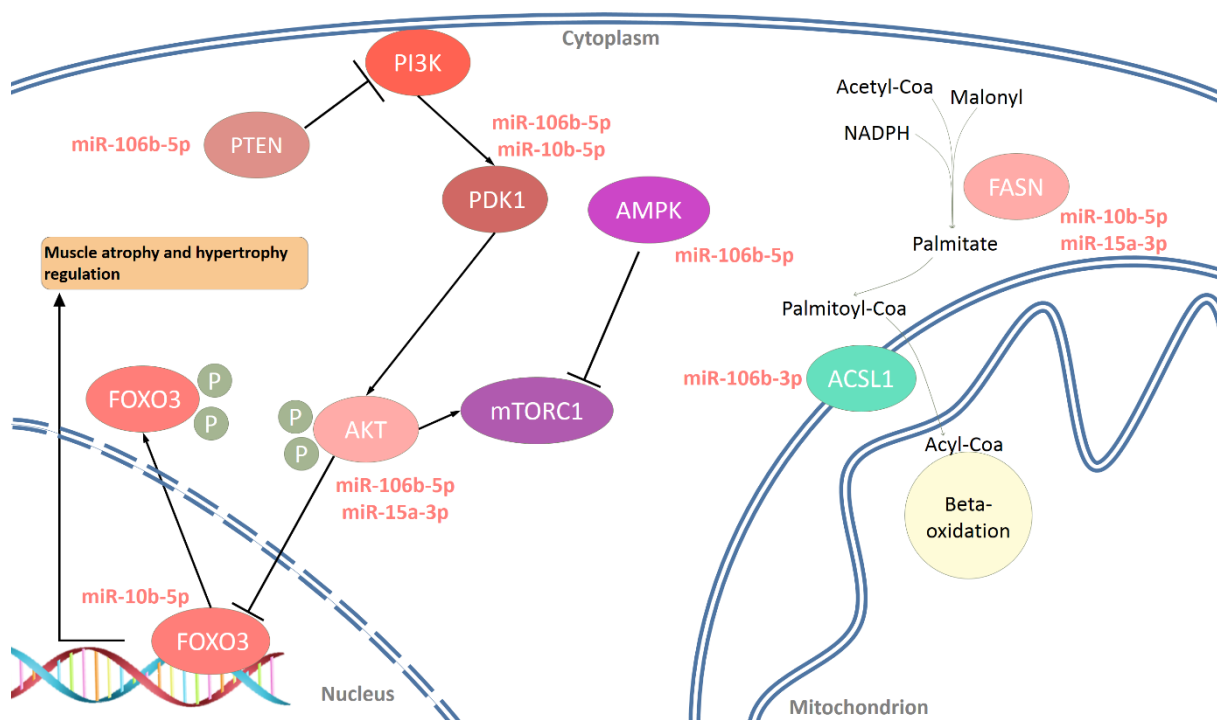
Figure 23. Overexpression of miRNAs in plasmas from FRDA patients downregulate their target mRNAs. Phosphatase and tensin homolog (PTEN), Phosphatidylinositol-4,5-bisphosphate 3-kinase (PI3K), 3-phosphoinositide-dependent protein kinase 1 (PDK1), Protein kinase B (AKT), Forkhead box 3 (FOXO3), mammalian target of rapamycin complex 1 (mTORC1), 5'-AMP-activated protein kinase catalytic subunit alpha-1 (AMPK), Fatty acid synthase (FASN), Long-chain-fatty-acid--CoA ligase 1 (ACSL1).

Other pathway that we found in our analysis was neurotrophin-signalling pathway. This pathway plays an important role in neural degeneration in FRDA context. We observed that Neurotrophic Receptor Tyrosine Kinase 2 (NTRK2) is targeted by miR-10b-5p, which expression levels were upregulated in SH-SY5Y frataxin-deficient cell lines compared with control SH-SY5Y cell lines. Thus, increased levels of miR-10b-5p might reduce NTRK2 receptor levels and alter development and maturation of the nervous system regulating neuron survival, proliferation, migration, differentiation, and synapse formation and plasticity.

AMPK signalling pathway was one of the most relevant pathways analysed. In this pathway, we found that *AMPK* gene was targeted by miR-106b-5p and Forkhead box protein 3 (*FOXO3*) gene was targeted by miR-10b-5p. AMPK is a protein also involved in mTOR signalling pathway, an important mechanism that is modulated in FRDA. Moreover, our analysis found that the AKT gene was regulated by miR-106b-5p and miR-15a-3p, 3-phosphoinositide-dependent

protein kinase 1 (PDK1) was targeted by miR-106b-5p and miR-10b-5p, and PTEN (phosphatase and tensin homolog) is targeted by miR-106b-5p (Figure 23).
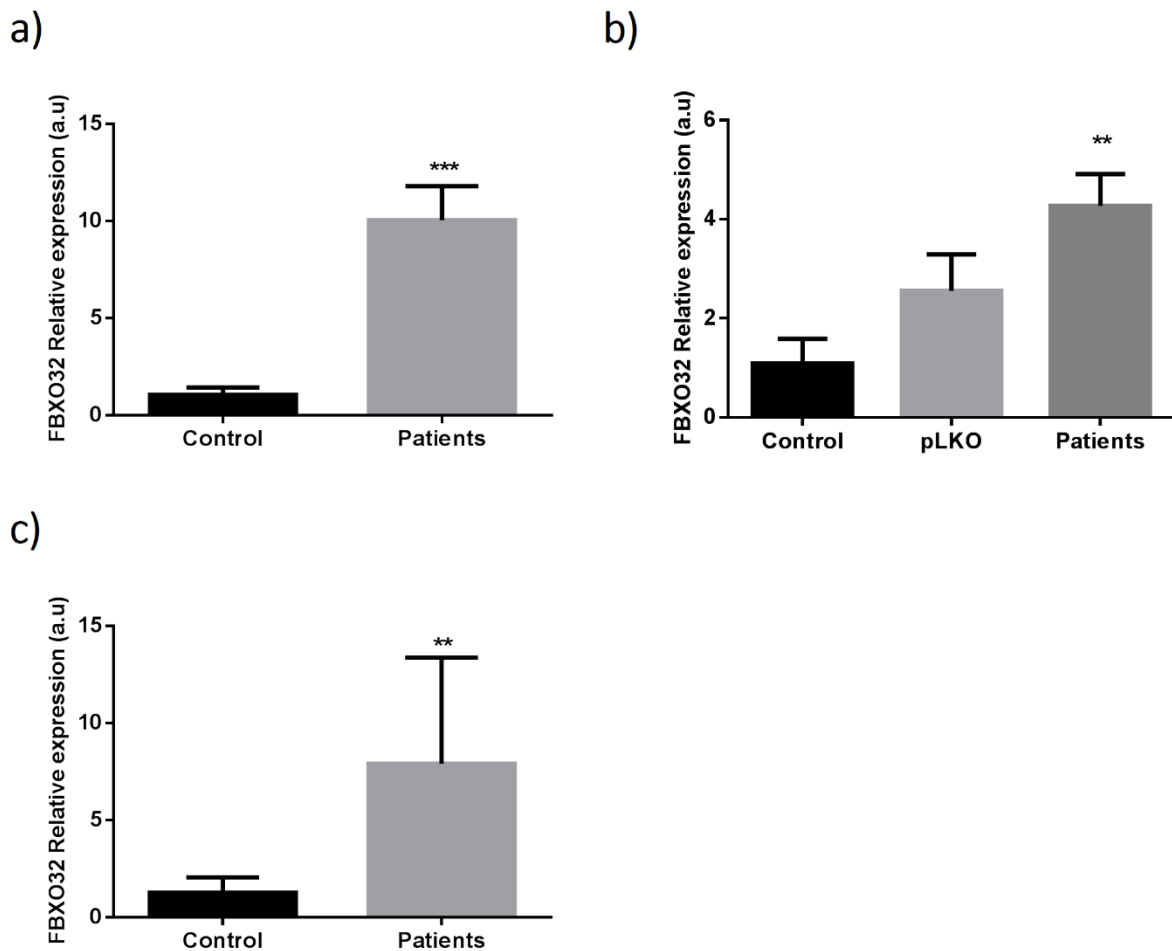
Figure 24. Relative expression levels of the F-box only protein 32 (FBXO32) gene found in samples of three cell models. Levels of FBXO32 in a) Olfactory mucosa stem cell of control (OControl) and olfactory mucosa stem cell of patients (OFRDA1 and OFRDA2); b) SH-SY5Y control (Control; n=3), pLKO control (pLKO; n=3), and deficient frataxin cell lines FXN-138.1 and FXN-138.1 (Patients n=3 each); c) control fibroblasts (Control1, Control2, and Control3; n=3) and fibroblasts from FRDA patients (FRDA1, FRDA2, and FRDA3; n=3). All results are represented as mean ± SD.** indicate p-values <0.01. *** indicate p-values<0.0001.

FOXO3 gene was involved in some pathways that we previously described. FOXO3 protein is a transcription factor involved in regulation of proteins that have a role in different pathways, such as regulation of muscle atrophy and hypertrophy targeting F-box protein 32 (FBXO32) gene, also known as atrogin-1 gene. As we describe above, FOXO3 was a target of miR-10b-5p, and this miRNA was upregulated in cell lines of patients (fibroblasts and olfactory mucosa stem cell) and frataxin-deficient cell lines (SH-SY5Y), when we compared to control cell lines. So, we decided to analyse FBXO32 in all cell lines. Surprisingly,

instead of a downregulation expected by the regulation of FOXO3 by miR-10b-5p, elevated levels of atrogin-1 gene in fibroblasts and olfactory mucosa stem cells from patients and frataxin-deficient (SH-SY5Y) cell lines were observed compared to control cell lines (Figure 24).

4.2.2. Epigenetic Biomarkers in human plasma

4.2.2.1. Clinical description of FRDA patients

Twenty-Five Caucasian FRDA patients from different families were enrolled in this study, all had their diagnosis confirmed by genetic testing. Participants with neoplastic diseases and active infection were excluded. Thirteen patients were men (52%), and the mean age of the group was 38 years. Table 14 shows the clinical characteristics of the patients participating in the study. Eight FRDA patients (32%) had also been diagnosed with cardiomyopathy. This diagnosis did not appear in the clinical records of the remaining 17 participants at the time of the study.

This study also included 25 healthy controls with no neoplastic diseases, active infection, cardiomyopathy, heart problems, hypertension, or diabetes. Of these healthy volunteers, 13 were men (52%), and the mean age of the group was 39 years (range: 16-68 years).

Table 14. Demographic and clinical features.

Patients (N)	25
Sex (M/F)	13 (52%) / 12 F (48%)
Age (mean/range)	39 years (16-68)
Age at onset (mean/range)	16 years (6-38)
Disease duration (mean/range)	22 years (8-35)
Expanded CAG repeats in the larger allele (mean/range)	665 (25-1185)
Punctuation SARA scale (average /range)	26,27 (9-37)
Diabetes (N/%)	5 (20%)
Smokers (N/%)	4 (16%)
Cardiomyopathy (N/%)	8 (32%)

4.2.2.2. Identification of differentially expressed miRNAs using NGS

We analysed miRNA samples from 25 FRDA patients and 17 healthy controls using next-generation sequencing. A preliminary exploration of the expression levels of all miRNAs showed that patient and control samples were well separated with the exception of five patients (corresponding to P.28, P.37, P.38, P.41 and P.43, Figure 25).
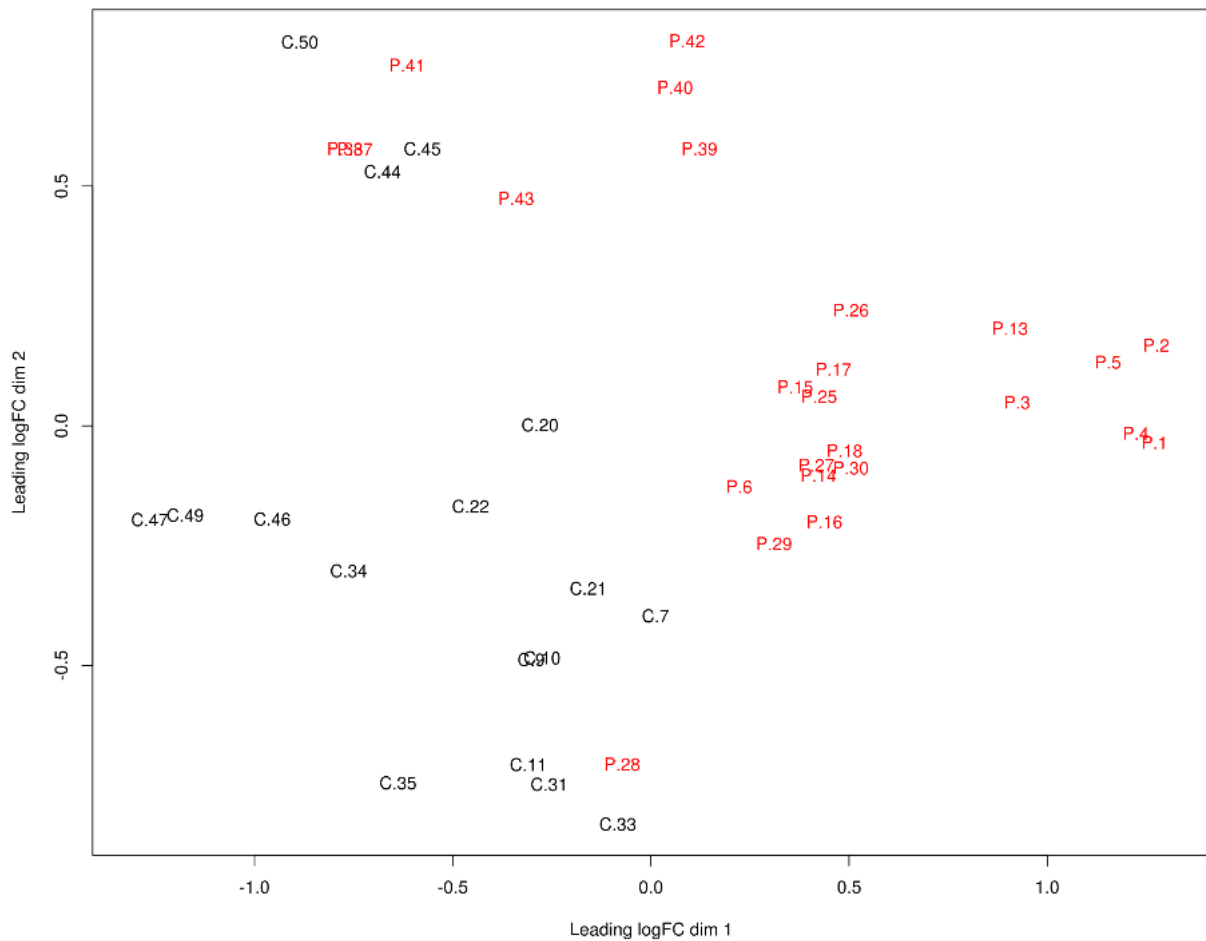
Figure 25. Multidimensional scale plot with all miRNAs and samples. The first component separates most of the patients (red) from the controls (black). However, 5 patients are misclassified (P.28, P.37, P.38, P.41 y P.43).

Differential expression analysis between patients and controls showed differential expression of 164 miRNAs between the two groups (false discovery rate < 0.05): 110 miRNAs were upregulated and 54 downregulated in samples from patients compared to controls. Among them we found 26 miRNAs with a false discovery rate (FDR) of less than 1e-4 and 12 with a correlation level lower than 0.7 (Figure 26). A LASSO logistic regression model with binomial distribution was fitted with 12 variables and 42 observations (considering all the samples). The

minimum leave-one-out cross-validation error was 0.071. The miRNAs identified at the optimal value were hsa-miR-128-3p, hsa-miR-625-3p, hsa-miR-130b-5p, hsa-miR-151a-5p, hsa-miR-330-3p, hsa-miR-323a-3p, and hsa-miR-142-3p. These seven miRNAs were upregulated in patients compared to controls (Figure 27).
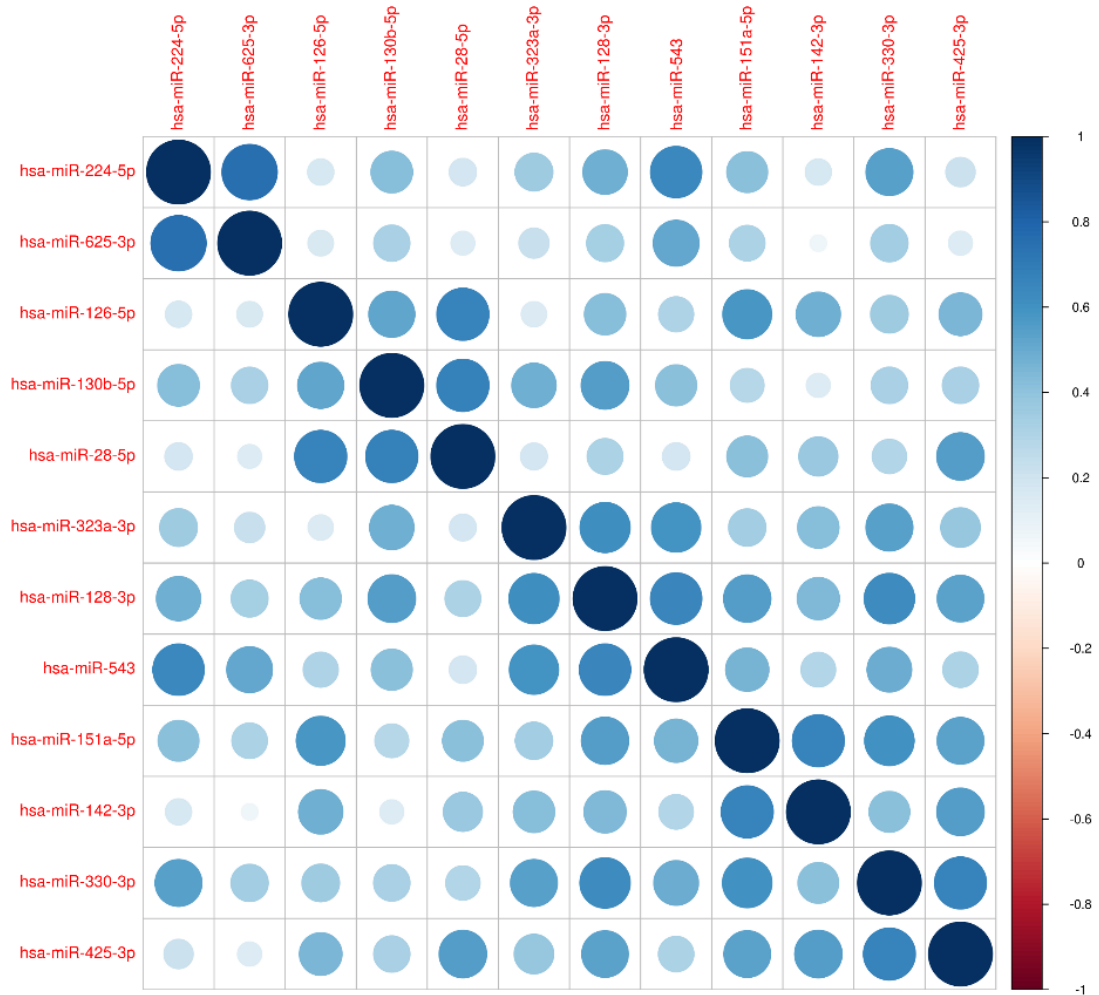
Figure 26. Correlation matrix. The miRNAs represented are those, which had a correlation level less than 0.7 among the most significant (FDR < 1e-4).
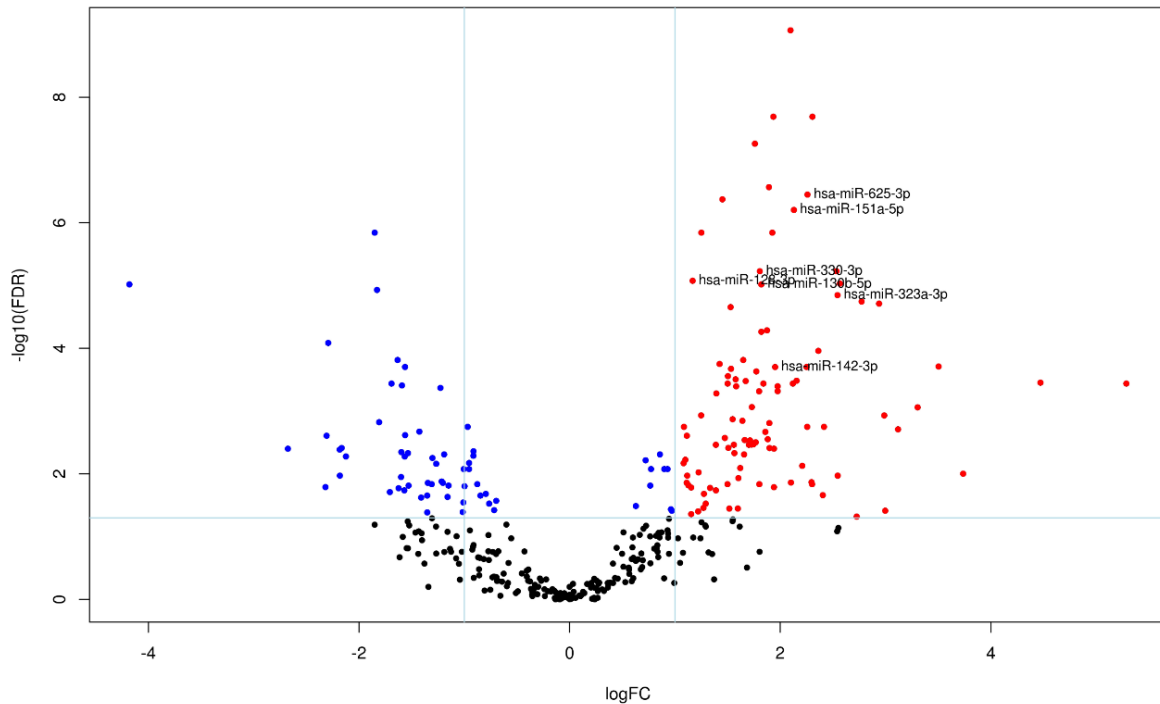
Figure 27. Volcano plot of differentially expressed human mature miRNAs in FRDA patients versus controls. Vertical lines indicate the threshold for a relative expression fold change (FC) of 2 or -2 fold compared to controls. The horizontal line represents the threshold of a 0.05 FDR value. The red and blue points lying in the top right and top left sectors are significantly up-regulated and down-regulated, respectively in patient versus control samples (FDR <0.05, FC ≥2 or ≤-2). Selected miRNAs by LASSO and cross validation are labelled.

4.2.2.3.   Validation of the differentially expressed miRNAs by RT-qPCR

The seven differentially expressed miRNAs detected by NGS were validated by RT-qPCR (Table 15). We analysed these miRNAs in the 25 FRDA patients and in the 25 controls (comprising 17 sequenced samples plus 8 additional controls). The two groups were matched by age, sex and race. We calculated relative expression levels for each miRNA, using hsa-miR-16-5p as an endogenous control due to its stable counts and threshold cycle (Ct) values in all the samples analysed by NGS and RT-qPCR, respectively. We detected a Ct of less than 39 in all miRNAs, with the exception of miR-130b-5p and miR-142-3p (Ct < 41). All miRNAs were present in plasma at higher levels in patients compared to healthy controls, in agreement with the results obtained by small RNA sequencing (Figure 28). The same differences were observed when we performed the analysis taking sex and age into account (all p-values less than 0.05; appendix tables 3 and 4).

Table 15. miRNAs selected as biomarkers for FRDA.

miRNA name	*Mature sequence*	*Accession*
hsa-miR-128-3p	ucacagugaaccggucucuuu	MIMAT0000424
hsa-miR-625-3p	gacuauagaacuuuccccuca	MIMAT0004808
hsa-miR-130b-5p	acucuuucccuguugcacuac	MIMAT0004680
hsa-miR-151a-5p	ucgaggagcucacagucuagu	MIMAT0004697
hsa-miR-330-3p	gcaaagcacacggccugcagaga	MIMAT0000751
hsa-miR-323a-3p	cacauuacacggucgaccucu	MIMAT0000755
hsa-miR-142-3p	uguaguguuuccuacuuuaugga	MIMAT0000434
hsa-miR-16-5p	uagcagcacguaaauauuggcg	MIMAT0000069
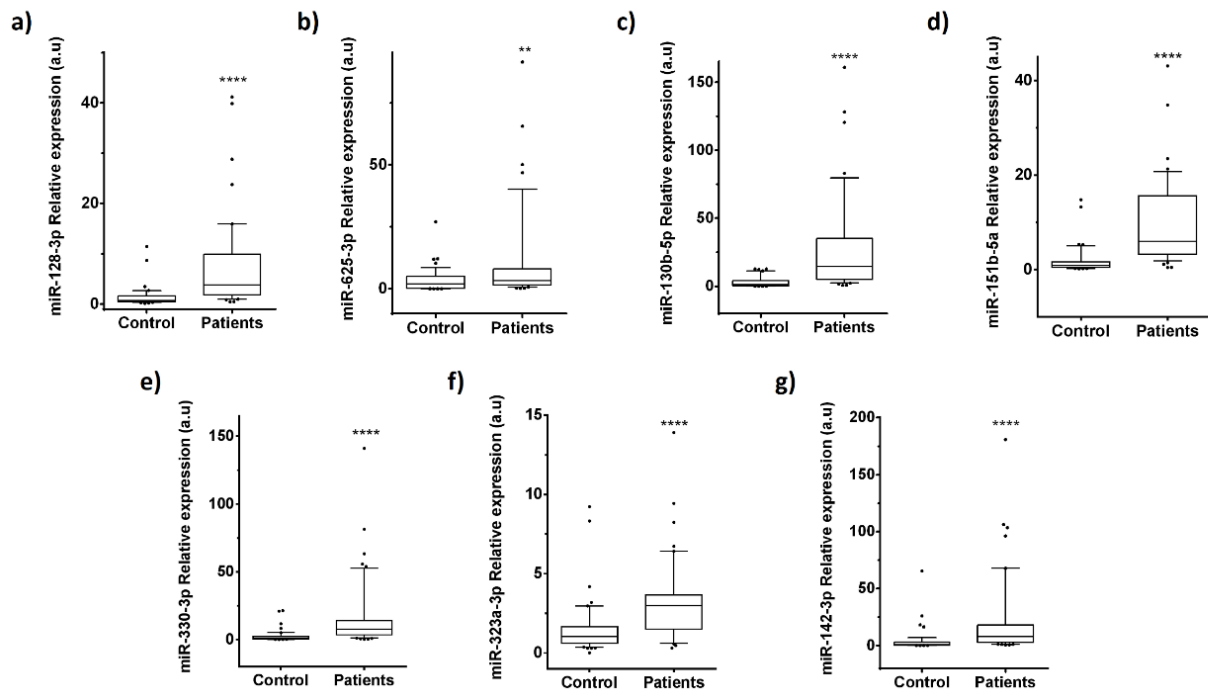
Figure 28. Relative expression levels of the miRNAs with different representation found in plasma of FRDA patients compared to control healthy subjects. Box plot of plasma levels of a) miR-128-3p (p<0.0001); b) miR-625-3p (p=0.0264); c) miR-130b-5p (p<0.0001); d) miR-151a-5p (p<0.0001); e) miR-330-3p (p<0.0001); f) miR-323a-3p (p<0.0001); and g) miR-142-3p (p<0.0001) in healthy normal subjects (Controls) (n = 25) and FRDA patients (n = 25). Expression levels of the miRNAs are normalized to miR-16. The lines inside the boxes denote the medians. The boxes mark the interval between the 25th and 75th percentiles. The whiskers denote the interval between the 10th and 90th percentiles. Filled circles indicate data points outside the 10th and 90th percentiles. Statistically significant differences were determined using Mann-Whitney tests. All P-values were two-sided and less than 0.05 was considered statistically significant.

Receiver operating characteristic (ROC) curve analyses performed to evaluate the diagnostic value of the seven circulating miRNAs revealed that all of them could be used to distinguish FRDA cases from healthy controls. The area

under the ROC curve (AUC), standard error, 95% confidence interval (CI), fold change cut-off value, sensitivity and specificity for each miRNA are shown in Table 16. Of the seven miRNAs analysed to elucidate their potential as biomarkers for FRDA diagnosis, miR-151a-5p showed the best ROC curve parameters (AUC=0.88, sensitivity=92.0%, specificity=80.0%).

Table 16. Area under ROC curves and standard error, and confidence interval (95%). Values for sensitivity, specificity and fold change optimal cut-off value.

miRNA	AUC	Standard error	95% CI	Fold Change optimal cut-off value	Sensitivity (%)	Specificity (%)
miR-128-3p	0.853	0.069	0.742-0.963	1.50	84.0	72.7
miR-625-3p	0.685	0.078	0.532-0.839	2.17	72.0	54.5
miR-130b-5p	0.895	0.046	0.805-0.984	2.80	92.0	72.7
miR-151a-5p	0.882	0.052	0.779-0.984	1.85	92.0	80.0
miR-330-3p	0.844	0.060	0.727-0.961	2.21	84.0	72.7
miR-323a-3p	0.802	0.069	0.666-0.938	1.48	88.0	72.7
miR-142-3p	0.847	0.058	0.734-0.961	2.14	88.0	72.7

4.2.2.4. *miRNA expression for phenotypical characterization of FRDA patients*

In a second approach, we analysed the expression of these seven miRNAs in plasma samples taken from the FRDA patients (n=25). This approach was selected in order to identify specific miRNA signatures corresponding to phenotypic and clinical features of FRDA. The patients were divided into subgroups according to sex, age, and comorbidities (diabetes and cardiomyopathy). We did not observe any significant differences in miRNA expression for sex, age, and diabetes. However, we found that miR-323a-3p was significantly upregulated in FRDA patients suffering of cardiomyopathy (n=8) in comparison with the remaining FRDA patients (n=17; table 17).

Table 17. Expression levels of selected miRNAs in FRDA cases. Fold change (FC); Standard deviation (SD) *Statistically significant differences were determined using Mann-Whitney tests. All P-values were two-sided and less than 0.05 was considered statistically significant.

miRNA	Cardiomyopathy		P value*
	Yes (n= 8) FC (SD)	No (n=17) FC (SD)	
miR-128-3p	5.02 (3.49)	7.07 (9.82)	>0.05
miR-625-3p	13.72 (29.55)	29.55 (63.14)	>0.05
miR-130b-5p	28.43 (39.70)	40.49 (47.31)	>0.05
miR-151a-5p	9.38 (9.64)	9.24 (7.00)	>0.05
miR-330-3p	12.19 (17.51)	17.51 (28.10)	>0.05
miR-323a-3p	4.82 (3.52)	2.56 (1.35)	0.048
miR-142-3p	23.35 (25.14)	20.43 (36.26)	>0.05

4.2.2.5. *miR-323a-3p is a biomarker for diagnosis of the use of cardiomyopathy in FRDA*

We performed the chi-squared test to test the association between miRNA-323a-3p fold change and cardiomyopathy, we found that of the eight FRDA patients with cardiomyopathy, seven (87.5%) showed a fold change above 2.5, and of those not affected by cardiomyopathy, just 41.2% presented a fold change value above 2.5 (p=0.048). In order to explore the value of this miRNA as a biomarker for cardiomyopathy, we studied the coefficient of variation (CV) for miR-323a-3p in a) 17 controls from our sequencing data study, b) 27 controls from an aortic stenosis circulating miRNA profile analysis[224], and c) seven controls from a study on miRNA analysis in adverse prognosis of myelodysplastic syndromes (https://www.ebi.ac.uk/arrayexpress/arrays/A-GEOD-18402/?ref=E-GEOD-76775). The CVs for miR-323a-3p in each analysed dataset were 0.38, 0.34 and 0.04, respectively. While the CVs of the first two datasets were similar, dataset c) gave a markedly lower value. This could be due to the smaller sample size of the third dataset in comparison with the other two, which would logically result in lower variability in expression levels.

Taking into account the sample size of each dataset and the nature of the data (human circulating miRNAs), we concluded that the miR-323a-3p CV in our control group was acceptable for assessing possible differences in expression among patient samples.

Afterwards, to examine the potential use of miR-323a-3p as a biomarker for cardiomyopathy in FRDA cases, we constructed the corresponding ROC curve, finding differences in miR-323a-3p fold change in FRDA patients with and without cardiomyopathy. We calculated the optimal cut-off value for the fold change as 2.79. Sensitivity and specificity were 88.9% and 62.5%, respectively, and the AUC was 0.75 (p= 0.042) (Figure 29).
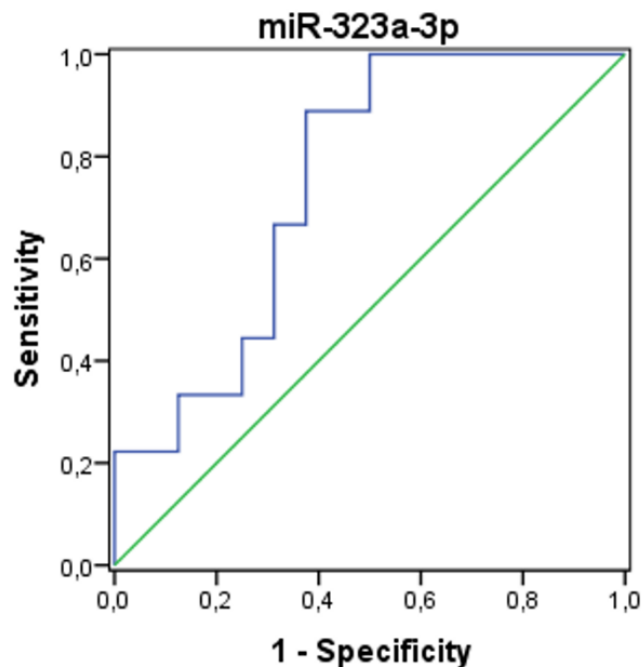
Figure 29. Area under curve of receiver operating characteristic (ROC) for miR-323a-3p.

4.2.2.6. *Analysis of miRNAs targets and pathway study in the context of FRDA*

In order to clarify the role of the identified miRNAs in FRDA, we analysed biochemical networks that were regulated by our seven validated miRNAs. We carried out a DIANA-miRPath v3.0 analysis and a Kyoto Encyclopaedia of Genes and Genomes (KEGG) pathway analysis to look for significantly enriched pathways. A total of 41 pathways with an FDR of less than 0.05 were retrieved in the first study. However, we focused our analysis on targets of selected miRNAs

in the context of FRDA pathophysiology and identified 12 relevant pathways, which are shown in Table 18.

Table 18. KEGG pathways targeted by differential expressed miRNAs in FRDA.

KEGG pathway	KEGG CODE
Fatty acid biosynthesis	hsa00061
Lysine degradation	hsa00310
Arrhythmogenic right ventricular cardiomyopathy (ARVC)	hsa05412
Central carbon metabolism in cancer	hsa05230
AMPK signalling pathway	hsa04152
mTOR signalling pathway	hsa04150
Ubiquitin mediated proteolysis	hsa04120
FoxO signalling pathway	hsa04068
Fatty acid metabolism	hsa01212
HIF-1 signalling pathway	hsa04066
Insulin signalling pathway	hsa04910
Signalling pathways regulating pluripotency of stem cells	hsa04550

As we previously said, one of the most relevant pathways found is AMPK signalling, in which genes such as FOXO1 and AMPK are directly targeted by miR-625 and miR-130b-5p. An important mechanism that is modulated in FRDA is the mTOR signalling pathway, in which a crosstalk protein AMPK is also involved in. Our analysis found that phosphatase and tensin homolog (PTEN) was a target of miR-151-5p and miR-625-3p. Interestingly, PTEN antagonizes PI3K. As a result, the downregulation of PTEN may increase phosphatidylinositol (3,4,5) triphosphate (PIP3) and produce subsequent activation of AKT. Our results also demonstrate the relevance of miR-625-3p regulating the HIF-1α signalling pathway, which plays a crucial role in ATP and ROS production[225]. In addition, 3-phosphoinositide-dependent protein kinase 1 (PDK1), pyruvate dehydrogenase alpha 1 (PDHA1) and lactate dehydrogenase A (LDHA) are regulated by miR-130b-5p; also miR-330-3p downregulates muscle pyruvate kinase (PKM) and transferrin receptor gene (TFRC) (Figure 30).

In our analysis, we found that miR-130b-5p regulates fatty acid synthase (FASN) and miR-142-3p targets adipose acyl-CoA synthetase-1 (ACSL1), thus regulating molecular pathways such as fatty acid metabolism and β-oxidation (Figure 30).
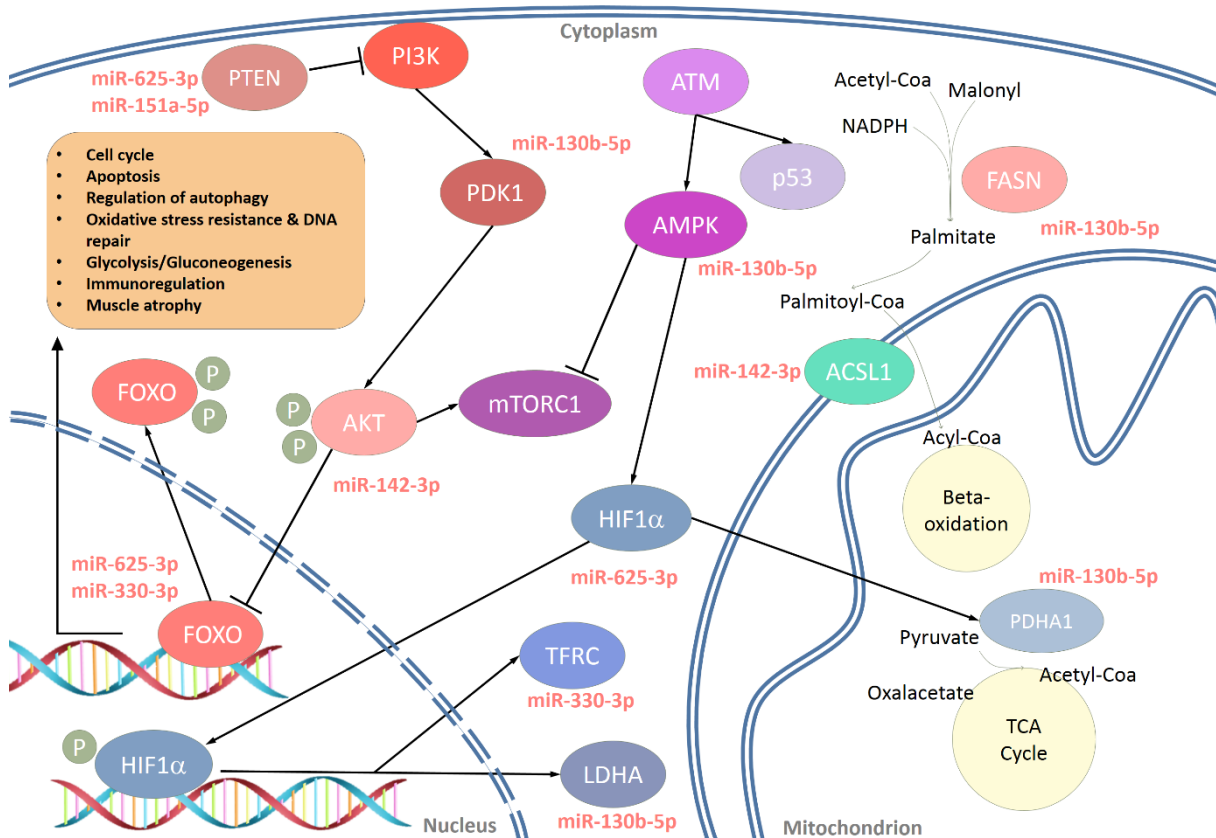
Figure 30. Overexpression of miRNAs in plasmas from FRDA patients downregulate their target mRNAs. Phosphatase and tensin homolog (PTEN), Phosphatidylinositol-4,5-bisphosphate 3-kinase (PI3K), 3-phosphoinositide-dependent protein kinase 1 (PDK1), Protein kinase B (AKT), Forkhead box (FOXO), mammalian target of rapamycin complex 1 (mTORC1), Hypoxia-inducible factor 1-alpha (HIF1α), Transferrin receptor (TFRC), L-lactate dehydrogenase A chain (LDHA), Ataxia telangiectasia mutated (ATM), 5'-AMP-activated protein kinase catalytic subunit alpha-1 (AMPK), Cellular tumour antigen p53 (p53), Fatty acid synthase (FASN), Long-chain-fatty-acid--CoA ligase 1 (ACSL1), Pyruvate dehydrogenase E1 component subunit alpha (PDHA1).

Other pathway analyses revealed that the insulin-signalling pathway is also targeted by miRNA candidates. In fact, glycogen synthase kinase 3 beta (GSK3β) is regulated by both miR-130b-5p and miR-625-3p. Finally, Wnt/β-catenin signalling related genes such as catenin (CTNNB1) and calcium-transporting ATPase sarcoplasmic reticulum type (ATP2A) are targets of some miRNAs: CTNNB1 is targeted by miR-151-5p and miR-625-3p and ATP2A2 is targeted by miR-142-3p, miR-323a-3p, and miR-151a5p.

4.2.2.7. *Validation of circulating miRNAs in cell lines models*

In order to identify the relevance of some miRNAs as potential contributors in FRDA disease mechanisms, we tested their expression in cell line models.

Expression analysis of our seven miRNAs in olfactory mucosa stem cells showed increased levels in FRDA's cell lines (OFRDA1 and OFRDA2) in case of miR-323a-3p (Figure 30g), as we observed in plasma miRNAs analysis. However, miR-625-3p, miR-128-3p, miR-151b-5p, and miR-142-3p did not present differences in their expression levels when we compared control and patients cell lines (Figure 31b, 31c, 31e, and 31f, respectively). On the contrary to plasma miRNAs analysis, we detected decreased levels of miR-330-3p and miR-130b-5p (Figure 31a and 31d, respectively).

Figure 31. Relative expression levels of the miRNAs with different expression levels found in olfactory mucosa stem cells. Levels of a) miR-330-3p; b) miR-625-3p; c) miR-128-3p; d) miR-130b-5p; e) miR-151a-5p; f) miR-142-3p; and g) miR-323a-3p in control cell line (OCONTROL; n=3) and patients (OFRDA1 and OFRDA2; n=3 each). All results are represented as mean ± SD.* indicates p-values <0.05.

SH-SY5Y cell models were analysed in order to find relevance of circulating miRNAs. In agreement with plasma miRNAs results, we observed increased expression levels of miR-330-3p and miR-323a-3p in frataxin-deficient cell lines FXN-138.1 and FXN-138.2 (Patients) compared with control cell lines (Figure 32a, and 32g, respectively). However, we did not detect differences in expression levels between frataxin-deficient cell lines and control cell lines of miR-625-3p, miR-128-3p, miR-130b-5p, miR-151b-5p, and miR-142-3p (Figure 32b, 32c, 32d, 32e, and 32f, respectively).
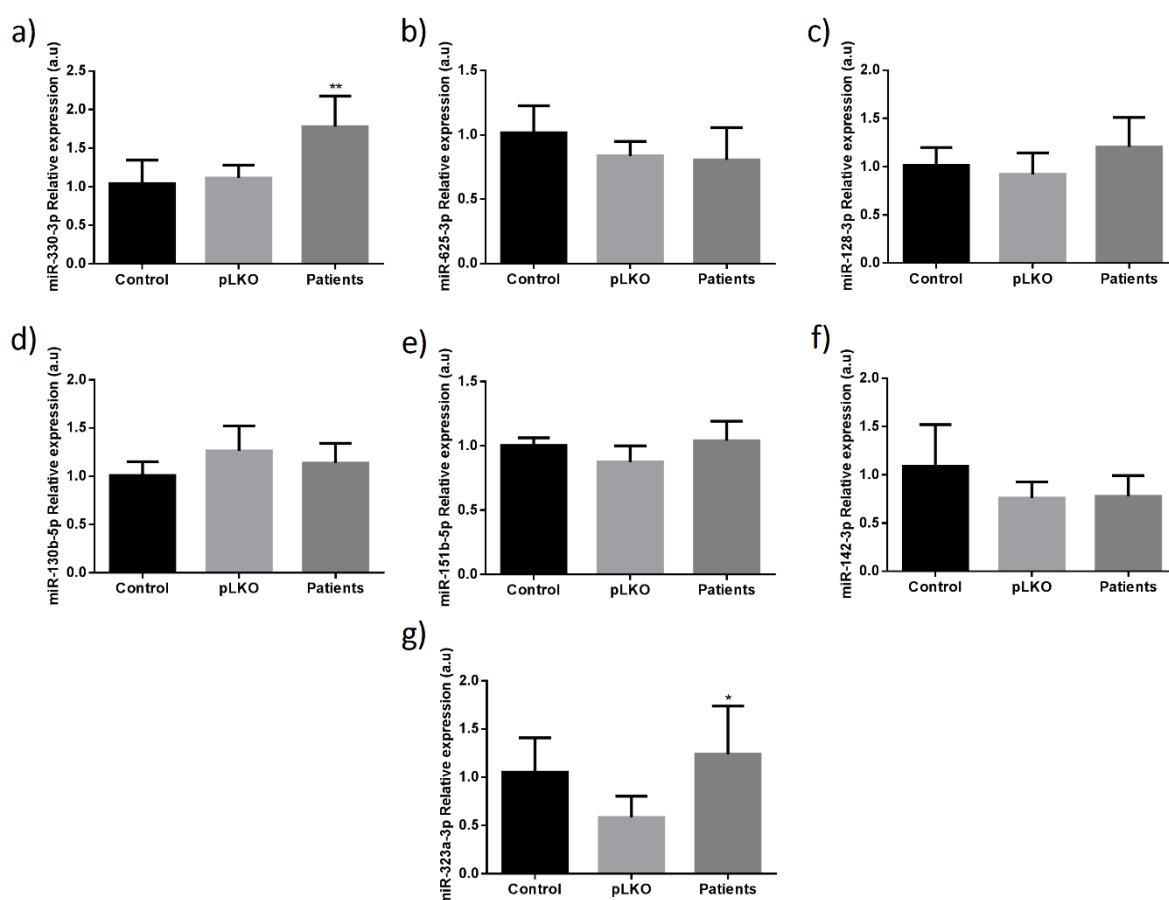
Figure 32. Relative expression levels of the miRNAs with different expression levels found in samples of SH-SY5Y cell models. Levels of a) miR-330-3p; b) miR-625-3p; c) miR-128-3p; d) miR-130b-5p; e) miR-151a-5p; f) miR-142-3p; and g) miR-323a-3p in SH-SY5Y control (n=3), pLKO control (n=3), and deficient frataxin cell lines FXN-138.1 and FXN-138.1 (Patients n=3). All results are represented as mean ± SD.* indicates p-values <0.05; ** indicates p-values <0.01.

Finally, miRNAs overrepresented in plasma were analysed in fibroblasts cell lines. miR-625-3p, miR-128-3p, miR-130b-5p, miR-151b-5p, miR-142-3p, and miR-323a-3p (Figure 33b, 33c, 33d, 33e, 33f, and 33g, respectively) did not show differences in expression levels when we compared fibroblasts from patients

(FRDA1, FRDA2 and FRDA3) and fibroblasts from control (Control 1, Control 2, and Control 3) cell lines, in disagreement with circulating miRNAs analysis in plasma. Moreover, miR-330-3p presented decreased levels in patient's fibroblasts when we compared with control's fibroblasts, just on the contrary to plasma miRNAs analysis (Figure 33a).
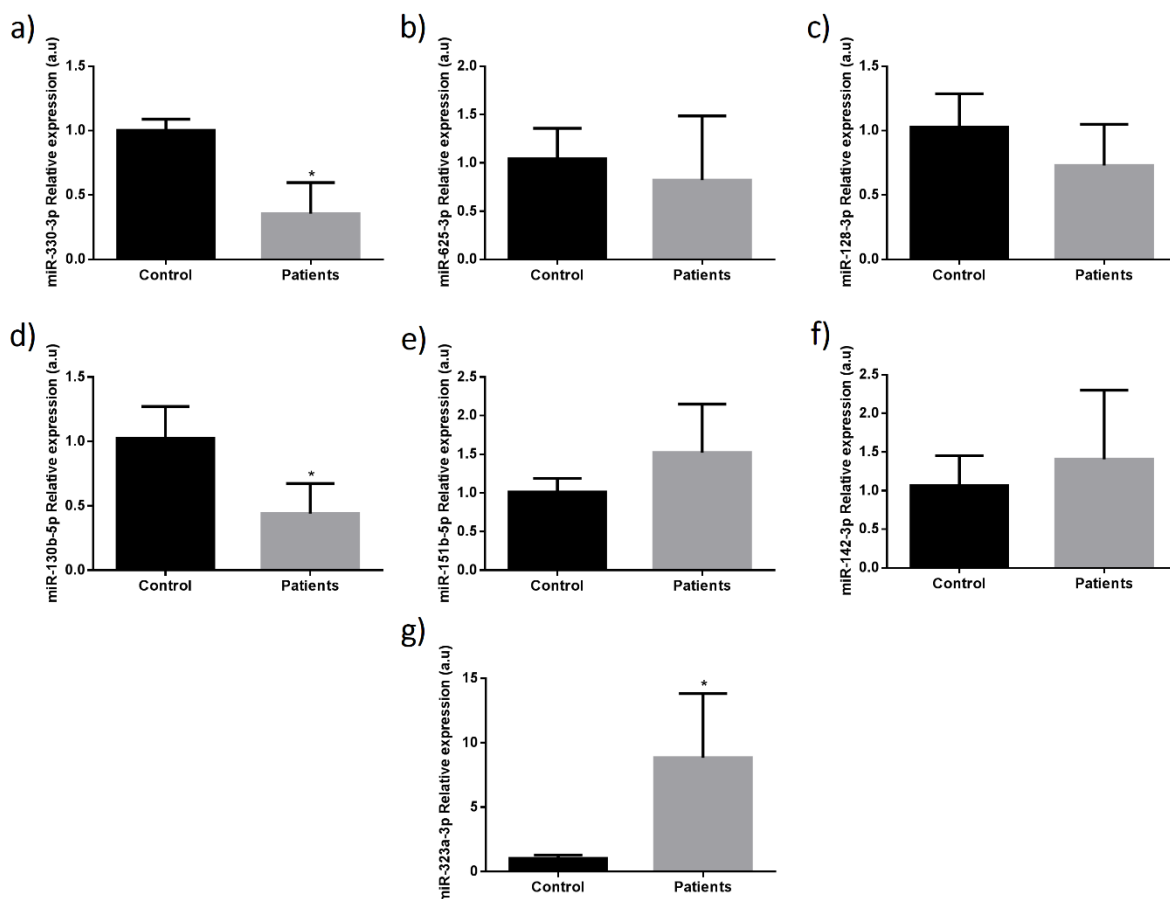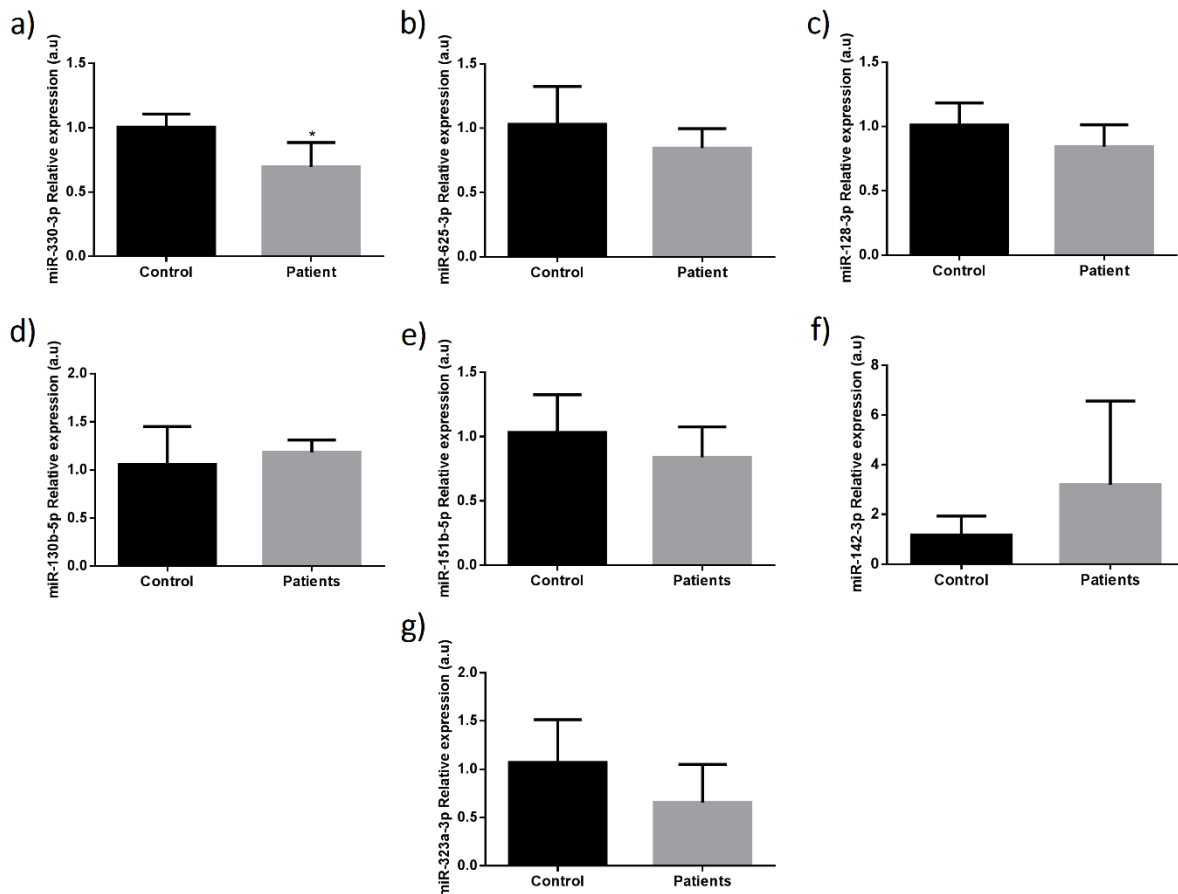

Figure 33. Relative expression levels of the miRNAs with different expression levels found in samples of fibroblasts cell lines. Levels of a) miR-330-3p; b) miR-625-3p; c) miR-128-3p; d) miR-130b-5p; e) miR-151a-5p; f) miR-142-3p; and g) miR-323a-3p in control fibroblasts (Control1, Control2, and Control3; n=3) and fibroblasts from FRDA patients (FRDA1, FRDA2, and FRDA3; n=3). All results are represented as mean ± SD.* indicates p-values <0.05.

4.2.2.8. Validation of the pathway in cell lines

In order to determine the importance of these miRNAs in the pathways analysed, we performed analysis of genes targeted by miRNAs. We focused our analysis on miR-330-3p, due to its differential expression levels in all cell lines and also in mir-130b-5p because of miRpath analysis identified this miRNA as having one of the largest numbers of gene targets in the selected pathways. For this reason, we analysed the gene expression of two targets of mir-130b-5p, Lactate Dehydrogenase A (LDHA) and Pyruvate Dehydrogenase Alpha 1 (PDHA1) and two

targets of mir-330-3p, Forkhead box O1 (FOXO1), and Manganese superoxide dismutase (SOD2).

Despite the fact that decreased levels of miR-130b-5p and miR-330-3p were detected in olfactory mucosa stem cell from patients (OFRDA1 and OFRDA2) compared with those from control (OCRONTROL; figure 31a and 31d, respectively), we did not observe differences in LDHA, PDHA1, and SOD2 gene expression (Figure 34a, 34b, and 34d). Unexpectedly, FOXO1 expression levels were downregulated in patient's cell lines compared with control cell lines (Figure 34c).
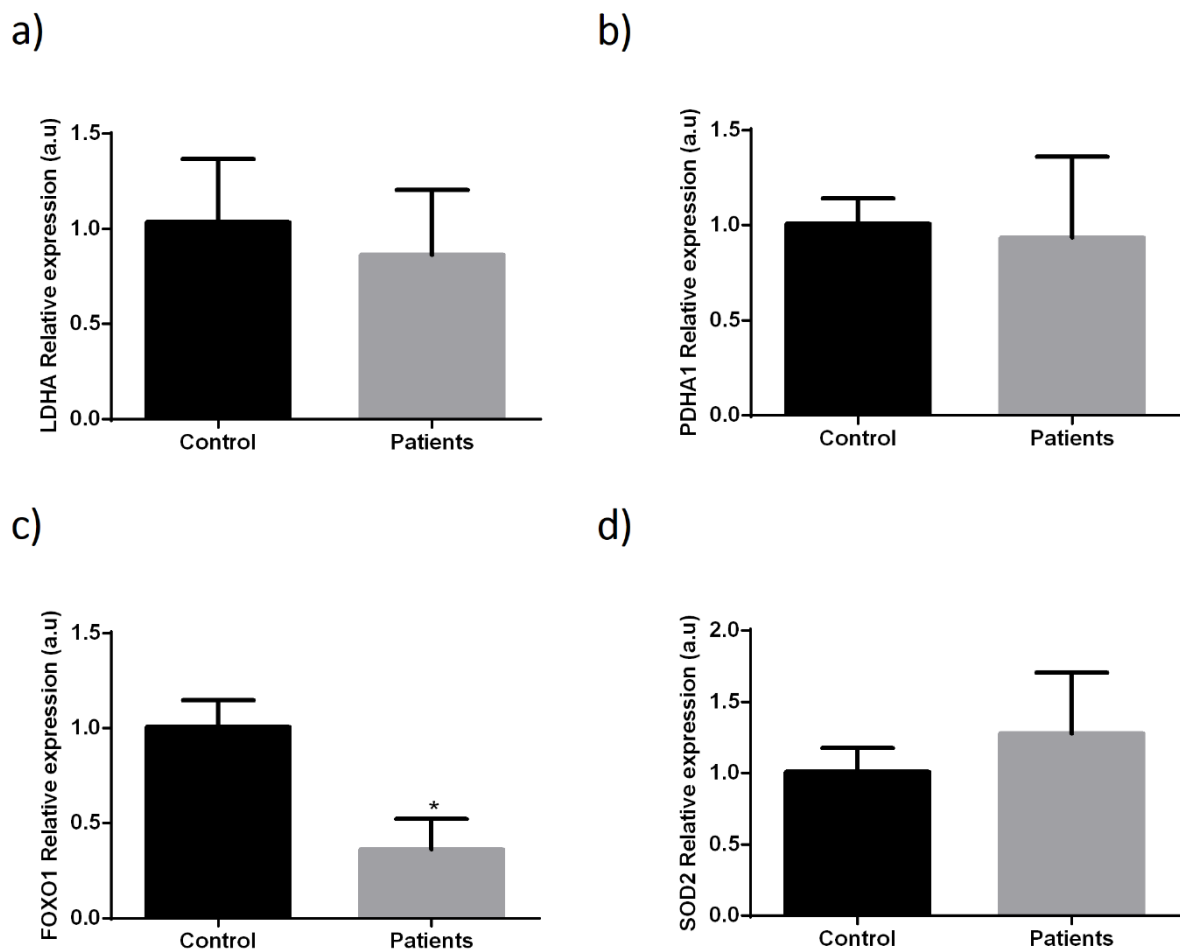
Figure 34. Relative expression levels of miR-130b-5p and miR-330-3p targeted genes in olfactory mucosa stem cells. Levels of a) Lactate Dehydrogenase A (LDHA) gene; b) Pyruvate Dehydrogenase Alpha 1 (PDHA1) gene; c) Forkhead box O1 (FOXO1) gene; and d) Manganese superoxide dismutase (SOD2) gene in control cell line (OCONTROL; n=3) and patients (OFRDA1 and OFRDA2; n=3 each). All results are represented as mean ± SD.* indicates p-values <0.05.

We performed gene expression analysis of miR-130b-5p and miR-330-3p targets in FXN-silenced SH-SYHY cell models. LDHA gene expression levels did not

present differences between frataxin-deficient cell lines (FXN-138.1 and FXN-128.2) compared with control cell lines (Figure 35a). This results agrees with non-differences observed in miR-130b-5p expression levels (Figure 32d). However, PDHA1 gene expression was upregulated in FXN-cell lines when we compared with controls (Figure 35b). Although miR-330-3p levels were uploaded in FXN-deficient cell lines compared with control cell lines (Figure 32a), SOD2 gene showed upregulated expression levels in FXN-cell lines (Figure 35d). Interestingly, we observed decreased expression levels of FOXO1 in FXN-silenced cell lines compared with the control line (Figure 35c). However, we also detected decreased FOXO1 gene expression levels in the pLKO negative control. This may indicate that FOXO1 gene expression levels were affected by the pLKO vector used in FXN-silenced cell line.

a)

b)

c)

d)
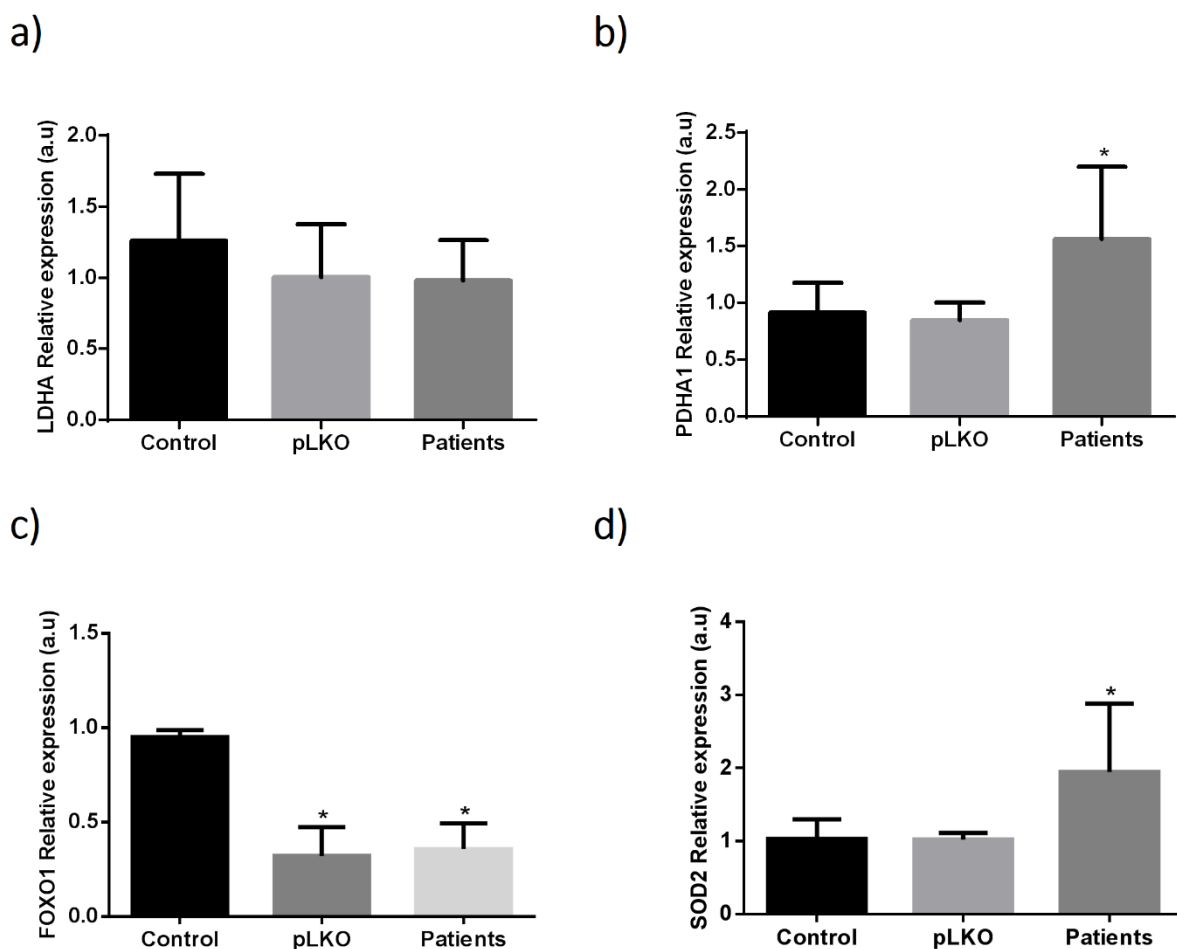
Figure 35. Relative expression levels of miR-130b-5p and miR-330-3p targeted genes in samples of SH-SY5Y cell models. Levels of a) Lactate Dehydrogenase A (LDHA) gene; b) Pyruvate Dehydrogenase Alpha 1 (PDHA1) gene; c) Forkhead box O1 (FOXO1) gene; and d) Manganese superoxide dismutase (SOD2) gene in SH-SY5Y control (n=3), pLKO control (n=3), and deficient frataxin cell lines FXN-138.1 and FXN-138.1 (Patients n=3). All results are represented as mean ± SD.* indicates p-values <0.05.

Finally, FOXO1, and SOD2 gene expression levels did not show differences in fibroblasts from patients (FRDA1, FRDA2 and FRDA3) when we compared with control (Control 1, Control 2, and Control 3) cell lines (Figure 36b, 36d) even though mir-330-3p presented decreased levels (Figure 34a). On the other hand, we did not observed differences in PDHA1 gene expression levels (36b) as could be expected for non-differences in miR-130b-5p expression levels (Figure 33d). Interestingly, we observed that LDHA gene showed decreased levels in fibroblasts from patients compared with fibroblasts from control cell lines (Figure 36a).
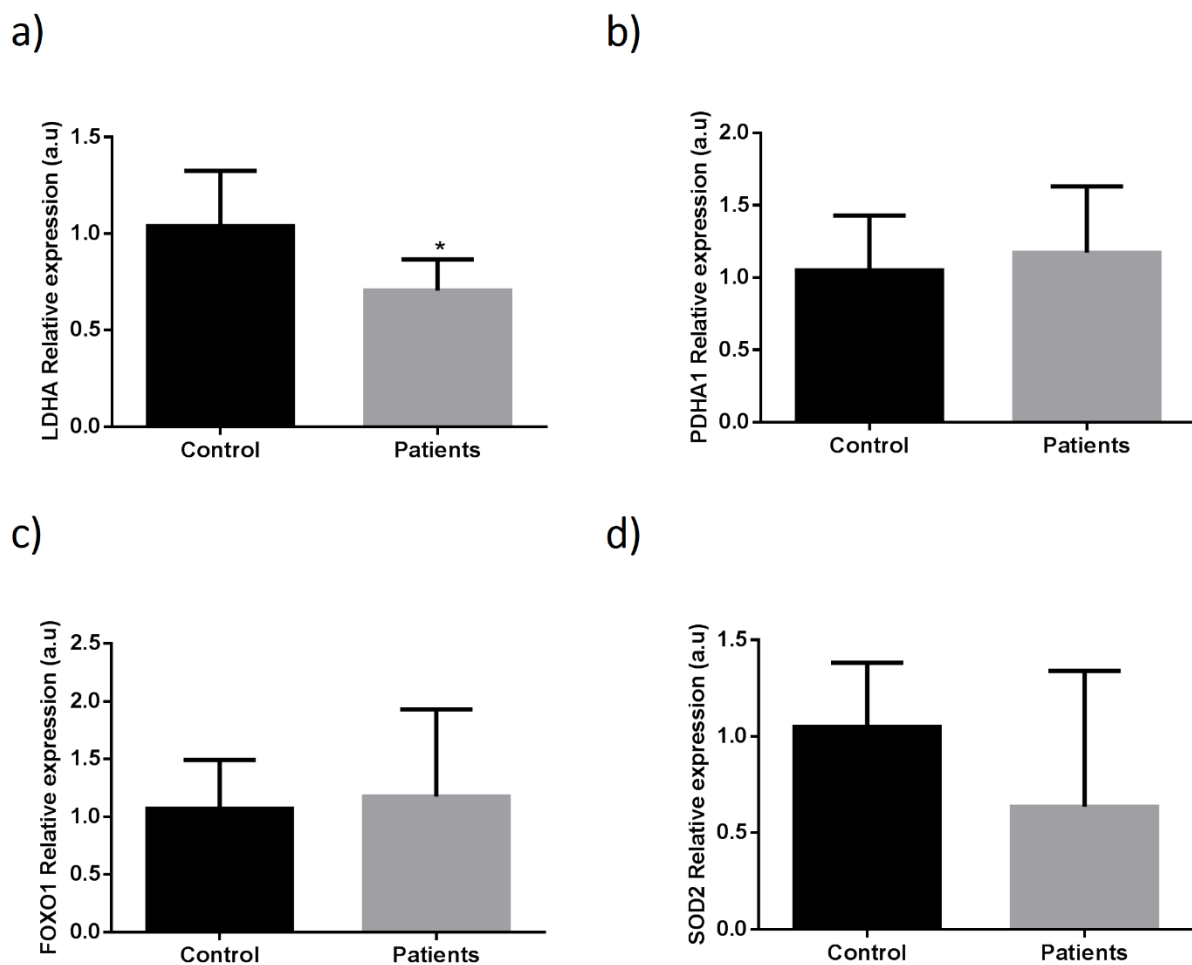
Figure 36. Relative expression levels of miR-130b-5p and miR-330-3p targeted genes in samples of fibroblasts cell lines. Levels of a) Lactate Dehydrogenase A (LDHA) gene; b) Pyruvate Dehydrogenase Alpha 1 (PDHA1) gene; c) Forkhead box O1 (FOXO1) gene; and d) Manganese superoxide dismutase (SOD2) gene in control fibroblasts (Control1, Control2, and Control3; n=3) and fibroblasts from FRDA patients (FRDA1, FRDA2, and FRDA3; n=3). All results are represented as mean ± SD.* indicates p-values <0.05.

5. Discussion

Discussion

Neuromuscular disorders show a heterogeneity and low frequency that challenge researchers to look for new effective diagnostic and treatment strategies. Specifically, the absence of reliable and monitorable clinical outcome measurements made more difficult to evaluate clinical trials of new therapies. Biomarkers could help researchers and clinicians in this issue, discovering the physiopathological mechanisms associated to such as diseases and playing a role as monitoring markers for response to drug treatment, progression and prognosis. Moreover, biomarkers could be useful for better stratification of patient cohorts thanks to a more accurate diagnosis and prognosis prediction.

Continuous development of high-throughput technologies involving genomics, transcriptomics and proteomics has increased the discovery of biomarkers. In this thesis, we use high-throughput technologies in order to find new biomarkers in two neurodegenerative diseases: Charcot-Marie-Tooth disease and Friedreich ataxia.

5.1. <u>Biomarkers in Charcot-Marie-Tooth</u>

5.1.1. Oxidative stress biomarkers

In this study, we analysed oxidative stress protein markers, such as carbonylation and nitrosylation, levels of lipoperoxidation using malondialdehyde (MDA), total antioxidant capacity, total glutathione (GSH) and the ratio between reduced GSH and its oxidized form (GSSG). Increased carbonylated protein levels had been observed in patients of multiple sclerosis[226] and triple transgenic Alzheimer mice models [227], being considered a good clinical marker for oxidative stress. However, we did not find differences in the three groups analysed (i.e. mild CMT patients, severe CMT patients, and controls). Moreover, nitrosylated protein levels did not show differences in a *GDAP1* fly model[228] as we observed in our data. Increased MDA levels were observed in people suffering other neurodegenerative disorders such as Friedreich's ataxia[229], nevertheless we did not detect differences in CMT patients. Interesting results of decreased total antioxidant capacity were observed in an Alzheimer disease rat model[230] that correlates well with increased oxidative stress, as described above. On the contrary, we did not observe significant changes in this total antioxidant capacity between the groups analysed. Finally, glutathione levels and

GSSG/GSH ratio showed no differences in our analysis as occurred in young flies with deficient *GDAP1* gene. In old flies, higher proportion of GSH than GSSG were found[228]. Taking all these results together, it seems that oxidative stress markers are not present in plasma of CMT1A patients, in contrast to what has been described in other neurodegenerative diseases, such as Alzheimer disease.

5.1.2. Proteomic biomarkers

With the aim of searching for new biomarkers in CMT, we performed 2D-DIGE analysis and subsequent identification of differentially expressed proteins in plasma from CMT patients (i.e. mild CMT patients and severe CMT patients) compared with healthy subjects. We identified twenty proteins (Table 8) with differential expression. Furthermore, the interactome showed those proteins which were phenotypically or functionally more related to PMP22 (Figure 13). In this regard, gelsolin was differentially expressed in mild CMT patients and severe CMT compared to controls. Looking at the interactome, gelsolin seems to be related with PMP22 through some genes with similar phenotype to PMP22. Previous results detected decreased levels of gelsolin in serum from patients with familial amyloidosis, Finnish type, when compared with serum of healthy subject [220]. Thus, we evaluated levels of gelsolin in plasma from the three groups studied (i.e. mild CMT patients, severe CMT patients, and controls). We did not observe any differences among them; also we did not find any correlation between age and gelsolin levels in CMT patients. These results suggest that gelsolin is not suitable for a biomarker of CMT disease. However, it is important to bear in mind that other possibility is that the stratification of CMT patients by using CMTN's scale could be not appropriate for phenotype characterization. In this regard, we used CMTN's scale to identify mild and severe patients but some of them could be misclassified, thus including some of them in an erroneous group. Therefore, new less subjective clinical scales should be developed. On the other hand, it is also possible that the results obtained by the ELISA kits commercially available are not reproducible enough when compared with values obtained by different lots of the kit. So, it might be possible that variability from CMTN's scale plus variability of results obtained from ELISA kit may have produced false negative results in our analysis.

Further proteins were detected in the proteomic analysis performed in plasma samples from CMT1A patients. One of these proteins that looks interesting was vitamin D binding protein (VDBP). This protein can bind different molecules, but its main role is as actin scavenger in extracellular fluids. In addition, increased levels of VDBP has been described in patients with Alzheimer's disease and postulated as a possible biomarker of dementia [231]. Importantly, this protein has been described as one of eight biomarkers in cerebrospinal fluid for Parkinson's disease [232].

Other remarkable protein is plasminogen. This zymogen is converted into plasmin protease by tissue plasminogen activator, and degrades fibrin and other extracellular proteins[233]. Diverse studies show that this protein participates in different processes in nervous system[234,235]. Furthermore, people with amyloid polyneuropathy showed decreased levels of plasminogen[236] as we observed in sample patients in our proteomic analysis.

Alpha-1-antitrypsine was observed with altered levels in patients of multiple sclerosis[237,238], however other studies did not show differences in alpha-1-antitrypsine levels[239,240]. Moreover, to these controversial results in multiple sclerosis, elevated levels of alpha-1-antitrypsine have been linked to patients with Alzheimer's disease[241].

Antithrombin III is an inhibitor of thrombin protein, its main role is related to anticoagulation. High levels of thrombin promote apoptotic cell death in nervous system[242]. For this reason, regulation of thrombin levels by antithrombin III is important in neuroprotective processes.

Other proteins with differential expression that we observed in our analysis were fibrinogen gamma (FGG) and vitronectin (VTN). Increased levels of vitronectin has been reported in endoneurium (part of peripheral nerve) of mostly CMT1 patients nerve biopsies [243]. Also, FGG forms together with FGG and fibrinogen beta (FGB) and fibrinogen alpha (FGA) the matrix of fibrin. Mutations in FGA produce an insoluble matrix which is associated with hereditary renal amyloidosis and peripheral neuropathy [244]. In addition, altered levels of FGG were reported in patients with Parkinson's disease [245]. Interestingly, mRNAs of these proteins in endoneurium of nerve biopsies were not found. Furthermore, it has been described that the expression of VTN and fibrinogen in the nerve is restricted to perineurium and blood vessels. So,

our decreased levels of VTN and FGG in plasma could be associated to an increased deposition of vitronectin in blood-nerve barrier [246].

Complement factor B and complement component 6 (C6) are proteins which were also detected in our analysis. These proteins are components of immune response. Little is known about complement factor B and neurodegenerative diseases, however some reports propose the implication of complement complex in demyelination of peripheral nerves [247,248]. Furthermore, C6 deficient rabbits showed typical neural phenotypical features of human neuroaxonal dystrophies[249].

Lipoprotein metabolism has been implicated in many neurodegenerative diseases. In our study, we observed differential expression in apolipoprotein E (APOE), apolipoprotein A1 (APO A1), clusterin (CLU; also known as apolipoprotein J), and apolipoprotein A4 (APO A4) lipid transporter proteins. Lower levels of APO A1 were described in people with Parkinson's disease[250] which correlate with dopaminergic system vulnerability [251] and earlier age at Parkinson's disease onset and greater motor severity[252]. Also, increased levels of APO A1 consequence of -75G/A promoter polymorphism in people with multiple sclerosis are associated with cognitive performance[253]. Elevated risk of Alzheimer's disease has been related with low levels of APO A1 and APO A4[254]. It has been described that mice with fatty liver dystrophy showed increased levels of APOA 4 associated with an abnormality of myelin formations as well as demyelination and axon degeneration [255]. Another neuropathy, Leber's hereditary optic neuropathy, has been characterized by increased levels of APO A4 [256]. It is well known that APO E4 allele has increased risk of Alzheimer's disease [257]. Also, recent studies have demonstrated that APO E4 allele is associated to an increased risk of severe diabetic polyneuropathy [258]. Moreover, several studies associates APOE with neuromuscular diseases [259]. Finally, knockout mice of CLU showed an impaired regeneration of sciatic nerves [260]. All these results that fits well with our proteomic results indicate a lipoprotein alteration in Charcot-Marie-Tooth disease. Furthermore, recent results demonstrated that PMP22 depletion causes severe disruption of cholesterol-enriched lipid rafts levels and localization [261].

Little is known about the role of Alpha-2-HS-glycoprotein, serotransferrin, kininogen-1, and haptoglobin in neurodegenerative diseases. Elevated levels of alpha-2-HS-glycoprotein in cerebrospinal fluid have been proposed as biomarker of active

multiple sclerosis[262]. Furthermore, increased levels of haptoglobin were observed in patients with chronic inflammatory demyelinating polyneuropathy[263].

In this proteomic study, we provide some potential biomarkers that could be useful for prognosis and clinical stratification of patients with Charcot-Marie-Tooth disease, after validation in well-characterized patient cohorts. Besides of our no significant results in gelsolin validation, further studies with the other proteins with differential expression should be performed. As we mentioned previously, almost all of the proteins have been associated with neurodegenerative diseases and their validation could provide suitable biomarkers that perhaps can provide a new stratification of CMT patients, which in turn may help clinicians in the prognosis and treatment. Moreover, these possible biomarkers could be also used for monitoring clinical treatments.

5.2. Biomarkers in FRDA

5.2.1. Biomarkers in cellular models of FRDA

We studied the miRNome in plasma from FRDA patients and in three different FRDA cell models, and examined how miRNAs can contribute to the characterization of new molecular and epigenetic regulatory mechanisms participating in the natural history of this neuromuscular disease. Indeed, miRNAs are promising molecules that can be used as biomarkers for the diagnosis, prognosis, and treatment monitoring of FRDA. This means that we could use miRNAs to screen and consolidate therapies, improving the quality of life of FRDA patients and reducing costs in clinical trials through the design of more personalized treatments and the identification of different molecular pathways underlying the progression of the disease.

The role of miRNAs is attracting significant interest in the area of neuromuscular disorders[264] and cardiovascular diseases[265]. Further, in this thesis, we described an investigation of miRNAs as epigenetic regulators in three FRDA cell models.

In the study of the miRNome in FRDA cell models, we detected a different miRNA profile between cases and controls of three cell lines models studied (i.e. fibroblasts, olfactory mucosa stem cells, and neuroblastoma cell line SH-SY5Y). Then, we looked for coincidences among miRNA profiles of these cellular models and we did not

observe any common miRNA with differential expression when comparing them. However, when we compared each line with each one of the other three different lines we observed that both cell lines, fibroblasts and SH-SY5Y cells present miR-10b-5p with differential expression compared against their respective controls. In addition, hsa-miR-409-3p, hsa-miR-3117-3p, hsa-miR-106b-3p, hsa-let-7a-2-3p, hsa-miR-15a-3p, and hsa-miR-106b-5p were differential expressed in both olfactory mucosa stem cells and SH-SY5Y. We validated four selected miRNAs from these comparison (Table 9) and we observed that in fibroblasts all these miRNAs showed the same tendency, in both SmallRNA-seq and RT-qPCR analysis (Table 19). Remarkably, only in miR-10b-5p the results were coincident for both analyses in the SH-SY5Y cell model. In olfactory mucosa stem cells model, the results were almost coincident and only miR-10b-5p showed an increased level in RT-qPCR that was not observed in the results obtained by SmallRNA-seq analysis (Table 19). The differences in the results between the two analyses might be explained by the different number of samples used in NGS, that are lower than those used in RT-qPCR. These results remark the importance of the validation of SmallRNA-seq results by other techniques such as RT-qPCR.

Table 19. Comparison of results from NGS analysis and RT-qPCR analysis for selected miRNAs in the three FRDA cell models. Dark blue arrows represent upregulation of miRNA; light blue arrows represent downregulation of miRNA; line represents no significant changes in miRNA expression. Red lines represent those miRNAs coincident in both analyses.

miRNA name	*Olfactory mucosa stem cells*		*SH-SY5Y*		*Fibroblasts*	
	NGS	*RT-qPCR*	*NGS*	*RT-qPCR*	*NGS*	*RT-qPCR*
hsa-miR-10b-5p	-	↑	↑	↑	↑	↑
hsa-miR-106b-3p	↓	↓	↑	↓	-	-
hsa-miR-106b-5p	↓	↓	↑	-	-	-
hsa-miR-15a-3p	↓	↓	↑	-	-	-

Some reports about these miRNAs in neurodegenerative diseases are commonly found in scientific literature. For example, mir-10b-5p was found overexpressed in prefrontal cortex samples of people with Parkinson's[266] and Huntington's[267] disease, as we found in FRDA cell models. Also, low levels of miR-106b-5p were observed in anterior temporal cortex of people with Alzheimer disease[268] and in different B cells from multiple sclerosis patients[269]. These data are in agreement with our results obtained from the study of the levels of miR-106b-5p in case of olfactory mucosa stem

cells. However, miR-106b-5p was upregulated in T cells from people with multiple sclerosis, but although our results were coincident in olfactory mucosa stem cells, we did not observe differential expression of this miRNA in fibroblasts and in SH-SY5Y by RT-qPCR analysis. This fact suggests that mir-106b-5p may have a tissue-specific expression and may play different roles in each tissue.

5.2.1.1. *Pathway analysis*

In our biological pathway analysis, we observed that mir-10b-5p and mir-15a-3p regulate fatty acid synthase (*FASN*) and mir-106b-3p regulates adipose acyl-CoA synthetase-4 (*ACSL4*). FASN is a lipogenic enzyme that synthesises *de novo* long-chain fatty acids from acetyl-CoA and malonyl-CoA[270]. On the other hand, ACSL4 is a long-chain fatty acyl-CoA synthetase that activates fatty acids in both synthesis of cellular lipids, and ß-oxidation degradation[271]. Altered lipid metabolism has been reported in a *Drosophila* model of FRDA[272]. In addition, lipid droplets in cardiac muscles of frataxin-deficient mouse line have been observed[159]. These observations fit with decreased levels of mir-15a-3p, which were observed in olfactory mucosa stem cells, and may result in higher levels of FAS, and in consequence higher levels of fatty acids. Interestingly, as a response to fatty acids overload, cell metabolism can promote their oxidation and esterification. Elevated oxidation of fatty acids generates elevated production of ROS, which in turn can lead to cardiomyopathy and myocardial dysfunction[273,274]. Also, these observations are consistent with our results that showed that mir-10b-5p was upregulated in the three cell models studied in this thesis, and mir-106b-3p was downregulated in olfactory mucosa stem cells and SH-SY5Y (RT-qPCR analysis), as a response of decrease of fatty acids by downregulation of FASN and possible upregulation of ACSL4, respectively, as a positive feed-back response of fatty acids overload. Other interesting point to take in mind of this pathway is the recent association of increased levels of ACSL4 with sensitivity to ferroptosis [275,276]. Ferroptosis is a form of cell death with different morphological, biochemical and genetic characteristics, and induced by the small molecule called erastin. Erastin interferes with cystine-glutamate antiporter that provides oxidised cysteine, an essential precursor of glutathione (GSH)[277]. GSH is necessary

for glutathione peroxidase 4 (Gpx4) detoxification process of lipid peroxidation [278]. Thus, decreased levels of GSH produce the accumulation of this lipid [279] and leads to cell death. Decreased levels of total GSH [280] and iron accumulation[156] have been described in FRDA patients. Hence, high levels of lipid peroxidation were described in these patients[229]. Taking these precedents all together, indicate that a process of cell death via ferroptosis might be plausible to occur in FRDA patients.

Low levels of miR-106-5p in olfactory mucosa stem cells may produce increased levels of ERO1-like protein alpha (*ERO1LA*) and ERO1-like protein beta (*ERO1LB*). Both are enzymes of endoplasmic reticulum that generate disulphide bonds in cysteine residues of proteins and contribute to decrease unfolded protein aggregates formed by ROS. Importantly, ERO1L isoforms have been found in a frataxin deficient model[281]. Also, increased levels of proteins related to unfolded protein response (UPR), were observed by Bolinches-Amorós *et. al.*[282].

Glucose-6-phosphatase catalytic subunit (*G6PC*) mRNA levels might be downregulated by elevated levels of miR-10b-5p in the three cell models, and as consequence a reduction in glucose formation may be expected.

In neurotrophin signalling pathway, we found that neurotrophic receptor tyrosine kinase 2 (*NTRK2*) is targeted by miR-10b-5p, which expression levels were upregulated in all FRDA cellular models analysed compared with control cell lines. Reduced levels of the protein encoded by *NTRK2* gene (BDNF/NT-3 growth factors receptor) produce that neurotrophins, which promote neural survival, bind to the low affinity receptor p75NTR, that they have in common, therefore promoting neuronal death [283,284].

One of the pathways identified in our study is the AMPK signalling pathway, which is known to be altered in Friedreich's ataxia. This pathway is responsible for altered ATP levels and deregulation of the mitochondrial biogenesis pathway, as previously described[201]. Our results showed increased levels of miR-10b-5p in the three FRDA cellular models compared to controls. This fact might produce a downregulation of the transcription factor *FOXO3.* However, when we analysed the expression levels of *FBXO32* gene by qRT-PCR, a target of *FOXO3*, we observed increased levels of this gene, which has been previously

described as an inhibitor of cardiac hypertrophy [285] in all cellular models. So, these results may indicate that transcription of *FBXO32* is increased maybe with the aim to reduce the signals that promote cardiac hypertrophy in FRDA patients. On the other hand, some post-translational regulation may produce an inhibition of atrogin-1 protein that seems to fail in hypertrophy inhibition. In addition, miR-10b-5p may be overexpressed in order to decrease *FBXO32* levels through its transcription factor. Also, in olfactory mucosa stem cells, decreased levels of miR-106b-5p may result in elevated AKt expression, which activates mTOR through Rheb protein[286]. This could explain the improvement in the motor phenotype in *Drosophila melanogaster* FRDA models treated with the TORC1 inhibitor, rapamycin[287]. However, miR-106b-3p and miR-15a-3p downregulated levels found in olfactory mucosa stem cells showed a different scenario. miR-106b-3p and miR-15a-3p, when are downregulated, may produce the upregulation of their target genes *AMPK* and *PTEN,* respectively. The up-regulated levels of *AMPK* and *PTEN* may produce consequently mTORC and AKt inhibition. Furthermore, it is not clear if PDK1 might be downregulated or upregulated, because miR-10b-5p is upregulated and miR-106b-5p is downregulated in olfactory mucosa stem cells. These controversial results point out that further studies in AKt/mTORC/AMPK signalling in FRDA patients should be performed in order to understand the regulation of this pathway and to discover biomarkers for patients' risk stratification or new targets for developing a possible treatment of this neurodegenerative disease.

5.2.2. Biomarkers in human plasma

In our study of smallRNA-seq using plasma from FRDA patients versus healthy controls, we found seven circulating miRNAs (hsa-miR-128-3p, hsa-miR-625-3p, hsa-miR-130b-5p, hsa-miR-151a-5p, hsa-miR-330-3p, hsa-miR-323a-3p, hsa-miR-142-3p) differentially represented in plasma samples. Some of these circulating miRNAs have been already found in other neurodegenerative disorders. For example, miR-128-3p was found overexpressed in plasma from people with Huntington's disease[288] and in

T cells from people with multiple sclerosis[289]. In contrast, lower levels of miR-142-3p were found in plasma from patients with Alzheimer's disease than in controls[290].

In an effort to identify biomarkers able to stratify patients' risk according to their phenotype, we found that miR-323a-3p was significantly upregulated in patients with cardiomyopathy compared to patients whose clinical records made no mention of this comorbidity. Our analysis demonstrated high sensitivity (88.9%) and acceptable specificity (62.5%) and the AUC was 0.75 (p= 0.042).

From a clinical point of view, the Mitochondrial Protection with Idebenone in Cardiac or Neurological Outcome (MICONOS) study group concludes that, irrespective of neurological status, all FRDA patients need an initial cardiac evaluation including cMRI (cardiac magnetic resonance imaging) and echocardiography and a regular echocardiographic follow-up[291]. Furthermore, these authors assert that clinical algorithms must be developed to manage and predict cardiomyopathies in rare diseases. The use of miR-323a-3p would help clinicians in this regard and could contribute to early diagnosis and prognosis of cardiomyopathy prior to detection by standard diagnostic procedures of clinical or morphological cardiac tissue manifestations.

5.2.2.1. *Fatty acids and central carbon metabolism Pathways*

In our pathway analysis of miRNAs in plasma, we identified fatty acid metabolism (hsa01212) and central carbon metabolism (hsa05230), as two additional pathways altered in FRDA. As these results show, lactate dehydrogenase A (LDHA) deregulation may alter the NAD+/NADH ratio, thus modifying energy metabolism through alteration of fatty acid oxidation[292] and the Krebs cycle[293] in cells. This deregulation of energy metabolism is a critical factor in FRDA cardiomyopathy. Linking these ideas with those concerning fatty acid pathway regulation based on our miRpath analysis, we found that miR-130b-5p regulates fatty acid synthase (FASN) and miR-142-3p targets adipose acyl-CoA synthetase-1 (ACSL1), resulting in increased uptake of fatty acids for use in ß-oxidation. In addition, a prolonged energy shift from fatty acid to glucose oxidation is a well-known feature of cardiac damage[294], and may contribute to FRDA cardiomyopathy.

5.2.2.2.   AMPK and AKT signalling pathways

In our study, one of the pathways identified was the AMPK signalling pathway. As we said before, this pathway, altered in Friedreich's ataxia, is responsible for deregulation of ATP levels and the mitochondrial biogenesis pathways[201]. AMPK, which is directly targeted by miR-625-3p and miR-130b-5p, is a crosstalk protein involved in the mTOR signalling pathway, an important mechanism that is altered in FRDA[201]. Calap-Quintana *et. al.* discovered that inhibition of TORC1 by the drug rapamycin improves the motor phenotype in *Drosophila melanogaster* FRDA models[287]. We found that miR-625-3p and miR-330-3p regulate transcription factors that play an important role in antioxidant gene regulation, protein quality control and autophagy. These transcription factors include FOXO [295-297], one of the pathways identified in our analysis. Ataxia telangiectasia mutated (ATM), among other proteins, is also regulated by miRNAs in the FOXO pathway. ATM participates in the regulation of DNA repair and controls DNA damage responses. Altered expression levels of ATM and p53 were previously detected in lymphocytes from FRDA patients[298]. FOXO transcription factors are involved in several physiological and pathological processes, including neurological diseases[297].

Our analysis also found that PTEN was a target of miR-151-5p and miR-625-3p. Interestingly, PTEN antagonizes PI3K, meaning the downregulation of PTEN may change the PIP3/PIP2 ratio. An increase in PIP3 could subsequently activate AKT. This pathway coordinates different steps of axon growth during development and in injury-induced axon regeneration[299]. PIP2 hydrolysis is responsible for the changes in Ca^{+2} homeostasis. Bolinches-Amorós *et. al.* showed that a decrease in frataxin levels induces mitochondrial dysfunction as a result of a bioenergetic deficit and abnormal Ca^{+2} metabolism[282]. Importantly, the Ca^{+2} signalling pathway regulates many pathways. Alterations in this pathway contribute to different disease states. For this reason, the discovery of biological modulators, like miRNAs, in this pathway is highly valuable.

Our results, also point out the relevance of HIF-1alfa signaling pathway. HIF-1alfa is targeted by miR-625-3p may produce a decreased levels of proteins

that are regulated by this transcriptional factor, among them those related with iron homeostasis. Also, nowadays it is known that hypoxia stimulate the frataxin expression through HIF-1alfa mediated mechanisms[300].

To validate some of the miRNAs we found in plasma, which are involved in the regulation of these pathways, we studied their expression in all three cellular models described in the previous section (i.e. olfactory mucosa stem cell, SH-SY5Y and fibroblasts). In all of them miR-330-3p showed differential expression, but only in SH-SY5Y we detected elevated levels of this miRNAs as occurred in plasma analysis, indicating that miR-330-3p could be interesting in FRDA. In addition, further analyses to understand the role of this miRNA were performed. We measured mRNA levels of some targets of miR-130b-5p (*LDHA* and *PDHA)* and mir-330-3p (*FOXO1* and *SOD2*) in SH-S5Y5 cell model and also in fibroblasts and olfactory mucosa stem cells. In olfactory mucosa stem cells, decreased levels of mir-330-3p were also observed, that may fit with increased levels of its target FOXO described previously in flies[287]. However, when we analysed mRNA levels of FOXO1 we showed decreased levels of expression. The different results with those described in *Drosophila*[287], may be explained by the diversity of the FOXO family in humans that is not found in the fly. So, we detect decreased levels of FOXO1, but maybe other protein/s of the FOXO family involved in FRDA physiopathology that could be upregulated. In fibroblasts, we detected low levels of mir-330-3p and by contrast downregulated levels of *LDHA* gene expression. On the contrary, elevated levels of lactate have been detected in blood of FRDA patients [134]. Furthermore, mir-130b-5p is also downregulated in olfactory mucosa stem cells and some of its targets, *PDK1*, *AMPK*, and *FASN* genes might have elevated levels of expression. PDK1 elevated levels may activate AKT promoting mTORC signalling and FOXO repression, however as we mentioned above, elevated levels of PDK1 inhibitor (*PTEN*) might also be promoted. Moreover, AMPK elevated levels may block mTORC activity. Thus, it is not clear if these pathways are activated or not. Elevated levels of PDK1 were observed in fly [301] and mice [302] models of frataxin deficiency, as well as increased levels of sphingolipid, iron accumulation and activation of Mef2 signalling pathway. In addition, elevated levels of *FASN* gene promote fatty acids synthesis, and elevated

oxidation of fatty acids generates ROS and cardiac problems[273,274] as we said above in cellular models. Finally, as already explained we observed elevated levels of mir-330-3p in the SH-SY5Y cell model, results that are coincident with those observed in plasma analysis. High levels of mRNA from *SOD2* gene were observed nevertheless high levels of mi-330-3p. These results are interesting, because low levels of *SOD2* transcript in fibroblasts from FRDA have been reported[201] , which fit well with our mir-330-3p expression results, however high levels of SOD2 expression have been described in *Drosophila* models of FRDA[287].

PGC-1α has been described as a regulator of PDHA1[303] and increased levels of PGC-1α has been found in fibroblasts from FRDA patients[287], so elevated PDHA1 gene expression may be related to high levels of PGC-1α more than an inhibition mediated by miR-330-3p. Moreover, decreased levels of *FOXO1* were observed in SH-SY5Y cell model, which was only congruent with miR-330-3p overexpression for frataxin-deficient cell lines. In addition, the repression of FOXO1 inhibits the transcription of pro-apoptotic protein BIM in neurons[304] and therefore inhibits apoptotic response, results that are in agreement with those described by Bolinches-Amorós *et. al.*[282] in which no differences in cytosolic cytochrome c levels were found. It will be interesting to tease out in future research the role of miR-330-3p/FOXO interplay in the regulation of neuronal survival in FRDA.

5.2.2.3. *Insulin signalling pathway*

Some of the miRNAs identified in our study regulate key genes in the insulin-signalling pathway, such as the eukaryotic translation initiation factor eIF4E, which is regulated by miR-142-3p, and Glycogen synthase kinase 3 beta (GSK3β), which is regulated by both miR-130b-5p and miR-625-3p. In addition, insulin-like growth factor I (IGF-I) has shown therapeutic effects in different cerebellar ataxias due to its protective effects on mitochondrial function and neuroprotective effects in frataxin deficient neuronal cultures[305] and Fxn-deficient mice[306]. Furthermore, diabetes is a metabolic disorder that affects one in every three Friedreich's ataxia patients. Insulin resistance and loss of glucose

tolerance are features found in the FRDA phenotype[307], and they seem to depend on the entry in senescence of the islets of Langerhans[308] and β-pancreatic cell survival.

5.2.2.4.   *Wnt/β-catenin signalling pathway*

Finally, we found that miR-151-5p and miR-625-3p target CTNNB1, and miR-142-3p, miR-323a-3p, and miR-151a-5p target ATP2A2. From our results it is feasible to hypothesize that an elevated cytosolic level of Ca^{+2} due to low levels of ATP2A2 (SERCA) may stimulate calmodulin protein (CaM), and in turn activate calcineurin (CaN), which dephosphorylates the nuclear factor of activated T cells (NFAT) being translocated into the nucleus. This transcription factor activates genes for cardiac growth and remodelling, resulting in increased cardiac hypertrophy (Figure 36). Recent studies in conditional gain-of-function of β-catenin (CTNNB1) cardiac endothelial cells from mice showed that Wnt/β-catenin signalling activation may be a cause of cardiac dysfunction through downregulation of the neuregulin-Erb-B pathway[309]. Reduced ATP2A2 mRNA levels have also been shown to affect heart function and are associated with hypertrophied hearts[310,311]. In addition, when we try to validate the circulating miRNAs in the cellular models described in this work, we found that miR-323a-3p was also upregulated in olfactory mucosa stem cells and SH-SY5Y cell model. These facts point out the importance of this miRNA in cardiomyopathy feature in FRDA. Moreover, we provide new candidate mechanisms to explain altered heart function in FRDA.
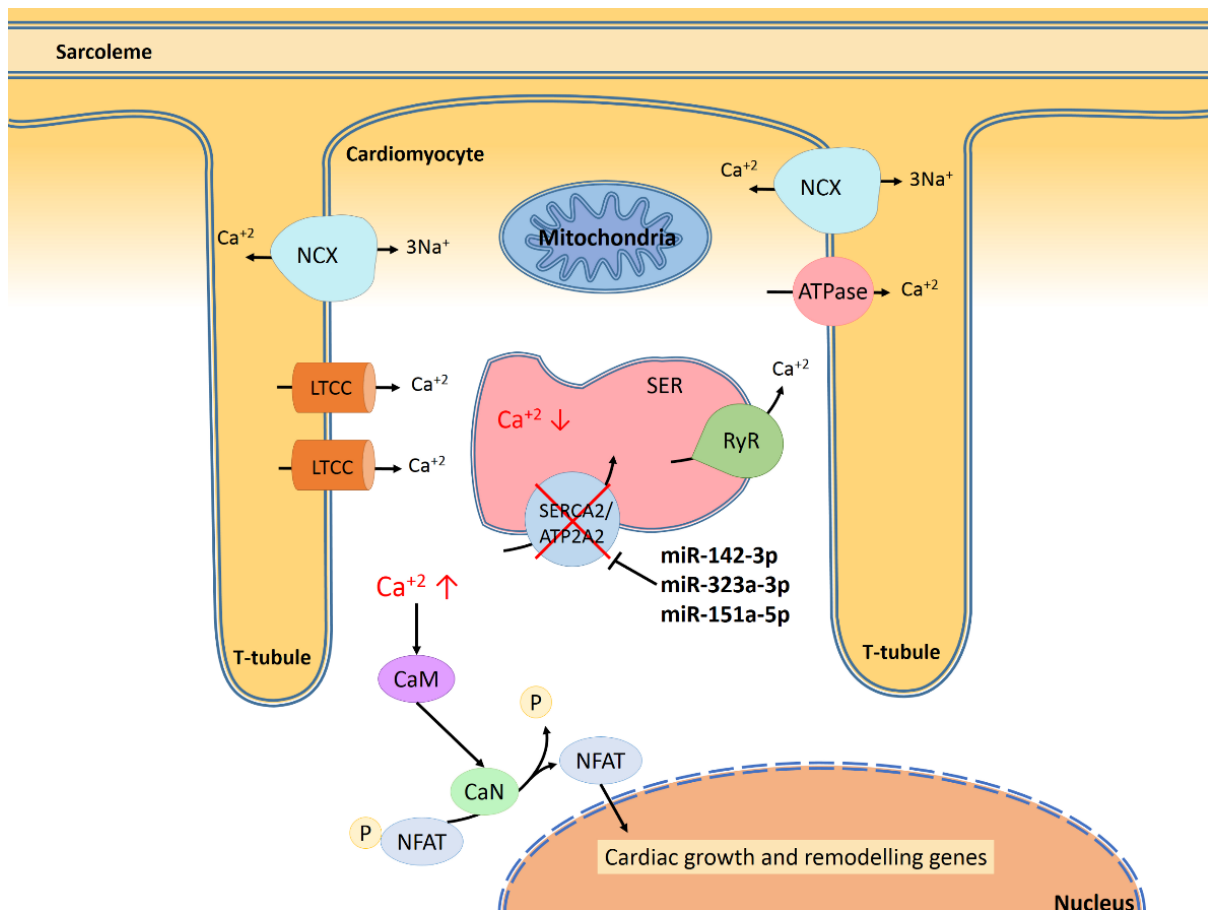
Figure 37. Overexpressed mir-142-3p, miR323a-3p and mir-151-5p may produce cardiac hypertrophy in FRDA patients by blocking ATP2A2. Sarcoplasmic/endoplasmic reticulum Ca+2 ATPase (SERCA2; also known as ATP2A2) and ryanodine receptor (RyR) regulate the Ca+2 input and output (respectively) of the sarcoplasmic endoplasmic reticulum (SER) in cardiomyocytes. In addition, sarcolemmal Na+/Ca+2 exchangers (NCX), ATPases, mitochondria, and L-type Ca+2 channels (LTCC) mediate the exchange of cytosolic Ca+2. Increased levels of mir-142-3p, miR323a-3p and mir-151-5p may decrease mRNA levels of SERCA and also SERCA protein levels. Low levels of SERCA produce an elevated cytosolic level of Ca2+ with a concomitant activation of calmodulin protein (CaM). Activated CaM can, in turn, stimulate the active form of calcineurin (CaN), which dephosphorylates the nuclear factor of activated T cells (NFAT) protein in the cytosol. This facilitates its translocation into the nucleus, and interacts with cardiac growth and gene promoter remodelling, resulting in increased cardiac hypertrophy.

5.2.2.5.   *Relevance of results in FRDA biomarkers*

Our results open new avenues for developing more personalized therapies focused on specific patients' symptoms. We identified seven miRNAs, all of which are associated with key molecular mechanisms underlying FRDA physiopathology. We found that miR-323-3p is a candidate for diagnosing cardiomyopathy in FRDA patients. Pilbrow *et al.* have described miR-323-3p as a candidate biomarker for coronary artery disease (CAD) in acute coronary syndrome (ACS) patients[312].

Previous studies have proposed that miRNAs play a direct or indirect role in cardiac hypertrophy in FRDA. In this regard, Kelly et al. found that miR-155 downregulates AGTR1, resulting in reduced production of AGTR1. However, the rs5186 C allele interrupts complementarity between miR-155 and the regulatory target site of AGTR1, thereby increasing AGTR1 levels, which may explain an increased degree of cardiac hypertrophy, oxidative stress, and fibrosis in FRDA patients[313]. We explored the expression of miR-155 in our series of patients and controls but found no significant differences. This could be because, as Kelly et al. propose, the effect may remain in the rs5186 C allele of AGTR1, but not in the different expression levels of miR-155.

Both clinicians and patients have called for new drugs to treat FRDA. However, these drugs do not always provide benefits, probably because underlying molecular mechanisms are not fully understood[314]. For example, variation in the efficacy of Idebenone in half of FRDA patients remains unexplained[315]. This drug decreases free fatty acid content[316]. Furthermore, as previously described, it decreases PGC1α[201], which cooperates with peroxisome proliferator-activated receptor alpha (PPARα) in transcriptional control of mitochondrial fatty acid oxidation enzymes[317]. As a result, altered regulation of fatty acid metabolism and fatty acid oxidation by microRNAs may help to regulate patients' different responses to Idebenone treatment.

In this regard, circulating miRNAs can detect pathological events, and could also monitor molecular signals participating in cardiomyopathy even before the appearance of clinical cardiac manifestations. To maximize the likelihood of detecting the onset or progression of cardiomyopathy, we suggest combining standard cardiac diagnostic procedures with the use of circulating microRNAs. This approach could provide more clinical information for evaluating cardiomyopathy progression in FRDA. In summary, miRNAs obtained in this study constitute new candidates for personalized therapy in FRDA patients.

6. Conclusions

Conclusions

1. Plasma from mild and severe Charcot-Marie-Tooth patients does not show differences in oxidative stress markers.

2. Twenty candidate proteomic biomarkers are detected in plasma from mild and severe Charcot-Marie-Tooth patients.

3. Further experiments and improvement of CMT diagnostic criteria irrespective to CMTNS should be performed in order to obtain clinical correlations with candidate proteomic markers.

4. Different expression profiles of miRNA are detected in cellular models of Friedreich's ataxia (i.e. olfactory mucosa stem cells, fibroblasts and SH-SY5Y) and plasma samples from FRDA patients compared to their respective controls, indicating that miRNAs play a relevant role in the physiopathology of FRDA.

5. miR-323a-3p is a biomarker of cardiomyopathy in patients with Friedreich's ataxia and may play a role in the deregulation of Ca^{+2} homeostasis in hypertrophic cardiomyopathy observed in FRDA patients.

Conclusions

7. Limitations

Limitations

The design of this study has certain limitations that are usually present in the study of most rare genetic diseases. Although this is a relatively large and well-characterized FRDA and CMT cohort, the small sample size of each sub-population limits the statistical power of the study to propose specific biomarkers that correlate with some of the clinical features analysed. Nevertheless, we are convinced that our study further increases the knowledge of molecular mechanisms underlying such a complex disease and constitutes a good starting point for launching a wider international effort to provide further insight. In any case, the potential use of these biomarkers must be seen as an additional help for clinicians and not as the main diagnostic tool. With the information provided by these biomarkers, clinicians can maintain a close follow-up of patients who show changes in the miRNA's signature.

Limitations

8. Bibliography

1.   Berthold CH, Fraher JP, King RHM, Rydmark M. Chapter 3 - Microscopic Anatomy of the Peripheral Nervous System A2 - Dyck, Peter J. In: Thomas PK, ed. Peripheral Neuropathy (Fourth Edition). Philadelphia: W.B. Saunders; 2005: 35-91.

2.   Salzer JL. Polarized domains of myelinated axons. *Neuron* 2003; **40**(2): 297-318.

3.   Brodal P. The central nervous system: structure and function: Oxford University Press; 2004.

4.   Chapter 12. The Nervous System and Nervous Tissue. In: Heyden RJ, editor. Anatomy & Physiology: Rice University.

5.   Richner M, Ulrichsen M, Elmegaard SL, Dieu R, Pallesen LT, Vaegter CB. Peripheral nerve injury modulates neurotrophin signaling in the peripheral and central nervous system. *Molecular neurobiology* 2014; **50**(3): 945-70.

6.   Honma Y, Kawano M, Kohsaka S, Ogawa M. Axonal projections of mechanoreceptive dorsal root ganglion neurons depend on Ret. *Development* 2010; **137**(14): 2319-28.

7.   Klein CJ, Duan X, Shy ME. Inherited neuropathies: clinical overview and update. *Muscle & nerve* 2013; **48**(4): 604-22.

8.   Luo L, O'Leary DD. Axon retraction and degeneration in development and disease. *Annu Rev Neurosci* 2005; **28**: 127-56.

9.   Weis J, Claeys KG, Roos A, et al. Towards a functional pathology of hereditary neuropathies. *Acta Neuropathol* 2017; **133**(4): 493-515.

10.   Mignarri A, Gallus GN, Dotti MT, Federico A. A suspicion index for early diagnosis and treatment of cerebrotendinous xanthomatosis. *J Inherit Metab Dis* 2014; **37**(3): 421-9.

11.   Depienne C, Stevanin G, Brice A, Durr A. Hereditary spastic paraplegias: an update. *Curr Opin Neurol* 2007; **20**(6): 674-80.

12.   Trott A, Houenou LJ. Mini-review: spinocerebellar ataxias: an update of SCA genes. *Recent Pat DNA Gene Seq* 2012; **6**(2): 115-21.

13.   Stone JR, Yang S. Hydrogen peroxide: a signaling messenger. *Antioxid Redox Signal* 2006; **8**(3-4): 243-70.

14.   Finkel T. Oxidant signals and oxidative stress. *Curr Opin Cell Biol* 2003; **15**(2): 247-54.

15.   Smythies J. The neurotoxicity of glutamate, dopamine, iron and reactive oxygen species: functional interrelationships in health and disease: a review-discussion. *Neurotox Res* 1999; **1**(1): 27-39.

16.   Dasuri K, Zhang L, Keller JN. Oxidative stress, neurodegeneration, and the balance of protein degradation and protein synthesis. *Free radical biology & medicine* 2013; **62**: 170-85.

17.   Di Meo S, Reed TT, Venditti P, Victor VM. Role of ROS and RNS Sources in Physiological and Pathological Conditions. *Oxidative medicine and cellular longevity* 2016; **2016**: 1245049.

18.   Nathan C, Xie QW. Nitric oxide synthases: roles, tolls, and controls. *Cell* 1994; **78**(6): 915-8.

19.   Pacher P, Beckman JS, Liaudet L. Nitric oxide and peroxynitrite in health and disease. *Physiol Rev* 2007; **87**(1): 315-424.

20.   Dizdaroglu M. Oxidative damage to DNA in mammalian chromatin. *Mutation Research/DNAging* 1992; **275**(3): 331-42.

21.   Loft S, Fischer-Nielsen A, Jeding IB, Vistisen K, Poulsen HE. 8-Hydroxydeoxyguanosine as a urinary biomarker of oxidative DNA damage. *J Toxicol Environ Health* 1993; **40**(2-3): 391-404.

22.   Hawkins CL, Morgan PE, Davies MJ. Quantification of protein modification by oxidants. *Free radical biology & medicine* 2009; **46**(8): 965-88.

23.   Loidl-Stahlhofen A, Hannemann K, Spiteller G. Generation of alpha-hydroxyaldehydic compounds in the course of lipid peroxidation. *Biochimica et biophysica acta* 1994; **1213**(2): 140-8.

24.   Pompella A, Visvikis A, Paolicchi A, De Tata V, Casini AF. The changing faces of glutathione, a cellular protagonist. *Biochemical pharmacology* 2003; **66**(8): 1499-503.

25.   Arner ES, Holmgren A. Physiological functions of thioredoxin and thioredoxin reductase. *Eur J Biochem* 2000; **267**(20): 6102-9.

26.   Wood ZA, Schroder E, Robin Harris J, Poole LB. Structure, mechanism and regulation of peroxiredoxins. *Trends Biochem Sci* 2003; **28**(1): 32-40.

27.   Uttara B, Singh AV, Zamboni P, Mahajan RT. Oxidative stress and neurodegenerative diseases: a review of upstream and downstream antioxidant therapeutic options. *Curr Neuropharmacol* 2009; **7**(1): 65-74.

28.   Marquardt D, Williams JA, Kucerka N, et al. Tocopherol activity correlates with its location in a membrane: a new perspective on the antioxidant vitamin E. *J Am Chem Soc* 2013; **135**(20): 7523-33.

29.   Berg RA, Steinmann B, Rennard SI, Crystal RG. Ascorbate deficiency results in decreased collagen production: under-hydroxylation of proline leads to increased intracellular degradation. *Arch Biochem Biophys* 1983; **226**(2): 681-6.

30.   Pop-Busui R, Sima A, Stevens M. Diabetic neuropathy and oxidative stress. *Diabetes Metab Res Rev* 2006; **22**(4): 257-73.

31.   Hayashi G, Cortopassi G. Oxidative stress in inherited mitochondrial diseases. *Free radical biology & medicine* 2015; **88**(Pt A): 10-7.

32.   Patel VP, Chu CT. Nuclear transport, oxidative stress, and neurodegeneration. *Int J Clin Exp Pathol* 2011; **4**(3): 215-29.

33.   Adelman R, Saul RL, Ames BN. Oxidative damage to DNA: relation to species metabolic rate and life span. *Proceedings of the National Academy of Sciences of the United States of America* 1988; **85**(8): 2706-8.

34.   Yan MH, Wang X, Zhu X. Mitochondrial defects and oxidative stress in Alzheimer disease and Parkinson disease. *Free radical biology & medicine* 2013; **62**: 90-101.

35.   Hollenbeck PJ, Saxton WM. The axonal transport of mitochondria. *Journal of cell science* 2005; **118**(Pt 23): 5411-9.

36.   Lu T, Pan Y, Kao SY, et al. Gene regulation and DNA damage in the ageing human brain. *Nature* 2004; **429**(6994): 883-91.

37. Koopman WJ, Willems PH, Smeitink JA. Monogenic mitochondrial disorders. *The New England journal of medicine* 2012; **366**(12): 1132-41.

38. Celsi F, Ferri A, Casciati A, et al. Overexpression of superoxide dismutase 1 protects against beta-amyloid peptide toxicity: effect of estrogen and copper chelators. *Neurochem Int* 2004; **44**(1): 25-33.

39. Rosen DR, Siddique T, Patterson D, et al. Mutations in Cu/Zn superoxide dismutase gene are associated with familial amyotrophic lateral sclerosis. *Nature* 1993; **362**(6415): 59-62.

40. Tozzi G, Nuccetelli M, Lo Bello M, et al. Antioxidant enzymes in blood of patients with Friedreich's ataxia. *Arch Dis Child* 2002; **86**(5): 376-9.

41. Clausen A, Xu X, Bi X, Baudry M. Effects of the superoxide dismutase/catalase mimetic EUK-207 in a mouse model of Alzheimer's disease: protection against and interruption of progression of amyloid and tau pathology and cognitive decline. *Journal of Alzheimer's disease : JAD* 2012; **30**(1): 183-208.

42. Umeda-Kameyama Y, Tsuda M, Ohkura C, et al. Thioredoxin suppresses Parkin-associated endothelin receptor-like receptor-induced neurotoxicity and extends longevity in Drosophila. *The Journal of biological chemistry* 2007; **282**(15): 11180-7.

43. Garcia-Gimenez JL, Seco-Cervera M, Aguado C, et al. Lafora disease fibroblasts exemplify the molecular interdependence between thioredoxin 1 and the proteasome in mammalian cells. *Free radical biology & medicine* 2013; **65**: 347-59.

44. Vernia S, Rubio T, Heredia M, Rodriguez de Cordoba S, Sanz P. Increased endoplasmic reticulum stress and decreased proteasomal function in lafora disease models lacking the phosphatase laforin. *PloS one* 2009; **4**(6): e5907.

45. Oh S, Hong HS, Hwang E, et al. Amyloid peptide attenuates the proteasome activity in neuronal cells. *Mechanisms of ageing and development* 2005; **126**(12): 1292-9.

46. McNaught KS, Jenner P. Proteasomal function is impaired in substantia nigra in Parkinson's disease. *Neuroscience letters* 2001; **297**(3): 191-4.

47. Lee M, Cho T, Jantaratnotai N, Wang YT, McGeer E, McGeer PL. Depletion of GSH in glial cells induces neurotoxicity: relevance to aging and degenerative neurological diseases. *FASEB journal : official publication of the Federation of American Societies for Experimental Biology* 2010; **24**(7): 2533-45.

48. Pastore A, Tozzi G, Gaeta LM, et al. Actin glutathionylation increases in fibroblasts of patients with Friedreich's ataxia: a potential role in the pathogenesis of the disease. *The Journal of biological chemistry* 2003; **278**(43): 42588-95.

49. Conte V, Uryu K, Fujimoto S, et al. Vitamin E reduces amyloidosis and improves cognitive function in Tg2576 mice following repetitive concussive brain injury. *Journal of neurochemistry* 2004; **90**(3): 758-64.

50. Ienco EC, LoGerfo A, Carlesi C, et al. Oxidative stress treatment for clinical trials in neurodegenerative diseases. *Journal of Alzheimer's disease : JAD* 2011; **24 Suppl 2**: 111-26.

51. Martin A, Youdim K, Szprengiel A, Shukitt-Hale B, Joseph J. Roles of vitamins E and C on neurodegenerative diseases and cognitive performance. *Nutr Rev* 2002; **60**(10 Pt 1): 308-26.

52.   Huntington Study Group Pre CI, Hyson HC, Kieburtz K, et al. Safety and tolerability of high-dosage coenzyme Q10 in Huntington's disease and healthy subjects. *Movement disorders : official journal of the Movement Disorder Society* 2010; **25**(12): 1924-8.

53.   Shults CW, Oakes D, Kieburtz K, et al. Effects of coenzyme Q10 in early Parkinson disease: evidence of slowing of the functional decline. *Arch Neurol* 2002; **59**(10): 1541-50.

54.   Braathen GJ, Sand JC, Lobato A, Hoyer H, Russell MB. Genetic epidemiology of Charcot-Marie-Tooth in the general population. *Eur J Neurol* 2011; **18**(1): 39-48.

55.   Kurihara S, Adachi Y, Wada K, Awaki E, Harada H, Nakashima K. An epidemiological genetic study of Charcot-Marie-Tooth disease in Western Japan. *Neuroepidemiology* 2002; **21**(5): 246-50.

56.   MacMillan JC, Harper PS. The Charcot-Marie-Tooth syndrome: clinical aspects from a population study in South Wales, UK. *Clin Genet* 1994; **45**(3): 128-34.

57.   Tazir M, Hamadouche T, Nouioua S, Mathis S, Vallat JM. Hereditary motor and sensory neuropathies or Charcot-Marie-Tooth diseases: an update. *Journal of the neurological sciences* 2014; **347**(1-2): 14-22.

58.   Harding AE, Thomas PK. The clinical features of hereditary motor and sensory neuropathy types I and II. *Brain : a journal of neurology* 1980; **103**(2): 259-80.

59.   Reilly MM. Axonal Charcot-Marie-Tooth disease: the fog is slowly lifting! *Neurology* 2005; **65**(2): 186-7.

60.   Mathis S, Goizet C, Tazir M, et al. Charcot-Marie-Tooth diseases: an update and some new proposals for the classification. *J Med Genet* 2015; **52**(10): 681-90.

61.   Pareyson D, Scaioli V, Laura M. Clinical and electrophysiological aspects of Charcot-Marie-Tooth disease. *Neuromolecular Med* 2006; **8**(1-2): 3-22.

62.   Shy ME, Lupski JR, Chance PF, Klein CJ, Dyck PJ. Chapter 69 - Hereditary Motor and Sensory Neuropathies: An Overview of Clinical, Genetic, Electrophysiologic, and Pathologic Features. Peripheral Neuropathy (Fourth Edition). Philadelphia: W.B. Saunders; 2005: 1623-58.

63.   Thomas PK, Marques W, Jr., Davis MB, et al. The phenotypic manifestations of chromosome 17p11.2 duplication. *Brain : a journal of neurology* 1997; **120 (Pt 3)**: 465-78.

64.   Hoogendijk JE, De Visser M, Bolhuis PA, Hart AA, Ongerboer de Visser BW. Hereditary motor and sensory neuropathy type I: clinical and neurographical features of the 17p duplication subtype. *Muscle & nerve* 1994; **17**(1): 85-90.

65.   Sghirlanzoni A, Pareyson D, Scaioli V, Marazzi R, Pacini L. Hereditary motor and sensory neuropathy type I and type II. *Ital J Neurol Sci* 1990; **11**(5): 471-9.

66.   Krajewski KM, Lewis RA, Fuerst DR, et al. Neurological dysfunction and axonal degeneration in Charcot-Marie-Tooth disease type 1A. *Brain : a journal of neurology* 2000; **123 (Pt 7)**: 1516-27.

67.   Dyck PJ, Karnes JL, Lambert EH. Longitudinal study of neuropathic deficits and nerve conduction abnormalities in hereditary motor and sensory neuropathy type 1. *Neurology* 1989; **39**(10): 1302-8.

68.   Burns J, Ryan MM, Ouvrier RA. Evolution of foot and ankle manifestations in children with CMT1A. *Muscle & nerve* 2009; **39**(2): 158-66.

69.   Garcia CA, Malamut RE, England JD, Parry GS, Liu P, Lupski JR. Clinical variability in two pairs of identical twins with the Charcot-Marie-Tooth disease type 1A duplication. *Neurology* 1995; **45**(11): 2090-3.

70.   Berciano J, Garcia A, Combarros O. Initial semeiology in children with Charcot-Marie-Tooth disease 1A duplication. *Muscle & nerve* 2003; **27**(1): 34-9.

71.   Suter U, Scherer SS. Disease mechanisms in inherited neuropathies. *Nat Rev Neurosci* 2003; **4**(9): 714-26.

72.   Jetten AM, Suter U. The peripheral myelin protein 22 and epithelial membrane protein family. *Prog Nucleic Acid Res Mol Biol* 2000; **64**: 97-129.

73.   Parmantier E, Cabon F, Braun C, D'Urso D, Muller HW, Zalc B. Peripheral myelin protein-22 is expressed in rat and mouse brain and spinal cord motoneurons. *Eur J Neurosci* 1995; **7**(5): 1080-8.

74.   Parmantier E, Braun C, Thomas JL, Peyron F, Martinez S, Zalc B. PMP-22 expression in the central nervous system of the embryonic mouse defines potential transverse segments and longitudinal columns. *The Journal of comparative neurology* 1997; **378**(2): 159-72.

75.   Suter U, Patel PI. Genetic basis of inherited peripheral neuropathies. *Hum Mutat* 1994; **3**(2): 95-102.

76.   Li J, Parker B, Martyn C, Natarajan C, Guo J. The PMP22 gene and its related diseases. *Molecular neurobiology* 2013; **47**(2): 673-98.

77.   Saberan-Djoneidi D, Sanguedolce V, Assouline Z, Levy N, Passage E, Fontes M. Molecular dissection of the Schwann cell specific promoter of the PMP22 gene. *Gene* 2000; **248**(1-2): 223-31.

78.   Desarnaud F, Do Thi AN, Brown AM, et al. Progesterone stimulates the activity of the promoters of peripheral myelin protein-22 and protein zero genes in Schwann cells. *Journal of neurochemistry* 1998; **71**(4): 1765-8.

79.   Desarnaud F, Bidichandani S, Patel PI, Baulieu EE, Schumacher M. Glucocorticosteroids stimulate the activity of the promoters of peripheral myelin protein-22 and protein zero genes in Schwann cells. *Brain research* 2000; **865**(1): 12-6.

80.   Zhang F, Seeman P, Liu P, et al. Mechanisms for Nonrecurrent Genomic Rearrangements Associated with CMT1A or HNPP: Rare CNVs as a Cause for Missing Heritability. *The American Journal of Human Genetics* 2010; **86**(6): 892-903.

81.   Chance PF, Alderson MK, Leppig KA, et al. DNA deletion associated with hereditary neuropathy with liability to pressure palsies. *Cell* 1993; **72**(1): 143-51.

82.   Jen J, Baloh RH, Ishiyama A, Baloh RW. Dejerine-Sottas syndrome and vestibular loss due to a point mutation in the PMP22 gene. *Journal of the neurological sciences* 2005; **237**(1-2): 21-4.

83.   Manfioletti G, Ruaro ME, Del Sal G, Philipson L, Schneider C. A growth arrest-specific (gas) gene codes for a membrane protein. *Molecular and cellular biology* 1990; **10**(6): 2924-30.

84.   Taylor V, Zgraggen C, Naef R, Suter U. Membrane topology of peripheral myelin protein 22. *Journal of neuroscience research* 2000; **62**(1): 15-27.

85.   Snipes GJ, Suter U, Welcher AA, Shooter EM. Characterization of a novel peripheral nervous system myelin protein (PMP-22/SR13). *J Cell Biol* 1992; **117**(1): 225-38.

86.   Taylor V, Welcher AA, Program AE, Suter U. Epithelial membrane protein-1, peripheral myelin protein 22, and lens membrane protein 20 define a novel gene family. *The Journal of biological chemistry* 1995; **270**(48): 28824-33.

87.   Pareek S, Suter U, Snipes GJ, Welcher AA, Shooter EM, Murphy RA. Detection and processing of peripheral myelin protein PMP22 in cultured Schwann cells. *The Journal of biological chemistry* 1993; **268**(14): 10372-9.

88.   D'Urso D, Muller HW. Ins and outs of peripheral myelin protein-22: mapping transmembrane topology and intracellular sorting. *Journal of neuroscience research* 1997; **49**(5): 551-62.

89.   Hasse B, Bosse F, Hanenberg H, Muller HW. Peripheral myelin protein 22 kDa and protein zero: domain specific trans-interactions. *Mol Cell Neurosci* 2004; **27**(4): 370-8.

90.   Myers JK, Mobley CK, Sanders CR. The peripheral neuropathy-linked Trembler and Trembler-J mutant forms of peripheral myelin protein 22 are folding-destabilized. *Biochemistry* 2008; **47**(40): 10620-9.

91.   Bosse F, Brodbeck J, Muller HW. Post-transcriptional regulation of the peripheral myelin protein gene PMP22/gas3. *Journal of neuroscience research* 1999; **55**(2): 164-77.

92.   Ryan MC, Notterpek L, Tobler AR, Liu N, Shooter EM. Role of the peripheral myelin protein 22 N-linked glycan in oligomer stability. *Journal of neurochemistry* 2000; **75**(4): 1465-74.

93.   Adlkofer K, Martini R, Aguzzi A, Zielasek J, Toyka KV, Suter U. Hypermyelination and demyelinating peripheral neuropathy in Pmp22-deficient mice. *Nature genetics* 1995; **11**(3): 274-80.

94.   Suter U, Snipes GJ. Biology and genetics of hereditary motor and sensory neuropathies. *Annu Rev Neurosci* 1995; **18**: 45-75.

95.   Brancolini C, Edomi P, Marzinotto S, Schneider C. Exposure at the cell surface is required for gas3/PMP22 To regulate both cell death and cell spreading: implication for the Charcot-Marie-Tooth type 1A and Dejerine-Sottas diseases. *Mol Biol Cell* 2000; **11**(9): 2901-14.

96.   Fabbretti E, Edomi P, Brancolini C, Schneider C. Apoptotic phenotype induced by overexpression of wild-type gas3/PMP22: its relation to the demyelinating peripheral neuropathy CMT1A. *Genes & development* 1995; **9**(15): 1846-56.

97.   Roux KJ, Amici SA, Fletcher BS, Notterpek L. Modulation of epithelial morphology, monolayer permeability, and cell migration by growth arrest specific 3/peripheral myelin protein 22. *Mol Biol Cell* 2005; **16**(3): 1142-51.

98.   Amici SA, Dunn WA, Jr., Murphy AJ, et al. Peripheral myelin protein 22 is in complex with alpha6beta4 integrin, and its absence alters the Schwann cell basal lamina. *The Journal of neuroscience : the official journal of the Society for Neuroscience* 2006; **26**(4): 1179-89.

99.   Taylor V, Suter U. Epithelial membrane protein-2 and epithelial membrane protein-3: two novel members of the peripheral myelin protein 22 gene family. *Gene* 1996; **175**(1-2): 115-20.

100.   Wadehra M, Iyer R, Goodglick L, Braun J. The tetraspan protein epithelial membrane protein-2 interacts with beta1 integrins and regulates adhesion. *The Journal of biological chemistry* 2002; **277**(43): 41094-100.

101.   Gudz TI, Schneider TE, Haas TA, Macklin WB. Myelin proteolipid protein forms a complex with integrins and may participate in integrin receptor signaling in oligodendrocytes. *The Journal of neuroscience : the official journal of the Society for Neuroscience* 2002; **22**(17): 7398-407.

102.   Feltri ML, Graus Porta D, Previtali SC, et al. Conditional disruption of beta 1 integrin in Schwann cells impedes interactions with axons. *J Cell Biol* 2002; **156**(1): 199-209.

103.   Notterpek L, Ryan MC, Tobler AR, Shooter EM. PMP22 accumulation in aggresomes: implications for CMT1A pathology. *Neurobiology of disease* 1999; **6**(5): 450-60.

104.   Ryan MC, Shooter EM, Notterpek L. Aggresome formation in neuropathy models based on peripheral myelin protein 22 mutations. *Neurobiology of disease* 2002; **10**(2): 109-18.

105.   Pareek S, Notterpek L, Snipes GJ, et al. Neurons promote the translocation of peripheral myelin protein 22 into myelin. *The Journal of neuroscience : the official journal of the Society for Neuroscience* 1997; **17**(20): 7754-62.

106.   Fortun J, Go JC, Li J, Amici SA, Dunn WA, Jr., Notterpek L. Alterations in degradative pathways and protein aggregation in a neuropathy model based on PMP22 overexpression. *Neurobiology of disease* 2006; **22**(1): 153-64.

107.   Isaacs AM, Jeans A, Oliver PL, et al. Identification of a new Pmp22 mouse mutant and trafficking analysis of a Pmp22 allelic series suggesting that protein aggregates may be protective in Pmp22-associated peripheral neuropathy. *Mol Cell Neurosci* 2002; **21**(1): 114-25.

108.   Dickson KM, Bergeron JJ, Shames I, et al. Association of calnexin with mutant peripheral myelin protein-22 ex vivo: a basis for "gain-of-function" ER diseases. *Proceedings of the National Academy of Sciences of the United States of America* 2002; **99**(15): 9852-7.

109.   Denzel A, Molinari M, Trigueros C, et al. Early postnatal death and motor disorders in mice congenitally deficient in calnexin expression. *Molecular and cellular biology* 2002; **22**(21): 7398-404.

110.   Notterpek L, Roux KJ, Amici SA, Yazdanpour A, Rahner C, Fletcher BS. Peripheral myelin protein 22 is a constituent of intercellular junctions in epithelia. *Proceedings of the National Academy of Sciences of the United States of America* 2001; **98**(25): 14404-9.

111.   Murphy SM, Herrmann DN, McDermott MP, et al. Reliability of the CMT neuropathy score (second version) in Charcot-Marie-Tooth disease. *J Peripher Nerv Syst* 2011; **16**(3): 191-8.

112.   Dortch RD, Dethrage LM, Gore JC, Smith SA, Li J. Proximal nerve magnetization transfer MRI relates to disability in Charcot-Marie-Tooth diseases. *Neurology* 2014; **83**(17): 1545-53.

113.	Nobbio L, Visigalli D, Radice D, et al. PMP22 messenger RNA levels in skin biopsies: testing the effectiveness of a Charcot-Marie-Tooth 1A biomarker. *Brain : a journal of neurology* 2014; **137**(Pt 6): 1614-20.

114.	Campuzano V, Montermini L, Molto MD, et al. Friedreich's ataxia: autosomal recessive disease caused by an intronic GAA triplet repeat expansion. *Science* 1996; **271**(5254): 1423-7.

115.	Justice CM, Den Z, Nguyen SV, et al. Phylogenetic analysis of the Friedreich ataxia GAA trinucleotide repeat. *J Mol Evol* 2001; **52**(3): 232-8.

116.	Labuda M, Labuda D, Miranda C, et al. Unique origin and specific ethnic distribution of the Friedreich ataxia GAA expansion. *Neurology* 2000; **54**(12): 2322-4.

117.	Hirayama K, Takayanagi T, Nakamura R, et al. Spinocerebellar degenerations in Japan: a nationwide epidemiological and clinical study. *Acta Neurol Scand Suppl* 1994; **153**: 1-22.

118.	Vankan P. Prevalence gradients of Friedreich's ataxia and R1b haplotype in Europe co-localize, suggesting a common Palaeolithic origin in the Franco-Cantabrian ice age refuge. *Journal of neurochemistry* 2013; **126 Suppl 1**: 11-20.

119.	Subramony SH, May W, Lynch D, et al. Measuring Friedreich ataxia: Interrater reliability of a neurologic rating scale. *Neurology* 2005; **64**(7): 1261-2.

120.	Schmitz-Hubsch T, Fimmers R, Rakowicz M, et al. Responsiveness of different rating instruments in spinocerebellar ataxia patients. *Neurology* 2010; **74**(8): 678-84.

121.	Trouillas P, Takayanagi T, Hallett M, et al. International Cooperative Ataxia Rating Scale for pharmacological assessment of the cerebellar syndrome. The Ataxia Neuropharmacology Committee of the World Federation of Neurology. *Journal of the neurological sciences* 1997; **145**(2): 205-11.

122.	Filla A, De Michele G, Cavalcanti F, et al. The relationship between trinucleotide (GAA) repeat length and clinical features in Friedreich ataxia. *Am J Hum Genet* 1996; **59**(3): 554-60.

123.	Pandolfo M. Friedreich ataxia: the clinical picture. *Journal of neurology* 2009; **256 Suppl 1**: 3-8.

124.	Delatycki MB, Corben LA. Clinical features of Friedreich ataxia. *Journal of child neurology* 2012; **27**(9): 1133-7.

125.	Koeppen AH. Friedreich's ataxia: pathology, pathogenesis, and molecular genetics. *Journal of the neurological sciences* 2011; **303**(1-2): 1-12.

126.	De Michele G, Di Salle F, Filla A, et al. Magnetic resonance imaging in "typical" and "late onset" Friedreich's disease and early onset cerebellar ataxia with retained tendon reflexes. *Ital J Neurol Sci* 1995; **16**(5): 303-8.

127.	Harding AE. Friedreich's ataxia: a clinical and genetic study of 90 families with an analysis of early diagnostic criteria and intrafamilial clustering of clinical features. *Brain : a journal of neurology* 1981; **104**(3): 589-620.

128.	Parkinson MH, Boesch S, Nachbauer W, Mariotti C, Giunti P. Clinical features of Friedreich's ataxia: classical and atypical phenotypes. *Journal of neurochemistry* 2013; **126 Suppl 1**: 103-17.

129. Santoro L, De Michele G, Perretti A, et al. Relation between trinucleotide GAA repeat length and sensory neuropathy in Friedreich's ataxia. *J Neurol Neurosurg Psychiatry* 1999; **66**(1): 93-6.

130. Furman JM, Perlman S, Baloh RW. Eye movements in Friedreich's ataxia. *Arch Neurol* 1983; **40**(6): 343-6.

131. Folker J, Murdoch B, Cahill L, Delatycki M, Corben L, Vogel A. Dysarthria in Friedreich's ataxia: a perceptual analysis. *Folia Phoniatr Logop* 2010; **62**(3): 97-103.

132. Rance G, Fava R, Baldock H, et al. Speech perception ability in individuals with Friedreich ataxia. *Brain : a journal of neurology* 2008; **131**(Pt 8): 2002-12.

133. Weidemann F, Rummey C, Bijnens B, et al. The heart in Friedreich ataxia: definition of cardiomyopathy, disease severity, and correlation with neurological symptoms. *Circulation* 2012; **125**(13): 1626-34.

134. Finocchiaro G, Baio G, Micossi P, Pozza G, di Donato S. Glucose metabolism alterations in Friedreich's ataxia. *Neurology* 1988; **38**(8): 1292-6.

135. McCabe DJ, Ryan F, Moore DP, et al. Typical Friedreich's ataxia without GAA expansions and GAA expansion without typical Friedreich's ataxia. *Journal of neurology* 2000; **247**(5): 346-55.

136. Greene E, Entezam A, Kumari D, Usdin K. Ancient repeated DNA elements and the regulation of the human frataxin promoter. *Genomics* 2005; **85**(2): 221-30.

137. Greene E, Mahishi L, Entezam A, Kumari D, Usdin K. Repeat-induced epigenetic changes in intron 1 of the frataxin gene and its consequences in Friedreich ataxia. *Nucleic acids research* 2007; **35**(10): 3383-90.

138. Lu C, Schoenfeld R, Shan Y, Tsai HJ, Hammock B, Cortopassi G. Frataxin deficiency induces Schwann cell inflammation and death. *Biochimica et biophysica acta* 2009; **1792**(11): 1052-61.

139. Sarsero JP, Li L, Wardan H, Sitte K, Williamson R, Ioannou PA. Upregulation of expression from the FRDA genomic locus for the therapy of Friedreich ataxia. *J Gene Med* 2003; **5**(1): 72-81.

140. Li K, Singh A, Crooks DR, et al. Expression of human frataxin is regulated by transcription factors SRF and TFAP2. *PloS one* 2010; **5**(8): e12286.

141. De Biase I, Chutake YK, Rindler PM, Bidichandani SI. Epigenetic silencing in Friedreich ataxia is associated with depletion of CTCF (CCCTC-binding factor) and antisense transcription. *PloS one* 2009; **4**(11): e7914.

142. Yandim C, Natisvili T, Festenstein R. Gene regulation and epigenetics in Friedreich's ataxia. *Journal of neurochemistry* 2013; **126 Suppl 1**: 21-42.

143. Kumari D, Usdin K. Is Friedreich ataxia an epigenetic disorder? *Clin Epigenetics* 2012; **4**(1): 2.

144. Adinolfi S, Iannuzzi C, Prischi F, et al. Bacterial frataxin CyaY is the gatekeeper of iron-sulfur cluster formation catalyzed by IscS. *Nature structural & molecular biology* 2009; **16**(4): 390-6.

145.   Gibson TJ, Koonin EV, Musco G, Pastore A, Bork P. Friedreich's ataxia protein: phylogenetic evidence for mitochondrial dysfunction. *Trends Neurosci* 1996; **19**(11): 465-8.

146.   Condo I, Ventura N, Malisan F, Rufini A, Tomassini B, Testi R. In vivo maturation of human frataxin. *Human molecular genetics* 2007; **16**(13): 1534-40.

147.   Koutnikova H, Campuzano V, Koenig M. Maturation of wild-type and mutated frataxin by the mitochondrial processing peptidase. *Human molecular genetics* 1998; **7**(9): 1485-9.

148.   Vazquez-Manrique RP, Gonzalez-Cabo P, Ros S, Aziz H, Baylis HA, Palau F. Reduction of Caenorhabditis elegans frataxin increases sensitivity to oxidative stress, reduces lifespan, and causes lethality in a mitochondrial complex II mutant. *FASEB journal : official publication of the Federation of American Societies for Experimental Biology* 2006; **20**(1): 172-4.

149.   Adinolfi S, Trifuoggi M, Politou AS, Martin S, Pastore A. A structural approach to understanding the iron-binding properties of phylogenetically different frataxins. *Human molecular genetics* 2002; **11**(16): 1865-77.

150.   Gomes CM, Santos R. Neurodegeneration in Friedreich's ataxia: from defective frataxin to oxidative stress. *Oxidative medicine and cellular longevity* 2013; **2013**: 487534.

151.   Marmolino D. Friedreich's ataxia: past, present and future. *Brain Res Rev* 2011; **67**(1-2): 311-30.

152.   Cossee M, Durr A, Schmitt M, et al. Friedreich's ataxia: point mutations and clinical presentation of compound heterozygotes. *Annals of neurology* 1999; **45**(2): 200-6.

153.   Cossee M, Puccio H, Gansmuller A, et al. Inactivation of the Friedreich ataxia mouse gene leads to early embryonic lethality without iron accumulation. *Human molecular genetics* 2000; **9**(8): 1219-26.

154.   Adamec J, Rusnak F, Owen WG, et al. Iron-dependent self-assembly of recombinant yeast frataxin: implications for Friedreich ataxia. *Am J Hum Genet* 2000; **67**(3): 549-62.

155.   Gakh O, Adamec J, Gacy AM, Twesten RD, Owen WG, Isaya G. Physical evidence that yeast frataxin is an iron storage protein. *Biochemistry* 2002; **41**(21): 6798-804.

156.   Lamarche JB, Cote M, Lemieux B. The cardiomyopathy of Friedreich's ataxia morphological observations in 3 cases. *Can J Neurol Sci* 1980; **7**(4): 389-96.

157.   Aloria K, Schilke B, Andrew A, Craig EA. Iron-induced oligomerization of yeast frataxin homologue Yfh1 is dispensable in vivo. *EMBO Rep* 2004; **5**(11): 1096-101.

158.   Huynen MA, Snel B, Bork P, Gibson TJ. The phylogenetic distribution of frataxin indicates a role in iron-sulfur cluster protein assembly. *Human molecular genetics* 2001; **10**(21): 2463-8.

159.   Puccio H, Simon D, Cossee M, et al. Mouse models for Friedreich ataxia exhibit cardiomyopathy, sensory nerve defect and Fe-S enzyme deficiency followed by intramitochondrial iron deposits. *Nature genetics* 2001; **27**(2): 181-6.

160.   Rotig A, de Lonlay P, Chretien D, et al. Aconitase and mitochondrial iron-sulphur protein deficiency in Friedreich ataxia. *Nature genetics* 1997; **17**(2): 215-7.

161.   Ramazzotti A, Vanmansart V, Foury F. Mitochondrial functional interactions between frataxin and Isu1p, the iron-sulfur cluster scaffold protein, in Saccharomyces cerevisiae. *FEBS letters* 2004; **557**(1-3): 215-20.

162.   Bridwell-Rabb J, Fox NG, Tsai CL, Winn AM, Barondeau DP. Human frataxin activates Fe-S cluster biosynthesis by facilitating sulfur transfer chemistry. *Biochemistry* 2014; **53**(30): 4904-13.

163.   Schmucker S, Martelli A, Colin F, et al. Mammalian frataxin: an essential function for cellular viability through an interaction with a preformed ISCU/NFS1/ISD11 iron-sulfur assembly complex. *PloS one* 2011; **6**(1): e16199.

164.   Shi Y, Ghosh MC, Tong WH, Rouault TA. Human ISD11 is essential for both iron-sulfur cluster assembly and maintenance of normal cellular iron homeostasis. *Human molecular genetics* 2009; **18**(16): 3014-25.

165.   Shan Y, Napoli E, Cortopassi G. Mitochondrial frataxin interacts with ISD11 of the NFS1/ISCU complex and multiple mitochondrial chaperones. *Human molecular genetics* 2007; **16**(8): 929-41.

166.   Taketani S. Aquisition, mobilization and utilization of cellular iron and heme: endless findings and growing evidence of tight regulation. *Tohoku J Exp Med* 2005; **205**(4): 297-318.

167.   Schoenfeld RA, Napoli E, Wong A, et al. Frataxin deficiency alters heme pathway transcripts and decreases mitochondrial heme metabolites in mammalian cells. *Human molecular genetics* 2005; **14**(24): 3787-99.

168.   Pastore A, Puccio H. Frataxin: a protein in search for a function. *Journal of neurochemistry* 2013; **126 Suppl 1**: 43-52.

169.   Soragni E, Miao W, Iudicello M, et al. Epigenetic therapy for Friedreich ataxia. *Annals of neurology* 2014; **76**(4): 489-508.

170.   Weidemann F, Liu D, Hu K, et al. The cardiomyopathy in Friedreich's ataxia - New biomarker for staging cardiac involvement. *Int J Cardiol* 2015; **194**: 50-7.

171.   Zhao Y, Ransom JF, Li A, et al. Dysregulation of cardiogenesis, cardiac conduction, and cell cycle in mice lacking miRNA-1-2. *Cell* 2007; **129**(2): 303-17.

172.   Bandiera S, Cartault F, Jannot AS, et al. Genetic variations creating microRNA target sites in the FXN 3'-UTR affect frataxin expression in Friedreich ataxia. *PloS one* 2013; **8**(1): e54791.

173.   Mahishi LH, Hart RP, Lynch DR, Ratan RR. miR-886-3p levels are elevated in Friedreich ataxia. *The Journal of neuroscience : the official journal of the Society for Neuroscience* 2012; **32**(27): 9369-73.

174.   Quesada MP, Jones J, Rodriguez-Lozano FJ, Moraleda JM, Martinez S. Novel aberrant genetic and epigenetic events in Friedreich's ataxia. *Experimental cell research* 2015; **335**(1): 51-61.

175.   Kapranov P, Cheng J, Dike S, et al. RNA maps reveal new RNA classes and a possible function for pervasive transcription. *Science* 2007; **316**(5830): 1484-8.

176.   Taft RJ, Pang KC, Mercer TR, Dinger M, Mattick JS. Non-coding RNAs: regulators of disease. *J Pathol* 2010; **220**(2): 126-39.

177.   Kozomara A, Griffiths-Jones S. miRBase: annotating high confidence microRNAs using deep sequencing data. *Nucleic acids research* 2014; **42**(Database issue): D68-73.

178.   Lee Y, Kim M, Han J, et al. MicroRNA genes are transcribed by RNA polymerase II. *The EMBO journal* 2004; **23**(20): 4051-60.

179.   Borchert GM, Lanier W, Davidson BL. RNA polymerase III transcribes human microRNAs. *Nature structural & molecular biology* 2006; **13**(12): 1097-101.

180.   Gregory RI, Yan KP, Amuthan G, et al. The Microprocessor complex mediates the genesis of microRNAs. *Nature* 2004; **432**(7014): 235-40.

181.   Hutvagner G, McLachlan J, Pasquinelli AE, Balint E, Tuschl T, Zamore PD. A cellular function for the RNA-interference enzyme Dicer in the maturation of the let-7 small temporal RNA. *Science* 2001; **293**(5531): 834-8.

182.   Bartel DP. MicroRNAs: genomics, biogenesis, mechanism, and function. *Cell* 2004; **116**(2): 281-97.

183.   Peters L, Meister G. Argonaute proteins: mediators of RNA silencing. *Molecular cell* 2007; **26**(5): 611-23.

184.   Hammond SM, Bernstein E, Beach D, Hannon GJ. An RNA-directed nuclease mediates post-transcriptional gene silencing in Drosophila cells. *Nature* 2000; **404**(6775): 293-6.

185.   Fevrier B, Raposo G. Exosomes: endosomal-derived vesicles shipping extracellular messages. *Curr Opin Cell Biol* 2004; **16**(4): 415-21.

186.   Mitchell PS, Parkin RK, Kroh EM, et al. Circulating microRNAs as stable blood-based markers for cancer detection. *Proceedings of the National Academy of Sciences of the United States of America* 2008; **105**(30): 10513-8.

187.   Park NJ, Zhou H, Elashoff D, et al. Salivary microRNA: discovery, characterization, and clinical utility for oral cancer detection. *Clin Cancer Res* 2009; **15**(17): 5473-7.

188.   Hanke M, Hoefig K, Merz H, et al. A robust methodology to study urine microRNA as tumor marker: microRNA-126 and microRNA-182 are related to urinary bladder cancer. *Urol Oncol* 2010; **28**(6): 655-61.

189.   Russo F, Scoyni F, Fatica A, et al. Chapter 12 - Circulating Noncoding RNAs as Clinical Biomarkers A2 - García-Giménez, José Luis. Epigenetic Biomarkers and Diagnostics. Boston: Academic Press; 2016: 239-58.

190.   Lopez-Serra P, Sandoval J. Chapter 27 - MicroRNA Deregulation in Lung Cancer and Their Use as Clinical Tools A2 - García-Giménez, José Luis. Epigenetic Biomarkers and Diagnostics. Boston: Academic Press; 2016: 539-55.

191.   Stefansson OA. Chapter 29 - MicroRNAs in Breast Cancer and Their Value as Biomarkers A2 - García-Giménez, José Luis. Epigenetic Biomarkers and Diagnostics. Boston: Academic Press; 2016: 587-612.

192.   Brennan E, McClelland A, Hagiwara S, Godson C, Kantharidis P. Chapter 31 - miRNAs in the Pathophysiology of Diabetes and Their Value as Biomarkers A2 - García-Giménez, José Luis. Epigenetic Biomarkers and Diagnostics. Boston: Academic Press; 2016: 643-61.

193.   Maciotta S, Meregalli M, Torrente Y. The involvement of microRNAs in neurodegenerative diseases. *Frontiers in cellular neuroscience* 2013; **7**: 265.

194.   Costa V, Matarazzo MR, Gagliardi M, Esposito R, Ciccodicola A. Chapter 11 - High-Throughput Analysis of Noncoding RNAs: Implications in Clinical Epigenetics A2 - García-Giménez, José Luis. Epigenetic Biomarkers and Diagnostics. Boston: Academic Press; 2016: 215-38.

195.   Fiore R, Khudayberdiev S, Saba R, Schratt G. MicroRNA function in the nervous system. *Prog Mol Biol Transl Sci* 2011; **102**: 47-100.

196.   Sebastiani G, Nigi L, Grieco GE, Mancarella F, Ventriglia G, Dotta F. Circulating microRNAs and diabetes mellitus: a novel tool for disease prediction, diagnosis, and staging? *J Endocrinol Invest* 2017.

197.   Zheng Y, Wang Z, Zhou Z. miRNAs: novel regulators of autoimmunity-mediated pancreatic beta-cell destruction in type 1 diabetes. *Cell Mol Immunol* 2017.

198.   White MC, Pang L, Yang X. MicroRNA-mediated maturation of human pluripotent stem cell-derived cardiomyocytes: Towards a better model for cardiotoxicity? *Food Chem Toxicol* 2016; **98**(Pt A): 17-24.

199.   Shy ME, Blake J, Krajewski K, et al. Reliability and validity of the CMT neuropathy score as a measure of disability. *Neurology* 2005; **64**(7): 1209-14.

200.   Schmitz-Hubsch T, du Montcel ST, Baliko L, et al. Scale for the assessment and rating of ataxia: development of a new clinical scale. *Neurology* 2006; **66**(11): 1717-20.

201.   Garcia-Gimenez JL, Gimeno A, Gonzalez-Cabo P, et al. Differential expression of PGC-1alpha and metabolic sensors suggest age-dependent induction of mitochondrial biogenesis in Friedreich ataxia fibroblasts. *PloS one* 2011; **6**(6): e20666.

202.   Lanza DC, Moran DT, Doty RL, et al. Endoscopic human olfactory biopsy technique: a preliminary report. *The Laryngoscope* 1993; **103**(7): 815-9.

203.   Biedler JL, Roffler-Tarlov S, Schachner M, Freedman LS. Multiple neurotransmitter synthesis by human neuroblastoma cell lines and clones. *Cancer research* 1978; **38**(11 Pt 1): 3751-7.

204.   Biedler JL, Helson L, Spengler BA. Morphology and growth, tumorigenicity, and cytogenetics of human neuroblastoma cells in continuous culture. *Cancer research* 1973; **33**(11): 2643-52.

205.   Wong SH, Knight JA, Hopfer SM, Zaharia O, Leach CN, Jr., Sunderman FW, Jr. Lipoperoxides in plasma as measured by liquid-chromatographic separation of malondialdehyde-thiobarbituric acid adduct. *Clinical chemistry* 1987; **33**(2 Pt 1): 214-20.

206.   Marouga R, David S, Hawkins E. The development of the DIGE system: 2D fluorescence difference gel analysis technology. *Analytical and bioanalytical chemistry* 2005; **382**(3): 669-78.

207.   Shevchenko A, Jensen ON, Podtelejnikov AV, et al. Linking genome and proteome by mass spectrometry: large-scale identification of yeast proteins from two dimensional gels. *Proceedings of the National Academy of Sciences of the United States of America* 1996; **93**(25): 14440-5.

208.   Rodriguez-Lopez R, Reyes-Palomares A, Sanchez-Jimenez F, Medina MA. PhenUMA: a tool for integrating the biomedical relationships among genes and diseases. *BMC Bioinformatics* 2014; **15**: 375.

209.   Liao Y, Smyth GK, Shi W. The Subread aligner: fast, accurate and scalable read mapping by seed-and-vote. *Nucleic acids research* 2013; **41**(10): e108.

210.   Liao Y, Smyth GK, Shi W. featureCounts: an efficient general purpose program for assigning sequence reads to genomic features. *Bioinformatics* 2014; **30**(7): 923-30.

211.   Robinson MD, Oshlack A. A scaling normalization method for differential expression analysis of RNA-seq data. *Genome biology* 2010; **11**(3): R25.

212.   Robinson MD, Smyth GK. Moderated statistical tests for assessing differences in tag abundance. *Bioinformatics* 2007; **23**(21): 2881-7.

213.   Robinson MD, Smyth GK. Small-sample estimation of negative binomial dispersion, with applications to SAGE data. *Biostatistics* 2008; **9**(2): 321-32.

214.   Friedman J, Hastie T, Tibshirani R. Regularization Paths for Generalized Linear Models via Coordinate Descent. *Journal of statistical software* 2010; **33**(1): 1-22.

215.   Paraskevopoulou MD, Georgakilas G, Kostoulas N, et al. DIANA-microT web server v5.0: service integration into miRNA functional analysis workflows. *Nucleic acids research* 2013; **41**(Web Server issue): W169-73.

216.   Vlachos IS, Zagganas K, Paraskevopoulou MD, et al. DIANA-miRPath v3.0: deciphering microRNA function with experimental support. *Nucleic acids research* 2015; **43**(W1): W460-6.

217.   McCarthy DJ, Chen Y, Smyth GK. Differential expression analysis of multifactor RNA-Seq experiments with respect to biological variation. *Nucleic acids research* 2012; **40**(10): 4288-97.

218.   Livak KJ, Schmittgen TD. Analysis of relative gene expression data using real-time quantitative PCR and the 2(-Delta Delta C(T)) Method. *Methods* 2001; **25**(4): 402-8.

219.   Bolstad BM, Irizarry RA, Astrand M, Speed TP. A comparison of normalization methods for high density oligonucleotide array data based on variance and bias. *Bioinformatics* 2003; **19**(2): 185-93.

220.   Paunio T, Kiuru S, Karonen S-L, Palo J, Peltonen L. Quantification of serum and cerebrospinal fluid gelsolin in familial amyloidosis, Finnish type (AGel). *Amyloid* 1994; **1**(2): 80-9.

221.   Missiaglia E, Shepherd CJ, Patel S, et al. MicroRNA-206 expression levels correlate with clinical behaviour of rhabdomyosarcomas. *British journal of cancer* 2010; **102**(12): 1769-77.

222.   Torres A, Torres K, Wdowiak P, Paszkowski T, Maciejewski R. Selection and validation of endogenous controls for microRNA expression studies in endometrioid endometrial cancer tissues. *Gynecol Oncol* 2013; **130**(3): 588-94.

223.   Manikandan M, Deva Magendhra Rao AK, Arunkumar G, Rajkumar KS, Rajaraman R, Munirajan AK. Down Regulation of miR-34a and miR-143 May Indirectly Inhibit p53 in Oral Squamous Cell Carcinoma: a Pilot Study. *Asian Pac J Cancer Prev* 2015; **16**(17): 7619-25.

224.   Coffey S, Williams MJ, Phillips LV, Jones GT. Circulating microRNA Profiling Needs Further Refinement Before Clinical Use in Patients With Aortic Stenosis. *J Am Heart Assoc* 2015; **4**(8): e002150.

225.   Semenza GL. HIF-1: upstream and downstream of cancer metabolism. *Current opinion in genetics & development* 2010; **20**(1): 51-6.

226.   Rommer PS, Greilberger J, Salhofer-Polanyi S, Auff E, Leutmezer F, Herwig R. Elevated levels of carbonyl proteins in cerebrospinal fluid of patients with neurodegenerative diseases. *Tohoku J Exp Med* 2014; **234**(4): 313-7.

227.   Shen L, Chen Y, Yang A, et al. Redox Proteomic Profiling of Specifically Carbonylated Proteins in the Serum of Triple Transgenic Alzheimer's Disease Mice. *Int J Mol Sci* 2016; **17**(4): 469.

228.   Lopez Del Amo V, Seco-Cervera M, Garcia-Gimenez JL, Whitworth AJ, Pallardo FV, Galindo MI. Mitochondrial defects and neuromuscular degeneration caused by altered expression of Drosophila Gdap1: implications for the Charcot-Marie-Tooth neuropathy. *Human molecular genetics* 2015; **24**(1): 21-36.

229.   Emond M, Lepage G, Vanasse M, Pandolfo M. Increased levels of plasma malondialdehyde in Friedreich ataxia. *Neurology* 2000; **55**(11): 1752-3.

230.   Tahirovic I, Sofic E, Sapcanin A, et al. Reduced brain antioxidant capacity in rat models of betacytotoxic-induced experimental sporadic Alzheimer's disease and diabetes mellitus. *Neurochemical research* 2007; **32**(10): 1709-17.

231.   Bishnoi RJ, Palmer RF, Royall DR. Vitamin D binding protein as a serum biomarker of Alzheimer's disease. *Journal of Alzheimer's disease : JAD* 2015; **43**(1): 37-45.

232.   Zhang J, Sokal I, Peskind ER, et al. CSF multianalyte profile distinguishes Alzheimer and Parkinson diseases. *Am J Clin Pathol* 2008; **129**(4): 526-9.

233.   Mayer M. Biochemical and biological aspects of the plasminogen activation system. *Clin Biochem* 1990; **23**(3): 197-211.

234.   Seeds NW, Williams BL, Bickford PC. Tissue plasminogen activator induction in Purkinje neurons after cerebellar motor learning. *Science* 1995; **270**(5244): 1992-4.

235.   Akassoglou K, Kombrinck KW, Degen JL, Strickland S. Tissue plasminogen activator-mediated fibrinolysis protects against axonal degeneration and demyelination after sciatic nerve injury. *J Cell Biol* 2000; **149**(5): 1157-66.

236.   Takahashi R, Ono K, Ikeda T, et al. Coagulation and fibrinolysis abnormalities in familial amyloid polyneuropathy. *Amyloid* 2012; **19**(3): 129-32.

237.   Lolin YI, Ward AM. Alpha-1-antitrypsin phenotypes and associated disease patterns in neurological patients. *Acta Neurol Scand* 1995; **91**(5): 394-8.

238.   Amin B, Maurer A, Voelter W, Melms A, Kalbacher H. New poteintial serum biomarkers in multiple sclerosis identified by proteomic strategies. *Curr Med Chem* 2014; **21**(13): 1544-56.

239.   Pearl GS, Mullins RE. Alpha 1-antitrypsin in cerebrospinal fluid of patients with neurologic diseases. *Arch Neurol* 1985; **42**(8): 775-7.

240.   Sladkova V, Mares J, Lubenova B, et al. Degenerative and inflammatory markers in the cerebrospinal fluid of multiple sclerosis patients with relapsing-remitting course of disease and after clinical isolated syndrome. *Neurol Res* 2011; **33**(4): 415-20.

241.   Nielsen HM, Minthon L, Londos E, et al. Plasma and CSF serpins in Alzheimer disease and dementia with Lewy bodies. *Neurology* 2007; **69**(16): 1569-79.

242.   Donovan FM, Pike CJ, Cotman CW, Cunningham DD. Thrombin induces apoptosis in cultured neurons and astrocytes via a pathway requiring tyrosine kinase and RhoA activities. *The Journal of neuroscience : the official journal of the Society for Neuroscience* 1997; **17**(14): 5316-26.

243.   Palumbo C, Massa R, Panico MB, et al. Peripheral nerve extracellular matrix remodeling in Charcot-Marie-Tooth type I disease. *Acta Neuropathol* 2002; **104**(3): 287-96.

244.   de Carvalho M, Linke RP, Domingos F, et al. Mutant fibrinogen A-alpha-chain associated with hereditary renal amyloidosis and peripheral neuropathy. *Amyloid* 2004; **11**(3): 200-7.

245.   Lu W, Wan X, Liu B, et al. Specific changes of serum proteins in Parkinson's disease patients. *PloS one* 2014; **9**(4): e95684.

246.   Previtali SC, Malaguti MC, Riva N, et al. The extracellular matrix affects axonal regeneration in peripheral neuropathies. *Neurology* 2008; **71**(5): 322-31.

247.   Koski CL, Vanguri P, Shin ML. Activation of the alternative pathway of complement by human peripheral nerve myelin. *J Immunol* 1985; **134**(3): 1810-4.

248.   Miyaji K, Paul F, Shahrizaila N, Umapathi T, Yuki N. Complement regulatory proteins (CD46, 55 and 59) expressed on Schwann cells: immune targets in demyelinating neuropathies? *Journal of neuroimmunology* 2014; **276**(1-2): 172-4.

249.   Giannini C, Monaco S, Kirschfink M, et al. Inherited neuroaxonal dystrophy in C6 deficient rabbits. *J Neuropathol Exp Neurol* 1992; **51**(5): 514-22.

250.   Swanson CR, Li K, Unger TL, et al. Lower plasma apolipoprotein A1 levels are found in Parkinson's disease and associate with apolipoprotein A1 genotype. *Movement disorders : official journal of the Movement Disorder Society* 2015; **30**(6): 805-12.

251.   Qiang JK, Wong YC, Siderowf A, et al. Plasma apolipoprotein A1 as a biomarker for Parkinson disease. *Annals of neurology* 2013; **74**(1): 119-27.

252.   Swanson CR, Berlyand Y, Xie SX, Alcalay RN, Chahine LM, Chen-Plotkin AS. Plasma apolipoprotein A1 associates with age at onset and motor severity in early Parkinson's disease patients. *Movement disorders : official journal of the Movement Disorder Society* 2015; **30**(12): 1648-56.

253.   Koutsis G, Panas M, Giogkaraki E, Karadima G, Sfagos C, Vassilopoulos D. An APOA1 promoter polymorphism is associated with cognitive performance in patients with multiple sclerosis. *Multiple sclerosis* 2009; **15**(2): 174-9.

254.   Lin Q, Cao Y, Gao J. Decreased expression of the APOA1-APOC3-APOA4 gene cluster is associated with risk of Alzheimer's disease. *Drug Des Devel Ther* 2015; **9**: 5421-31.

255.   Langner CA, Birkenmeier EH, Roth KA, Bronson RT, Gordon JI. Characterization of the peripheral neuropathy in neonatal and adult mice that are homozygous for the fatty liver dystrophy (fld) mutation. *The Journal of biological chemistry* 1991; **266**(18): 11955-64.

256.   D'Aguanno S, Barassi A, Lupisella S, et al. Differential cerebro spinal fluid proteome investigation of Leber hereditary optic neuropathy (LHON) and multiple sclerosis. *Journal of neuroimmunology* 2008; **193**(1-2): 156-60.

257.   Corder EH, Saunders AM, Strittmatter WJ, et al. Gene dose of apolipoprotein E type 4 allele and the risk of Alzheimer's disease in late onset families. *Science* 1993; **261**(5123): 921-3.

258.   Monastiriotis C, Papanas N, Trypsianis G, Karanikola K, Veletza S, Maltezos E. The epsilon4 allele of the APOE gene is associated with more severe peripheral neuropathy in type 2 diabetic patients. *Angiology* 2013; **64**(6): 451-5.

259.   Bedlack RS, Strittmatter WJ, Morgenlander JC. Apolipoprotein E and neuromuscular disease: a critical review of the literature. *Arch Neurol* 2000; **57**(11): 1561-5.

260.   Wright MC, Mi R, Connor E, et al. Novel roles for osteopontin and clusterin in peripheral motor and sensory axon regeneration. *The Journal of neuroscience : the official journal of the Society for Neuroscience* 2014; **34**(5): 1689-700.

261.   Lee S, Amici S, Tavori H, et al. PMP22 is critical for actin-mediated cellular functions and for establishing lipid rafts. *The Journal of neuroscience : the official journal of the Society for Neuroscience* 2014; **34**(48): 16140-52.

262.   Harris VK, Donelan N, Yan QJ, et al. Cerebrospinal fluid fetuin-A is a biomarker of active multiple sclerosis. *Multiple sclerosis* 2013; **19**(11): 1462-72.

263.   Zhang HL, Zhang XM, Mao XJ, et al. Altered cerebrospinal fluid index of prealbumin, fibrinogen, and haptoglobin in patients with Guillain-Barre syndrome and chronic inflammatory demyelinating polyneuropathy. *Acta Neurol Scand* 2012; **125**(2): 129-35.

264.   Alexander MS, Kunkel LM. Skeletal muscle microRNAs: their diagnostic and therapeutic potential in human muscle diseases. *Journal of Neuromuscular Diseases* 2015; **2**(1): 1-11.

265.   van Rooij E, Olson EN. MicroRNA therapeutics for cardiovascular disease: opportunities and obstacles. *Nature reviews Drug discovery* 2012; **11**(11): 860-72.

266.   Hoss AG, Labadorf A, Beach TG, Latourelle JC, Myers RH. microRNA Profiles in Parkinson's Disease Prefrontal Cortex. *Front Aging Neurosci* 2016; **8**: 36.

267.   Hoss AG, Kartha VK, Dong X, et al. MicroRNAs located in the Hox gene clusters are implicated in huntington's disease pathogenesis. *PLoS genetics* 2014; **10**(2): e1004188.

268.   Hebert SS, Horre K, Nicolai L, et al. Loss of microRNA cluster miR-29a/b-1 in sporadic Alzheimer's disease correlates with increased BACE1/beta-secretase expression. *Proceedings of the National Academy of Sciences of the United States of America* 2008; **105**(17): 6415-20.

269.   Sievers C, Meira M, Hoffmann F, Fontoura P, Kappos L, Lindberg RL. Altered microRNA expression in B lymphocytes in multiple sclerosis: towards a better understanding of treatment effects. *Clinical immunology* 2012; **144**(1): 70-9.

270.   Menendez JA, Lupu R. Fatty acid synthase and the lipogenic phenotype in cancer pathogenesis. *Nature reviews Cancer* 2007; **7**(10): 763-77.

271.   Grevengoed TJ, Klett EL, Coleman RA. Acyl-CoA metabolism and partitioning. *Annual review of nutrition* 2014; **34**: 1-30.

272.   Navarro JA, Ohmann E, Sanchez D, et al. Altered lipid metabolism in a Drosophila model of Friedreich's ataxia. *Human molecular genetics* 2010; **19**(14): 2828-40.

273.   Iozzo P. Myocardial, perivascular, and epicardial fat. *Diabetes Care* 2011; **34 Suppl 2**: S371-9.

274.   Giacco F, Brownlee M. Oxidative stress and diabetic complications. *Circulation research* 2010; **107**(9): 1058-70.

275.   Yuan H, Li X, Zhang X, Kang R, Tang D. Identification of ACSL4 as a biomarker and contributor of ferroptosis. *Biochemical and biophysical research communications* 2016; **478**(3): 1338-43.

276.   Doll S, Proneth B, Tyurina YY, et al. ACSL4 dictates ferroptosis sensitivity by shaping cellular lipid composition. *Nat Chem Biol* 2017; **13**(1): 91-8.

277.   Dixon SJ, Lemberg KM, Lamprecht MR, et al. Ferroptosis: an iron-dependent form of nonapoptotic cell death. *Cell* 2012; **149**(5): 1060-72.

278.   Ishii T, Sugita Y, Bannai S. Regulation of glutathione levels in mouse spleen lymphocytes by transport of cysteine. *J Cell Physiol* 1987; **133**(2): 330-6.

279.   Ursini F, Maiorino M, Valente M, Ferri L, Gregolin C. Purification from pig liver of a protein which protects liposomes and biomembranes from peroxidative degradation and exhibits glutathione peroxidase activity on phosphatidylcholine hydroperoxides. *Biochimica et biophysica acta* 1982; **710**(2): 197-211.

280.   Piemonte F, Pastore A, Tozzi G, et al. Glutathione in blood of patients with Friedreich's ataxia. *Eur J Clin Invest* 2001; **31**(11): 1007-11.

281.   Lu C, Cortopassi G. Frataxin knockdown causes loss of cytoplasmic iron-sulfur cluster functions, redox alterations and induction of heme transcripts. *Arch Biochem Biophys* 2007; **457**(1): 111-22.

282.   Bolinches-Amoros A, Molla B, Pla-Martin D, Palau F, Gonzalez-Cabo P. Mitochondrial dysfunction induced by frataxin deficiency is associated with cellular senescence and abnormal calcium metabolism. *Frontiers in cellular neuroscience* 2014; **8**: 124.

283.   Barde YA. Trophic factors and neuronal survival. *Neuron* 1989; **2**(6): 1525-34.

284.   Majdan M, Miller FD. Neuronal life and death decisions functional antagonism between the Trk and p75 neurotrophin receptors. *Int J Dev Neurosci* 1999; **17**(3): 153-61.

285.   Li HH, Kedar V, Zhang C, et al. Atrogin-1/muscle atrophy F-box inhibits calcineurin-dependent cardiac hypertrophy by participating in an SCF ubiquitin ligase complex. *The Journal of clinical investigation* 2004; **114**(8): 1058-71.

286.   Inoki K, Li Y, Xu T, Guan KL. Rheb GTPase is a direct target of TSC2 GAP activity and regulates mTOR signaling. *Genes & development* 2003; **17**(15): 1829-34.

287.   Calap-Quintana P, Soriano S, Llorens JV, et al. TORC1 Inhibition by Rapamycin Promotes Antioxidant Defences in a Drosophila Model of Friedreich's Ataxia. *PloS one* 2015; **10**(7): e0132376.

288.   Diez-Planelles C, Sanchez-Lozano P, Crespo MC, et al. Circulating microRNAs in Huntington's disease: Emerging mediators in metabolic impairment. *Pharmacological research* 2016; **108**: 102-10.

289.   Guerau-de-Arellano M, Smith KM, Godlewski J, et al. Micro-RNA dysregulation in multiple sclerosis favours pro-inflammatory T-cell-mediated autoimmunity. *Brain : a journal of neurology* 2011; **134**(Pt 12): 3578-89.

290.   Kumar P, Dezso Z, MacKenzie C, et al. Circulating miRNA biomarkers for Alzheimer's disease. *PloS one* 2013; **8**(7): e69807.

291.   Jensen MK, Bundgaard H. Cardiomyopathy in Friedreich ataxia: exemplifying the challenges faced by cardiologists in the management of rare diseases. *Circulation* 2012; **125**(13): 1591-3.

292.   Hirschey MD, Shimazu T, Goetzman E, et al. SIRT3 regulates mitochondrial fatty-acid oxidation by reversible enzyme deacetylation. *Nature* 2010; **464**(7285): 121-5.

293.   Ahn BH, Kim HS, Song S, et al. A role for the mitochondrial deacetylase Sirt3 in regulating energy homeostasis. *Proceedings of the National Academy of Sciences of the United States of America* 2008; **105**(38): 14447-52.

294.   Neubauer S. The failing heart--an engine out of fuel. *The New England journal of medicine* 2007; **356**(11): 1140-51.

295.   Kofman AE, McGraw MR, Payne CJ. Rapamycin increases oxidative stress response gene expression in adult stem cells. *Aging* 2012; **4**(4): 279-89.

296.   Robida-Stubbs S, Glover-Cutter K, Lamming DW, et al. TOR signaling and rapamycin influence longevity by regulating SKN-1/Nrf and DAF-16/FoxO. *Cell metabolism* 2012; **15**(5): 713-24.

297.   Webb AE, Brunet A. FOXO transcription factors: key regulators of cellular quality control. *Trends Biochem Sci* 2014; **39**(4): 159-69.

298.   Haugen AC, Di Prospero NA, Parker JS, et al. Altered gene expression and DNA damage in peripheral blood cells from Friedreich's ataxia patients: cellular model of pathology. *PLoS genetics* 2010; **6**(1): e1000812.

299.   Park KK, Liu K, Hu Y, Kanter JL, He Z. PTEN/mTOR and axon regeneration. *Experimental neurology* 2010; **223**(1): 45-50.

300.   Guccini I, Serio D, Condo I, et al. Frataxin participates to the hypoxia-induced response in tumors. *Cell death & disease* 2011; **2**: e123.

301.   Chen K, Lin G, Haelterman NA, et al. Loss of Frataxin induces iron toxicity, sphingolipid synthesis, and Pdk1/Mef2 activation, leading to neurodegeneration. *Elife* 2016; **5**.

302.   Chen K, Ho TS, Lin G, Tan KL, Rasband MN, Bellen HJ. Loss of Frataxin activates the iron/sphingolipid/PDK1/Mef2 pathway in mammals. *Elife* 2016; **5**.

303.   Lucas EK, Dougherty SE, McMeekin LJ, et al. PGC-1alpha provides a transcriptional framework for synchronous neurotransmitter release from parvalbumin-positive interneurons. *The Journal of neuroscience : the official journal of the Society for Neuroscience* 2014; **34**(43): 14375-87.

304.   Zhou J, Li H, Li X, et al. The roles of Cdk5-mediated subcellular localization of FOXO1 in neuronal death. *The Journal of neuroscience : the official journal of the Society for Neuroscience* 2015; **35**(6): 2624-35.

305.   Franco C, Fernandez S, Torres-Aleman I. Frataxin deficiency unveils cell-context dependent actions of insulin-like growth factor I on neurons. *Molecular neurodegeneration* 2012; **7**: 51.

306.   Franco C, Genis L, Navarro JA, et al. A role for astrocytes in cerebellar deficits in frataxin deficiency: Protection by insulin-like growth factor I. *Mol Cell Neurosci* 2017; **80**: 100-10.

307.   Cnop M, Mulder H, Igoillo-Esteve M. Diabetes in Friedreich ataxia. *Journal of neurochemistry* 2013; **126 Suppl 1**: 94-102.

308.   Molla B, Riveiro F, Bolinches-Amoros A, Munoz-Lasso DC, Palau F, Gonzalez-Cabo P. Two different pathogenic mechanisms, dying-back axonal neuropathy and pancreatic senescence, are present in the YG8R mouse model of Friedreich's ataxia. *Disease models & mechanisms* 2016; **9**(6): 647-57.

309.   Nakagawa A, Naito AT, Sumida T, et al. Activation of endothelial beta-catenin signaling induces heart failure. *Scientific reports* 2016; **6**: 25009.

310.   Piacentino V, 3rd, Weber CR, Chen X, et al. Cellular basis of abnormal calcium transients of failing human ventricular myocytes. *Circulation research* 2003; **92**(6): 651-8.

311.   Mercadier JJ, Lompre AM, Duc P, et al. Altered sarcoplasmic reticulum Ca2(+)-ATPase gene expression in the human ventricle during end-stage heart failure. *The Journal of clinical investigation* 1990; **85**(1): 305-9.

312.   Pilbrow AP, Cordeddu L, Cameron VA, et al. Circulating miR-323-3p and miR-652: candidate markers for the presence and progression of acute coronary syndromes. *Int J Cardiol* 2014; **176**(2): 375-85.

313.   Kelly M, Bagnall RD, Peverill RE, et al. A polymorphic miR-155 binding site in AGTR1 is associated with cardiac hypertrophy in Friedreich ataxia. *J Mol Cell Cardiol* 2011; **51**(5): 848-54.

314.   Garcia-Gimenez JL, Sanchis-Gomar F, Pallardo FV. Could thiazolidinediones increase the risk of heart failure in Friedreich's ataxia patients? *Movement disorders : official journal of the Movement Disorder Society* 2011; **26**(5): 769-71.

315.   Hausse AO, Aggoun Y, Bonnet D, et al. Idebenone and reduced cardiac hypertrophy in Friedreich's ataxia. *Heart* 2002; **87**(4): 346-9.

316.   Kakihana M, Yamazaki N, Nagaoka A. Effects of idebenone on the levels of acetylcholine, choline, free fatty acids, and energy metabolites in the brains of rats with cerebral ischemia. *Archives of gerontology and geriatrics* 1989; **8**(3): 247-56.

317.   Vega RB, Huss JM, Kelly DP. The coactivator PGC-1 cooperates with peroxisome proliferator-activated receptor alpha in transcriptional control of nuclear genes encoding mitochondrial fatty acid oxidation enzymes. *Molecular and cellular biology* 2000; **20**(5): 1868-76.

9. Appendix

Appendix Documents 1. Documents of approval Biomedical Research Ethics Committee (CEIB) of Hospital La Fe (Valencia), Hospital de Bellvitge (Barcelona), Hospital La Paz (Madrid), and Hospital Virgen del Rocio (Sevilla).

GENERALITAT VALENCIANA
CONSELLERIA DE SANITAT

AGÈNCIA VALENCIANA DE SALUT

La Fe
DEPARTAMENT DE SALUT
FPNT-CEIB-04 (A)

DICTAMEN DEL COMITÉ ÉTICO DE INVESTIGACIÓN BIOMÉDICA

Don Serafín Rodríguez Capellán, Secretario del Comité Ético de Investigación Biomédica del Hospital Universitario y Politécnico La **Fe,**

C E R T I F I C A

Que este Comité ha evaluado en su sesión de fecha **6 de Noviembre de 2012**, el Proyecto de Investigación titulado **"TRANSLATIONAL RESEARCH, EXPERIMENTAL MEDICINE AND THERAPEUTICS ON CHARCOT-MARIE-TOOTH. TREAT-CMT"**, con nº de registro **2011/0537**.

Que dicho proyecto se ajusta a las normativas éticas sobre investigación biomédica con sujetos humanos y es viable en cuanto al planteamiento científico, objetivos, material y métodos, etc, descritos en la solicitud, así como la Hoja de Información al Paciente y el Consentimiento Informado.

En consecuencia este Comité acuerda emitir **INFORME FAVORABLE** de dicho Proyecto de Investigación que será realizado en el Hospital Universitario y Politécnico La Fe por el/la **Dr. / Dra. TERESA SEVILLA MANTECON** del servicio de **NEUROLOGÍA** como Investigador Principal.

Miembros del CEIB:

Presidente:
Dr. Juan B. Salom Sanvalero. (Unidad de Circulación Cerebral Experimental)

Vicepresidente:
Dr. José Vicente Cervera Zamora. (Hematología)

Secretario:
D. Serafín Rodríguez Capellán. (Asesor jurídico)

Miembros:
Dr. Melchor Hoyos García. (Gerente del Departamento de salud Valencia La Fe)
Dr. José Vicente Castell Ripoll. (Director de Investigación)
Dr. Salvador Aliño Pellicer. (Farmacólogo Clínico - Hospital U. i P. La Fe)
Dra. Remedios Clemente García. (Medicina Intensiva)
Dra. Mª Luisa Martínez Triguero. (Análisis Clínicos)
Dr. José Luis Vicente Sánchez. (Jefe de sección - Unidad de Reanimación)
Dr. Isidro Vitoria Miñana. (Pediatría)
Dra. Belén Beltrán Niclós. (Medicina Digestiva)
Dra. Inmaculada Calvo Penadés. (Reumatología Pediátrica)
Dr. Alfredo José Perales Marin (Jefe de Servicio - Obstetricia)
Dra. Begoña Polo Miquel (Gastroenterología Pediátrica).
Dr. Enrique Viosca Herrero (Jefe de Servicio - Medicina Física y Rehabilitación)
Dra. Eugenia Pareja Ibars (Unidad de Cirugía y Trasplante Hepático).
Dr. Jaime Sanz Caballer (Grupo Acreditado en Hematología y Hemoterapia)
Dr. José Luis Ponce Marco (Unidad de Cirugía Endocrino Metabólica)
Dr. José Antonio Aznar Lucea (Jefe de Unidad - Hemostasia y Trombosis)

FPNT-CEIB-04 (A)

Dra. Pilar Sáenz González (Neonatología)
Dr. Rafael Botella Estrada (Dermatología)
Dr. José Luis Mullor Sanjose (Grupo de Investigación Traslacional en Enfermedades Neurosensoriales)
Dr. Francisco Javier Pemán García (Grupo Acreditado multidisciplinar para el estudio de la Infección Grave)
Dra. María José Gómez-Lechón Moliner (Grupo Acreditado en Hepatología Experimental)
Dr. Ramiro Jover Atienza. (Unidad de Bioquímica y Biología Molecular)
Dra. María Tordera Baviera. (Farmacéutica del Hospital)
D. Jesús Delgado Ochando. (Diplomado en Enfermería)

Lo que firmo en Valencia, a 6 de Noviembre de 2012

Fdo.: Don Serafín Rodríguez Capellán
Secretario del Comité Ético de Investigación Biomédica

**INFORME DEL COMITÉ ÉTICO DE INVESTIGACIÓN CLÍNICA
SOBRE PROYECTOS DE INVESTIGACIÓN**

El Comité Ético de Investigación Clínica del Hospital Universitari de Bellvitge, en su reunión de fecha 05 de Julio de 2012 (Acta 13/12), tras examinar toda la documentación presentada sobre el proyecto de investigación con nuestra ref. **PR184/12**, titulado:

"TRANSLATIONAL RESEARCH, EXPERIMENTAL MEDICINE AND THERAPEUTICS ON CHARCOT-MARIE-TOOTH DISEASE"

Presentado por el Dr. Carlos Casasnovas Pons del Servicio de Neurología del Hospital Universitari de Bellvitge – IDIBELL, como investigador principal, ha acordado emitir INFORME FAVORABLE al mencionado proyecto.

Convocatoria ISCIII CIBERER Biobank Centro de Investigación Biomédica en Red de Enfermedades Raras

Fdo. Dr. Enric Sospedra Martínez
Secretario del CEIC

L'Hospitalet de Llobregat, 5 de Julio de 2012

Hospital Universitari de Bellvitge
Feixa Llarga s/n
08907 L'Hospitalet de Llobregat
Tel. 932 607 500
www.bellvitgehospital.cat

C. E. I. C.
Hospital
Universitario
La Paz

HOJA DE EVALUACION   **Estudio**

TRANSLATIONAL RESEARCH, EXPERIMENTAL MEDICINE AND THERAPEUTICS ON CHARCOT-MARIE-TOOTH DISEASE.

INVESTIGADOR PRINCIPAL: el Dr. Samuel Ignacio Pascual Pascual del Servicio de Neurología del Hospital Infantil del Hospital Universitario "La Paz"
CEIC DE REFERENCIA: CIUTAT SANITÀRIA I UNIVERSITÀRIA DE BELLVITGE

TIPO DE ESTUDIO: NO-EPA

CÓDIGO HULP: PI-1378   ACTA: 17/2012
CÓDIGO PROMOTOR: PROMOTOR:

			Asistencia
Presidente	ANTONIO GIL AGUADO	Jefe de Sección. Medicina Interna	☑
Vicepresidente	JESÚS FRÍAS INIESTA	Jefe de Sección. Farmacología Clínica	☑
Secretaria	ROSARIO MADERO JARABO	Adjunto Bioestadística. Dpto. de Investigación	☑
Vocal	MARIO ARANCÓN MONGE	Médico Adjunto. Atención Primaria. Área 5	☐
Vocal	ELENA VILLAMAÑÁN BUENO	Farmacéutica Adjunta. Servicio de Farmacia	☑
Vocal	FILIBERTO CHULIÁ FERNÁNDEZ	Abogado. Jefe de Servicio. Asesoría Jurídica.	☑
Vocal	ALEJANDRO BALSA CRIADO	Médico Adjunto. Servicio de Reumatología. H.R.T.	☑
Vocal	JAVIER ARPA GUTIERREZ	Jefe de Sección. Servicio de Neurología. H. G.	☑
Vocal	MANUEL JIMÉNEZ LENDÍNEZ	Jefe de Servicio. Medicina Intensiva. H. G.	☑
Vocal	CARLOS A. HERNÁNDEZ GIL	Médico Adjunto. Servicio de Traumatología. H.R.T.	☐
Vocal	JAIME FERNÁNDEZ-BUJARRABAL	Médico Adjunto. Servicio de Neumología	☑
Vocal	RAFAEL DEL RIO VILLEGAS	Médico Adjunto. Servicio de Neurofisiología	☑
Vocal	ELENA GARCÍA HIGUERA	Médico Adjunto. Servicio de Anestesia y Reanimación	☐
Vocal	ANTONIO BUÑO SOTO	Médico Adjunto. Servicio de Análisis Clínicos	☑
Vocal	JAIME FELIU BATLLE	Médico Adjunto. Servicio de Oncología Médica	☐
Vocal	FERNANDO CABAÑAS GONZÁLEZ	Médico Adjunto. Servicio de Neonatología	☐
Vocal	FILOMENA TROCOLI GONZÁLEZ	Enfermera. Servicio de Nefrología	☑
Vocal	ÁNGEL ROBLES MARHUENDA	Médico Adjunto. Servicio de Medicina Interna	☑
Vocal	LUIS ASENSIO PRIANES	Médico Adjunto. Servicio de Cirugía General	☑
Vocal	ALMUDENA CASTRO CONDE	Médico Adjunto. Servicio de Cardiología	☑
Vocal	JOSÉ RAMÓN PAÑO PARDO	Médico Adjunto. Servicio de Medicina Interna	☐
Vocal	R. USANDIZAGA ELIO	Jefe de Sección. Servicio de Ginecología	☑
Vocal	J.A. SÁNCHEZ.-MORENO MÍNGUEZ	Abogado. Miembro no sanitario, ajeno a la Institución	☑

RESOLUCIÓN:
☐ Se delega   ☐ Aprobación
☒ Condicionada   ☐ Denegación
☐ No afecta a nuestro centro   ☐ Se ratifica la aprobación

ACLARACIONES Y MODIFICACIONES SOLICITADAS

La ratificación de la aprobación está pendiente de la recepción del certificado de la póliza de seguro de responsabilidad civil para el estudio

Madrid, 23 de octubre de 2012

Firmado: Rosario Madero Jarabo
Secretaria del CEIC

C. E. I. C.
Hospital
Universitario
La Paz

HOJA DE EVALUACION   **Estudio**

TRANSLATIONAL RESEARCH, EXPERIMENTAL MEDICINE AND THERAPEUTICS ON CHARCOT-MARIE-TOOTH DISEASE.

INVESTIGADOR PRINCIPAL: el Dr. Samuel Ignacio Pascual Pascual del Servicio de Neurología del Hospital Infantil del Hospital Universitario "La Paz"
CEIC DE REFERENCIA: CIUTAT SANITÀRIA I UNIVERSITÀRIA DE BELLVITGE

TIPO DE ESTUDIO: NO-EPA
CÓDIGO HULP: PI-1378   ACTA: 17/2012
CÓDIGO PROMOTOR: PROMOTOR:

			Asistencia
Presidente	ANTONIO GIL AGUADO	Jefe de Sección. Medicina Interna	☑
Vicepresidente	JESÚS FRÍAS INIESTA	Jefe de Sección. Farmacología Clínica	☑
Secretaria	ROSARIO MADERO JARABO	Adjunto Bioestadística. Dpto. de Investigación	☑
Vocal	MARIO ARANCÓN MONGE	Médico Adjunto. Atención Primaria. Area 5	☐
Vocal	ELENA VILLAMAÑÁN BUENO	Farmacéutica Adjunta. Servicio de Farmacia	☑
Vocal	FILIBERTO CHULIÁ FERNÁNDEZ	Abogado. Jefe de Servicio. Asesoría Jurídica.	☑
Vocal	ALEJANDRO BALSA CRIADO	Médico Adjunto. Servicio de Reumatología. H.R.T.	☑
Vocal	JAVIER ARPA GUTIERREZ	Jefe de Sección. Servicio de Neurología. H. G.	☑
Vocal	MANUEL JIMÉNEZ LENDÍNEZ	Jefe de Servicio. Medicina Intensiva. H. G.	☑
Vocal	CARLOS A. HERNÁNDEZ GIL	Médico Adjunto. Servicio de Traumatología. H.R.T.	☐
Vocal	JAIME FERNÁNDEZ-BUJARRABAL	Médico Adjunto. Servicio de Neumología	☑
Vocal	RAFAEL DEL RÍO VILLEGAS	Médico Adjunto. Servicio de Neurofisiología	☑
Vocal	ELENA GARCÍA HIGUERA	Médico Adjunto. Servicio de Anestesia y Reanimación	☐
Vocal	ANTONIO BUÑO SOTO	Médico Adjunto. Servicio de Análisis Clínicos	☑
Vocal	JAIME FELIU BATLLE	Médico Adjunto. Servicio de Oncología Médica	☐
Vocal	FERNANDO CABAÑAS GONZÁLEZ	Médico Adjunto. Servicio de Neonatología	☐
Vocal	FILOMENA TROCOLI GONZÁLEZ	Enfermera. Servicio de Nefrología	☑
Vocal	ÁNGEL ROBLES MARHUENDA	Medico Adjunto. Servicio de Medicina Interna	☑
Vocal	LUIS ASENSIO PRIANES	Médico Adjunto. Servicio de Cirugía General	☑
Vocal	ALMUDENA CASTRO CONDE	Médico Adjunto. Servicio de Cardiología	☑
Vocal	JOSÉ RAMÓN PAÑO PARDO	Medico Adjunto. Servicio de Medicina Interna	☐
Vocal	R. USANDIZAGA ELÍO	Jefe de Sección. Servicio de Ginecología	☑
Vocal	J.A. SÁNCHEZ-MORENO MÍNGUEZ	Abogado, Miembro no sanitario, ajeno a la Institución	☑

RESOLUCIÓN:
☐ Se delega   ☐ Aprobación
☐ Condicionada   ☐ Denegación
☐ No afecta a nuestro centro   ☒ Se ratifica la aprobación

ACLARACIONES Y MODIFICACIONES SOLICITADAS

Madrid, a 2 de octubre de 2012

Firmado: Rosario Madero Jarabo
Secretaria del CEIC

Servicio Andaluz de Salud
CONSEJERÍA DE SALUD Y BIENESTAR SOCIAL

INFORME DEL COMITÉ DE ÉTICA DE LA INVESTIGACIÓN DE CENTRO H.U. VIRGEN DEL ROCIO

El Comité de Ética de la Investigación de Centro H.U. Virgen del Rocío de Sevilla, en Sesión celebrada el día veinticinco de julio de dos mil doce (Acta 07/12):

1.   Ha procedido a la revisión del estudio:

- Código de CEI **2012PI/164**
- Presentado por **D. Celedonio Márquez Infante**
- Titulado **"Investigación Traslacional, Medicina Experimental y Terapéutica de la Enfermedad de Charcot-Marie-Tooth" (TREAT-CMT)".**
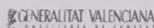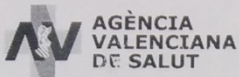
2.   Tras su valoración procede a emitir **INFORME FAVORABLE** del mismo.

Y para que conste y surta los efectos oportunos se expide la presente certificación en Sevilla, a veintisiete de julio de dos mil doce

Fdo.: Javier Bautista Paloma
Presidente

Appendix Documents 2. Documents of approval Biomedical Research Ethics Committee (CEIB) of Hospital Hospital Clínic Universitari de València and the ethics and scientific committees of the Basque Biobank for Research-OEHUN and (www.biobancovasco.org) and the Biobank for Biomedical Research and Public Health of the Valencian Community (IBSP-CV) through the Spanish National Biobank Network (RNBB 2013/12).

GENERALITAT VALENCIANA

AGÈNCIA VALENCIANA DE SALUT

INFORME DEL COMITE ETICO DE INVESTIGACION CLINICA DEL HOSPITAL CLINIC UNIVERSITARI DE VALENCIA

D. Manuel Labiós Gómez, Secretario del Comité Ético de Investigación Clínica del Hospital Clínic Universitari de Valencia
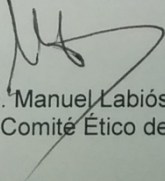
CERTIFICA

Que en este Comité, en su reunión de fecha 4 de octubre de 2013, y según consta en el acta de la misma, se han analizado los aspectos éticos y científicos relacionados al proyecto de investigación que lleva por título:

Estudio de miRNAs en pacientes de ataxia de Friedreich. Implicaciones diagnósticas terapéuticas.

Que será llevado a cabo en el Departamento de Fisiología de la Facultad de Medicina de la Universidad de Valencia y cuyo investigador principal es el Dr. Federico Pallardó, acordando que reúne las características adecuadas referentes a información a los pacientes y cumplimiento de los criterios éticos para la investigación médica y biomédica establecidos en la *Declaración de Helsinki* (Junio 1964, Helsinki, Finlandia) de la Asamblea Médica Mundial, y sus revisiones (Octubre 1975, Tokio, Japón), (Octubre 1983, Ve necia, Italia), (Septiembre 1989, Hong Kong), (Octubre 1996, Somerset West, Sudáfrica), (Octubre 2000, Edimburgo) y (Octubre 2008 Seúl, Corea) en la *Declaración Universal sobre el Genoma Humano y los Derechos del Hombre de la UNESCO* y los acuerdos del *Protocolo Adicional del Consejo de Europa para la protección de los Derechos del Hombre y de la dignidad del ser humano frente a la aplicaciones de la biología y de la medicina* (París 12-1-1998, ratificado el 23-7-1999).

Lo que certifico a efectos oportunos de la convocatoria de Ayudas de Proyectos de Investigación en Salud .

Valencia, 4 de octubre de 2013

Fdo. : Dr. D. D. Manuel Labiós Gómez
Secretario del Comité Ético de Investigación Clínica

GENERALITAT VALENCIANA
Conselleria de Sanitat

AGÈNCIA VALENCIANA DE SALUT

Federico Pallardó
Departamento de Fisiología
Facultad de Medicina
Universidad de Valencia

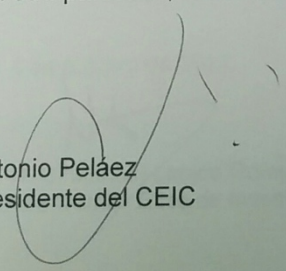Valencia, 10 de octubre de 2013.

Estimado Dr. Pallardó,

El motivo de la presente es informarle que en la pasada reunión del Comité de Ética del Hospital clínico Universitario de Valencia de fecha 4 de octubre de 2013, ha sido evaluado el proyecto titulado "Estudio de miRNAs en pacientes de ataxia de Friedreich. Implicaciones diagnósticas terapéuticas." del cual usted es el investigador principal.

En dicha evaluación, se acordó informar favorablemente.

Así mismo, se le informa que la legislación vigente en investigaciones donde se va a proceder a la toma de muestras de pacientes, es la Ley 14/2007 de 3 de julio, de Investigación Biomédica y estas investigaciones deberán cumplir dicha normativa.

En caso de requerir información adicional, no dude en ponerse en contacto con la secretaría del Comité.

Sin otro particular, reciba un cordial saludo.

Antonio Peláez
Presidente del CEIC

GENERALITAT VALENCIANA

CENTRO SUPERIOR DE INVESTIGACIÓN EN SALUD PÚBLICA

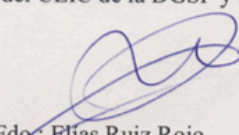**DICTAMEN DEL COMITÉ ÉTICO DE INVESTIGACIÓN CLÍNICA**

D. Elías Ruiz Rojo, Secretario del CEIC de la DGSP y CSISP.

CERTIFICA:

Que este CEIC ha evaluado en la reunión del día 31 de enero de 2014 la solicitud de muestras de la Red Valenciana de Biobancos con **REFERENCIA: RVB13011CPR,** para el proyecto de investigación denominado **"Estudio de miRNAs en pacientes de ataxia de Friedreich. Implicaciones diagnósticas y terapéuticas",** siendo su investigador principal el Dr. Pallardó. Considerándose procedente:

✓ Autorizar la cesión al proyecto de las muestras solicitadas que cuentan con CI específico de Biobanco.

✓ Autorizar la cesión al proyecto de las muestras solicitadas obtenidas con anterioridad a la entrada en vigor de la Ley de Investigación Biomédica que no disponen de CI.

✓ Autorizar la cesión al proyecto de las muestras solicitadas de donantes que han fallecido.

✓ Autorizar la cesión al proyecto de las muestras solicitadas de aquellos donantes que no han sido localizados.

✓ Autorizar la cesión al proyecto de las muestras solicitadas de aquellos donantes que han sido localizados, que no cuentan con CI, condicionada a la obtención del mismo y tras la comunicación a este CEIC.

Valencia a 4 de febrero de 2014
Secretario del CEIC de la DGSP y CSISP

Fdo.: Elías Ruiz Rojo
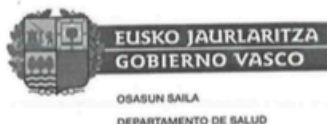
INFORME DEL COMITE ETICO DE INVESTIGACION CLINICA DE EUSKADI (CEIC-E)

Dª Iciar Alfonso Farnós como Secretaria del CEIC de la Comunidad Autónoma del País Vasco (CEIC-E)
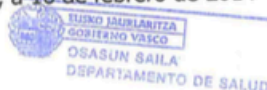
CERTIFICA

Que este Comité, actuando como comité ético externo del Biobanco Vasco de Bioef, ha evaluado la solicitud de cesión de muestras del biobanco vasco de la Fundación Vasca de Innovación e Investigación Sanitarias (BIOEF) para la realización del proyecto de investigación, titulado **"Estudio de miRNAs en pacientes de ataxia de Friedreich. Implicaciones diagnósticas y terapéuticas."**, y en el que actuará como investigador principal:

- Federico Vicente Pallardó (Universidad de Valencia)

Y que este Comité reunido el 29 de Enero de2014 (recogido en acta 02/2014), ha decidido emitir informe **favorable** a la solicitud de aprobación de cesión de muestras.

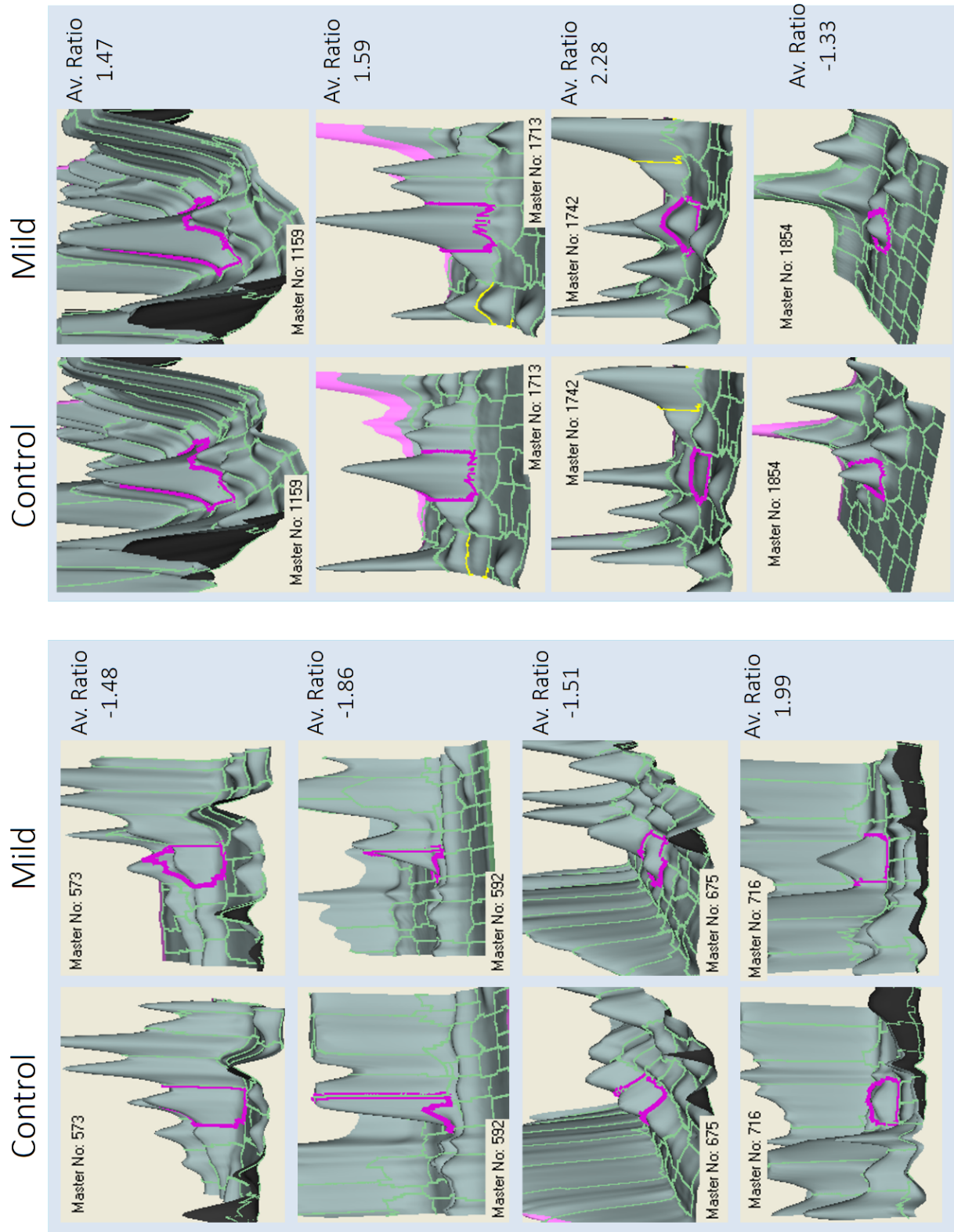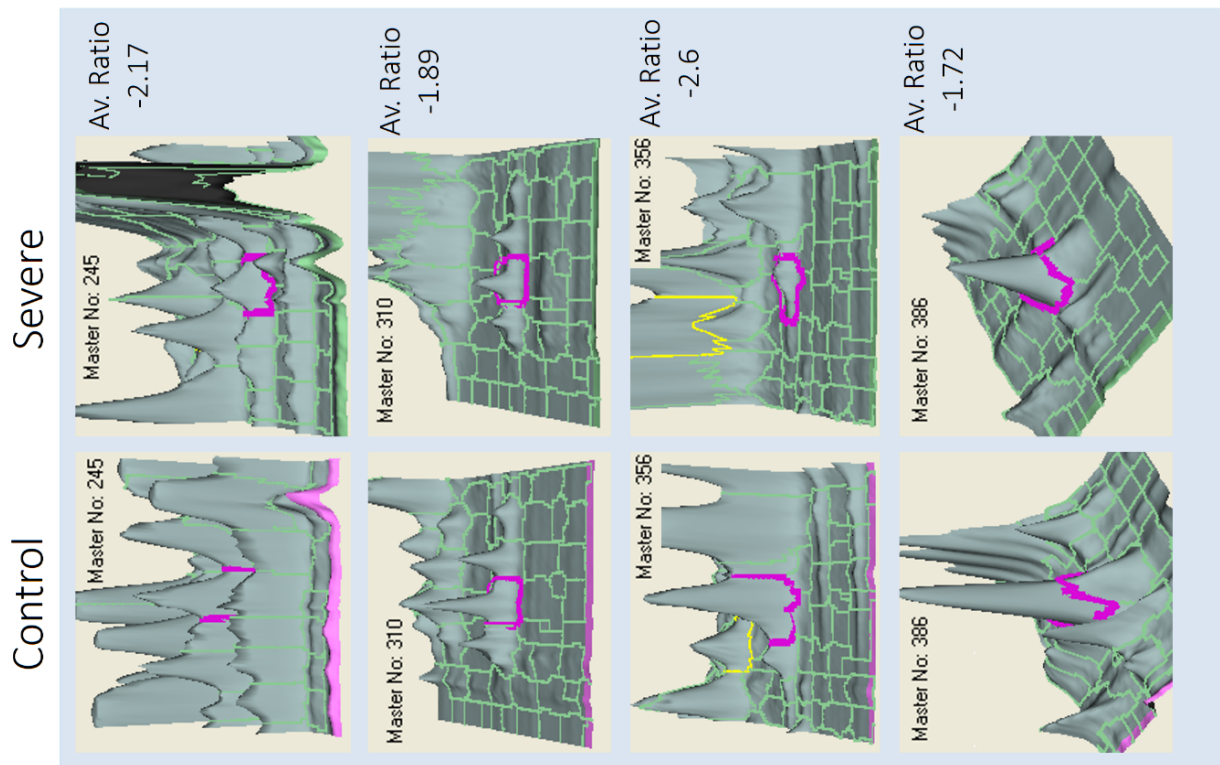Lo que firmo en Vitoria, a 10 de febrero de 2014

Fdo:

Dra. Iciar Alfonso Farnós
Secretaria del CEIC de la Comunidad Autónoma del País Vasco (CEIC-E)

Appendix Figure 1. Graphic representation of fluorescence intensity pics in 2D-DIGE analysis for mild CMT patients and healthy subjects. Identification number for each pick (Master No) and average ratio (Av. Ratio) was indicated for each pick.

(Continue)

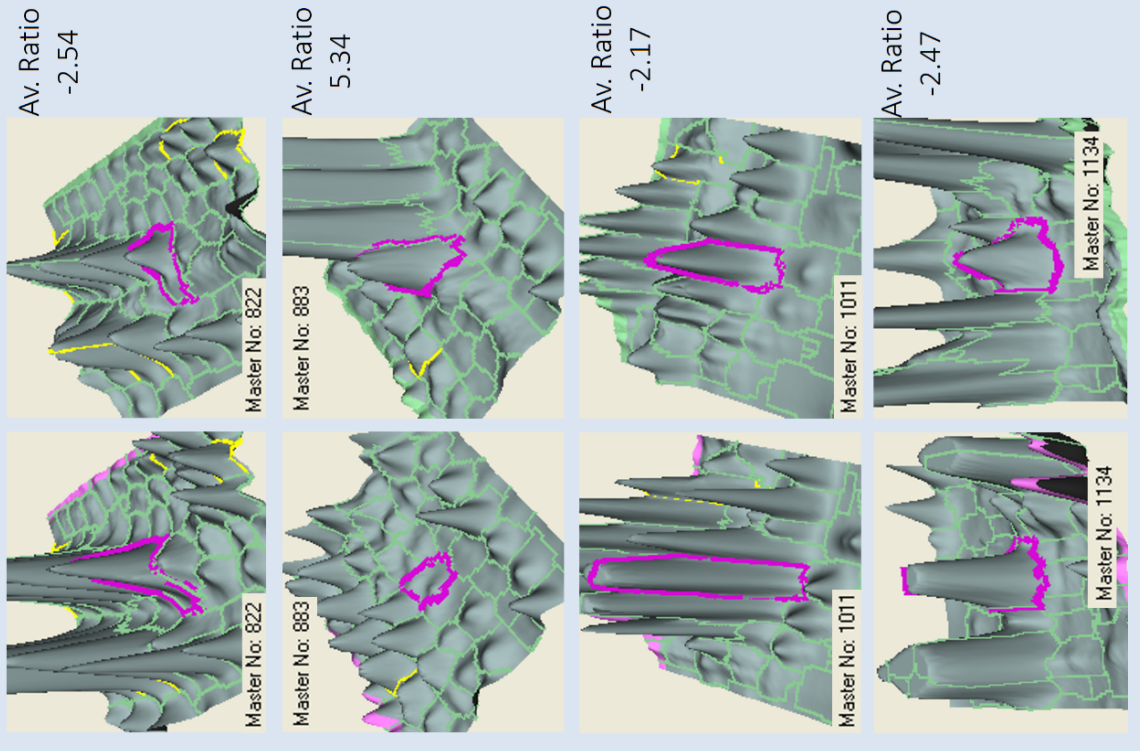Av. Ratio 2.91 — Severe — Master No: 1413 / Control — Master No: 1413

Av. Ratio 3.15 — Severe — Master No: 1426 / Control — Master No: 1426

Av. Ratio 4.93 — Severe — Master No: 1507 / Control — Master No: 1507

Av. Ratio 4.38 — Severe — Master No: 1529 / Control — Master No: 1529

Av. Ratio 7.05 — Severe — Master No: 1190 / Control — Master No: 1190

Av. Ratio 2.25 — Severe — Master No: 1278 / Control — Master No: 1278

Av. Ratio 3.36 — Severe — Master No: 1331 / Control — Master No: 1331

Av. Ratio 2.99 — Severe — Master No: 1353 / Control — Master No: 1353
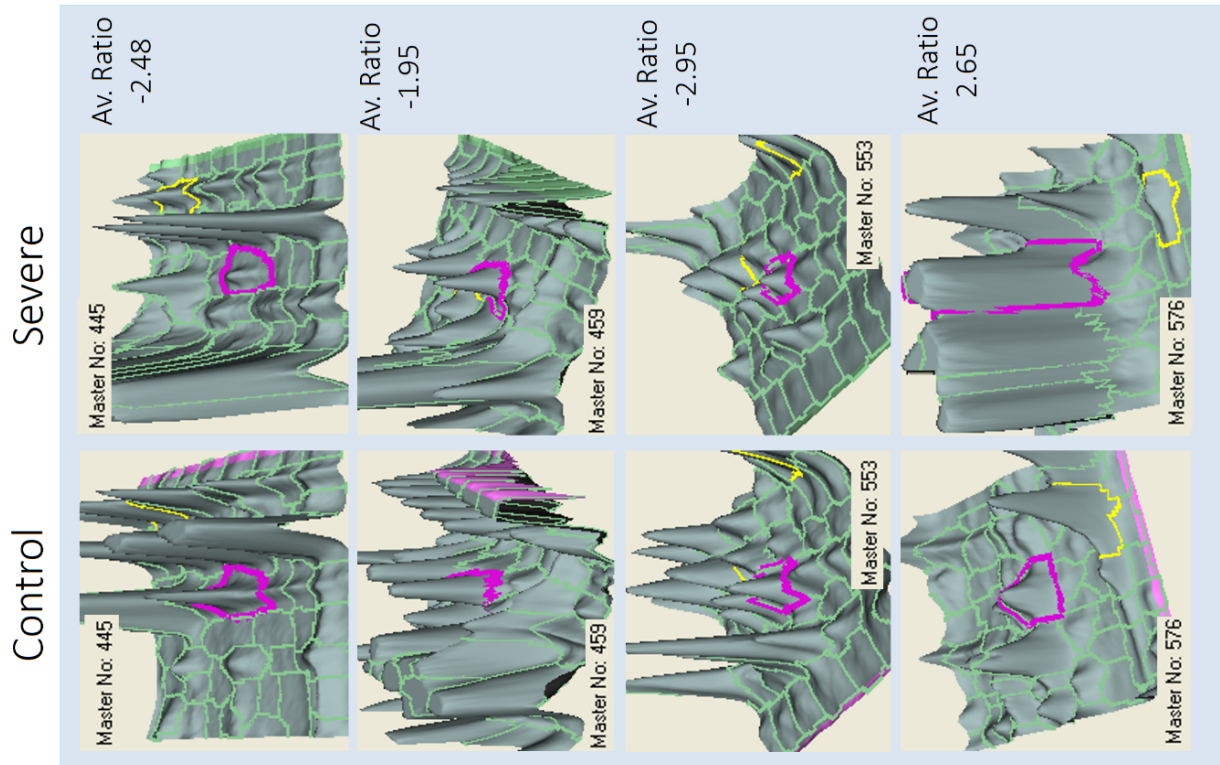
(Continue)

(Continue)

Apendix Figure 2. Graphic representation of fluorescence intensity pics in 2D-DIGE analysis for severe CMT patients and healthy subjects. Identification number for each pick (Master No) and average ratio (Av. Ratio) was indicated for each pick.
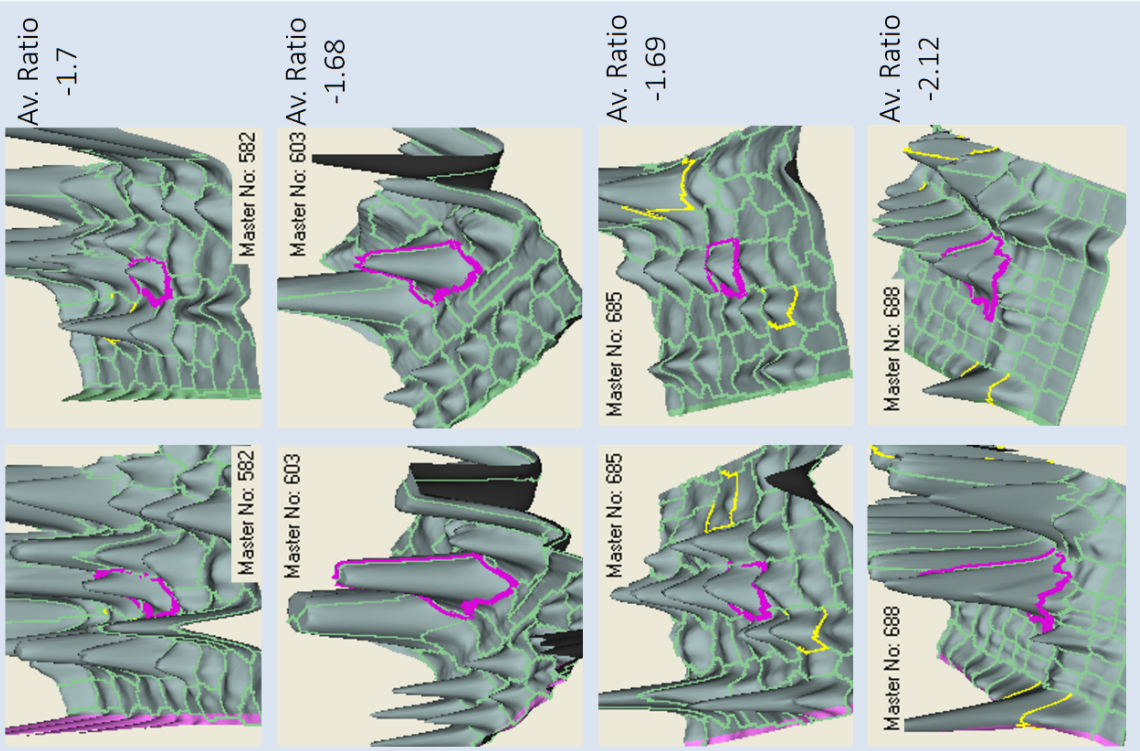
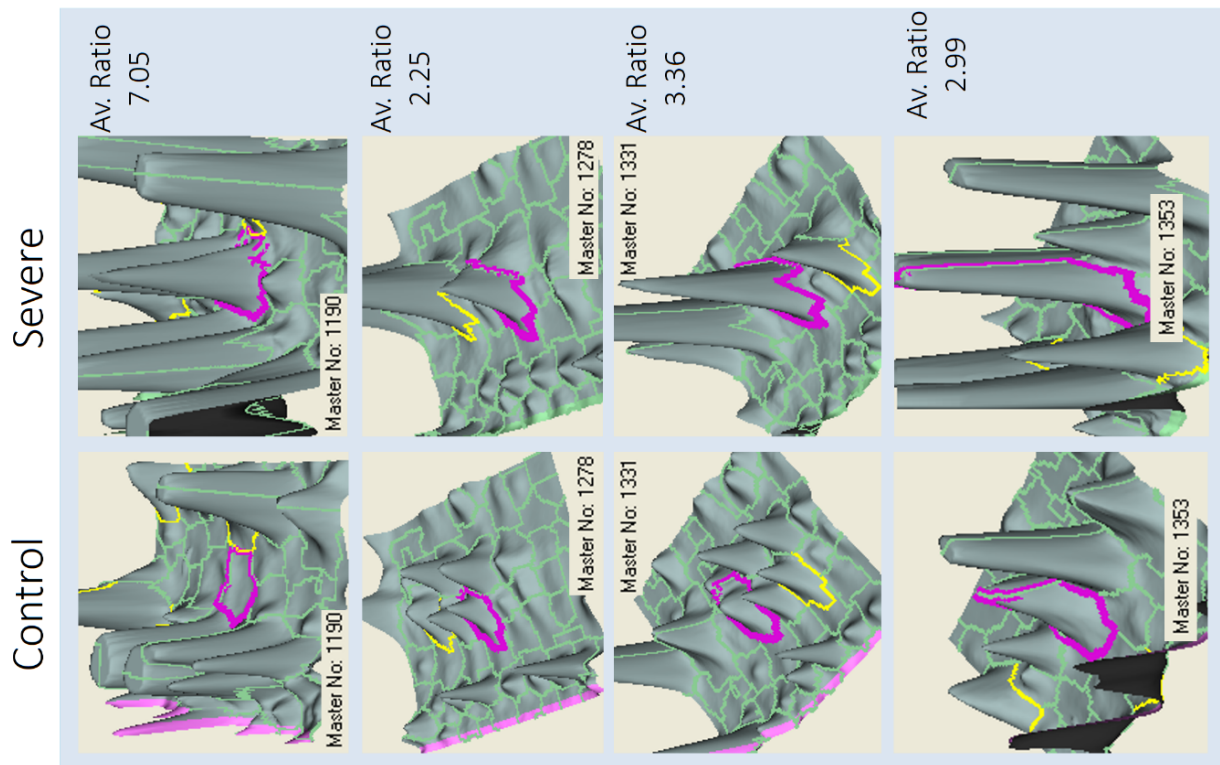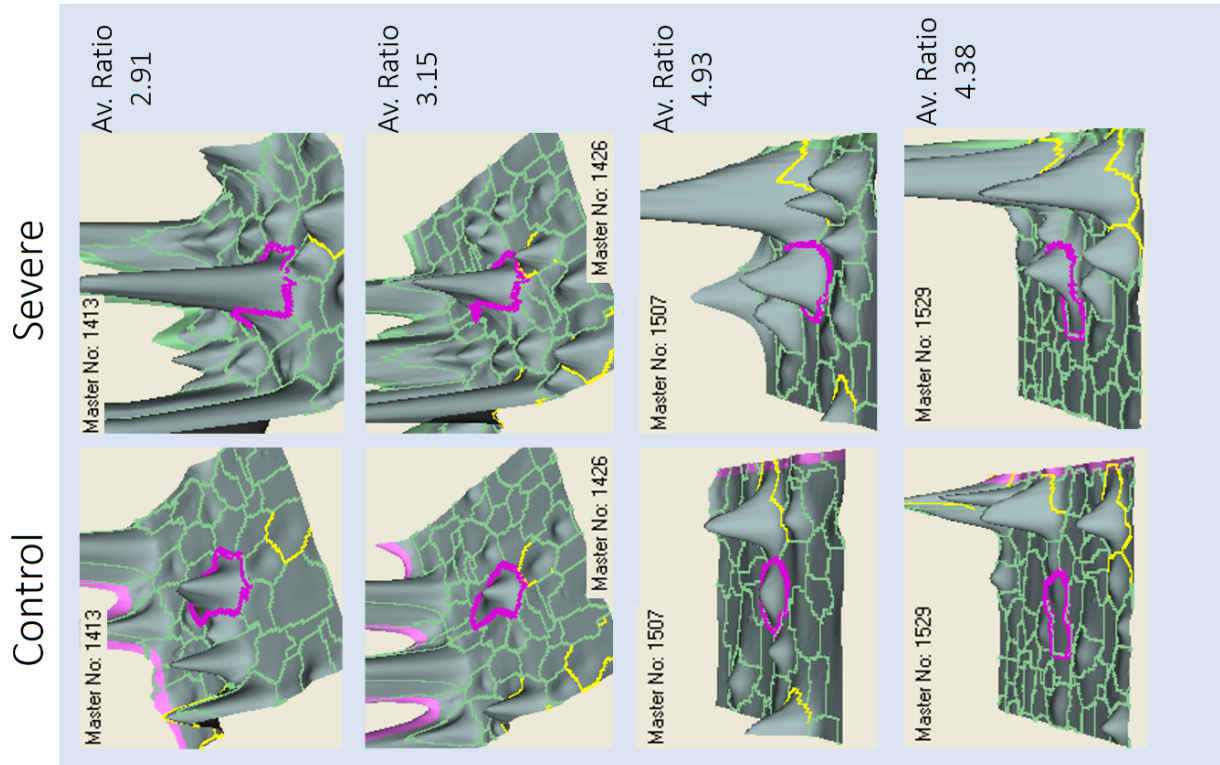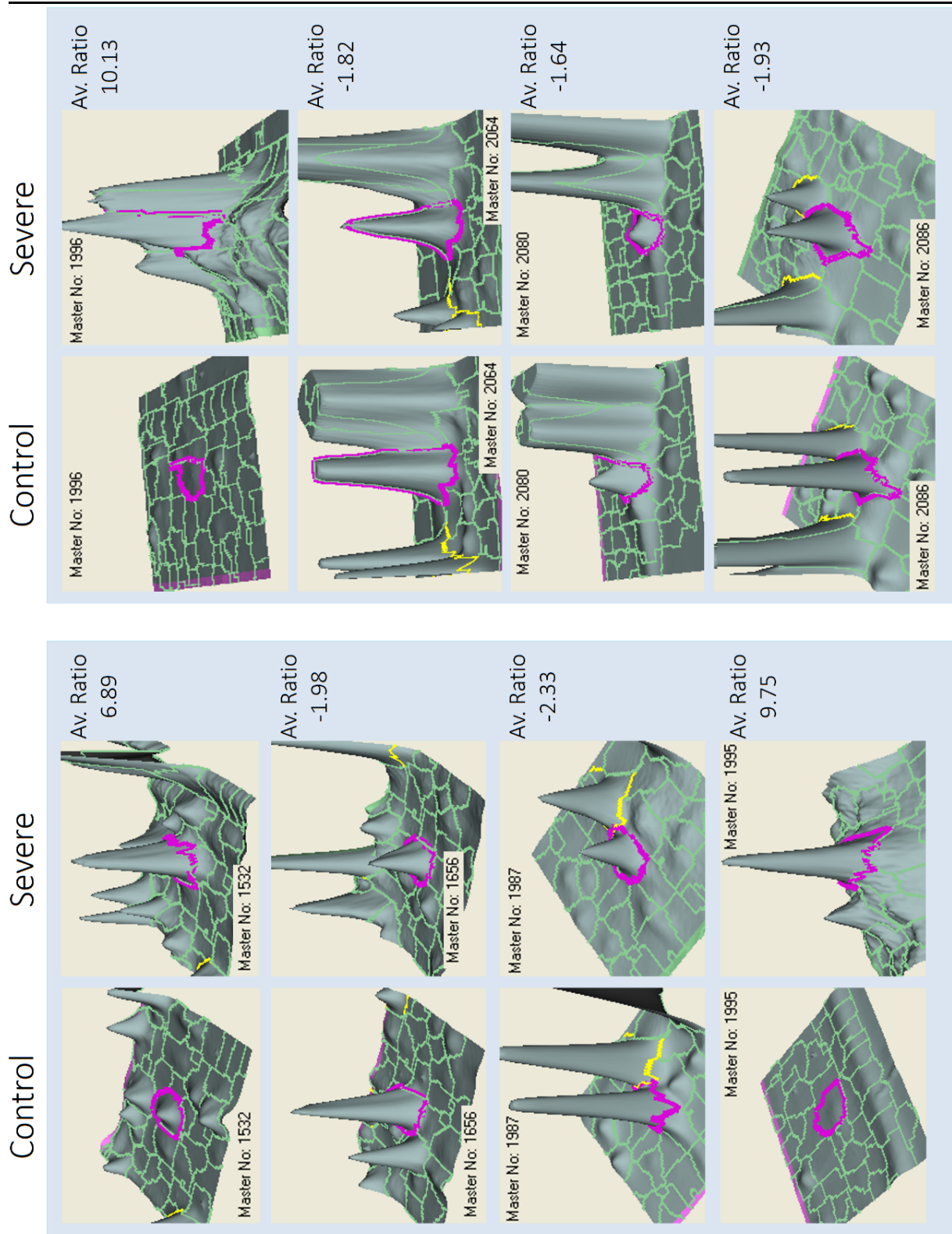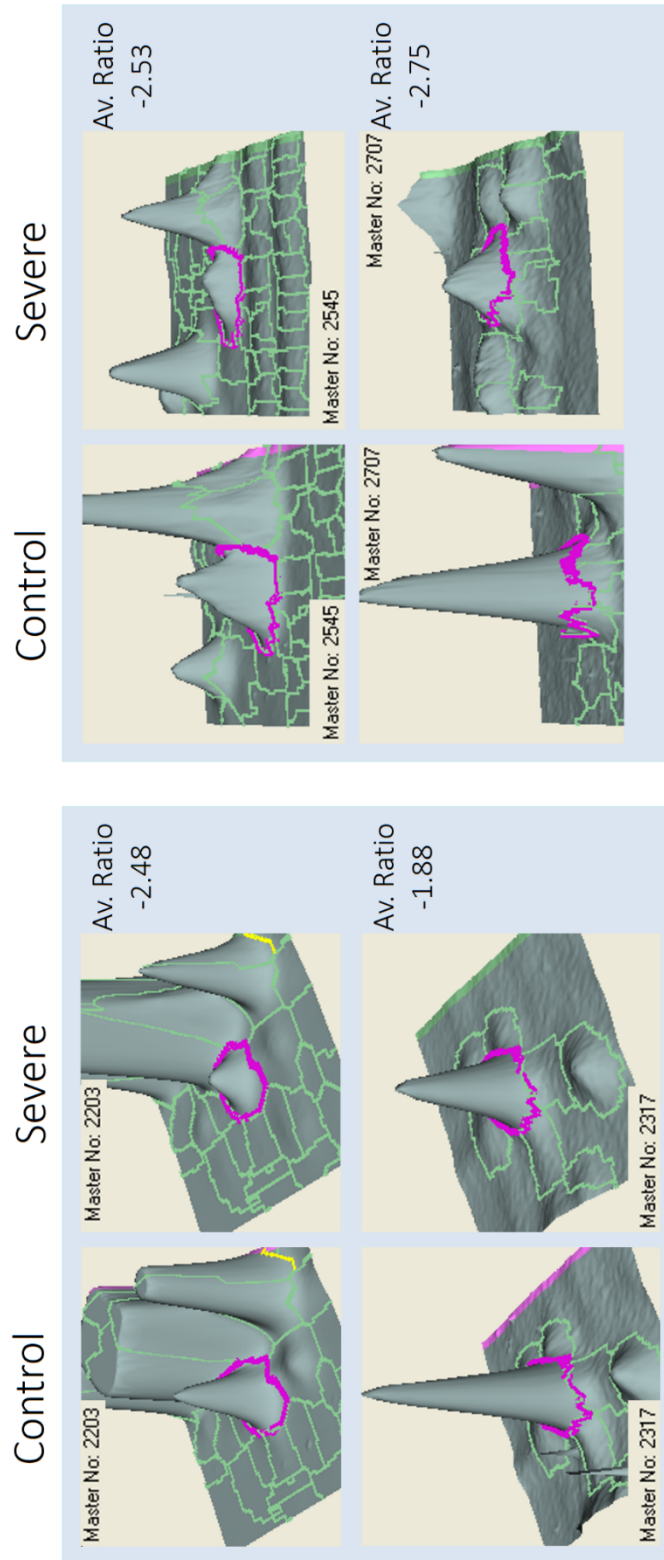**Appendix Table 1. Data from protein identification for mild CMT patients compared with healthy subjects.** Identification number for each pick (Master No), detection method used, protein identification code with the best accession, protein name, p-value for assignation for protein, and average ratio (Av. Ratio).

Master No	Detection method	Best Protein Accession	Protein Name	T-test	Av. Ratio
573	MALDITOFTOF	PLMN_HUMAN	Plasminogen	0,032	-1,48
592	LCMSMS	CFAB_HUMAN	Complement factor B	0,023	-1,86
675	MALDITOFTOF	AFAM_HUMAN	Afamin	0,046	-1,51
716	MALDITOFTOF	GELS_HUMAN	Gelsolin	0,005	1,99
1159	MALDITOFTOF	ANT3_HUMAN	Antithrombin-III	0,017	1,47
1713	MALDITOFTOF	APOA4_HUMAN	Apolipoprotein A-IV	0,047	1,59
1742	LCMSMS	HPT_HUMAN	Haptoglobin	0,037	2,28
1854	LCMSMS	CLUS_HUMAN	Clusterin	0,0085	-1,33
573	MALDITOFTOF	PLMN_HUMAN	Plasminogen	0,032	-1,48

Appendix Table 2. Data from protein identification for severe CMT patients compared with healthy subjects. Identification number for each pick (Master No), detection method used, protein identification code with the best accession, protein name, p-value for assignation for protein, and average ratio (Av. Ratio). Not congruent refers to a mixture of proteins.

Master No	Detection method	Best Protein Accession	Protein Name	T-test	Av. Ratio
245	LCMSMS	CO6_HUMAN	Complement component C6	0,00012	-2,17
310	LCMSMS	PLMN_HUMAN	Plasminogen	0,00083	-1,89
356	LCMSMS	CFAB_HUMAN	Complement factor B	0,0022	-2,60
386	LCMSMS	GSN_HUMAN	Gelsolin	0,0027	-1,72
445	LCMSMS	CFAB_HUMAN	Complement factor B	0,00021	-2,48
459	MALDITOFTOF	AFAM_HUMAN	Afamin	0,00038	-1,95
553	LCMSMS	VTNC_HUMAN	Vitronectin	0,0014	-2,95
576	MALDITOFTOF	TRFE_HUMAN	Serotransferrin	0,009	2,65
582	LCMSMS	A1BG_HUMAN	Alpha-1B-glycoprotein	0,0039	-1,70
603	LCMSMS	TRFE_HUMAN	Serotransferrin	0,00077	-1,68
685	LCMSMS	KNG1_HUMAN	Kininogen-1	0,048	-1,69
688	LCMSMS	AACT_HUMAN	Alpha-1-antichymotrypsin	0,0025	-2,12
822	LCMSMS	KNG1_HUMAN	Kininogen-1	0,00013	-2,54
883	LCMSMS	A1AT_HUMAN	Alpha-1-antitrypsin	0,00028	5,34
1011	LCMSMS	FETUA_HUMAN	Alpha-2-HS-glycoprotein	0,0015	-2,17
1134	LCMSMS	FIBG_HUMAN	Fibrinogen gamma chain	0,00021	-2,47
1190	LCMSMS	VTDB_HUMAN	Vitamin D-binding protein	0,0038	7,05
1278	LCMSMS	HPT_HUMAN	Haptoglobin	0,017	2,25
1331	MALDITOFTOF	HPT_HUMAN	Haptoglobin	0,00089	3,36
1353	MALDITOFTOF	APOA4_HUMAN	Apolipoprotein A-IV	0,0014	2,99
1413	LCMSMS	HPT_HUMAN	Haptoglobin	0,0067	2,91
1426	LCMSMS	HPT_HUMAN	Haptoglobin	0,0034	3,15
1507	LCMSMS	HPT_HUMAN	Haptoglobin	0,00046	4,93
1529	LCMSMS	HPT_HUMAN	Haptoglobin	0,00031	4,38
1532	LCMSMS	HPT_HUMAN	Haptoglobin	0,00028	6,89
1656	MALDITOFTOF	APOE_HUMAN	Apolipoprotein E	0,0013	-1,98
1987	MALDITOFTOF	Not Congruent	N/A	N/A	-2,33
1995	LCMSMS	IGKC_HUMAN	Ig kappa chain C region	0,00032	9,75
1996	LCMSMS	IGKC_HUMAN	Ig kappa chain C region	0,00021	10,13
2064	MALDITOFTOF	APOA1_HUMAN	Apolipoprotein A-I	0,0011	-1,82
2080	MALDITOFTOF	APOA1_HUMAN	Apolipoprotein A-I	0,032	-1,64
2086	MALDITOFTOF	APOA1_HUMAN	Apolipoprotein A-I	0,00011	-1,93
2203	LCMSMS	Not Congruent	N/A	N/A	-2,48
2317	LCMSMS	Not Congruent	N/A	N/A	-1,88
2545	LCMSMS	Not Congruent	N/A	N/A	-2,53
2707	LCMSMS	Not congruent	N/A	N/A	-2,75

Appendix Table 3. Expression levels of selected miRNAs in FRDA patients and controls stratified by age.
*Statistically significant differences were determined using Mann Whitney tests. All P-values were two-tailed and less than 0.05 was considered statistically significant.

miRNA	<39 years			>39 years		
	Patients (n=14) FC (SD)	Controls (n=11) FC (SD)	P value*	Patients (n=11) FC (SD)	Controls (n=14) FC (SD)	P value*
miR.128-3p	4.24 (4.56)	1.63 (2.41)	0.021	9.18 (11.10)	1.04 (0.75)	< 0.0001
miR-625-3p	13.46 (21.05)	1.48 (2.02)	0.007	20.38 (30.24)	2.72 (2.10)	0.034
miR-130b-5p	33.66 (50.49)	4.08 (4.67)	0.039	40.41 (37.69)	1.87 (2.18)	< 0.0001
miR-151a-5p	7.03 (6.72)	2.06 (4.00)	0.002	12.16 (10.40)	1.58 (1.57)	< 0.0001
miR-330-3p	11.73 (18.15)	3.03 (6.11)	0.021	21.00 (30.79)	1.93 (2.29)	< 0.0001
miR-323a-3p	2.84 (2.00)	1.63 (2.41)	0.049	3.83 (2.78)	1.30 (0.92)	< 0.0001
miR-142-3p	18,64 (26.50)	5.35 (13.46)	0.008	24.83 (40.17)	2.54 (3.85)	< 0.0001

Appendix Table 4. Expression levels of selected miRNAs in FRDA patients and controls stratified by sex.
*Statistically significant differences were determined using Mann Whitney tests. All P-values were two-tailed and less than 0.05 was considered statistically significant.

miRNA	Males			Females		
	Patients (n=12) FC (SD)	Controls (n=13) FC (SD)	P value*	Patients (n=13) FC (SD)	Controls (n=12) FC (SD)	P value*
miR.128-3p	8.02 (11.45)	1.08 (0.64)	0.001	4.93 (3.54)	1.54 (2.63)	0.002
miR-625-3p	14.47 (23.20)	2.44 (1.96)	0.05	17.80 (26.94)	1.67 (2.28)	0.007
miR-130b-5p	49.27 (57.21)	3.39 (3.40)	< 0.0001	24.96 (25.72)	2.17 (3.65)	< 0.0001
miR-151a-5p	11.14 (11.17)	1.18 (0.78)	< 0.0001	7.57 (5.63)	2.46 (4.00)	0.005
miR-330-3p	22.59 (33.66)	1.49 (1.05)	< 0.0001	9.55 (8.00)	3.43 (6.12)	0.011
miR-323a-3p	2.62 (1.20)	1.26 (0.72)	0.004	3.89 (3.02)	1.80 (2.40)	0.016
miR-142-3p	28.82 (44.32)	1.47 (1.34)	< 0.0001	14.48 (14.77)	6.29 (13.10)	0.008